

## **General Disclaimer**

### **One or more of the Following Statements may affect this Document**

- This document has been reproduced from the best copy furnished by the organizational source. It is being released in the interest of making available as much information as possible.
- This document may contain data, which exceeds the sheet parameters. It was furnished in this condition by the organizational source and is the best copy available.
- This document may contain tone-on-tone or color graphs, charts and/or pictures, which have been reproduced in black and white.
- This document is paginated as submitted by the original source.
- Portions of this document are not fully legible due to the historical nature of some of the material. However, it is the best reproduction available from the original submission.

MASSACHUSETTS INSTITUTE OF TECHNOLOGY

NASA CR-

141898

# APOLLO

## GUIDANCE, NAVIGATION AND CONTROL

R-700

MIT'S ROLE IN PROJECT APOLLO  
FINAL REPORT ON CONTRACTS  
NAS 9-153 AND NAS 9-4065

VOLUME II

OPTICAL, RADAR, AND  
CANDIDATE SUBSYSTEMS

MARCH 1972



**MIT INSTRUMENTATION  
LABORATORY**  
CAMBRIDGE 39, MASSACHUSETTS

(NASA-CF-141898) MIT'S ROLE IN PROJECT  
APOLLO. VOLUME 2: OPTICAL, RADAR, AND  
CANDIDATE SUBSYSTEMS Final Report  
(Massachusetts Inst. of Tech.) 261 p HC  
\$8.50

N75-28110

CSCI 22E G3/19

Unclas  
28646

# APOLLO

## GUIDANCE, NAVIGATION AND CONTROL

Approved David G. Hoag Date 3/1/72  
D. G. HOAG, DIRECTOR  
APOLLO GUIDANCE AND NAVIGATION PROGRAM

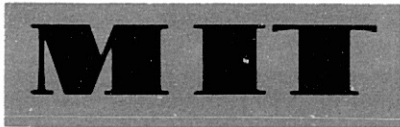
Approved Ralph A. Ragan Date 5 Mar 1972  
R. R. RAGAN, DEPUTY DIRECTOR  
THE CHARLES STARK DRAPER LABORATORY

R-700  
MIT's ROLE IN PROJECT APOLLO  
FINAL REPORT ON CONTRACTS  
NAS 9-153 AND NAS 9-4065

VOLUME II

OPTICAL, RADAR, AND  
CANDIDATE SUBSYSTEMS

MARCH 1972



CAMBRIDGE 39, MASSACHUSETTS

# INSTRUMENTATION LABORATORY

COPY # \_\_\_\_\_

## ACKNOWLEDGMENTS

This report was prepared under DSR Project 55-23890, sponsored by the Manned Spacecraft Center of the National Aeronautics and Space Administration.

The publication of this document does not constitute approval by the National Aeronautics and Space Administration of the findings or conclusions contained herein. It is published for the exchange and stimulation of ideas.

**REPRODUCTION RESTRICTIONS OVERRIDDEN**  
NASA Scientific and Technical Information Facility

© Copyright by the Massachusetts Institute of Technology  
Published by the Charles Stark Draper Laboratory of the  
Massachusetts Institute of Technology  
Printed in Cambridge, Massachusetts, U.S.A., 1972

**REPRODUCTION RESTRICTIONS OVERRIDDEN**

NASA Scientific and Technical Information Facility

## FOREWORD

The title of these volumes, "MIT's Role in Project Apollo", provides but a modest hint of the enormous range of accomplishments by the staff of this Laboratory on behalf of the Apollo program. Man's rush into spaceflight during the 1960s demanded fertile imagination, bold pragmatism, and creative extensions of existing technologies in a myriad of fields. The achievements in guidance and control for space navigation, however, are second to none for their critical importance in the success of this nation's manned lunar-landing program, for while powerful space vehicles and rockets provide the environment and thrust necessary for space flight, they are intrinsically incapable of controlling or guiding themselves on a mission as complicated and sophisticated as Apollo. The great achievement of this Laboratory was to supply the design for the primary hardware and software necessary to solve the Apollo guidance, navigation and control problem. It is to the credit of the entire team that this hardware and software have performed so dependably throughout the Apollo program.

The quantum leap in technology nurtured by the Apollo program has been and should continue to be of immensely significant benefit to this country—socially, economically and in terms of its national esteem. It is the responsibility of all those who contributed to the proud achievements of Apollo to convince their countrymen of the directions this nation ought to follow in implementing these newly gained—and hard fought for—advances.

C. Stark Draper, President  
Charles Stark Draper Laboratory

## ABSTRACT

This report presents the Draper Laboratory's efforts in Project APOLLO for Optical, Radar, and Candidate Subsystems from original contract award in mid-1961 through July 1969.

The design and development of the optical subsystems for both the APOLLO command and lunar spacecraft are described in Chapter I. Generally, the chapters are written for the design engineer, i. e., design approaches, problems, and solutions are discussed.

Chapter II discusses the evolution and current status of the radar interfaces with the GN&C system which involved both hardware and software in a relatively complex interrelationship.

Chapter III discusses the design and development of three candidate subsystems that were considered for use in APOLLO, but which, for the reasons stated, were not incorporated into the final GN&C system. The three subsystems discussed are the star tracker-horizon photometer, the map and data viewer and the lunar module optical rendezvous system.

PRECEDING PAGE BLANK NOT FILMED

PRECEDING PAGE BLANK NOT FILMED

TABLE OF CONTENTS

<u>Chapter</u>		<u>Page</u>
I	OPTICAL SUBSYSTEMS. . . . .	1
1.0	EVOLUTION OF OPTICAL SUBSYSTEM REQUIREMENTS . .	5
1.1	INITIAL DECISIONS AND REASONING. . . . .	5
1.2	APPROACHES, PROBLEMS, AND SOLUTIONS. . . . .	5
	1.2.1 General Design Evolution . . . . .	5
	1.2.2 Environmental Problems . . . . .	7
	1.2.3 Eye Problems . . . . .	8
	1.2.4 Resolver Design . . . . .	8
	1.2.5 Placement of the Optical Subsystem . . . . .	9
2.0	OPTICAL SUBSYSTEM, COMMAND MODULE . . . . .	11
2.1	SUBSYSTEM DESIGN . . . . .	11
	2.1.1 General Description . . . . .	11
	2.1.1.1 Block I-0 Optical Subsystem . . . . .	18
	2.1.1.2 Block I-50 Optical Subsystem. . . . .	19
	2.1.1.3 Block I-100 Optical Subsystem . . . . .	19
	2.1.1.4 Block II Optical Subsystem. . . . .	21
	2.1.2 Interfaces . . . . .	21
	2.1.3 Optical Unit Assembly Design Evaluation . . . . .	23
2.2	PROBLEMS AND SOLUTIONS . . . . .	26
	2.2.1 Block I-0 Optical Subsystem . . . . .	26
	2.2.2 Block I-50 Optical Subsystem . . . . .	27
	2.2.3 Block I-100 Design . . . . .	27
	2.2.4 Block II Design. . . . .	28
2.3	FLIGHT EXPERIENCE, COMMAND MODULE . . . . .	29
2.4	ERROR ANALYSIS . . . . .	30
2.5	DESIGN CRITIQUE OF THE BLOCK II OPTICAL SUBSYSTEM . . . . .	30
3.0	LUNAR MODULE OPTICS, ALIGNMENT OPTICAL TELESCOPE . . . . .	33
3.1	DESIGN REQUIREMENTS AND FUNCTIONAL DESCRIPTION . . . . .	33
	3.1.1 Requirements . . . . .	33
	3.1.2 Functional Description . . . . .	37
3.2	PROBLEMS AND SOLUTIONS . . . . .	38

TABLE OF CONTENTS (Cont)

<u>Chapter</u>	<u>Page</u>
3.3	FLIGHT EXPERIENCE, LUNAR MODULE (AOT). . . 39
3.4	ERROR ANALYSIS . . . . . 39
3.5	CRITIQUE . . . . . 40
4.0	VISIBILITY STUDIES . . . . . 43
4.1	INTRODUCTION . . . . . 43
4.2	TESTS AND RESULTS. . . . . 44
5.0	MATERIAL AND COMPONENT PROBLEMS AND SOLUTIONS. . . . . 47
5.1	BERYLLIUM FABRICATION TECHNIQUES . . . . . 47
5.2	MOTOR-TACHOMETER OPERATIONS IN VACUUM . 47
5.3	DEVELOPMENT OF A 64-SPEED RESOLVER . . . . 48
5.4	BEARING LUBRICATION . . . . . 48
	5.4.1 Lubricant Characteristics. . . . . 49
	5.4.2 Labyrinth Seals . . . . . 49
5.5	VACUUM WELDING. . . . . 49
5.6	LOCKING COMPOUNDS . . . . . 50
5.7	OUTGASSING PRODUCTS . . . . . 50
6.0	OPTICAL SUBSYSTEM ANALYSIS . . . . . 51
6.1	EARTH-HORIZON DEFINITION PROGRAMS . . . . . 51
	6.1.1 Program Objectives . . . . . 51
	6.1.2 Program Tasks . . . . . 54
	6.1.3 Program Schedule . . . . . 57
6.2	THE VISUAL HORIZON . . . . . 59
	6.2.1 Beamsplitter Effects of the Apollo Optics . . . 61
	6.2.2 Sources of Horizon Measurement Error . . . 63
	6.2.3 Selection of Locators . . . . . 66
	6.2.4 Geometric Aspects of Navigation Sighting . . . 67
	6.2.5 Summary of Sighting Constraints. . . . . 70
	6.2.6 Optical Simulation Results . . . . . 71
	6.2.6.1 Stars Against Uniform Background . 71
	6.2.6.2 Stars Against Horizon and Landmarks. . . . . 72
	6.2.6.3 Horizon Against Scattered Light . . . 73
	6.2.7 Scattered Light Intensity . . . . . 73
6.3	POST FLIGHT MEASUREMENT EVALUATIONS . . . . 82

## TABLE OF CONTENTS

<u>Chapter</u>	<u>Page</u>
II RADAR SUBSYSTEM. . . . .	85
1.0 INTRODUCTION . . . . .	87
2.0 ORIGINAL RADAR REQUIREMENTS . . . . .	89
3.0 EVOLUTION OF THE RADAR SPECIFICATION . . . . .	91
4.0 RENDEZVOUS RADAR (RR) . . . . .	93
4.1 RADAR FUNCTIONAL REQUIREMENTS . . . . .	93
4.2 OPERATING LIMITS . . . . .	93
4.3 ANGULAR COVERAGE . . . . .	94
4.4 MEASUREMENT ACCURACY . . . . .	96
4.5 DESCRIPTION OF RENDEZVOUS RADAR . . . . .	96
4.5.1 Summary . . . . .	96
4.5.2 Rendezvous Radar Parameters . . . . .	102
4.5.3 Operation . . . . .	102
4.5.4 Antenna . . . . .	103
4.5.5 Receiver . . . . .	104
4.5.6 Frequency Synthesizer . . . . .	104
4.5.7 Frequency Tracker . . . . .	104
4.5.8 Range Tracker . . . . .	105
4.5.9 Servo Electronics . . . . .	105
4.5.10 Signal Data Converter . . . . .	106
4.5.11 Self-Test . . . . .	106
4.6 TRANSPONDER . . . . .	107
4.6.1 General . . . . .	107
4.6.2 Transponder Parameters. . . . .	107
4.6.3 Operation. . . . .	107
4.6.4 Transponder Self-Test. . . . .	108
4.7 TRANSPONDER ACQUISITION SEQUENCE . . . . .	108
4.8 RENDEZVOUS RADAR-COMPUTER ANGLE INTERFACE. . . . .	108
4.9 RENDEZVOUS RADAR-COMPUTER DIGITAL INTERFACE. . . . .	110
4.10 RENDEZVOUS RADAR INTERFACE SOFTWARE . . . . .	114
4.10.1 Computer Angle Control of the Rendezvous Radar . . . . .	115
4.10.2 Rendezvous Radar Search Routine . . . . .	120

TABLE OF CONTENTS (Cont)

<u>Chapter</u>		<u>Page</u>
	4.10.3 Rendezvous Radar Angular Mode Control and Limits . . . . .	121
	4.10.4 Radar Angle Limit Protection . . . . .	124
	4.10.5 Aided Acquisition . . . . .	125
	4.10.6 Angle Bias Estimation . . . . .	125
	4.10.7 Functional Protection of the Rendezvous Radar	129
5.0	LANDING RADAR . . . . .	131
5.1	FUNCTIONAL REQUIREMENTS . . . . .	131
5.2	OPERATING LIMITS . . . . .	131
5.3	MEASUREMENTS ACCURACY . . . . .	132
5.4	DESCRIPTION OF THE LANDING RADAR. . . . .	132
	5.4.1 Antenna Coordinate System . . . . .	132
	5.4.2 Physical Description . . . . .	135
	5.4.3 Landing Radar Operation . . . . .	135
	5.4.4 Landing Radar Design Features to Counter Vehicle Effects . . . . .	139
	5.4.5 Landing Radar - Computer Interface . . . . .	140
5.5	LANDING RADAR INTERFACE SOFTWARE . . . . .	143
	5.5.1 Computer Processing of Velocity Data . . . . .	145
	5.5.2 Landing Radar Reasonableness Test . . . . .	146
6.0	VHF RANGING SYSTEM . . . . .	147
6.1	FUNCTIONAL REQUIREMENTS . . . . .	147
6.2	OPERATIONAL CHARACTERISTICS . . . . .	147
6.3	OPERATING LIMITS . . . . .	148
6.4	MEASUREMENT ACCURACY . . . . .	148
6.5	COMPUTER-VHF RANGING INTERFACE . . . . .	149
6.6	INTERFACE EVALUATION TESTS . . . . .	149
	6.6.1 VHF Interface Simulator . . . . .	151
	6.6.2 Evaluation . . . . .	151
6.7	VHF RANGING SYSTEM INTERFACE SOFTWARE . . . . .	151
7.0	FLIGHT TEST PROGRAM . . . . .	155
7.1	GENERAL . . . . .	155
7.2	FACILITIES . . . . .	155
7.3	MIT/IL RANDEZVOUS RADAR TESTS . . . . .	156
	7.3.1 Rendezvous Radar Lunar-Stay Simulation Tests . . . . .	157
	7.3.2 Rendezvous Radar Rendezvous Simulation Tests . . . . .	157
	7.3.3 Polarization Tests . . . . .	158
	7.3.4 Rendezvous Radar Pearl-X Test . . . . .	163
7.4	LANDING RADAR TESTS . . . . .	163
	7.4.1 Landing Radar Mission Simulation Tests . . . . .	164

TABLE OF CONTENTS (Cont)

<u>Chapter</u>		<u>Page</u>
	7.4.2 Zero-Doppler Dropout Test . . . . .	164
	7.4.3 Cross Beam Lock-on Tests . . . . .	164
	7.4.4 Deceleration and Attitude Angle-Rate Tests . . . . .	166
	7.4.5 Range Beam Tests . . . . .	166
	7.5 FLIGHT TEST REFERENCES . . . . .	166
8.0	INTERFACE TEST PROGRAM . . . . .	169
8.1	INTRODUCTION . . . . .	169
8.2	PHASE I TEST PROGRAM . . . . .	169
	8.2.1 Phase I Test Equipment . . . . .	170
	8.2.2 Problems Encountered in the Phase I Tests . . . . .	173
	8.2.3 Test Results . . . . .	177
8.3	PHASE II TEST PROGRAM . . . . .	179
	8.3.1 Evaluation of Rendezvous Radar Angle Inter- face . . . . .	179
	8.3.1.1 Servo Evaluation . . . . .	181
	8.3.1.2 Comparison with MIT/IL Digital Simulation Model . . . . .	182
	8.3.1.3 Dither Problems . . . . .	186
	8.3.1.4 Computer Program Evaluation . . . . .	186
	8.3.2 Evaluation of Landing Radar Data Readout . . . . .	187
	8.3.2.1 Statistical Characteristics of Data Readout Using Simulated Input Signals . . . . .	188
	8.3.2.1.1 Random Errors and Readout Delays . . . . .	191
	8.3.2.1.2 Frequency Tracker Noise Investigation . . . . .	193
	8.3.2.2 Processing Of Flight Test Data . . . . .	193
	8.3.2.2.1 1966/1967 Flight Test Data . . . . .	197
	8.3.2.2.2 1968 Flight Test Data . . . . .	200

## TABLE OF CONTENTS

<u>Chapter</u>	<u>Page</u>
III CANDIDATE SUBSYSTEMS. . . . .	205
1.0 GENERAL INTRODUCTION . . . . .	205
2.0 TRACKER-PHOTOMETER . . . . .	206
2.1 INTRODUCTION . . . . .	206
2.2 STAR TRACKER. . . . .	206
2.3 HORIZON PHOTOMETER. . . . .	208
2.4 NAVIGATION TECHNIQUE WITH THE TRACKER - PHOTOMETER . . . . .	210
2.5 CONCLUSIONS . . . . .	210
3.0 LUNAR MODULE OPTICAL RENDEZVOUS SYSTEM . . . . .	215
3.1 INTRODUCTION . . . . .	215
3.2 FUNCTIONAL CAPABILITIES. . . . .	215
3.3 OPTICAL RENDEZVOUS SYSTEM COMPONENT DESCRIPTION. . . . .	216
3.3.1 Optical Tracker. . . . .	216
3.3.2 Lunar Module Computer Control . . . . .	221
3.3.3 Command Module Luminous Beacon . . . . .	222
3.4 REFERENCES. . . . .	222
4.0 MAP AND DATA VIEWER. . . . .	225
4.1 INTRODUCTION . . . . .	225
4.2 GENERAL DEVELOPMENT . . . . .	225
4.3 MAP AND DATA VIEWER PHYSICAL DESCRIPTION. . . . .	227
4.3.1 General Construction . . . . .	227
4.3.1.1 Housing and Moisture Seal Assembly	230
4.3.1.2 Film Cartridge . . . . .	230
4.3.1.3 Access Door Assembly . . . . .	230
4.3.1.4 Electronics Assembly . . . . .	232
4.3.2 Map and Data Viewer Mechanization . . . . .	232
4.3.3 Optical System . . . . .	234
4.3.4 Operation . . . . .	236
4.4 DEVELOPMENT TESTING OF BLOCK II CONFIGURATION . . . . .	236
4.4.1 Sine-Wave Vibration Tests . . . . .	236

TABLE OF CONTENTS (Cont)

Chapter

	<u>Page</u>
4.4.2 Random Vibration Tests . . . . .	238
4.4.3 Pressure Tests . . . . .	238
4.4.4 Moisture Tests . . . . .	239
4.4.5 Drop Test . . . . .	240
4.5 PORTABLE CONFIGURATION . . . . .	240

PRECEDING PAGE BLANK NOT FILMED

LIST OF ILLUSTRATIONS

Chapter I

<u>Figure</u>		<u>Page</u>
2-1	Sextant Schematic . . . . .	12
2-2	Scanning Telescope Schematic . . . . .	12
2-3	Optical Unit Assembly . . . . .	13
2-4	Apollo Optical Unit . . . . .	14
2-5	Optical Subsystem Axes . . . . .	16
2-6	Block I-50 OSS Functional Diagram . . . . .	20a
2-7	Block I-100 OSS Functional Diagram . . . . .	22a
2-8	Block II OSS Functional Diagram . . . . .	24a
3-1	Alignment Optical Telescope Optical Schematic. . . . .	34
3-2	AOT Cutaway View . . . . .	35
3-3a	Depicts the Principles of Measurement . . . . .	36
3-3b	Depicts the Principles of Measurement . . . . .	36
3-1	Typical Horizon Profile . . . . .	53
6-2	Relationships between the Projects in the Horizon Program . . . . .	55
6-3	Major Activities in the Program . . . . .	58
6-4	A Typical Horizon Profile . . . . .	60
6-5	Illustration of Cloud Top Problem with the Use of Apparent Horizon as a Location. . . . .	62
6-6	Variation in Half-Maximum Intensity Altitude . . . . .	64
6-7	Variation in Half-Maximum Intensity Altitude . . . . .	64
6-8	Typical Midcourse Navigation Situation . . . . .	68
6-9	Projected OSS Field of View in Typical Navigation Situation . . . . .	69
6-10	Star Visibility Test Data . . . . .	74
6-11	Sextant Star Visibility Contours for Sun $10^{\circ}$ from LLOS . . . . .	75
6-12	Sextant Star Visibility Contours for Sun $15^{\circ}$ from LLOS . . . . .	76
6-13	Sextant Star Visibility Contours for Sun $20^{\circ}$ from LLOS . . . . .	77
6-14	Sextant Star Visibility Contours for Sun $30^{\circ}$ from LLOS . . . . .	78
6-15	Sextant Star Visibility Contours for Sun $40^{\circ}$ from LLOS . . . . .	79
6-16	Sextant Star Visibility Contours for Sun $45^{\circ}$ from LLOS . . . . .	80

LIST OF ILLUSTRATIONS (Cont)

Chapter I

<u>Figure</u>	<u>Page</u>
6-17 Sextant Star Visibility Contours for Sun 50° from LLOS . . . . .	81
6-18 P23 Activity for G-Mission Translunar and Transearth Trajectories	83
6-19 Apollo 8 Translunar Midcourse Navigation . . . . .	84

Chapter II

4-1 Rendezvous Radar Antenna Assembly . . . . .	95
4-2 Shaft Mode Limits Expressed in Shaft Resolver Angles . . . . .	97
4-3 Mode Limits and Hard Stop Locations Expressed in Resolver Angles	98
4-4 Rendezvous Radar Block Diagram . . . . .	99
4-5 Transponder, Block Diagram . . . . .	100
4-6 RR-LGC Interface, Block Diagram . . . . .	111
4-7 RR Stable Angle Lock-up Locations . . . . .	116
4-8 Typical RR Angle Designate . . . . .	119
4-9 RR Search Pattern. . . . .	122
4-10 RR Search Mode-Maximum Continuous Exposure Time(s) vs Angle from Designated LOS . . . . .	123
4-11 RR-LM Angle Coverage . . . . .	126
5-1 L.R. Antenna Coordinate System . . . . .	133
5-2 Angles Defining Orientation of LR Antenna Axes with Respect to the Navigation Base Coordinate System . . . . .	134
5-3 LR Antenna and Electronic Assemblies . . . . .	136
5-4 LR Antenna and Electron Assemblies Block Diagram . . . . .	137
5-5 LGC - LR Interface . . . . .	141
6-1 DRG Interface Block Diagram . . . . .	150
6-2 General Configuration of VHF Interface Simulator. . . . .	152
6-3 General Configuration of VHF Interface Simulator. . . . .	153
7-1 T-33 Flight Trajectories - ALT. 12K FT. . . . .	159
7-2 SH-3A Flight Trajectories - ALT. 3K FT. . . . .	160
7-3 White Sands Test Pass 1: Run 1 Theta Bias vs Time . . . . .	161
7-4 White Sands Test Pass 1: Run 1 Beta Bias vs Time . . . . .	162
7-5 LR Dropout Points . . . . .	165
8-1 Block Diagram of Phase I Interface Test . . . . .	171
8-2 Rendezvous Radar Digital Interface Unit . . . . .	172
8-3 Landing Radar Digital Interface Unit. . . . .	174

LIST OF ILLUSTRATIONS (Cont)

Chapter II

<u>Figure</u>	<u>Page</u>
8-4 Digital Interface Simulator . . . . .	175
8-5 Computer Simulator . . . . .	176
8-6 Rendezvous Radar Antenna Simulator . . . . .	180
8-7 RR Antenna Servo Digital Simulation . . . . .	184
8-8 Digital Simulation of Antenna Angle Designation (Trunnion Angle) . .	185
8-9 Test Setup for Simulated Radar Signal . . . . .	189
8-10 Data Readout Simulation of Landing Radar . . . . .	190
8-11 V-Velocity Tracker Error - Probability Density . . . . .	194
8-12 Flight Test Operations . . . . .	196
8-13 LR Helicopter "Yo-Yo" Flight vs Time . . . . .	198
8-14 Three Velocity Components in Antenna Coordinates . . . . .	198
8-15 LR Slant Range Errors . . . . .	199
8-16 LR Vertical Velocity Error . . . . .	199
8-17 LR Cross-Track Velocity Error . . . . .	199
8-18 LR Track Velocity Error . . . . .	199

Chapter III

2-1 V-30 Apollo Optical Unit . . . . .	207
2-2 Star Tracker Block Diagram . . . . .	209
2-3 Horizon Sighting Geometry . . . . .	211
2-4 Horizon Photometer, Block Diagram . . . . .	212
3-1 Optical Tracker Cross Section . . . . .	217
3-2 LORS System Logic Block Diagram . . . . .	218
3-3 LORS Modulation Techniques . . . . .	220
3-4 Luminous Beacon . . . . .	223
3-5 Luminous Beacon Block Diagram . . . . .	224
4-1 Lower Display and Control Panel . . . . .	226
4-2a Map and Data Viewer . . . . .	229
4-2b M and DV, Top View . . . . .	229
4-3 Cartridge and Film Alignment . . . . .	231
4-4 Access Door Assembly . . . . .	231
4-5 Gearbox and Cartridge Mechanization . . . . .	233
4-6 M&DV Optical System Functional Diagram . . . . .	235
4-7 Projection Lamp Control Circuit . . . . .	237
4-8 Map and Data Viewer - Portable Configuration . . . . .	242

LIST OF TABLES

Chapter I

<u>Table</u>		<u>Page</u>
3-I	Inflight Alignment Errors . . . . .	41
3-II	Lunar Surface Alignment . . . . .	41
6-I	Comparison of Visual Horizon Locations . . . . .	65
6-II	Description and Summary of Locators with Typical Beamsplitter . .	67
6-III	Minimum Star Intensity . . . . .	70
6-IV	Minimum Sun Elevation Angle . . . . .	71
6-V	Maximum Slant Angle. . . . .	71

Chapter II

4-I	RR Measurement Accuracy . . . . .	101
4-II	RR-LGC Status Discretes . . . . .	113
5-I	Landing Radar Measurement Performance Summary . . . . .	132
5-II	Landing Radar Status Discretes . . . . .	142
8-I	Base Motion Disturbance . . . . .	183
8-II	System, Summary of Data Readout Errors for Simulated Input Signals	192
8-III	Error Statistics of Landing Radar Flight Tests . . . . .	203
8-IV	Error Statistics of Landing Radar End to End Flight Test. . . . .	204

Chapter III

4-I	Characteristics of Block I and II Map and Data Viewer . . . . .	228
-----	---	-----

PRECEDING PAGE BLANK NOT FILMED

## PREFACE

"I believe this nation should commit itself to achieving the goal before this decade is out of landing a man on the moon and returning him safely to earth." With these words, spoken on 25 May 1961, President John Fitzgerald Kennedy stated for all Americans the challenge of the APOLLO project. The Massachusetts Institute of Technology Instrumentation Laboratory\* was selected to design and develop the hardware and software of the APOLLO Guidance, Navigation and Control system for safe and self-sufficient translunar flight, lunar landing, and return. This Final Report describes that work — a most demanding, innovative, and rewarding task.

This report presents the Draper Laboratory's efforts in Project APOLLO from the original contract award in mid-1961 through July 1969. The report is organized in five volumes:

VOLUME I: PROJECT MANAGEMENT AND SYSTEMS DEVELOPMENT

VOLUME II: OPTICAL, RADAR, AND CANDIDATE SUBSYSTEMS

VOLUME III: COMPUTER SUBSYSTEM

VOLUME IV: INERTIAL SUBSYSTEM

VOLUME V: THE SOFTWARE EFFORT

Volume I emphasizes what was done in terms of resource allocation and systems development and contains Appendices A and B; Volumes II through IV describe the hardware subsystems in detail, with emphasis on the final design configurations; Volume V fully treats the Laboratory's software effort. Appendix A presents abstracts of significant research and engineering reports and theses written under Contracts NAS 9-153 and NAS 9-4065. Appendix B is a bibliography of all such reports and theses prepared through June 1969. This date is also the cutoff for all discussions within this report, except for APOLLO 11 — the first manned lunar landing and return.

---

\*The Laboratory was renamed the Charles Stark Draper Laboratory in January 1970.

CHAPTER I  
OPTICAL SUBSYSTEMS

ACKNOWLEDGMENT

The following individuals contributed significantly to this chapter: Philip N. Bowditch, Donald R. Giller, James A. Hand, George Karthas, Ronald L. Morey, and Lawrence Yorgy.

The design and development of the optical subsystems for both the APOLLO command and lunar module spacecraft are described in this chapter. Generally, the chapter is written for the design engineer; i.e., optical design approaches, problems, and solutions are discussed.

The first section is a synopsis of the evolution of optical sensor design requirements for the command module. Section 2 then describes the two major blocks of design configurations. This is followed by the design description of the lunar module optics. One of the major findings of the APOLLO optical design and flight experience has demonstrated the seriousness of the scattered light environment in space flight—such visibility studies are the topic of the fourth section. Problems and solutions in materials and components are described in the fifth section. The last section of the chapter summarizes the analyses of the overall navigation sighting function and principal error sources.

PRECEDING PAGE BLANK NOT FILMED

SECTION 1.0  
EVOLUTION OF OPTICAL SUBSYSTEM REQUIREMENTS

1.1 INITIAL DECISIONS AND REASONING

The initial requirement of the APOLLO mission was a complete, self-contained, onboard guidance and navigation capability. No ground or peripheral control of the spacecraft's motion was envisioned (see also Vol. 1, Chapter II). Thus, it was clear that some form of inertial measurement unit (IMU), able to be erected from within a space vehicle, would have to be designed. From the beginning of MIT/IL's involvement in the design of a GN&C system, it was expected that the duration of the lunar mission would necessitate that the inertial measurement unit be turned off periodically during flight to conserve power. Alternatively, if the inertial unit were not turned off, gyro drift rates would be intolerable, so that a requirement would exist for re-erection of the unit to the inertial coordinate frame with star sightings.

To achieve the necessary navigational accuracy in updating the vehicle's state vector, a dual line-of-sight (LOS) sextant observation was required. This would provide a capability of instantaneously measuring the plane angle between two celestial objects, a near body and star. A dual line-of-sight device would allow much higher accuracy than could be accomplished with a single instrument used to obtain sequential sightings referenced to the inertial measurement unit stable member through a resolver chain and a mechanical alignment system.

1.2 APPROACHES, PROBLEMS, AND SOLUTIONS

The following section describes the evolution of the optical subsystem (OSS) sextant and scanning telescope designs from their initial conception through the Block II type which was used in the manned APOLLO flights.

1.2.1 General Design Evolution

Early in the planning phase, several sextant designs were tried, each in an attempt to provide as much independent motion as possible for the line of sight. Each of these designs had its own drawback. The first space sextant, called Mark I, was composed of a simple theodolite with 28-power eyepiece configured to have two

PRECEDING PAGE BLANK NOT FILMED

lines of sight, both movable in shaft and trunnion. A precision angle measurement was included between the two lines of sight. The Mark I was originally a combined sextant-scanning telescope with low and high powers on a single head and two eyepieces.

The Mark I design was rejected because two independent lines of sight fail to alleviate spacecraft attitude control restrictions for midcourse measurements. It was also concluded that the low power part of the instrument was primarily a "finder" device, having nothing in common with the high power requirements. It was thus decided to design two separate instruments. One would be a scanning telescope (SCT) and the other a rather conventional sextant (SXT), except that one line of sight would be immovable.

These considerations led to a design involving a double-dove beamsplitter that would allow one fixed line of sight to go through, and another steerable line of sight to be singly reflected by the double-dove. The two lines of sight would have been mutually inverted; this was judged to be a major perceptual difficulty. It was decided to have erect images throughout, and the double-dove sextant design was abandoned.

Landmark tracking was defined early in the design effort as a desirable instrument function, with the scanning telescope to be used for this purpose. Because NASA required a fail-safe backup manual control, manual drives and angle readouts were placed on the telescope. With these drives, the telescope could be aimed in a known direction (with respect to the body axes) and thus the inertial measurement unit aligned even in the case of complete optical subsystem failure.

On the Block I-0 optical subsystem, a fixed polarizer on the beamsplitter and a manually moved polarizer in the eyepiece of the sextant would allow variable attenuation of the landmark line of sight (LLOS) without influencing the star line of sight (SLOS). This approach was dropped after testing indicated the polarizer might not meet some of the severe thermal requirements.

Also at the Block I-0 stage, a submode was installed to allow the optical axis of the telescope to be offset from the sextant landmark line of sight by 25 degrees. This offset field allowed acquisition of stars by the telescope over the entire available field of view without losing sight of the landmark image in the sextant during star-landmark navigation measurements.

The next major change in the optical subsystem occurred in the Block I-100 design. A star tracker-horizon photometer was incorporated into the optics. The optical

unit assembly was modified, incorporating 0.8-inch aperture systems that used tuning forks for light modulation and a photomultiplier as the sensing element. The tracker was to lock onto a star using an articulating index mirror, which was integral with the sextant star line of sight. The horizon-photometer line of sight was steered manually with the minimum impulse controller, using the scanning telescope as a visual reference of the horizon.

Problems arose in the development of peripheral packaging for the tracker-photometer. Because of general difficulties in assembly, schedules, and cost, the device was deleted at the Block II assembly stage, although dummy electronic modules remained. A more detailed treatment of the development of the tracker-photometer is presented in Chapter III, Candidate Subsystems, Section 2.0.

### 1.2.2 Environmental Problems

The original environmental specifications (circa 1962) were based on the worst imaginable guided missile environment, based on extrapolation from booster rocket experience. Though these excessively severe specifications were modified after approximately four years, the original design work was done under the constraints of the earlier environmental specifications.

The navigation base (NB) throughout the Block I optical subsystem design was constructed of beryllium and was shockmounted to protect the optics from launch thrusts. Once out of the atmosphere, the 5-psi differential between operational cabin pressure and the vacuum in space would have resulted in approximately 800 lb of outward force on the optical subsystem, thus loading up the shockmounts. In the Block II design, the new navigation base incorporated an aluminum shell filled with rigid foam and was hard-mounted to the spacecraft structure. A flexible seal was employed around the optics separating cabin and space environment.

The vehicle and environmental specifications made it likely that a large amount of moisture condensation would form on the lens elements. To preclude the possibility of this condition, heaters were added to the eyepiece to ensure that the lenses remained above ambient temperature. Because the early environmental specifications were so rigid and because a thermal model was not originally defined, spaces were provided in the base of the optics for a coolant system. This system was never used since the actual thermal environment was not as severe as envisioned.

The protective doors over the optics were typical motor-powered airframe doors with a backup manual drive. After installation on the first vehicle, it was found by

the spacecraft manufacturer that these doors would not meet the design requirements. The door design was deleted, making necessary the placement of ablative thermal shielding for atmospheric reentry on the optical subsystem. Another company was subcontracted by NASA to design a thermal shield for the optics.

### 1.2.3 Eyepiece Problems

The optical subsystem originally included a three-power eyepiece. NASA decided to delete this feature since the low power telescope optics were to be used primarily in a finder mode, and little advantage could be seen for any magnification. The Block I and II subsystems were therefore designed with a one-power eyepiece.

Long-relief eyepieces were at one time considered as an interface technique between the helmeted astronaut and the optical subsystem. Helmet specifications were not readily available, delaying long-relief eyepiece design. Another issue involving human engineering considerations was that of allowing the eyepieces to be removable. Originally, the eyepieces were screwed on in a straightforward threading operation. They were stored in a niche and screwed to the optical unit assembly panel. This arrangement was judged undesirable, however, because of operating time involved and other considerations. A quick-release eyepiece and its mount were therefore designed.

After considerable delay, space for eyepiece storage was allotted in the area vacated by the abandoned map and data viewer. MIT/IL initiated the design of a storage unit that was completed and manufactured by AC Electronics.

### 1.2.4 Resolver Design

The earliest attempt at a precision angle-measurement device involved a worm drive. Upon test, this device showed a very large cyclical tooth error. Another approach involved a theodolite, designed by MIT/IL. But this was a complicated, delicate device with many fragile optical elements, and was not considered feasible in the optical subsystem design.

A multipole resolver, designed by Bendix, had the desirable aspects of averaging of 64 poles, requiring few mechanical tolerances, and fitting neatly into a package. It also provided the desired accuracy. A single- and 64-speed Bendix resolver was thus incorporated into the optical subsystem design for measurement of the sextant angle between the star and landmark lines of sight.

### 1.2.5 Placement of the Optical Subsystem

It was decided to place the GN&C equipment in the area of the lower equipment bay. The optics was to be the only system, with the exception of the life support system, to penetrate the skin of the spacecraft. Care was taken not to compromise the pressure integrity of the cabin.

PRECEDING PAGE BLANK NOT FILMED

## SECTION 2.0 OPTICAL SUBSYSTEM, COMMAND MODULE

### 2.1 SUBSYSTEM DESIGN

#### 2.1.1 General Description

The optical subsystem consists of an optical unit assembly (OUA), coupling data units (CDUs), and portions of the power and servo assembly (PSA) and guidance and navigation indicator and control panel (GNICP). The optical subsystem, incorporated into a complete GN&C system, performs two major functions: navigation and inertial platform alignment. If the spacecraft is near a planet, navigation can be performed by providing the computer with data obtained from successive angle measurements between a line of sight to a near-body landmark and a reference direction obtained from the inertial measurement unit and computer. When the spacecraft is far from a planet, earth or moon, data for navigation can be obtained from two lines of sight to celestial objects—one of which must be the earth or moon. Optical tracking of the lunar module also permits rendezvous navigation. Alignment is performed by providing the computer with angular data from a single line of sight, established by sightings on selected stars, the angular data being stored on MARK command and processed by the APOLLO guidance computer (AGC) to establish an inertial reference.

The optical unit assembly consists of two servo-operated optical instruments: a scanning telescope and a sextant. Figures 2-1, 2-2, and 2-3 depict the scanning telescope, the sextant, and the optical unit assembly, respectively. The scanning telescope is a unity-power, single line of sight, wide field-of-view instrument used for coarse target acquisition for the sextant, orbital tracking of the lunar module, landmark tracking, and general viewing. The sextant is a high magnification (28-power), dual line-of-sight instrument used for accurate angular measurements. Each instrument has two degrees of rotational freedom, around both the shaft and trunnion axes. Rotation about the shaft axis, which is fixed with respect to the spacecraft, defines a shaft angle ( $A_S$ ). Rotation about the trunnion axis, which is perpendicular to and rotates with the shaft axis, defines a trunnion angle ( $A_T$ ). Of the two sextant lines of sight, one is fixed parallel to the shaft axis, and the other is movable (articulating) and can be positioned with respect to the fixed line of sight by rotations of the shaft and trunnion axes. Figure 2-4 is a simplified optical schematic of the optical unit showing the optical axes and line-of-sight geometry.

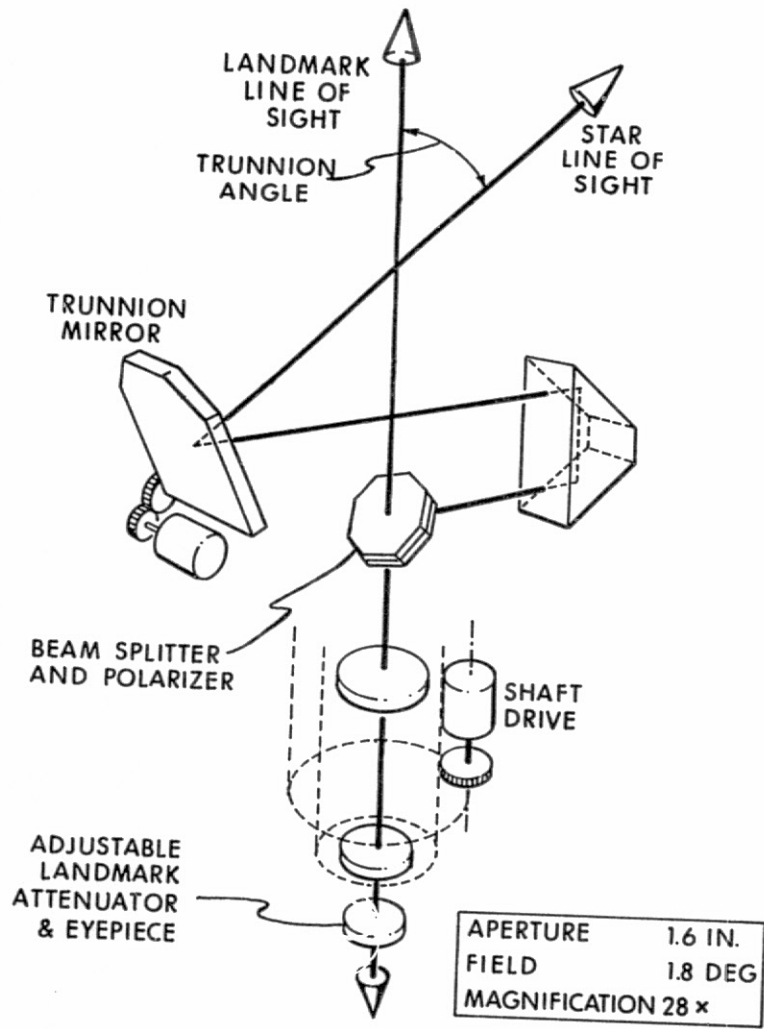


Fig. 2-1 Sextant Schematic

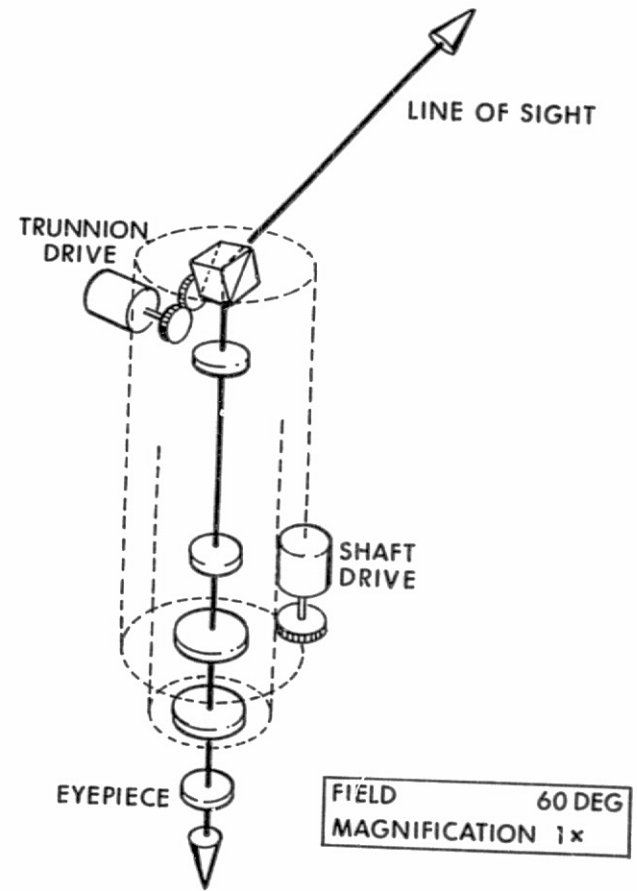


Fig. 2-2 Scanning Telescope Schematic

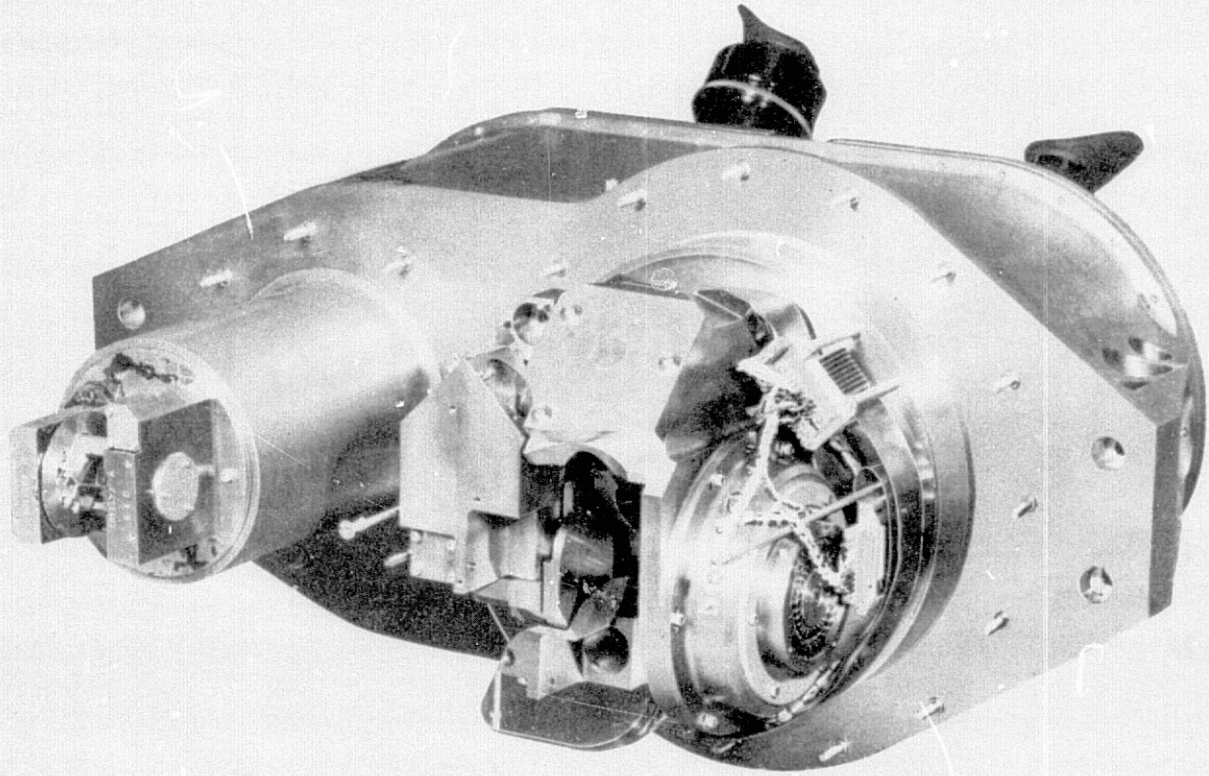


Fig. 2-3 Optical Unit Assembly

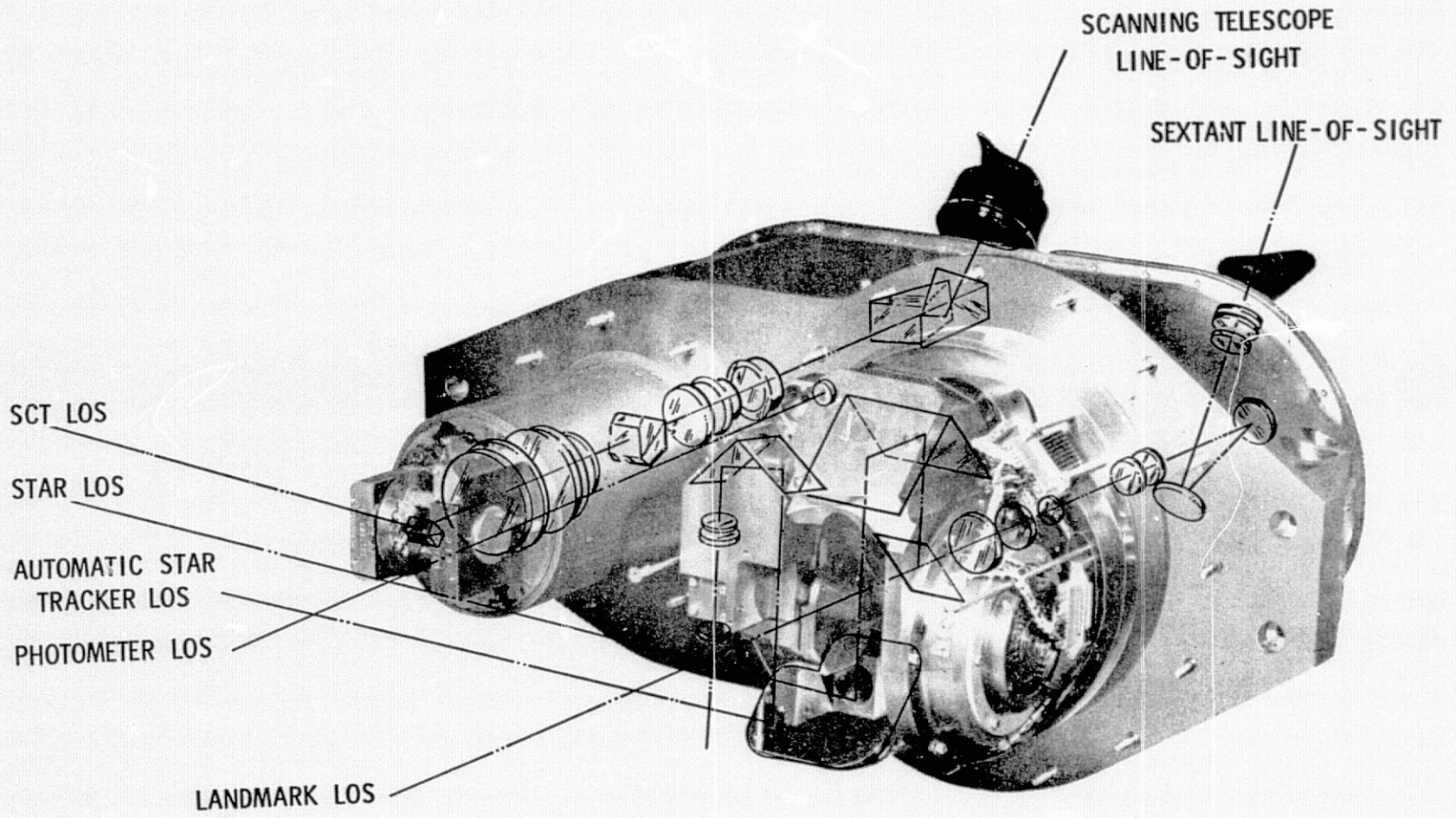


Fig. 2-4 Apollo Optical Unit

The optical subsystem allows the navigator to sight celestial and/or planetary reference objects in the field of view of the optical instruments, to position the reference objects in the field of view by means of the servo controls in order to make precision angular measurements, and to initiate a MARK command, causing the computer to record the angles via the coupling data unit. The optical unit is mounted on the navigation base to maintain the optics shaft axis in the required relationship to the coordinate frame of the inertial measurement unit. The servo controls are in the optics portion of the control panel, and the electronic circuitry associated with the optics is in the power and servo assembly. In case of electronic circuitry failure, the navigator can position the scanning telescope line of sight by means of manual drives, and read off the angles from telescope precision angle counters (TPAC), the drives and counters being available on the telescope panel. This backup function would enable inertial platform alignment of accuracy sufficient to accomplish safe return of the APOLLO spacecraft to earth. However, the backup function has been superseded by another manual optical device, the crew optical alignment sight (COAS).

Optical line-of-sight motion is about two right-hand orthogonal sets of axes. One set rotates with shaft rotation while the other set rotates with the trunnion rotation of both the sextant and telescope. The articulating, or star line of sight, angle is twice the trunnion axis rotation angle because of the doubling effect of the trunnion mirror in the sextant and the double-dove prism in the telescope. Figure 2-5 shows the optical subsystem axes for conditions of zero rotation, rotation of the shaft axis, and rotation of both trunnion and shaft axes.

The optical subsystem provides control of the direction of the star line of sight with respect to the landmark line of sight, which is fixed. The astronaut can select various modes of optics operation by positioning switches on the optics portion of the control panel. These modes are: Manual Direct, Manual Resolved, Zero Optics, and Computer Control.

The optical subsystem in the Manual mode positions the star line of sight according to command signals from the astronaut by way of the optics hand controller (H/C) and Speed Selector switch on the control panel. In the Direct mode, an up or down motion of the controller results in a positive or negative rotation of the optics trunnion drive axis (TDA), with a corresponding motion of the star line of sight in the trunnion direction. A right or left motion of the controller causes a positive or negative rotation of the optics shaft drive axis (SDA), with a corresponding rotation of the star line about the landmark line of sight. In other words, the Manual Direct mode commands result in direct rotations of the optics trunnion drive and shaft drive

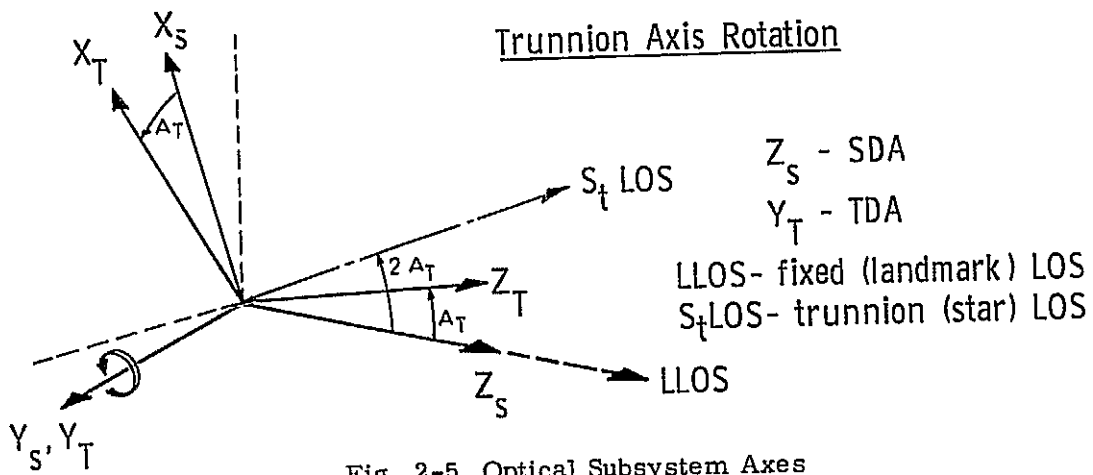
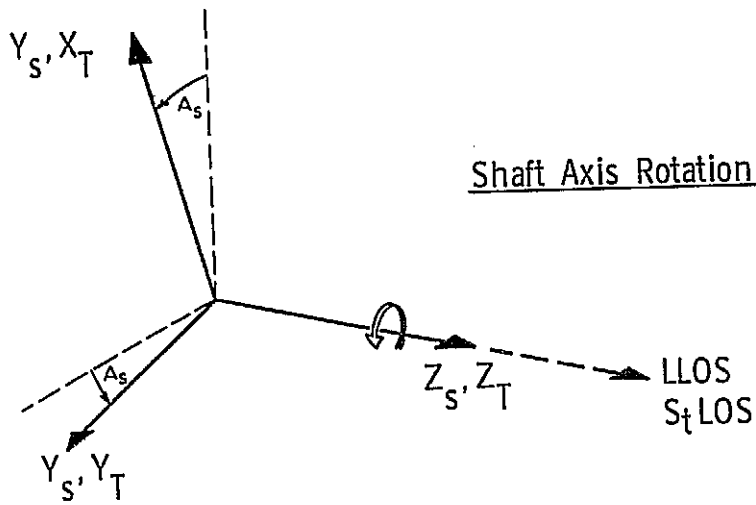
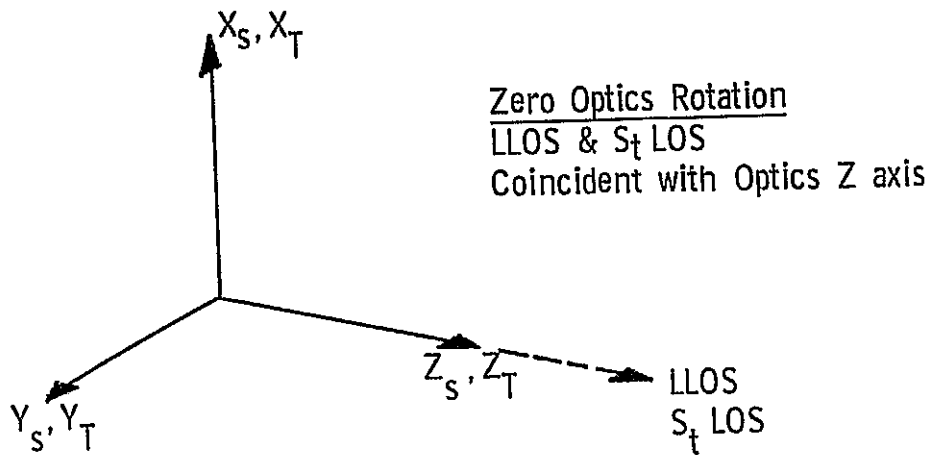


Fig. 2-5 Optical Subsystem Axes

axes. In the Manual Resolved mode, command signals from the controller are operated upon so that up, down, right, and left movements produce up, down, right, and left target movement, respectively, in the field of view, or target movement in the astronaut's X and Y coordinate system. In addition, apparent target rate is controlled so that it is directly proportional to the hand controller deflection. The Speed Selector switch enables three maximum rates of optics trunnion and shaft drive axes rotations for maximum deflection of the controller, depending upon the position of the Speed Selector switch: LO, MED, or HI. Manual mode operation is commanded by the astronaut when he sets the optics Mode switch to Manual, and the Submode switch to either Direct or Resolved.

The Zero Optics mode is initiated by the astronaut prior to making any optical sightings to assure synchronization between the optical line-of-sight angles and the computer's knowledge of these angles. The Zero Optics mode results in the closing of optical subsystem servo loops upon themselves to drive the optics trunnion and shaft drive axes of the optical instruments and the encoders to both mechanical and electrical zero. The Zero Optics mode is commanded when the astronaut sets the optics Mode switch to ZO.

The Computer mode enables automatic drive of the optics trunnion and shaft drive axes to the desired shaft and trunnion angles as calculated by an automatic optics routine. The computer drives the optics trunnion and shaft drive axes by generating a series of pulses fed to the optics digital-to-analog converter (DAC). Then the converter converts the pulse train to an analog electrical signal that drives the optics trunnion and shaft drive axes toward the desired angles. The pulse train is generated by bit differencing. Approximately every half-second the computer recycles until the bit difference or position error between the desired and actual optics trunnion and shaft drive axes position is zero. The astronaut selects the Computer mode by positioning the optics Mode switch to CMC. This automatic aid to the required alignment and navigational sightings has been used repeatedly in the manned APOLLO flights to date.

In addition to the four preceding primary mode configurations, three submodes for the telescope trunnion are available when the subsystem is in the Manual mode: SLOS, LLOS 0 degree, and Offset 25 degrees. When in the SLOS mode, the telescope line of sight is servo-configured to be parallel to the sextant star line of sight. When in the landmark line of sight 0 degree mode, the telescope line of sight is fixed parallel to the sextant landmark line of sight. When in the Offset 25 degree mode, the telescope line of sight is offset 25 degrees in trunnion, remains fixed at

this offset angle independently of sextant star line of sight trunnion, but is servo-configured so that the shaft drive rotations of both instruments are identical. This feature provides for the largest acquisition field for the scanning telescope.

Section 2.1.2 outlines the interface characteristics common to all the optical subsystem configurations (Block I-0, I-50, I-100, and II); the following sections describe the differences between them.

#### 2.1.1.1 Block I-0 Optical Subsystem

In the Block I-0 optical subsystem, the optical unit assembly is the Block 0 version, and the coupling data units are electromechanical assemblies. The servo configurations are such that all commands to position the optical lines of sight are generated by commanding the trunnion and shaft coupling data units to various positions. The positioning can be commanded in three ways: two by the astronaut, with the hand controller in the Manual mode or by selection of the Zero Optics mode; and the third through the D/A converters in the Computer mode. The servo loop mechanizations operate in a coarse/fine resolver system for the sextant and a coarse resolver system for the telescope. The servo loops send position information from the coupling data units to each instrument where the optics servomotors drive the optics lines of sight to the positions commanded.

Anticreep protection is provided by removing the reference voltage from the coupling data unit servomotors with microswitches in the hand controller that open at the null or zero-control voltage position. A sextant power switch was incorporated in this system for inhibiting the sextant servomotors by removing reference excitation voltage, thus allowing only the telescope to be exercised in a single speed follow-up servo configuration. NASA Dwg 1021036 gives a complete description of the optical subsystem, the optical unit assembly, and the various modes of operation.

The Block I-0 optical subsystem was conceived as a learner or prototype model. All subsystem components were to be designed, manufactured, tested, assembled, and finally tested and exercised at subsystem and system levels. Knowledge gained from these exercises would then be used as a basis for a final design suitable for manned lunar flights. Because of pressure for earlier flight schedules, it was decided to fly with a subsystem that would be available before the final design could be produced. The unit for this first manned flight was to be a Block I-0 with modifications, and was called Block I-50.

### 2.1.1.2 Block I-50 Optical Subsystem

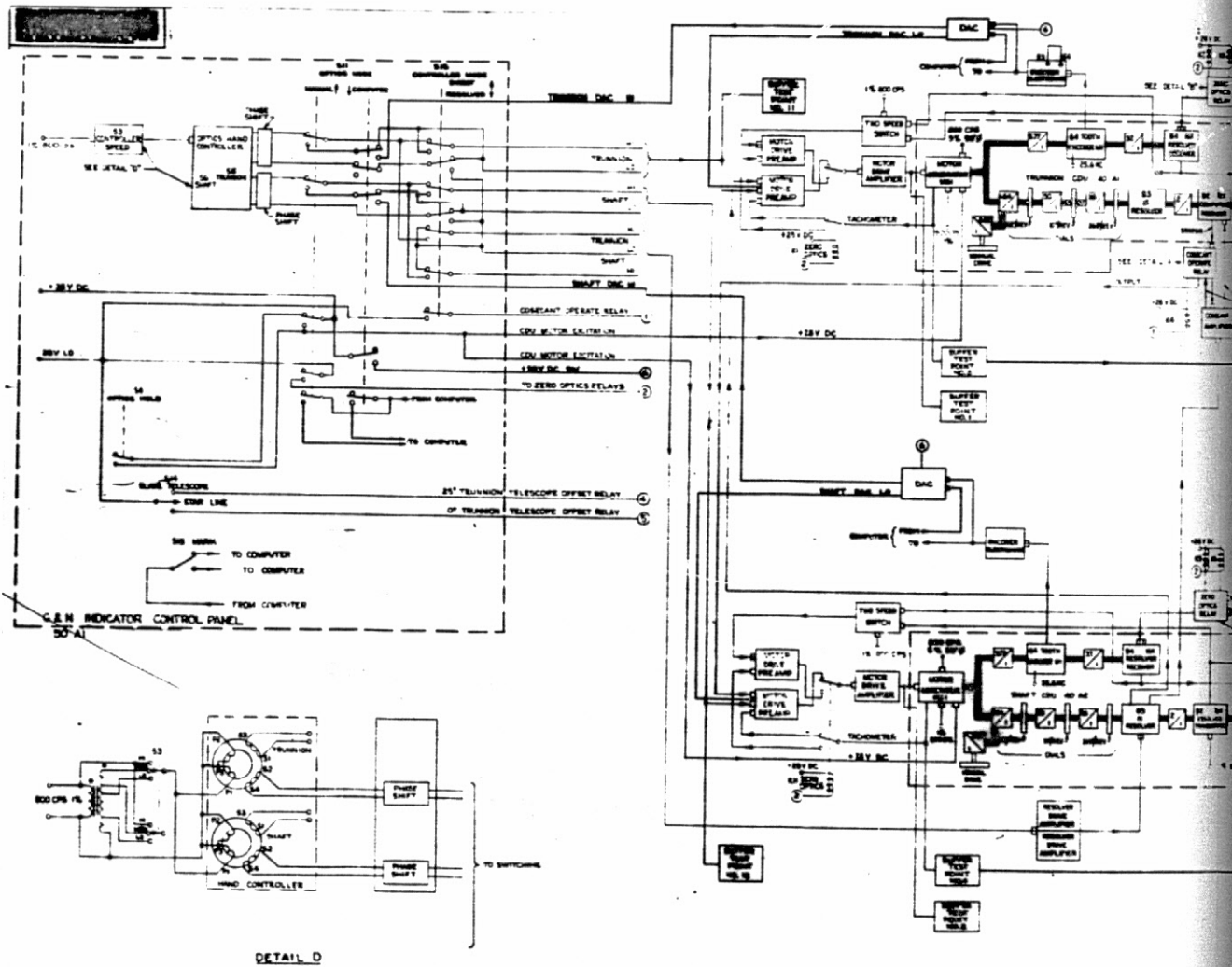
The Block I-50 optical subsystem was the same as the Block I-0 except for the following modifications incorporated to make the Block I-0 subsystem suitable for space flight: a single sextant reticle used in preflight testing was replaced by a dual reticle to compensate for shift in focus when moving from an atmospheric to a vacuum environment. Tachometer feed forward, from the shaft and trunnion coupling data units to the telescope shaft and trunnion motor drive amplifiers, was incorporated to reduce servo velocity error to an acceptable value during lunar module tracking; and finally, switching transients that fed erroneous angle data to the computer upon activation of the optics Mode switch were eliminated by changing hand controller anticreep switching from 800 Hz to direct current, and by hard-wiring the D/A converter output load to the optics 0-Vdc supply instead of switching via the optics Mode switch.

Figure 2-6, the functional diagram for the Block I-50 subsystem, gives the signal flows and the various components of the subsystem. E-1899, APOLLO Operations Handbook, Section 2.2, gives a complete description of the optical subsystem, optical unit assembly, and various modes of operation.

### 2.1.1.3 Block I-100 Optical Subsystem

In the Block I-100 subsystem, the optical unit assembly is the Block II version and the coupling data units are electromechanical assemblies. The servo configurations are such that all commands to position the optical lines of sight are generated through the signals to the sextant electronics and thus to its servomotors. The servo loop mechanizations operate in a coarse/fine resolver system for the coupling data units and a coarse resolver system for the telescope. With information sent from the sextant shaft and trunnion by the servo loops, the coupling data unit and the telescope servomotors drive the coupling data unit readouts and the line of sight to the position commanded by the sextant.

A major change in the Block I-100 design was the addition of a tracker-photometer to the Block II optical unit. The star tracker is an electro-optical device that, in conjunction with the associated electronics of the optical subsystem, maintains automatic star lock-on after the astronaut or the automatic optics routine acquires a star. With this lock-on capability, automatic inertial measurement unit realignment is possible. Error signals generated in the star tracker electronics control the sextant star line of sight by driving the trunnion and shaft servomotors (see Chapter III Candidate Subsystems).



DETAIL D

**FOLDOUT FRAME**

FOLDOUT

NOT FILMED

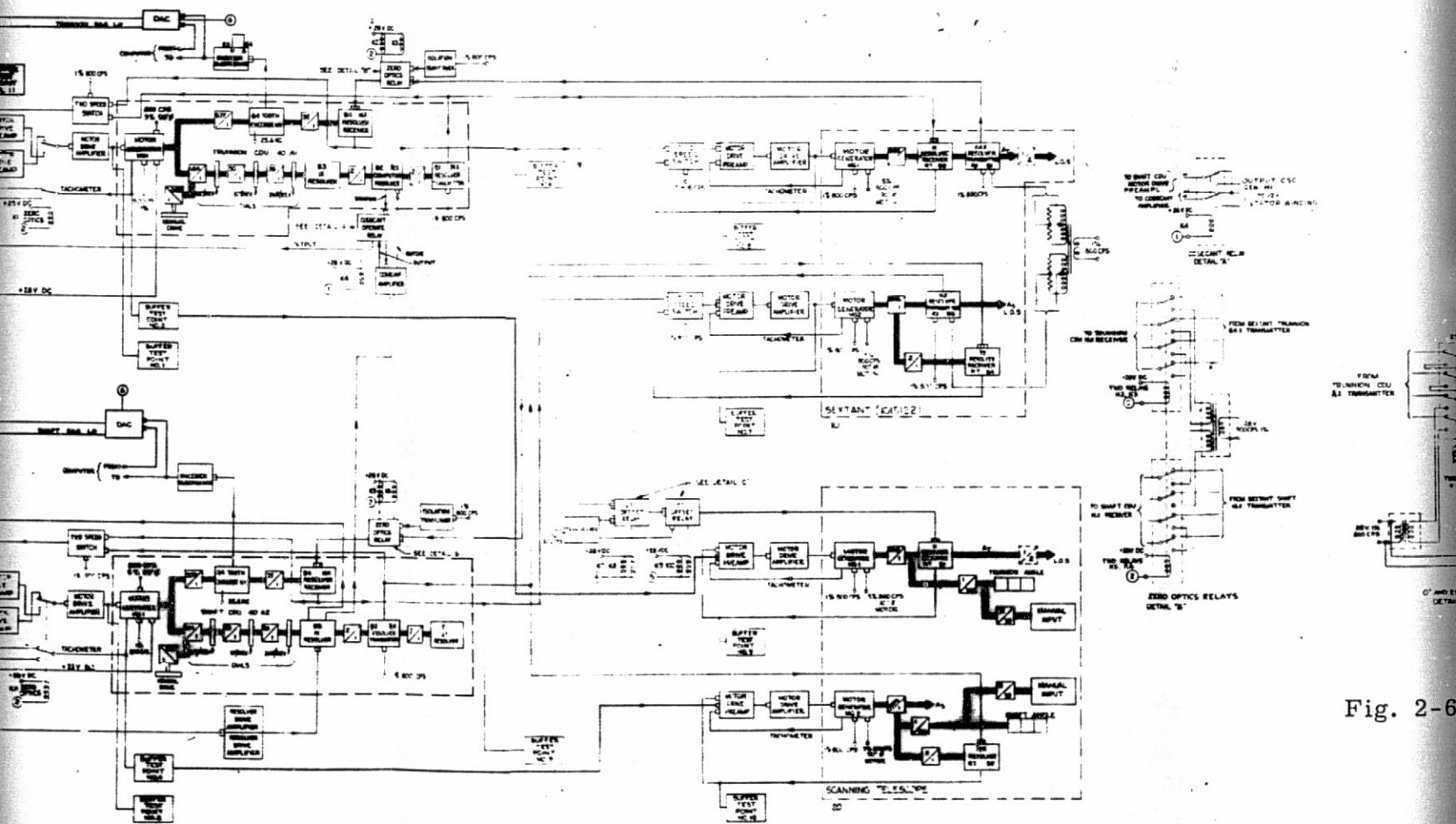


Fig. 2-6

FOLDOUT FRAME

2

PRECEDING PAGE BLANK NOT FILMED

FOLDOUT FRAME

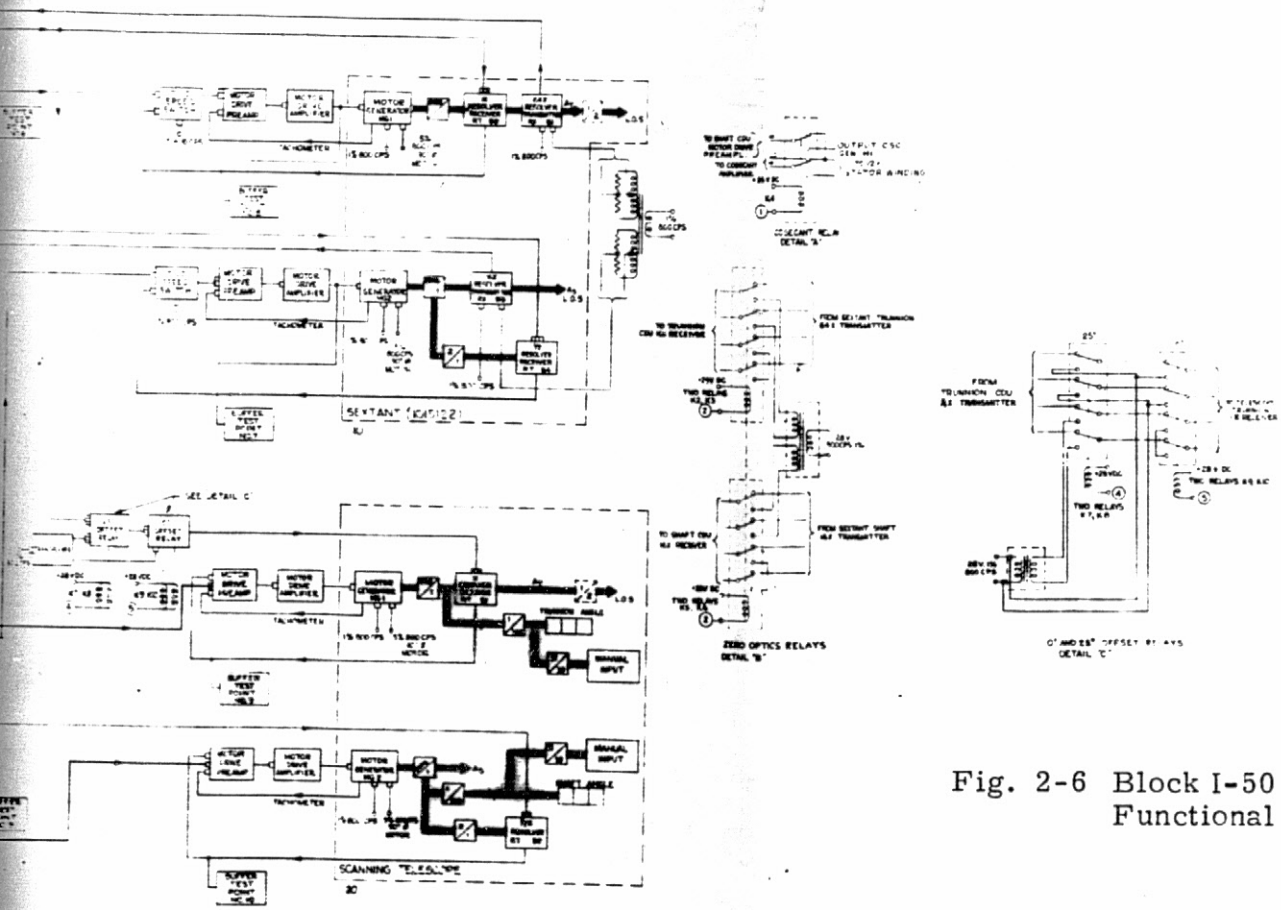


Fig. 2-6 Block I-50 OSS Functional Diagram

REVISIONS		APPROVED FOR		DATE	
NO.	DESCRIPTION	BY	DATE	BY	DATE
1	INITIAL DESIGN				
2	REVISION				
3	REVISION				
4	REVISION				
5	REVISION				
6	REVISION				
7	REVISION				
8	REVISION				
9	REVISION				
10	REVISION				

**FUNCTIONAL DIAGRAM OPTICAL SYSTEM**  
REF. GEN. 074012  
M. C. S.

2

PRECEDING

EOLDOUT FRAME 3

Designed in conjunction with the star tracker, the horizon photometer is an electro-optical device that senses horizon radiance. It locates a relatively fixed altitude above the earth, within plus or minus 1 kilometer, by sensing the altitude where the horizon radiance is 50 percent of peak value. To operate the photometer, the astronaut acquires a preselected star in the telescope (Acquisition mode) and switches the star tracker to ON, at which point the tracker drives the sextant trunnion and shaft to track the selected star. The astronaut then maneuvers the spacecraft so that the horizon line of sight scans the earth's horizon in a plane normal to the earth's horizon that contains the tracked star; the scan direction is from the earth to space. The photometer, sensing the horizon radiance, monitors and stores the maximum intensity, and issues an automatic MARK to the computer when the horizon radiance becomes 50 percent of the measured peak value. At the time of MARK, the computer records the angle between the star and the earth's horizon. This angle is a precision measurement used by the computer in deriving improved estimates of spacecraft state vector.

Figure 2-7, the functional diagram for the Block I-100 optical subsystem, gives the signal flows and the various components of the system.

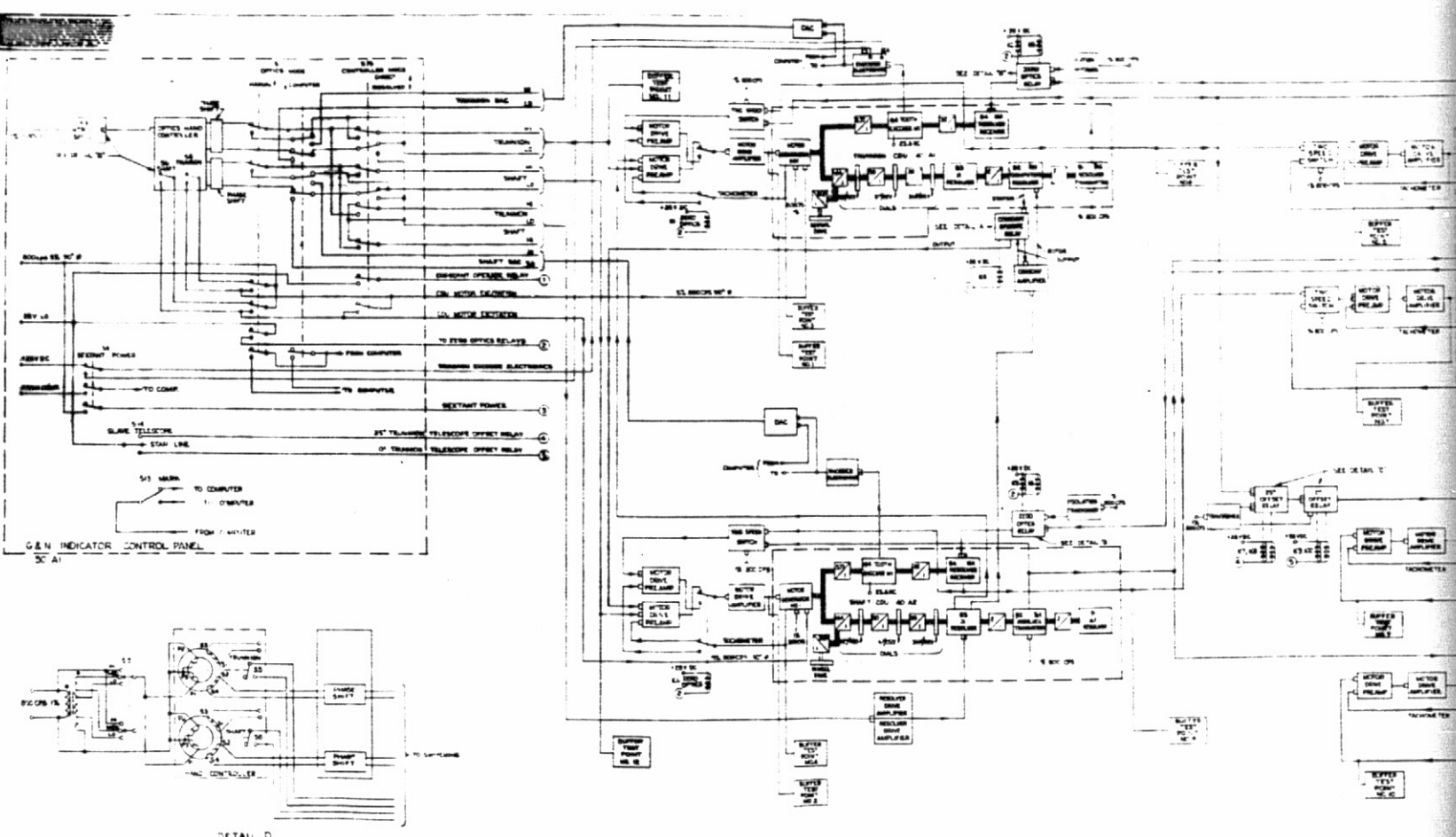
#### 2.1.1.4 Block II Optical Subsystem

The Block II optical subsystem design is the same as the Block I-100 except for the removal of the tracker-photometer optical and electronic components, and for the replacement of the electromechanical coupling data units by an electronic coupling data unit (ECDU). The tracker-photometer modules in the optical unit assembly were replaced by dummy modules. Wiring for these instruments currently remains in the power and servo assembly. Figure 2-8, the functional diagram for the Block II optical subsystem, gives the signal flows and various components of the subsystem.

#### 2.1.2 Interfaces

There are no operational interfaces of the optical subsystem which are external to the primary GN&C system except for direct visual sightings made by the astronaut with the optical instruments. Optical subsystem interfaces with the GN&C system are as follows:

1. The electronic coupling data unit in Block II enables optics angle data to be presented to the computer and optics position commands to be delivered to the optical subsystem.



FOLDOUT FRAME /



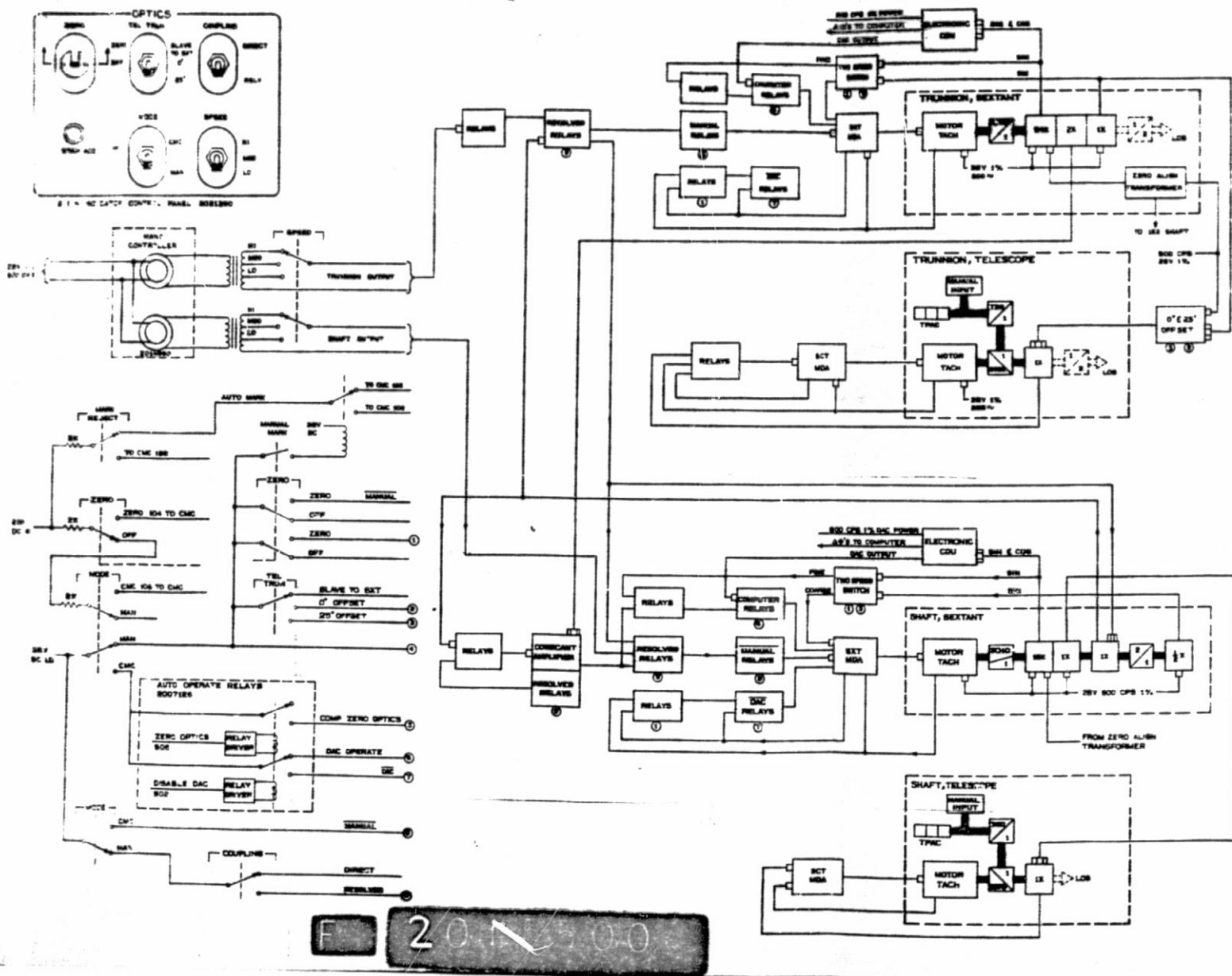
2. The coupling data units, in all optical subsystems other than Block II, in conjunction with the encoder and D/A converter electronics in the power and servo assembly, enable the optics angle data to be presented to the computer and optics position commands to be delivered to the optics from the computer.
3. The GN&C control power is the man-machine interface with which the astronaut selects and controls the various operating modes of the optical subsystem.
4. The navigation base provides the mounting surfaces for both the optical unit and the inertial measurement unit. The navigation base contains precision-machined mounting surfaces so that the plane of the inertial measurement unit mounting surface is precisely located with respect to the plane of the optics unit assembly mounting surface, and provides a rigid correspondence between the operational axes of the inertial measurement unit and the optical unit.
5. The power and servo assembly contains the optical subsystem electronic hardware.

### 2.1.3 Optical Unit Assembly Design Evaluation Program

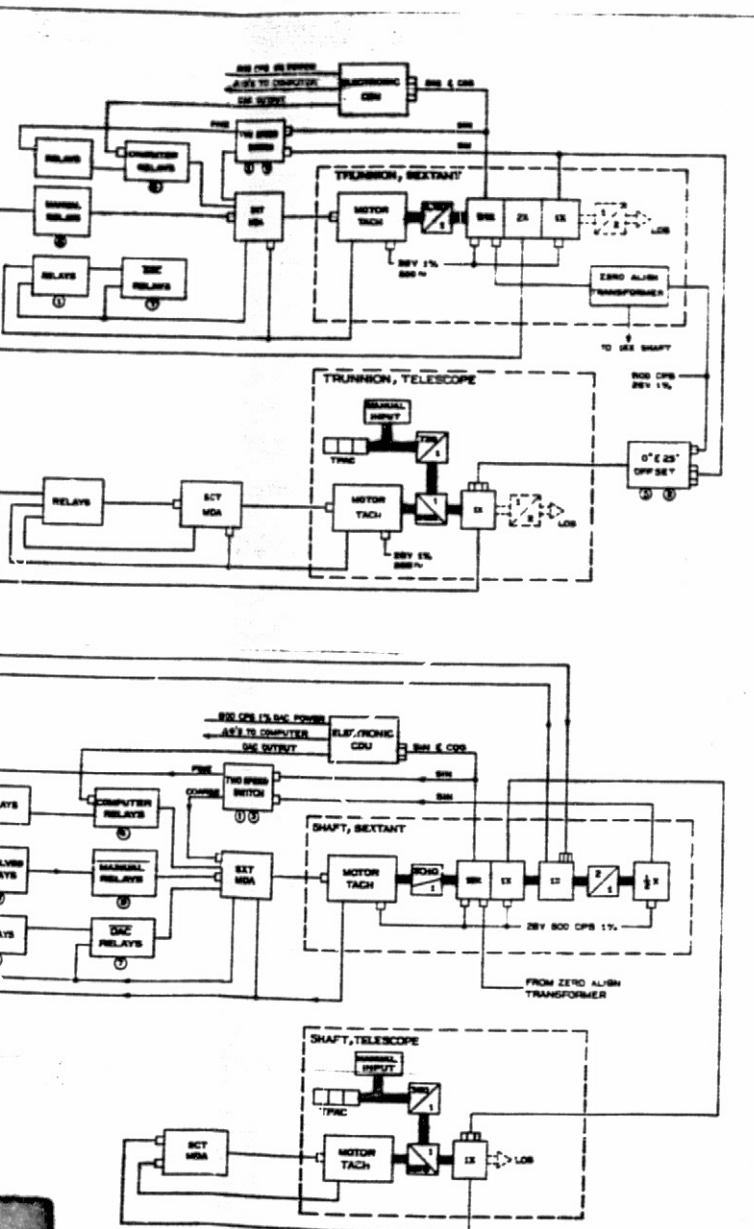
The design evaluation effort for the optical unit was divided into three main categories: thermal-vacuum tests, including humidity and salt spray; mechanical integrity tests, including vibration and shock; and servo tests to check stiction and rate characteristics. In the Block I test program, the tests on the optical unit were divided between Kollsman Instrument Corporation and MIT/IL. In Block II testing, all tests were performed at Kollsman under MIT/IL surveillance, except that special tests on the sextant head assembly were conducted at MIT/IL to evaluate the tracker-photometer design.

Problems that occurred during Block II testing and which did not appear in the earlier program (see E-1978 and E-2034 for detailed test program reports) are listed below:

1. Shifts occurred in the telescope objective lens assembly during vibration tests, evidently because the lens doublets were not completely seated as a result of a change in assembly techniques. The O-rings used to center the middle doublet and to seal the locking ring had created enough resistance to require iterations on torquing up the ring. The optimum technique suggested was to subject the components to vibration during assembly.



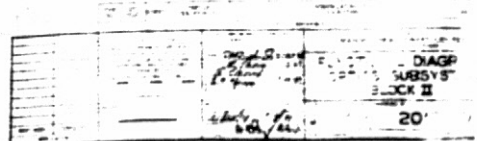
FOLDOUT FRAME I



TRUNNION LOS 0 (+0, -10) TO +90 (+10, -0) DEGREES  
 SHAFT LOS +270 (-0, +10) TO -270 (-10, +0) DEGREES  
 MAXIMUM TRUNNION LOS RATE = 10°/SEC  
 MAXIMUM SHAFT LOS RATE = 10°/SEC  
 TRUNNION LOS GRANULARITY = 10 SEC/BIT  
 SHAFT LOS GRANULARITY = 40 SEC/BIT

TEST POINTS:  
 MOTOR CONTROL WINDINGS (.4.7x)  
 TACHMETER MONITOR POINTS 50K  
 PREAMP MONITOR POINTS 51K

Fig. 2-8 Block II OSS Functional Diagram



FOLDOUT FRAME I

PREVIOUS PAGE BEHIND, NOT FILMED

2. Relay lens locking rings became loose, attributable to inadequate applications of Loctite compound. This problem also showed up in the design of the alignment optical telescope.
3. Shifts in the sextant index mirror were caused by debris underneath the mirror pads. To minimize this possibility, selectively fitted bushings were used in the mirror mount holes to prevent the mirror from moving around on the pads during vibration.
4. The entire sextant head was found susceptible to rotation within the limits of a diamond shaped locating pin, allowing shifts of 1 or 2 arcminutes. To solve this problem without removing the heads, right angle bars were epoxied at the head-base joint to prevent rotation. The Block II mechanical design evaluation unit was tested at MIT/IL to isolate the shift.
5. To prevent the tuning fork assembly interfaces in the tracker and photometer designs from shifting in vibration testing, it was found necessary to use dowel or taper pins at final assembly.
6. The most significant problem uncovered in thermal vacuum tests was the fact that, in the presence of a thermal gradient, the index mirror mount (sextant trunnion axis) would bow because it was unable to expand along its bearing axis. As a result, the index mirror changed in trunnion angle because of the arrangement of the mounting screws.

There were numerous other problems associated with materials selection and qualification (to be discussed in a separate section), but two further areas are discussed here: vacuum shift in the sextant and the radiation environment.

During early vacuum tests, a shift in sextant focus was discovered. The shift was attributed to the change in focal length of the T2-type objective from normal atmospheric pressure to vacuum. As a remedy, a double reticle was conceived with two reticle patterns: each produced on a face of a glass wafer, 0.023-inch thick and protected with two cover glasses. The air reticle pattern was deposited so that it would not be illuminated by the reticle lamps. The vacuum reticle pattern was engraved and filled. Without the introduction of the double reticle, the instrument would have demanded exhaustive testing in a vacuum chamber both at the factory and in the field, a very expensive requirement.

The radiation hazards in space are only beginning to be appreciated by the designers of manned spacecraft. It is only due to our uncertainty in the actual radiation levels present that no major changes in the APOLLO hardware were effected to provide guaranteed protection for the equipment and the astronauts. Specifications defined tolerable radiation levels for the instruments. Basically, such specifications cover

the effects of about two weeks of solar wind exposure (mainly low energy protons of 1-keV average energy), Van Allen belt radiation of short-term exposure (mainly medium-energy electrons and protons), and the occurrence of one major (1 percent) solar flare (mainly high-energy protons of about 30-MeV average energy). The main impact on the optical systems is that ordinary glass turns brown and becomes opaque at long exposures to radiation. Specially treated glass, such as Cerium, offers about 100 times more resistance to browning at a small percentage sacrifice of normal transmission, but for protection to be effective for more than three or four weeks in space, protective covers must be provided.

Tests were performed on a Block II index mirror and dove prism for solar wind exposures. No damage or changes were visible. Tests on samples were also made for gamma-ray exposures to determine the levels at which the glass turned brown. Additional tests with electron fluxes were performed by Langley Research Center in coordination with Bellcomm personnel. Since a simulation of the solar flare radiation (high-energy protons) was impracticable, extrapolation was necessary to determine the response of the APOLLO optics. MIT/IL concluded that, with the nominal specifications, the telescope dove prism and possibly the alignment optical telescope prism may experience about 25-percent loss in transmission near the end of a nominal lunar landing mission. Although no changes were made on the optics in response to the radiation problem, the narrow bandpass filter for the Block I-100 photometer was changed to a quartz substrate to improve its radiation resistance. No degradation attributable to radiation exposure has occurred on the APOLLO missions already flown.

## 2.2 PROBLEMS AND SOLUTIONS

### 2.2.1 Block I-0 Optical Subsystem

Major problems became apparent during testing of the Block I-0 optical subsystem. Several of these problems, namely servo velocity error in the telescope and optics mode-switching transients, have already been explained (Section 2.1.1.2). The other major problems included the following:

1. Telescope shaft and trunnion position errors. Accuracy tests of the telescope revealed conditions in the shaft and trunnion coupling data unit dial readouts and pulses to the computer which did not satisfy the specifications. The position errors were found to be caused by unbalanced loading of the coupling data unit resolvers (1/2x shaft and 1/4x trunnion) that resulted from the connection of the Zero Optics

two-speed switches to the resolver sine winding with no compensation across the cosine winding. The shaft position error was corrected by adding a compensation resistor in the resistor and capacitor module across the coupling data unit shaft 1/2x cosine windings. The trunnion position error would have been corrected in the same manner, but the new electronic components were never incorporated; a change in tray wiring of the power and servo assembly would have been necessary because no easily accessible location was available in which to place a compensating resistor.

2. Sextant shaft oscillation. Subsystem testing revealed two types of sextant shaft oscillation. The first type, induced in at least one subsystem tested when driving the sextant shaft at a low constant velocity, was due to the combination of gear train backlash, low-load coulomb friction, and the antibacklash spring. This oscillation was greatly reduced by tightening up the antibacklash spring and by increasing load coulomb friction through tighter engagement between the shaft drive gear and bull gear. The second type of oscillation was caused by nonlinearities in the shaft servo loop arising from saturation of the motor drive amplifier and the two-speed switch. This problem was eliminated by increasing the sextant shaft tachometer feedback and reducing the amplifier forward gain, thus increasing the minor loop damping while maintaining the  $A\beta$  at nearly the original value.

### 2.2.2 Block I-50 Optical Subsystem

The problems and solutions with the Block I-50 optical subsystem were similar to those that were corrected in the Block I-0 design and already explained in Section 2.1.1.2. An additional problem, which could have caused complete failure of the subsystem (both Block I-0 and I-50) had the subsystem been used for extended operation in a manned flight, was with the sextant and telescope servo drive motors. If the optics were operated in a space environment, the motor rotors would overheat, expand, and tend to bind. Also, the high temperature affected the tachometer characteristic and tended to change the servo loop performance. The Block I-100 subsystem was designed with improved (Block II) servo drive motors as well as improved star tracker-horizon photometer circuitry. The new motors also had higher torque outputs and better temperature operating characteristics that improved servo performance of the Block I-100 and II optical subsystems.

### 2.2.3 Block I-100 Design

As noted previously, one of the major changes in the Block I-100 design was the servo configuration whereby the coupling data units and the telescope followed the

sextant. The Block I-0 unit had an insufficient torque-to-inertia ratio and would have been unable to follow the sextant position at its highest drive rates. Thus, a Block I-100 optics coupling data unit design was required to have increased accelerating and synchronizing capabilities in order to follow the motions of the sextant. To achieve this, the Block I-0 units were modified by replacing the servo drive motors with the Block II optical unit motors and removing the flywheel, thus creating Block I-100 optics coupling data units. The Block I-100 motor drive amplifiers were thus designed to optimize the servo performance of all elements of the subsystem, and changes were made to Block I-0 and I-50 electronics (resolver-drive amplifier, cosecant amplifier, and two-speed switch) for noise suppression and more linear operation. These changes did not result from flight problems but were effected to optimize the design based upon deficiencies noted in the previous subsystems tested. No optics problems were encountered during testing of the Block I-100 configurations, though several out-of-specification conditions occurred that were caused by anomalies existing at the component level. These are fully described in AC Electronics Division document XDE34-T-55. Schedule and cost difficulties combined to cause removal of the star tracker and horizon photometer prior to design evaluation testing.

#### 2.2.4 Block II Design

Several problems became apparent during testing of the first few Block II optical subsystems, all involving image motion in the sextant field of view under conditions when no motion should have occurred. The problems were the result of the attempt to control image motions in the subsystem at low-level slew rates and at standstill. Specifically, the problems were the following:

1. Image creep due to hand controller and motor-tachometer voltage. The Block II subsystem was mechanized with anticreep protection to prevent undesirable random image motion due to controller and motor-tachometer residual voltages present when the controller is returned to mechanical null. The anticreep protection was obtained by controlling the B+ voltage to the sextant drive amplifiers, using the controller output voltage to regulate the anticreep electronics, which in turn applied or removed the B+ to or from the amplifiers. The anticreep electronics contained a time delay of approximately 0.3 sec that maintained the B+ voltage to the amplifiers after removal of the hand controller signal, and thus allowed tachometer feedback to stop any sextant line-of-sight motion after the controller was returned to its neutral or null position. With the B+ voltage removed from the amplifiers, the sextant servo loops

were deenergized and, theoretically, the unwanted image motions would have been inhibited. However, with the system in a deenergized state, unwanted image motion was found to occur because of insidious torques, mechanical imbalances, and electrical anomalies.

2. Image hop. Upon reapplication of B+ voltage to the sextant motor drive amplifiers, an electrical transient resulted in a jump motion of the sextant lines of sight. This problem was eliminated by rewiring so that only the power output stage of the amplifiers had the B+ voltage controlled; the remainder had a constant B+ supply.
3. Shaft residual image motion; trunnion drag and motor reverse drive by antibacklash spring. After opening of the shaft servo loop by the anticreep circuit, an image motion caused by a sextant shaft rotation was noted. This was caused by torque supplied by the flex-print wiring of the sextant. Investigation of this problem revealed a hesitation of the image motion (trunnion drag) for low rate constant trunnion commands. This was caused by torque supplied by the trunnion resolver lead wires overcoming the trunnion dead zone takeup spring torque. No easy solution was available for the shaft residual image motion, but the trunnion drag could be removed by increasing the dead zone takeup spring torque. Increasing this spring torque could, however, cause the spring to drive the trunnion when the anticreep circuitry opened the trunnion servo loop.
4. Image creep resulting from motor single phasing and from motor drive amplifier feedthrough. These problems were both encountered on the sextant trunnion. With the anticreep circuitry opening the trunnion servo loop and the very low friction of the trunnion gear train, trunnion motion could occur because of the motor control winding source impedance (single phasing) and/or residual voltages present in the motor drive amplifier (feedthrough).

All the above problems, except for trunnion drag, were associated with the anticreep protection, while the trunnion drag could be corrected if there were no anticreep protection. The final solution was to remove the anticreep electronics from the power servo and to increase the trunnion dead zone spring torque. Image motions due to the hand controller and tachometer residual voltages are present in the Block II design, but have been found to be within acceptable limits for the various subsystems which were produced.

### 2.3 FLIGHT EXPERIENCE, COMMAND MODULE

Of the optical units flown on the first 11 APOLLO flights, only one experienced mechanical failure. During the APOLLO 9 mission, a pin in the telescope shaft

angle counter became loosened, floated around inside the optical unit base, and finally lodged itself between the elements of the shaft resolver split gear. The telescope was thus made unusable for nominal landmark-tracking. Because the operation of the sextant was unaffected, mission success and safety were not compromised.

All inertial measurement unit alignments and realignments attempted with the optical subsystems on all manned APOLLO flights have been successfully completed. Typically, the sighting measurement error, defined as the difference between the known angular separation between the two stars sighted versus the measured separation, was 0.012 degree, or less. Flight experience to date, in using the optics for navigational sightings, is summarized in Section 6 of this report.

## 2.4 ERROR ANALYSIS

In the Block II GN&C system, the optical subsystem interfaces with the computer through the electronic coupling data unit. In operation, the computer reads the positions of the telescope and sextant optical lines of sight by summing the pulses received from the two optics channels of the coupling data unit. The data unit generates pulses, the granularity being approximately equal to 10 arcseconds for the trunnion angle and 40 arcseconds for the shaft angle. Since these pulses are the main interface between the optics and the computer, this section shows the static accuracy of all the optical subsystems tested. The raw data used in the accuracy calibrations can be found in AC Electronics APOLLO Engineering Memorandum AP-M 12001 (Revision G), OSS Test Results for Block II Systems.

Fourteen separate optical subsystems were tested. The following are the average static accuracy results, expressed as one-sigma values:

- |                              |                  |
|------------------------------|------------------|
| 1. Sextant trunnion angle:   | 12.9 arcseconds  |
| 2. Telescope trunnion angle: | 162 arcseconds   |
| 3. Sextant shaft angle:      | 28.4 arcseconds  |
| 4. Telescope shaft angle:    | 116.4 arcseconds |

## 2.5 DESIGN CRITIQUE OF THE BLOCK II OPTICAL SUBSYSTEM

The following critique constitutes a number of conclusions and recommendations as a result of operational analysis of the Block II optical subsystem configuration.

## 1. Automatic Sensors

During the return from the moon, it is difficult to find suitable earth landmarks for visual sightings. The earth's horizon provides a suitable navigation reference. The horizon-photometer permits an accurate determination of the horizon reference attitude, which is several times better than can be done manually. The photometer would also permit onboard earth reference during unmanned flights.

The star tracker would be a considerable aid to the astronaut during navigation measurements. During unmanned flights it would permit automatic onboard navigation and automatic inertial measurement unit realignment.

## 2. Optics Control System Design

Residual torques in optical unit components (flex-print, resolver leads, etc) caused subsystem problems by moving the lines of sight when no input commands have been applied to the servos. An increase in friction load of the sextant gear trains should eliminate this kind of problem.

Error sensing feed forward from the sextant to telescope would minimize acceleration errors during high rate tracking tasks with the telescope.

## 3. Optical Design

A factor-of-three improvement in the telescope resolution can be realized by optimal optical design. The present design fulfills APOLLO requirements, but the resolution improvement would also improve light transmission and light scatter characteristics.

## 4. Mechanical Design

An optics protective door would improve optical subsystem performance, reliability, and durability. The door should be designed as an integral part of the subsystem to maximize its performance in conjunction with the optics.

More extensive purging and sealing of optics subsystems are desirable. Greater care is required to reduce the problem of dust accumulation along the optical paths.

The general utility of the optics as a navigation tool is somewhat limited by scattered light and reduced field of view. The optics baffling and spacecraft structure should be redesigned with more emphasis on visibility requirements.

SECTION 3.0  
LUNAR MODULE OPTICS, ALIGNMENT OPTICAL TELESCOPE

3.1 DESIGN REQUIREMENTS AND FUNCTIONAL DESCRIPTION

3.1.1 Requirements

The alignment optical telescope originated from the need for a method of aligning the inertial measurement unit onboard the lunar module. Since navigational tasks were assigned primarily to the radar systems, the sole task of the telescope was to make star sightings accurate to about 1 mrad. Because of its single important function, the simplest practicable design was implemented; i.e., having no electronic components or interfaces, except for reticle illumination.

Astronauts on the lunar surface must be able to identify stars for inertial measurement unit alignment or realignment. The optical telescope therefore requires a large field of view (60 degrees) for pattern recognition with high transmission. Another requirement, protection from the adverse scattered light environment, was not achieved until late in the program because of changes in both hardware and concepts of star identifiability. Since the axis of the telescope had to be located vertically, a periscopic design was adopted. Optical and mechanical schematics are presented in Figures 3-1 and 3-2.

MIT/IL checked and verified the optical performance of the alignment optical telescope. (The optics were designed by Kollsman Instrument Corporation.) The telescope is of unity magnification and, with high efficiency antireflection coatings, achieves about 60-percent luminous transmission. The design includes the use of an aspherical first lens (fourth-order correction) for control of pupil location. A spiral reticle pattern provides readout capability; both the rotational and radial position of a target can be determined by one degree of freedom (i.e., reticle rotation). An angle counter, located on the reticle drive shaft, provides mechanical readout readable to 0.01 degree. For in-flight inertial measurement unit realignments, stars cross the rectilinear pattern of the reticle as a result of spacecraft motion. (Figure 3-3a and b depicts the principles of measurement.)

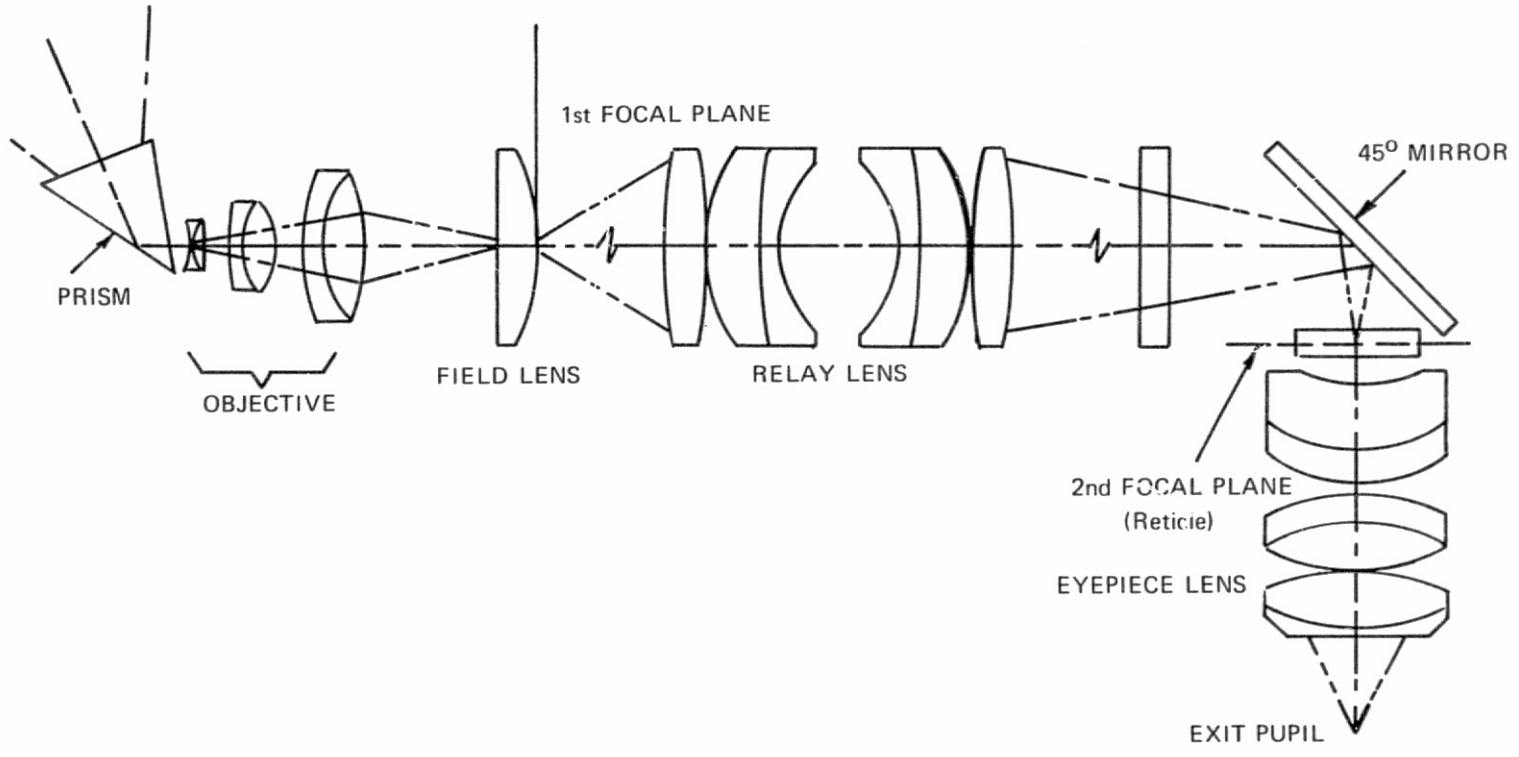


Fig. 3-1 Alignment Optical Telescope Optical Schematic

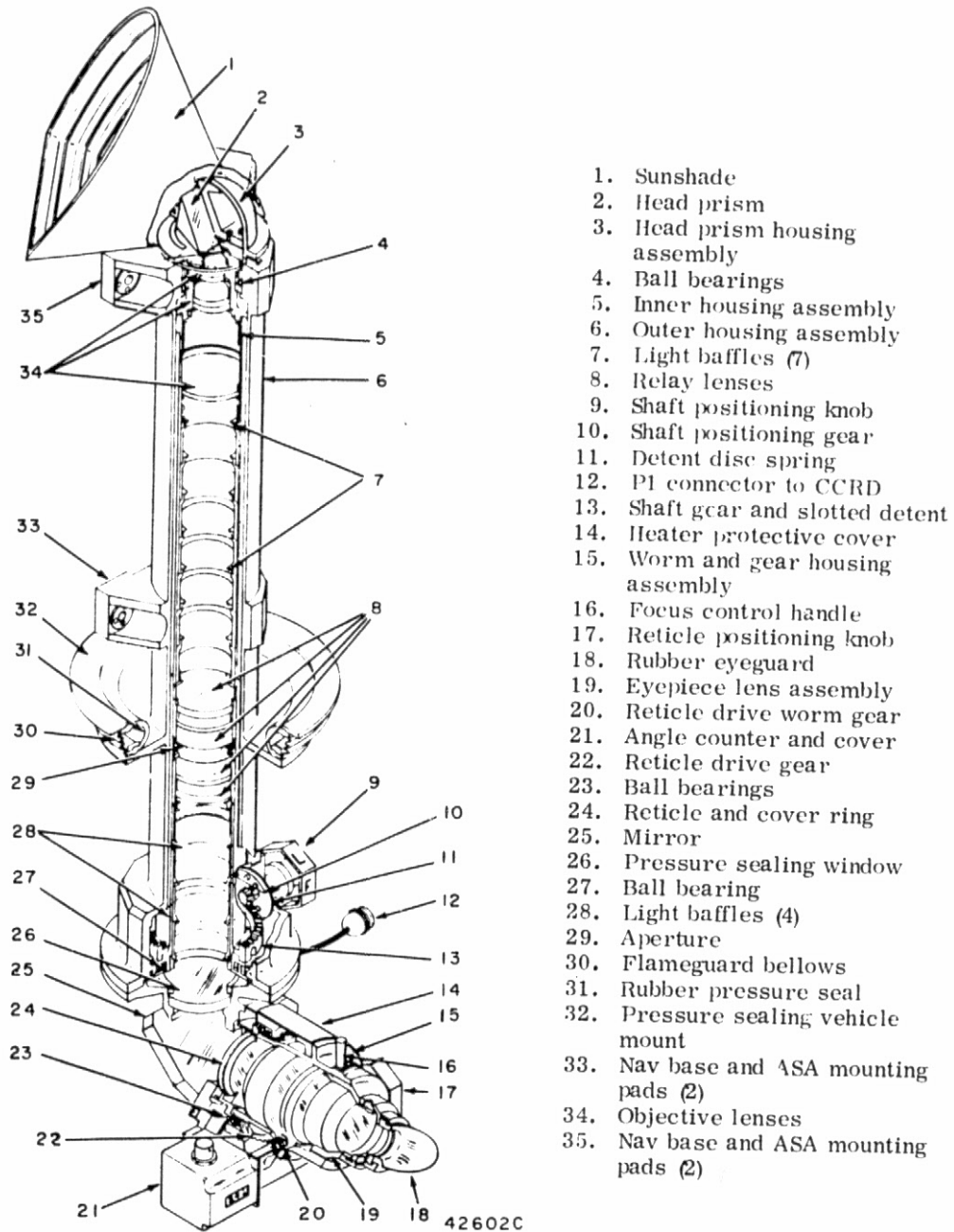


Fig. 3-2 AOT Cutaway View

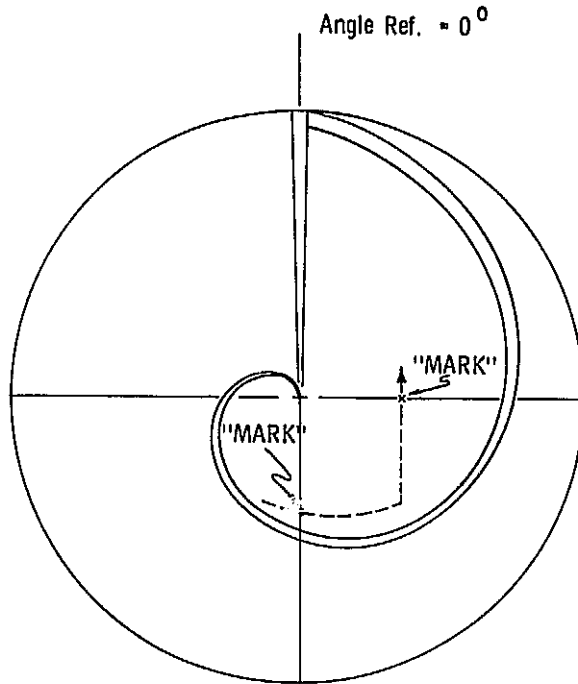


Fig. 3-3a Depicts the Principles of Measurement

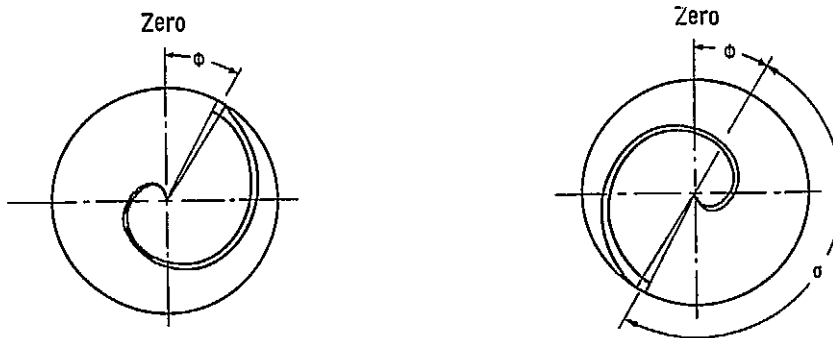
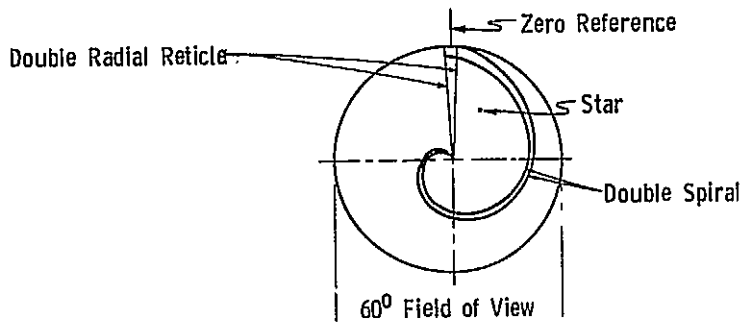


Fig. 3-3b Depicts the Principles of Measurement

### 3.1.2 Functional Description

As may be visualized in Figure 3-3a, the lunar-surface, star-position measurement technique utilizes a polar coordinate system, where the radial angle is obtained by use of a double Archimedean spiral.

Superimposition of the star and the double radial reticle provides a direct shaft angle measurement ( $\phi$  in the figure) when the angle counter geared to the reticle rotation is read. Subsequent rotation of the reticle to superimpose a star between the double spiral yields an angle difference ( $\sigma$ ) analogous to trunnion angle simply by:

$$\text{trunnion} = \frac{360 - (\theta - \phi)}{12}$$

where:  $\phi$  = rotation to radial reticle

$\theta$  = the total rotation to spiral crossing

$$\frac{30}{360} = 1/12 = \text{proportionality constant; i. e., spiral tracks from zero trunnion to 30-degree field rotation in 360-degree counter rotation}$$

The onboard computer determines unambiguous star position in the field of view, relative to the center, by use of the above equation, the angles inserted by the astronaut, and by a time mark through a pushbutton command. (Since the moon rotates in inertial space, and since the two angle measurements are not simultaneous, and because the two star sightings needed for realignment are not simultaneous, care is taken to optimize the sighting mark schedule.)

The azimuth and elevation angles of the center of the telescope field, referred to the navigation base coordinate frame, are stored in the computer. Therefore, each star position in a two-star sighting sequence is known and the present-versus-desired stable member orientation can be determined for inertial measurement unit alignment or realignment.

There are six viewing detents that provide for rotation of the field about the longitudinal axis of the telescope to known sighting positions referred to the navigation base coordinates. The locus of the line described by the center of the field in this rotation is a line of constant latitude nominally inclined 45 degrees to the Y-Z plane of the navigation base and lunar module spacecraft. Measured in this plane, the viewing positions are separated by 60 degrees. In the forward detent the center of the telescope field lies nominally in the X-Z plane of the craft.

The forward detect position is normally used for inflight sightings. An automatic spacecraft maneuver places the selected target star near the center of the field. Thereafter, minimum-impulse attitude commands by a hand controller cause the target to apparently cross the X-X (horizontal) and Y-Y (vertical) reticle lines. The X-Y mark pairs (recorded inertial measurement unit gimbal angles) provide a pointing vector in the basic inertial reference frame; multiple mark pairs provide the required accuracy for each vector and two-star sighting sequences permit inertial measurement unit realignment. After the stable member realignment, an automatic spacecraft maneuver to point the telescope reticle center at a third star yields assurance, if need be, that the realignment was not erroneous.

### 3.2 PROBLEMS AND SOLUTIONS

During the course of the alignment optical telescope design evaluation program, several important problems were revealed. The most significant follow:

1. Because the second focal plane of the telescope was to be used for off-axis measurements, all optical elements in advance of the reticle had to be stabilized against cross-axis mechanical shifts of a few ten-thousandths of an inch. Ultimately, the only means of accomplishing this stabilization involved epoxying all lens elements in their respective housings and taper-pinning all mechanical interfaces. A detailed discussion of the extensive evaluation associated with this problem can be found in reports E-1978 and E-2034.
2. The shift of focus at the second focal plane from air to vacuum conditions amounted to 0.025 inch (0.4 diopter), an amount sufficient to introduce significant parallax errors. To solve this problem, the alignment optical telescope had to be focused and aligned under simulated vacuum conditions. Because provisions for evacuating the inner tube of the telescope were not readily available at the APOLLO field sites, special techniques had to be established for testing purposes. If the telescope were subjected to excessive stress before flight deployment, it would require return to the manufacturer to be checked for all possible deviations from specification.
3. Another major source of parallax-related error occurs because the focal surface is curved, while the reticle is flat. Because star images are not coincident everywhere with the sharpest reticle image, movement of the eye across the exit pupil creates a relative motion between star and reticle. To minimize this effect, the focus was designed to be optimum halfway out in the field, and sightings within 5 degrees of the edge of the field of view were not recommended.

4. To provide better coverage of the celestial sphere, the telescope has six detented viewing positions about the axis of the tube. At first, only the three forward positions were to be used (the three rear positions were obstructed by a protective cap); thus, accurate coordinates for the centers of only the forward fields of view were determined by optical measurement on a precision fixture. The test fixtures lacked the ability of testing the rear detent positions, since this was not an original design requirement. With the replacement of the protective cap by a scattered light shield, the rear positions could be of use; a mathematical technique was devised to calculate the rear detent coordinates on the basis of the three forward positions.
5. At about the midpoint of the telescope production schedule, a serious scattered light problem was revealed in tests simulating the operation of the instrument on the lunar surface in sunlight. The rendezvous radar gyro package assembly in front of the telescope had been painted white, thereby increasing to intolerable levels the amount of stray light hitting the telescope head prism. Also, NASA/MSO engineers and astronauts had established a threshold visibility requirement ensuring perception of fourth-magnitude stars, a magnitude fainter than MIT/IL's criterion. To correct these problems, a conical sun shade was designed and implemented to provide the required shielding from sunlight.

### 3.3 FLIGHT EXPERIENCE, LUNAR MODULE (AOT)

Although no explicit mechanical failure has been revealed in the flight operation of the telescope, the extrapolated accuracies of inertial measurement unit realignments placed some doubts upon the performance characteristics of the telescope prior to the APOLLO 12 mission. Since most of the error budget is attributed to observer (parallax) error, additional experience with observational techniques was needed to reduce inflight errors. The outstanding pinpoint landing of APOLLO 12—prepared for by a very accurate inflight realignment preparatory to the thrusting maneuvers—indicated that the instrument could be used to the limit of its intended design accuracy. Moreover, post-flight analyses of inertial measurement unit realignment data made on the lunar surface with the telescope were within the specified accuracy limits (ref. MIT/IL 235 memo 70-15, 3 March 1970).

### 3.4 ERROR ANALYSIS

A detailed RMS analysis of alignment optical telescope-inertial measurement unit alignment accuracies was performed to ascertain the degree to which the guidance

and navigation system satisfied specifications. Error sources were separated into two groups: alignment (fixed) errors and random (variable) errors. Because of relatively large parallax (random) errors, especially in lunar surface realignments, it is beneficial to require multiple readings on stars. In fact, in the case of lunar surface realignments, two or more sets of readings are required to satisfy the specification (2 mrad, 3 sigma per inertial measurement unit axis). Tables 3-I and 3-II demonstrate the effects of multiple readings.

### 3.5 CRITIQUE

The sole significant area critical to the design of the alignment optical telescope was the requirement for accurate off-axis measurement. In the future, if a wide-angle telescope is employed for angle measurement, it should have two degrees of freedom, allowing marks to be made in the center of the field of view.

TABLE 3-I  
INFLIGHT ALIGNMENT ERRORS

INFLIGHT ALIGNMENT ERRORS  $1\sigma$

<u>OVERALL 3d IMU ALIGNMENT ERROR</u>	<u>ERROR PER AXIS</u>	<u>NO. OF SIGHTINGS PER STAR</u>
153 sec	89 sec	1
114 sec	66 sec	3
108 sec	62 sec	4
99 sec	57 sec	7

$3\sigma$  (per axis) = 1.3 mils for  $n = 1$ ; 1 mil for  $n = 3$ .

<u>OVERALL 3d ERROR TRANSMITTED TO AGS</u>	<u>ERROR PER AXIS</u>	<u>NO. OF SIGHTINGS PER STAR</u>
161 sec	93 sec	1
125 sec	72 sec	3
119 sec	69 sec	4
111 sec	64 sec	7

$3\sigma$  (per axis) = 1.4 mils for  $n = 1$ ; 1.1 mils for  $n = 3$ .

TABLE 3-II  
LUNAR SURFACE ALIGNMENT ERRORS

LUNAR SURFACE ALIGNMENT ERRORS  $1\sigma$

<u>OVERALL 3d IMU ALIGNMENT ERROR</u>	<u>ERROR PER AXIS</u>	<u>NO. OF SIGHTINGS PER STAR (n)</u>
258 sec	150 sec	1
167 sec	97 sec	3
152 sec	88 sec	4
130 sec	75 sec	7

$3\sigma$  (per axis) = 2.2 mils for  $n = 1$ ; 1.4 mils for  $n = 3$ .

<u>OVERALL 3d ERROR TRANSMITTED TO AGS</u>	<u>ERROR PER AXIS</u>	<u>NO. OF SIGHTINGS PER STAR (n)</u>
263 sec	152 sec	1
175 sec	100	3
160 sec	93 sec	4
140 sec	81 sec	7

$3\sigma$  (per axis) = 2.3 mils for  $n = 1$ ; 1.5 mils for  $n = 3$ .

PRECEDING PAGE BLANK NOT FILMED

## SECTION 4.0 VISIBILITY STUDIES

### 4.1 INTRODUCTION

The chief optical problem in space navigation is to be able to see and/or track a star of magnitude +3 or +4 in the presence of another star (the sun) some 30 magnitudes brighter. In more familiar units, 30 stellar magnitudes is 120 decibels on an energy scale; an acoustical engineer would recognize immediately the impossibility of hearing a faint sound near the threshold of audibility in the presence of a sound so loud as to cause pain. Fortunately, the length of light waves is so much shorter than the length of sound waves that the focused image of a star formed by a properly designed optical system tends to be isolated from its surroundings. Partly for the same reason, optical baffles are more effective than acoustical baffles. Even so, there is always a residuum of scattered light in the field of view and MIT/IL has from the outset been keenly aware of the deleterious effect of stray radiations.

In the design of optical systems, rays of light from a single point source are traced through the system, whose elements are modified until the resulting image resembles a point whose minimum size is set by diffraction. The effect of scattered light is ignored during design procedures. This is expedient because as soon as the system has been fabricated, it is a relatively simple exercise to evaluate its performance in the presence of extraneous sources.

The assumption that the sun is the only source of stray radiations was an oversimplification, because a spacecraft near the earth or moon can receive almost as much unwanted luminous power from either of these celestial bodies as from the sun itself. (Intrinsically, the luminance of the sun is enormously greater than the luminance of either planet; but the solid angle subtended by the sun can be a tiny fraction of the solid angle subtended by the earth or the moon.) Indeed, the spacecraft itself must be regarded as an additional celestial body, and any sunlit area thereof is suspect in proportion to the solid angle that that area subtends at the window of an onboard instrument.

The structure of the spacecraft itself has been modified from time to time, and these modifications can potentially restrict the capability of the three principal optical

devices (scanning telescope, sextant, and optical telescope), even when the modified structure lies outside the actual field of view of the instrument.

## 4.2 TESTS AND RESULTS

This section summarizes the tests and results that have direct bearing on the visibility through the current configuration of the APOLLO optical subsystems. The information can be classified in the following categories:

1. Thresholds in the absence of sources of scattered light
2. Visibility in the presence of scattered light from direct sunlight alone
3. Visibility in the presence of scattered light from illuminated spacecraft structures
4. Visibility in the presence of a bright target (e.g., moon, earth) in the field of view
5. Star-landmark and star-horizon visibility through the sextant.

In the absence of stray light, the visibility through a telescope is a function of the light transmission, collecting aperture, and unaided eye adaptation. The transmission of the Block I sextant and scanning telescope was measured; scanning telescope transmission runs about 30 percent, sextant star line of sight 25, landmark line of sight 4. Sell-off requirements refer to the luminous transmission of the telescope and both lines of sight of the sextant. Changes in the Block II system have increased the telescope transmission by 10 percent and the star line of sight transmission of the sextant by about 15 percent. As a rule, transmission can be determined very accurately by calculation on the basis of curves for glass and coatings. The alignment optical telescope transmission runs about 60 percent.

Lengthy tests were run with four of five subjects during 1964 to determine the liminal stellar magnitude observable with the unaided eye and with the scanning telescope. The results were as follows: 6.5 magnitude (50 percent detection) threshold for unaided eye, and 5.5 magnitude through the telescope. These results agreed very well with predictions and the work of others. Much time was spent in verifying the eye pupil diameter versus adaptation level curve in order to be able to approach scattered light problems analytically. In general, the approach was to verify experimentally some of the basic relationships between photometric quantities and visibility terms, then to proceed to take photometric data during the actual tests and deduce the visibility limits from them. Occasionally, a visual situation would be set up during a specific test configuration to reinforce the evaluation technique.

Most of the scattered light tests at MIT/IL have been concerned with sun input alone. A good deal of the work done in late 1964 and 1965 was made inapplicable for APOLLO because the external part of the command module optics was modified significantly with the introduction of the ablative covers to replace the optics doors. The work mainly involved mapping the plane of the scanning telescope under direct solar illumination. The results of this work and also a summary of the threshold studies were reported at MSC status review meetings at MIT/IL during the period mentioned.

Work during late 1965 and early 1966 was devoted primarily to the alignment optical telescope simulations. Most of the results are still applicable to the present telescope except that a conical sunshade design made the instrument less vulnerable to scattered light. The alignment optical telescope tests utilized a wooden model of the rendezvous radar antenna assembly that is in front of the telescope and obstructs some of the forward field of view. After the bulk of these tests were run, the gyro package of the rendezvous radar assembly was painted diffuse white. As a result, the scattered light environment was seriously changed. It was around this time that MSC decided to engage in its own full scale alignment optical telescope-lunar module simulations, the results of which led to the approval of a very effective baffle which had been recommended by MIT/IL.

Work on the Block I-100 series sextant under solar illumination was accomplished in March 1966. From the results, predictions were made of sextant performance with the ablative cover installed on the basis of the additional mechanical protection afforded by the cover. Further simulation in 1968 on the present sextant configuration led to final conclusions. Tests in mid-1967, reported at the August 1967 quarterly review meeting, revealed the basic sun-angle restriction for the present scanning telescope configuration. The ablative cover design for this instrument is, in general, an improvement over the previous cover design, except that a region around -90 degrees shaft angle is made useless because of an overlap of the sextant crown rim. Also, the scanning telescope is still vulnerable to lunar module structure contact.

Because of the overriding requirements concerned with reentry ablative action, no changes on the scanning telescope and sextant which would improve the present visibility were possible. However, a significant change was effected in time on the telescope cover to prevent the viewer from seeing the edge of the ablative crown and the command module outer skin.

Realistic simulation of spacecraft structures which are significant scattered light sources was possible at MIT/IL only for the alignment optical telescope. Effects

of both the lunar module surface around the telescope and the rendezvous radar assembly were simulated. Initial plans were made to represent lunar module interference with the command module optics by using a silhouette at one-fourth scale, but the idea was dropped because it would have been difficult to justify the results based on such a poor imitation of the shape of the lunar module. MSC realized the difficulties in this area (mainly facility and budgetary problems) and constructed a life-sized model of the capsules for scattered-light testing.

Early attempts were made in 1964 to evaluate effects of bright targets in the field of view. Results based on the simulations indicated that constellation recognition was not possible in the scanning telescope when a full moon or a brighter target was in the field of view. One major difficulty in simulating the earth is the large radiant power required to provide for a target subtending 20 degrees. There is much to be gained, with regard to future applications of visual star-finding telescopes, by constructing a meaningful simulation of bright, extended targets in the field of view.

Star-landmark visibility in the use of the APOLLO sextant has been the subject of much analysis and testing at MIT/IL. The basic work associated with the choice of the beamsplitter characteristics in the landmark line of sight was accomplished during 1964 and 1965. In brief, the goal in designing the beamsplitter was to optimize the land-sea contrast for earth landmarks. The main subject, visibility of stars against bright landmarks, was analyzed photometrically. The results of this analysis were verified by observation and reported to MSC. For situations relevant to a typical APOLLO mission, the sextant star-landmark visibility was found adequate. A 3.5 magnitude or brighter star can be seen on the brightest lunar feature and a 2.5 magnitude star or brighter can be seen against a typically bright earth landmark. No substantial previous work had been done on the use of the earth horizon visually, mainly because an automatic horizon sensor had been provided until the Block II design, and a problem in the availability of earth landmarks during the last half of a transearth trajectory was not revealed until late in the program. In practice, star-earth landmark observations are seriously hampered by cloud cover appearing in the star line of sight.

Much work has been done by MSC personnel with an alignment optical telescope-lunar module simulation. Such tests indicated the necessity for additional protection of the prism from backscatter from the radar assembly. This protection took the form of a conical shaped horn, recommended by MIT/IL and developed by MSC, to be fastened to the telescope head prism housing. During the course of the telescope tests, MSC was able to verify the visibility predicted from its own photometric readings, but, because of the unavoidable presence of backscatter from air particles, it was difficult to perform a visual test that would satisfy the astronauts.

## SECTION 5.0 MATERIAL AND COMPONENT PROBLEMS AND SOLUTIONS

### 5.1 BERYLLIUM FABRICATION TECHNIQUES

Originally, sintered blocks of beryllium were machined using conventional tools, but difficulties were realized in that the crystal lattice is sensitive to such techniques. Electric discharge machining was then employed and found successful. Extreme caution was exercised in the removal of material during machining since an excessive rate of metal removal allowed the formation of compounds such as beryllium carbide, resulting in an uneven surface. Such surfaces can act as sites for corrosion either by entrapping machining fluid or entrapping solvents and moisture during subsequent cleaning operations.

The machining of screw holes appeared to be a problem area, but the use of layer tap drills obviated any difficulties. Inserts were a problem but special tools and techniques were developed to facilitate their fabrication.

In general, beryllium is a corrosion-resistant material, but only if the material can be kept clean. Due to excessive handling, some corrosion did occur and several corrosion prevention techniques were developed. A method for anodizing large intricate pieces was developed, but a number of auxiliary anodes was necessary. The final solution was to anodize the less intricate components and to paint the outside of the optics unit assembly base. A number of corrosion-prevention schemes for the inside of the base were tried with the final utilization of a passivation process using a potassium dichromate-phosphoric acid solution forming a complex beryllium-chromium-phosphorous compound. An integral part of this process was the prior cleaning with oxalic acid.

### 5.2 MOTOR-TACHOMETER OPERATIONS IN VACUUM

Difficulties were encountered in operating motor tachometers that had been designed for air operations. Since, in a vacuum, there is no heat transfer due to convection, the rotor reached high temperatures and caused binding of the motor bearing and rapid degradation of the lubricant in the bearings. Design modifications included blackening of the rotor drag cup to increase heat transfer, using bearings of increased radial play to prevent binding, and adding extra lubricant to the bearings. Extreme

care had to be taken during manufacture to prevent contamination, and tolerances had to be strictly controlled. The motors underwent comprehensive acceptance tests in a thermal-vacuum environment to eliminate motors which did not conform to the specifications. Because the rotors in the motor tachometers operated in a high temperature environment, bearings with metal ribbon retainers had to be employed, thus precluding the use of lubricant reservoirs.

### 5.3 DEVELOPMENT OF A 64-SPEED RESOLVER

Manufacturing problems made continuous liaison between contractor and vendor mandatory. The connector potting disintegrated, necessitating a change in the silicone potting material from type RTV 11 to RTV 881. Accuracy requirements necessitated strict dimensional tolerances on resolver and mounting. The resolver failed the insulation resistance test, necessitating a change in the insulation test. The stability of the unit was a continuing problem, as resolver shifts occurred after running in a thermal vacuum environment. This caused further manufacturing modifications, including dowel potting.

### 5.4 BEARING LUBRICATION

Silicone oils were chosen for use as a lubricant for bearings and gears, both inside the command module in an oxygen environment and in the optical subsystem when exposed to a vacuum environment. A methyl chlorophenyl silicone fluid was utilized. A mixture of grease and the oil was used to reduce creepage losses. The lubricant was chosen after considering the operational and environmental factors involved, based upon the following lubricant requirements:

1. Low viscosity and thermal coefficient of viscosity, making it suitable for lubrication of instrument bearings over a wide temperature range
2. Low evaporation rate in vacuum
3. Stability in an oxygen environment
4. Low toxicity hazard
5. Test results run by a number of organizations, including MIT/IL, on operational life in a vacuum environment.

The evaporation rate was considered a major factor in determining if liquids and greases would serve satisfactorily at elevated temperatures. Simulated tests were run to determine the effects of evaporation, degradation, and dissociation.

#### 5.4.1 Lubricant Characteristics

Silicone oils are synthetic compounds containing the elements silicon and oxygen as an inorganic backbone, with organic side groups substituted on the silicon along the polymer chain. The silicone oils are of relatively short polymer size and have few or no crosslinks.

The volatility of the silicone fluids is dependent on the viscosity or molecular weight, and in vacuum it is primarily due to volatilization of the lower molecular-weight polymers. The silicone oils do have a flash point but offer a greater degree of flame resistance than do many organic lubricants. A problem with the use of silicone fluids is that they exhibit very low surface tension with ensuing creepage problems. The value for surface tension is lower than for most mineral oils. However, the silicone fluids still possess some of the best viscosity-temperature characteristics of the commercially available liquid lubricants.

The shear characteristics of an oil are important in lubricant applications. These silicone fluids behave as Newtonian fluids up to shear rates of  $10\ 000\ \text{sec}^{-1}$ . This means that the apparent viscosity under shear is independent of the shearing rate.

#### 5.4.2 Labyrinth Seals

Labyrinth seals were utilized to reduce losses of lubricant due to the hard vacuum environment. Simulated tests were run using narrow passages, and from these tests it was deduced that all bearings and gears on the space side of the optics would actually operate in a soft vacuum, i.e., approximately  $10^{-5}$  torr as opposed to  $10^{-12}$  torr in a hard vacuum.

### 5.5 VACUUM WELDING

In a vacuum environment, once the oxide layer that is present on metal surfaces is ruptured or an adsorbed layer is evaporated, there is no possibility of reformation. With similar metals and metals of compatible crystal structure, welding and bonding may occur. Some metals are less prone to weld and where possible such materials were utilized in the design. By the use of labyrinth seals, the vacuum inside the optical unit seal is not as severe as the vacuum outside, thus giving surface-adsorbed layers much longer life. Silicone lubricant was added on the gear teeth to prevent metal-to-metal contact and reduce friction.

## 5.6 LOCKING COMPOUNDS

To prevent loosening of several components during vibration, anaerobic sealing compounds were used for locking. Surface preparation of parts is critical prior to application of such compounds and a minimum amount of compound was found to be necessary; failures below the minimum occurred during vibration tests.

## 5.7 OUTGASSING PRODUCTS

The use of certain plastics (such as silicones) as gasket material caused some concern; such plastics would exude a fluid during vacuum exposure. The problem was overcome by vacuum-baking such materials or by changing to a fluorocarbon gasket material that would not exude. Haze on the spacecraft windows during flight was attributable partly to adsorbed liquid derived from the fluid used during electric discharge machining operations, and partly to the silicone gaskets. A more efficient cleaning operation of the optics base and a change in the gasket material solved the problem, even though no difficulties of this origin arose in flights.

All materials used in the optical subsystem were subjected to tests for outgassing, but supplier variations sometimes caused difficulties.

SECTION 6.0  
OPTICAL SUBSYSTEM ANALYSIS

6.1 EARTH-HORIZON DEFINITION PROGRAM

This section discusses the general objectives of the APOLLO earth-horizon definition program, an effort toward making possible autonomous spacecraft navigation in cislunar space. It describes the objectives and major components of the program effort and outlines the time schedule followed. Finally, it discusses the relative magnitudes of the major sources of horizon measurement error substantiated by an evaluation of C<sup>1</sup>-Mission (APOLLO 8) cislunar navigation. At this writing the data evaluation from APOLLO missions 10 through 12 and the horizon definition sightings planned for APOLLO 13 are areas of the program not yet completed.

6.1.1 Program Objectives

The objective of this program was to define the characteristics of the earth's horizon that are pertinent to the APOLLO optical subsystem. The fundamental parameters are the altitude of the horizon above the earth's geoid and the statistical variations in this altitude. The geometric constraints involving sun and spacecraft position are also of great importance.

The horizon, seen by an observer in space, is not the terrestrial surface but rather some part of the atmosphere. The optical thickness of the atmosphere is only about 0.1 or 0.3 in the vertical direction, so it appears transparent to observers looking through it at a steep angle. However, the navigation measurement line of sight is tangent to the surface so it looks through the atmosphere edgewise. The horizontal optical thickness of the atmosphere is 80 times the vertical thickness so the optical thickness of the navigation line of sight is at least 10.<sup>1</sup> If a sharp demarcation is seen in the horizon, it is either a high altitude cloud formation or an atmospheric aerosol layer; it is never the solid earth.

---

1. Transmission of light (T) is related to optical thickness  $\tau$  by the equation  $T = e^{-\tau}$ .

The visual appearance of the horizon is determined by the light-scattering properties of the atmosphere. The visible horizon extends 40 or 50 km above the surface. The intensity and color characteristics of the horizon change considerably between the upper and lower regions. Figure 6-1 illustrates a typical horizon profile in terms of eye response parameters. The intensity is nearly constant at low altitudes, but decreases exponentially with altitude in the upper region. When the horizon is viewed through neutral optics, the hue (dominant wavelength) is a blue (4700Å) varying from 80 percent purity at high altitudes to 25 percent, or nearly white, at lower altitudes. The APOLLO sextant optics contains a beamsplitter designed for spectral contrast between landmark and sea; it transmits red light, but blocks the blue light. The horizon appears orange when viewed through this filter as shown by the second set of lines in Figure 6-1. Unless high-altitude clouds or aerosol layers are present, the variations are smooth and continuous, and no distinct transitions are visible. The difficulty of the locator sighting task is further compounded by the fact that the sextant reticle was designed for landmark sightings; it is not optimized for marking on the substellar point of the horizon.

The visible horizon that the earth presents to the space navigator lacks a salient feature that can be used as an altitude reference, analogous to the sea level reference used by the nautical navigator. The navigator must define a feature that he can subjectively identify on the horizon profile, and use this as his reference point when making angular measurements. Typical candidates for this locator might be the whitest point, the bluest point, the upper threshold, or some point midway between the blue and white. The selection of an optimum locator requires an analysis of the statistical properties of each candidate. The statistical characteristics can be divided into two categories: human eye response and atmospheric optical properties.

The major factors that influence the optical properties of the horizon are air density, sun angle, clouds, ground albedo, and aerosols. Density at certain altitudes can vary by as much as 50 percent due to temperature variations. Seasonal latitude and diurnal variations are systematic and their average values are predictable. However, local weather patterns can cause large deviations from nominal conditions.

The appearance of the horizon is dependent upon the sun elevation angle. This dependency is especially evident at low sun angles. The sun angle that the navigator in a returning APOLLO vehicle sees depends on the orientation of the measurement plane and varies throughout the trajectory in accordance with the day of the lunar month during which the flight takes place. The most critical navigation situation occurs 2 to 5 hours before reentry. This is the latest time at which optical measurements, useful for state vector updates preparatory to reentry, can be made.

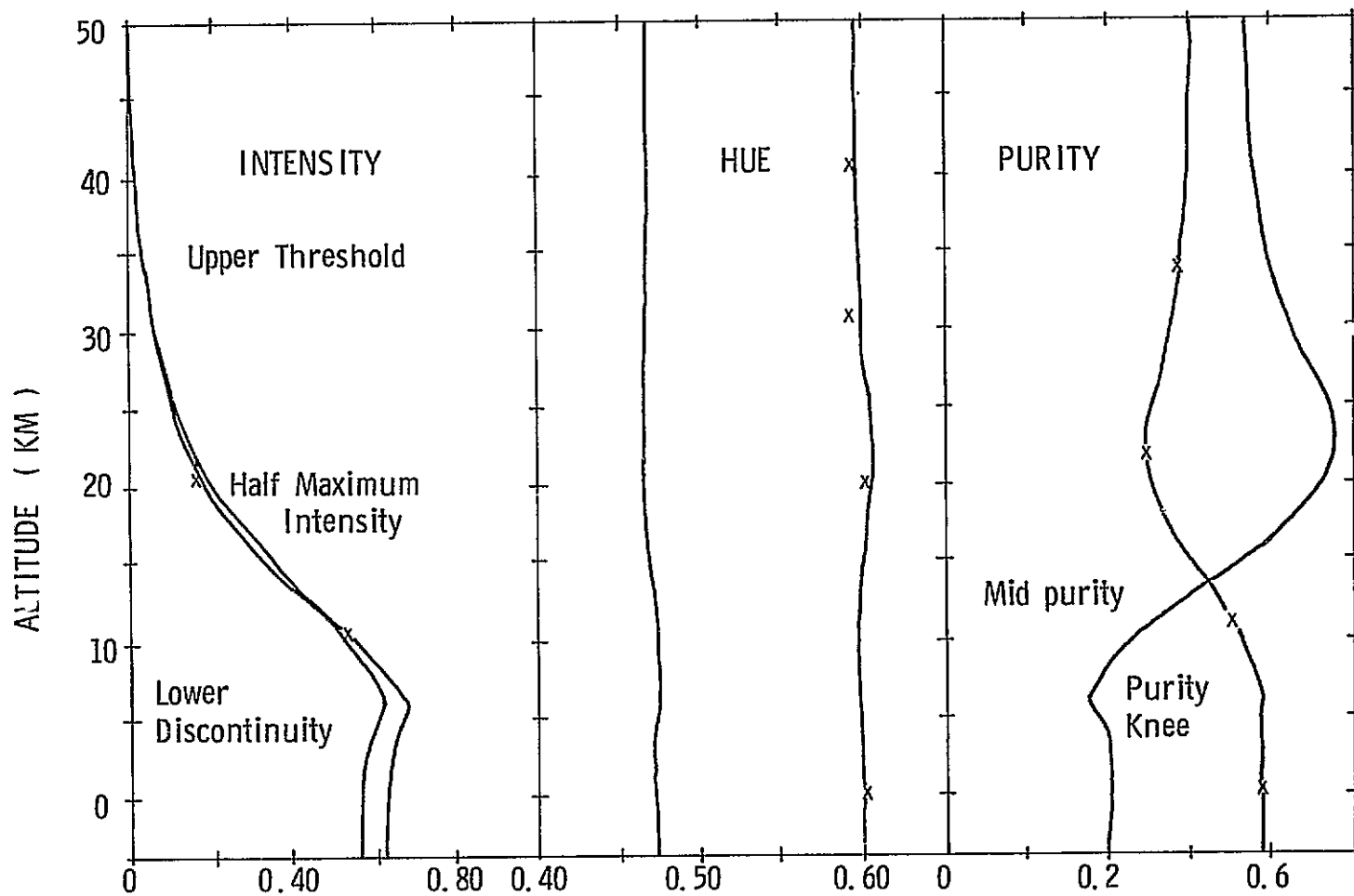


Fig. 6-1 Typical Horizon Profile

At this point in time the spacecraft is near enough to the earth that horizon errors dominate over sextant errors. Unfortunately, in this critical situation, the elevation angle of the sun above the local horizon is very small, making the effects of sun angle very important. Therefore, establishing an error model of the horizon measurement that includes the effects of sun angle and establishing the geometric constraints under which the model and the measurement are valid became important objectives of this program.

Ground albedo influences the horizon by regulating the amount of light that is absorbed or reflected by the lower boundary of the atmosphere. Clouds affect the horizon in two ways: their high reflectance changes the apparent albedo of the lower boundary, and, if the cloud amount is high, the lower boundary is raised from ground level to cloud top level. Secondly, if the cloud tops are at high altitude, they will stand out as distinct features on the otherwise smoothly varying horizon profile. This effect obscures features that are present in the lower part of the profile in the absence of clouds and distracts and disorients a navigator looking for subtler horizon features in the profile.

Atmospheric aerosols (haze, dust, smog, etc.) affect atmospheric scattering to a significant degree. At very low altitudes, aerosol scattering is more prevalent than scattering due to the presence of air molecules. Aerosol distributions vary substantially in different geographic locations and from day to day in any one location. Aerosol density generally decreases with an increase in altitude more rapidly than air density; aerosols are therefore less important at high altitudes than at low. However, a thin aerosol layer of low density can have very substantial optical significance when viewed edgewise. These layers are more significant than their total density would suggest because they, like high altitude clouds, cause perceptible distortion of an otherwise smoothly varying profile.

The principal situation under investigation was the daytime sunlit horizon. However, a number of other situations were considered. The backlit horizon, the twilight horizon, and the moonlit horizon are all of interest to the APOLLO navigator.

#### 6.1.2 Program Tasks

The overall horizon definition program was composed of 13 separate tasks or projects. A block diagram showing the relationships between these projects is shown in Figure 6-2. Part of the project was experimental and the remainder a mathematical evaluation combining both experimental and theoretical data.

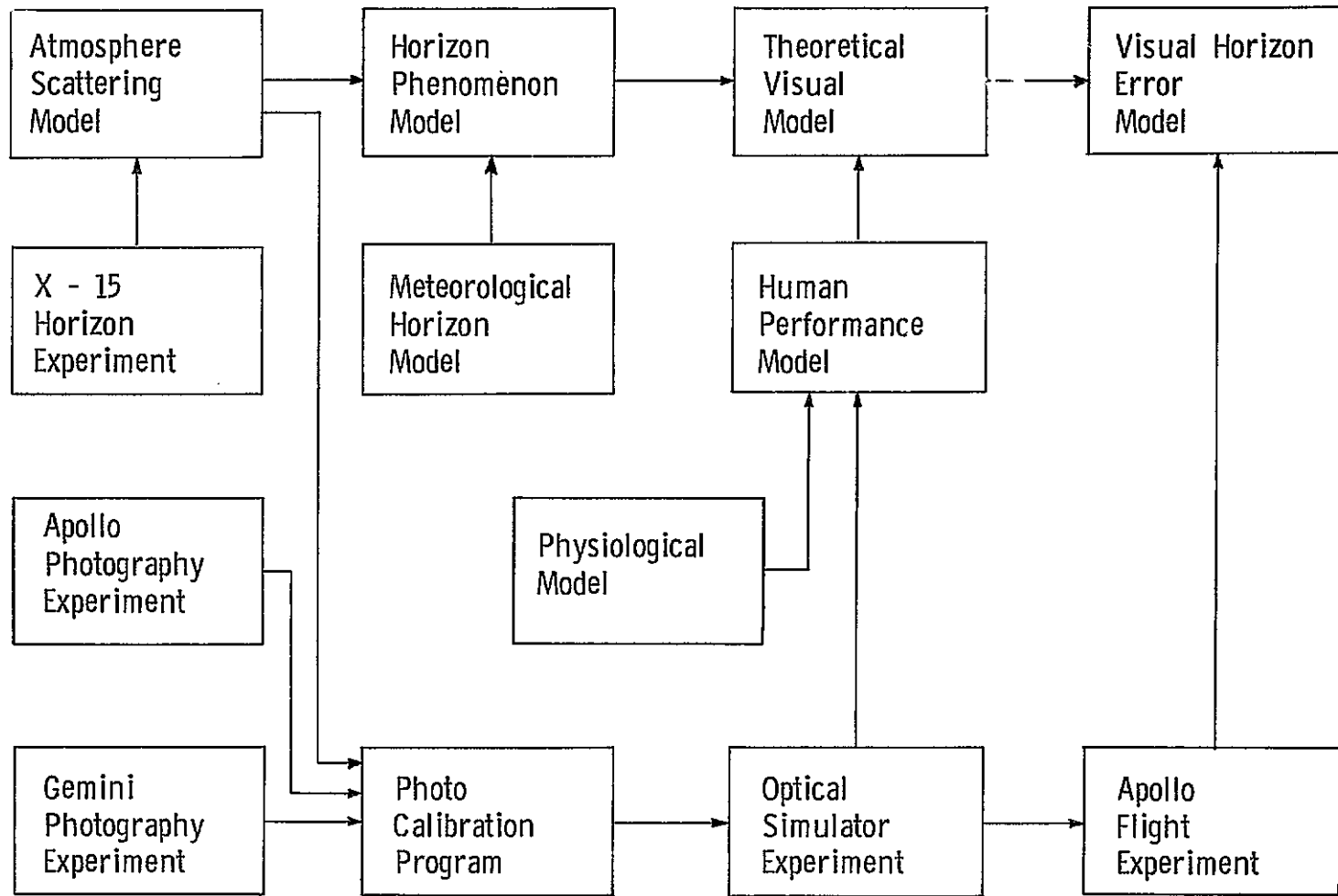


Fig. 6-2 Relationships between the Projects in the Horizon Program

The general outline of the program is as follows. An atmospheric scattering model, based on the optical properties of the atmosphere, is developed. This project yields a computer program that can calculate the horizon profile for any specified meteorological condition. This program, combined with a meteorological model, determines the shape and the statistical properties of the horizon profile. This result, combined with a human performance model, allows prediction of the theoretical accuracy of a horizon measurement.

The MIT/IL optical simulator made several important contributions to the program. It is used to train astronauts for the flight experiments, as well as for the actual navigation procedure, and to provide human performance data for the theoretical evaluation. Human performance in visual tasks is very sensitive to the circumstances of the situation and to the "gamesmanship" of the test. While a vast amount of data were available on human response, none were specifically applicable to the APOLLO horizon navigation situation. While some of the available data could be used to make preliminary estimates, new data, taken in as realistic a simulation as possible, were required to determine human performance.

The simulator also provides an important reference against which theoretical plans, evaluations, and predictions can be tested for feasibility, realism, and order of magnitude accuracy prior to flight testing.

Horizon photographs were required for the simulator activities. Artificially generated scenes can be used to evaluate some human performance parameters. However, due to the complexity of the horizon phenomena and the importance of subtle visual clues, the problems of generating realistic scenes are prohibitive. A number of photographs taken on GEMINI flights were suitable for this experiment. A number of additional photographs taken of specific horizon situations would be required if the full potential of the simulator were to be realized.

Color photography is a very inexact process. While an accurate theory of color reproduction exists, the nature of the photographic process is such that implementation of the ideal procedure is impossible. Photometric calibration of the photographs were used, first to verify that the photo is a reasonable representation of the theoretical horizon and secondly to provide benchwork calibration of the eye response data from the simulator experiment.

The optical simulator cannot be used directly to evaluate the altitude and variation of horizon locators because of the infidelity of the photographic process. Instead, the simulator provides human performance data for a situation similar to the

navigation task. Simulator performance, calibrated by the photo calibration project, is transformed to performance in the real situation by applying a human performance model to theoretical horizon profiles.

The atmospheric scattering model is the fundamental building block in this program. It provides the horizon profile reference definition and sets the standards by which photographs for the simulator are accepted. The X-15 horizon definition experiment provides accurate, well documented experimental data to verify the accuracy of the scattering model (see report R-648). Without this confirmation, the validity of the theoretical horizon profiles would be difficult to verify.

The guideline which has been used in defining this program is that every theoretical component should be backed up by experimental measurements and that each experimental component should be examined theoretically for consistency and for statistical significance. This philosophy provides redundancy within the program so that results could be obtained even if unforeseen problems were to hinder some of the projects, and it enhanced confidence in the results through the cross-checks between components.

### 6.1.3 Program Schedule

The schedule of the major activities in this program is outlined in Figure 6-3. The horizontal bars indicate the development of major projects. The arrows between blocks indicate the flow of essential information between projects.

The first activity for the first quarter of 1968 was the evaluation of preliminary data from the atmospheric scattering model to identify the parameters that are most significant in influencing the physical appearance of the horizon. Simulation data indicated that a well defined target can be marked with an accuracy of 5 to 10 arcseconds, one sigma (0.25 to 0.5 mile at a range of 10 000 n. mi.) by a navigator using the APOLLO optics. Therefore, meteorological and other natural factors that perturb the horizon by more than 0.5 km are significant.

Using this criterion, the required meteorological data were identified and located. The next step in the meteorological project was to collect extreme values of the parameters and compute the variations in locator altitude caused by these perturbations, thereby showing which factors dominated the variability. Since statistical properties of the dominating factors (cloud cover, sun angle, and eye response) determine the statistical properties of the navigation measurement errors, all factors were not examined in the same detail. The dominating factors were examined

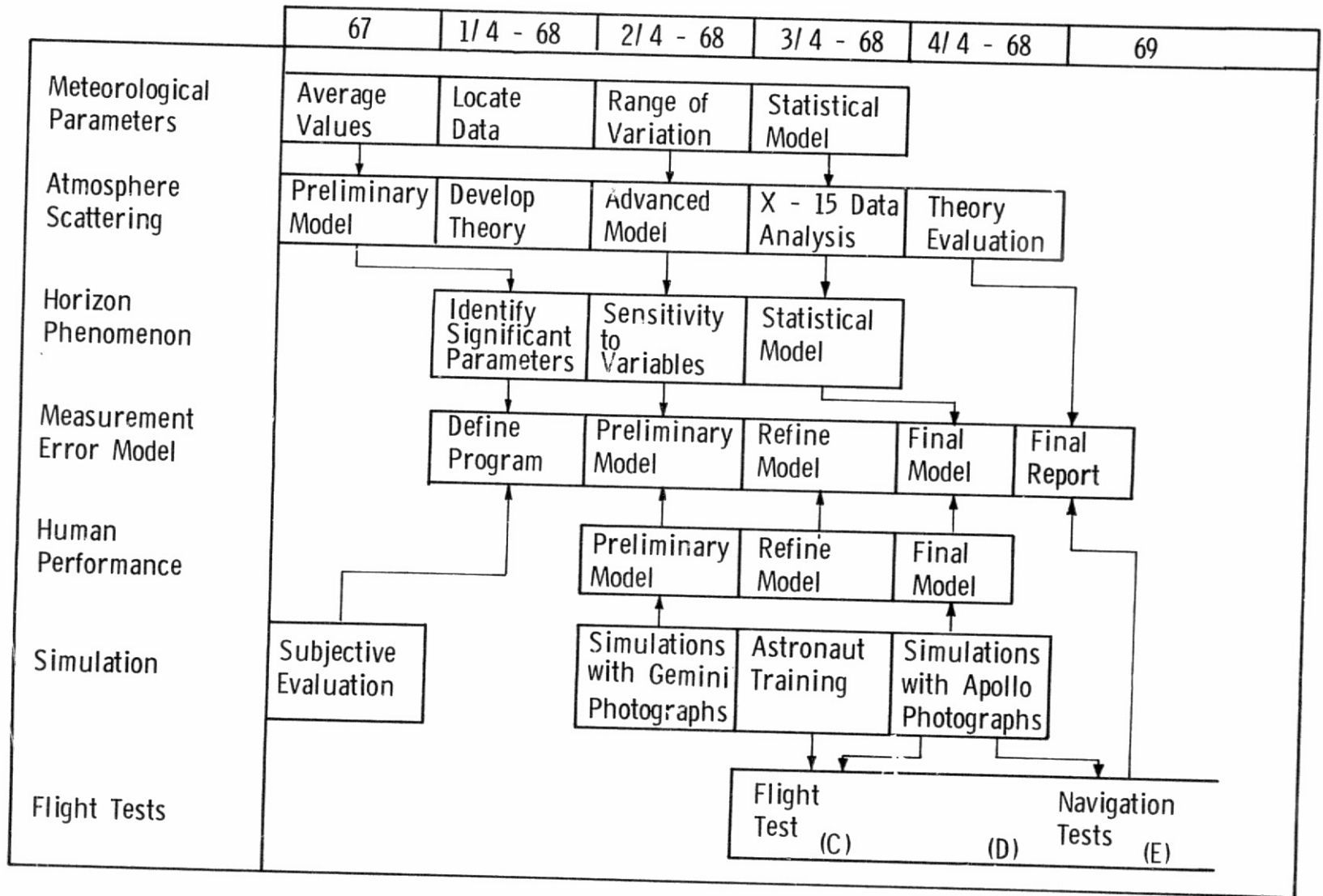


Fig. 6-3 Major Activities in the Program

to determine their statistical properties while the lesser factors were examined only to demonstrate that their maximum effect is small compared to that of the dominant factors.

The atmospheric scattering model was updated to include all the significant factors and to perform the calculations to the required accuracy. The necessary physical and optical theory was developed and the computational procedure was formulated.

When the results of the X-15 horizon definition experiment became available, they were used to verify the accuracy of the theoretical model. The meteorological conditions of the air mass observed by the X-15 were used as inputs to the scattering model. The final phase of the scattering model project was an evaluation of its accuracy based on the X-15 results.

Optical simulation experiments began in the second quarter of 1968. These simulations used GEMINI horizon photographs and other scenes to provide preliminary data on human performance that could be combined with the horizon phenomenon variation model. At this point many different horizon locators could be compared and the optimum one selected. This allowed the definition of a preliminary measurement error model to be used in navigation analysis in the GSOP for the early APOLLO flights.

As soon as a preliminary measurement error model was defined, the simulator could be used to train crew members for both the general navigation procedure and for the photography and navigation experiments that support this program.

## 6.2 THE VISUAL HORIZON

A typical horizon profile is shown in Figure 6-4. The three parameters plotted against altitude are 1) intensity (relative brightness to human eye), 2) hue (dominant wavelength), and 3) spectral purity (zero purity is white, 100 percent purity is monochromatic light). While the hue remains constant at 4800A (blue), the purity changes from 10 to 40 percent which is sufficient to change the apparent color from white to blue. This effect can be seen on any color photo of the horizon taken on MERCURY or GEMINI flights.

The atmospheric horizon profile is determined by light scattered from air molecules, dust and aerosol particles, and clouds. Both direct sunlight and reflected light from the ground, the lower atmosphere, and low altitude clouds illuminate these scattering sources. Ozone, which absorbs light in part of the visible spectrum, is another important factor in atmospheric optics.

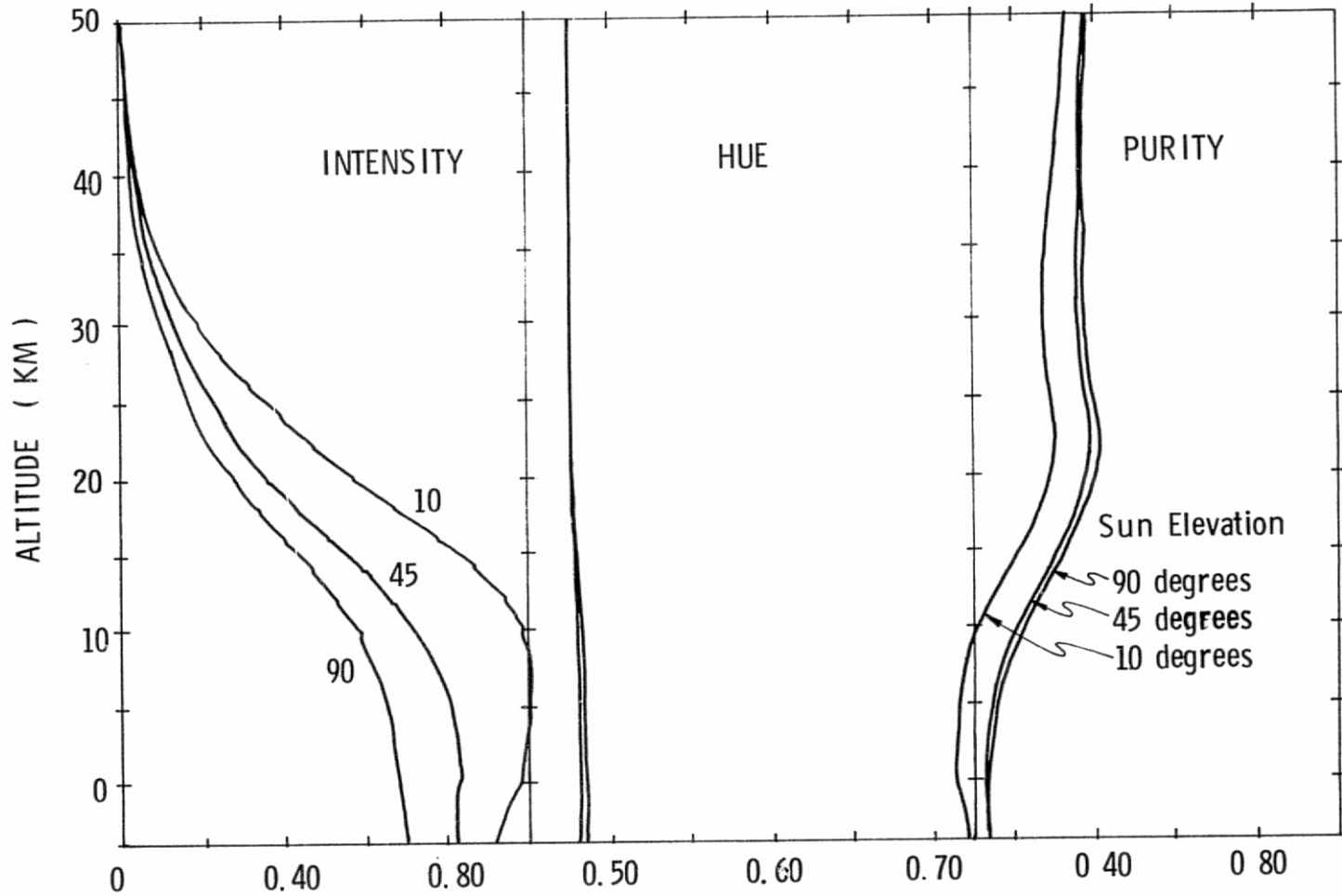


Fig. 6-4 A Typical Horizon Profile

The lower part of the horizon (10 km and below) is dominated by cloud cover effects. While the atmosphere appears to be nearly transparent to an observer looking through it vertically, it is so thick when viewed edgewise (as is the case in horizon observations) that the surface of the earth or even low altitude clouds cannot be seen at the horizon. An additional factor that prevents observation of the terrestrial horizon is the high occurrence of cloud cover. If an apparent solid earth horizon is seen in the white diffuse horizon layer, the feature is actually either a high altitude cloud or a foreground cloud. Figure 6-5 illustrates the geometry for these situations. If the low altitude discontinuity was used as a navigation reference, its uncertainty would probably be about 4 to 6 km,  $1\sigma$ .

The mid-altitude horizon (10 to 20 km) is most strongly affected by variations in air and aerosol density. Variations in aerosol amount can affect the contrast between the blue and white regions, and variations in either air or aerosol affect the altitude at which the blue-white transition occurs.

Two types of air density variations occur: systematic variations with latitude and season, and random variations associated with local weather disturbances. Dust and aerosol variations are partly systematic with season and geographic area and partly random. The random variations of both air and aerosol are about the same magnitude as the systematic variations so corrections for known variations would not improve the navigation accuracy by a substantial amount. The horizon altitude uncertainty caused by dust and aerosols ( $\sigma = 1$  to 3 km) is slightly greater than the air density contribution ( $\sigma = 1$  or 2 km). Dust and aerosol distribution and variability are very poorly documented and are the most serious limitations in theoretical studies of horizon profiles.

The upper part of the horizon (above 20 km) is sensitive to air density, sun angle, and earth albedo variations. The altitude uncertainty of this part of the horizon is about 3 to 5 km,  $1\sigma$ . Here, systematic variations with latitude, season, and time of day dominate the random variations, and a very complicated model would be required to compensate for these variations. Even if such a compensation was employed, the random variations would still make this altitude region less accurate as a navigation reference than the middle altitude region.

#### 6.2.1 Beamsplitter Effects of the APOLLO Optics

The most significant feature of the APOLLO optics is the dichroic beamsplitter that is used to combine the star and landmark lines of sight. The beamsplitter transmits part of the red but almost none of the blue light, from the landmark line

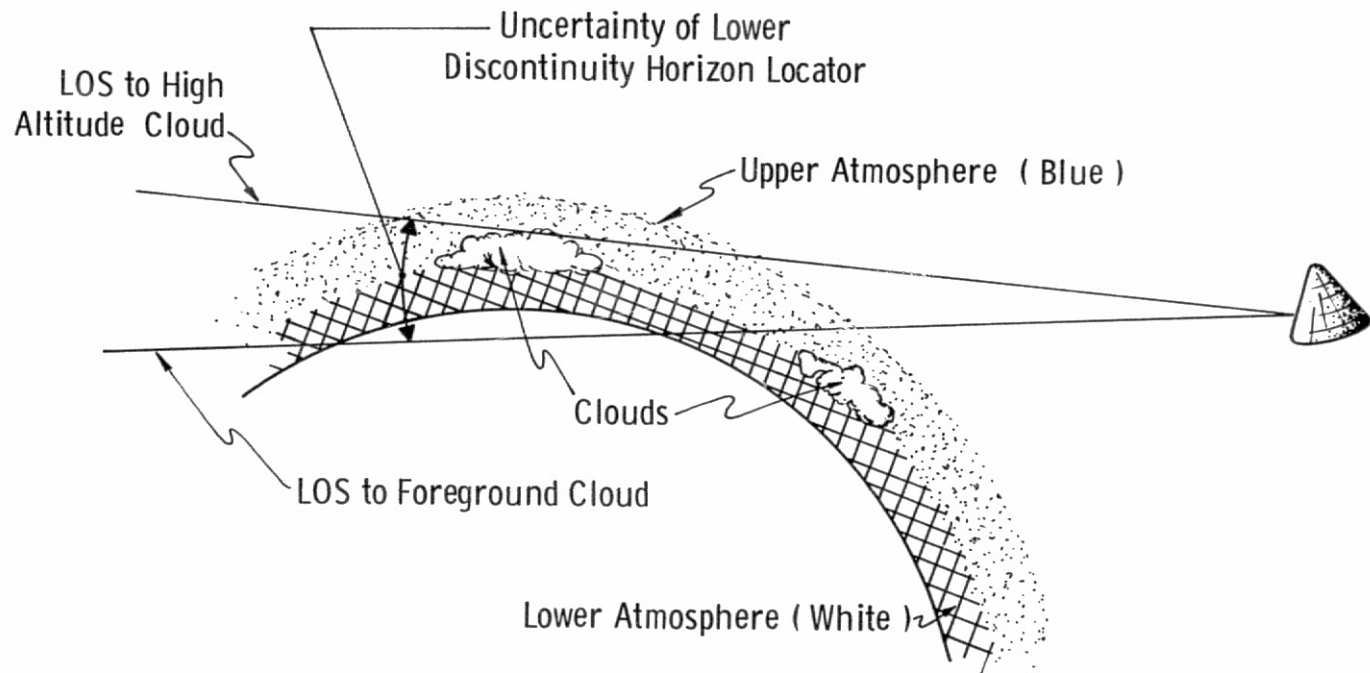


Fig. 6-5 Illustration of Cloud Top Problem with the Use of Apparent Horizon as a Location

of sight to the eyepiece and reflects most of the light from the star line of sight to the eyepiece.

The beamsplitters transmit red but no blue, causing the horizon to appear as a different color through the sextant than when viewed normally. The resulting change is that the lower part appears red or orange rather than white, and the top appears pink or gray rather than blue. The disadvantages of this for horizon sightings are 1) red light is more susceptible to variations of clouds, aerosols, and albedo than blue light, and 2) the unnatural color complicates the astronaut's task.

### 6.2.2 Sources of Horizon Measurement Error

The relative importance of the major sources of uncertainty are discussed below. The magnitudes presented are based on preliminary investigations and are intended only to illustrate major factors.

The first categorization in analyzing an accuracy of an optical measurement is to separate the characteristics of the detector and phenomenon. When discussing horizon phenomenon, two factors must be specified: the pertinent wavelengths and the altitude of the locator. These distinctions are necessary because the factors that determine the horizon profile, weather, ozone, albedo, aerosols, and clouds have different effects at different wavelengths and are often localized in altitude.

Figures 6-6 and 6-7 illustrate the variation in half-maximum intensity altitude due to albedo and sun angle variations as a function of wavelength. These curves have notable minimums in a region around 3800A making that wavelength ideal for navigation such as the APOLLO tracker-photometer, which uses electro-optical sensors. The reason for this minimum is that ozone absorption has two peaks centered at 2500A and 6000A, and is nearly zero at 3800A. Daily and geographic variations in ozone density cause perturbations at the wavelengths where absorption is strong. In addition to a direct attenuation proportional to density, the ozone absorption complicates the effects of albedo and sun angle.

The wavelengths longer than 3800A are more variable than the shorter wavelengths because they penetrate to lower altitudes where they are susceptible to albedo and cloud variations. The shorter wavelengths see a much thicker atmosphere so air density, which is more stable than clouds or albedo, is the dominant variable.

Human eye response, which determines the wavelength of interest to visual observations, is restricted to the 4500 to 6500A range. The transmission characteristics

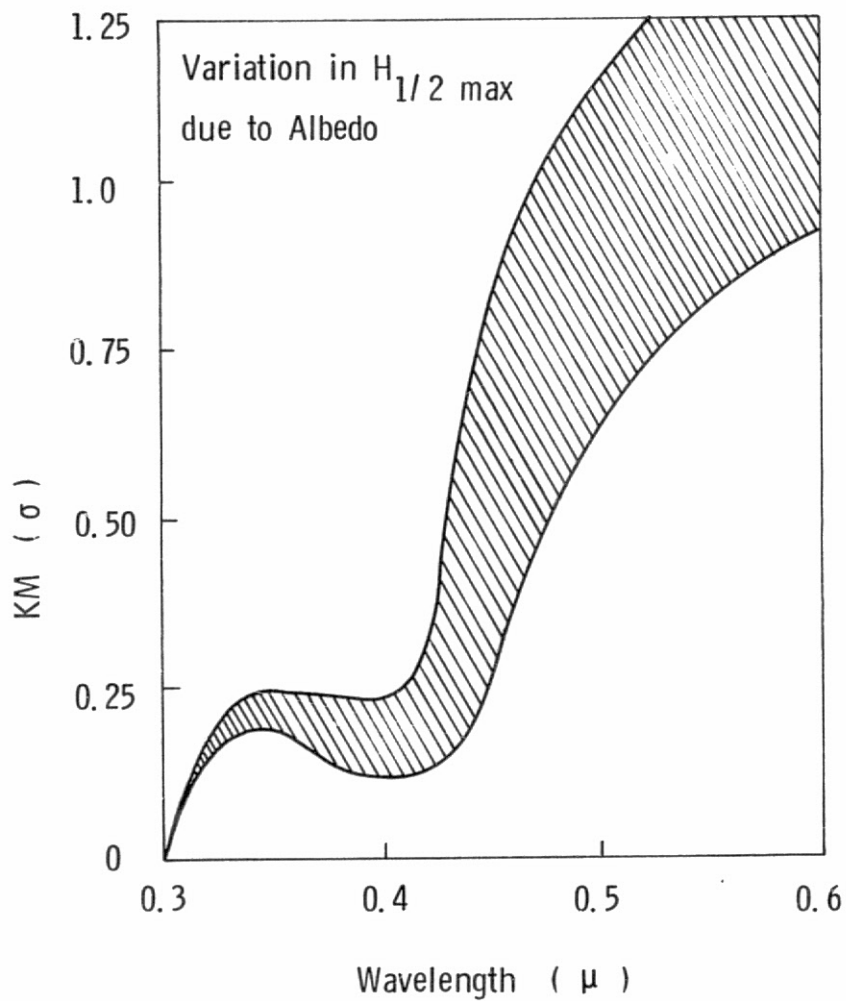


Fig. 6-6 Variation of Half-Maximum  
Intensity Altitude

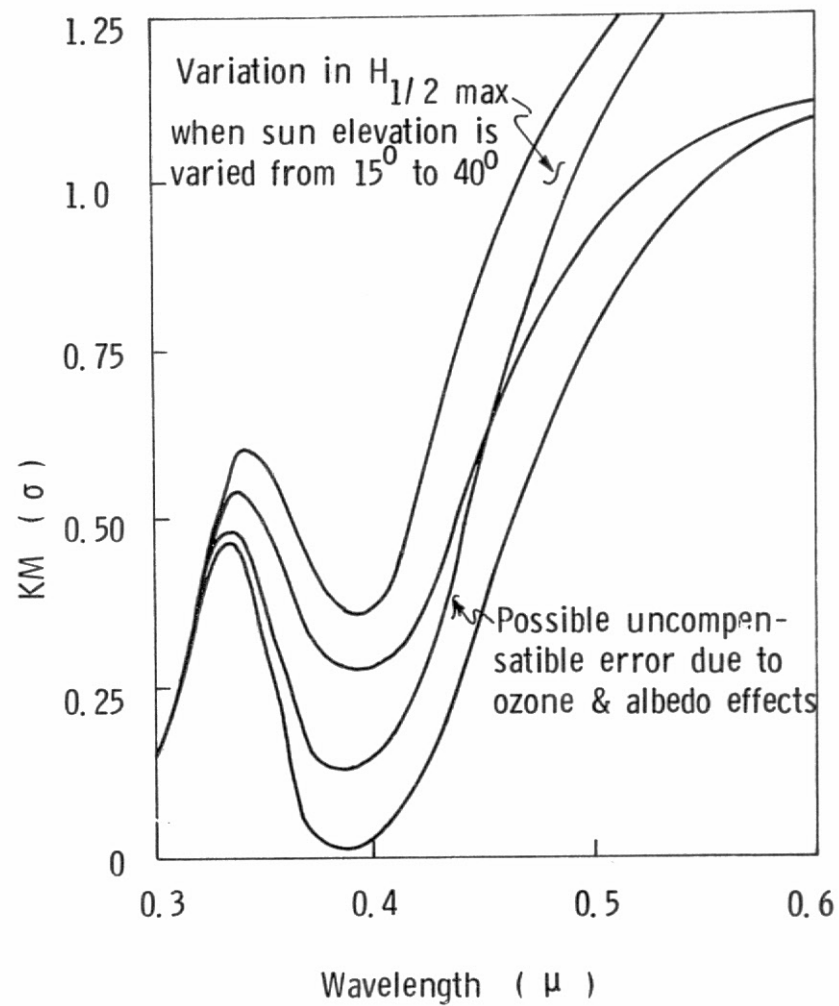


Fig. 6-7 Variation of Half-Maximum  
Intensity Altitude

of the dichroic beamsplitter in the APOLLO optics restrict the applicable range to 5500 to 6500A, which is the region of greatest sensitivity to phenomenological variations.

A number of visual locators are feasible and each has a different sensitivity to phenomenon variations. Low altitude locators such as point of maximum intensity or lower discontinuity are most sensitive to cloud and aerosol perturbations. High-altitude locators, such as threshold or upper discontinuity, are sensitive to ozone and albedo perturbations. Middle altitude locators, such as half intensity and point of color change, are susceptible to sun angle and ozone variations. Table 6-I lists several of these locators and preliminary estimates of the relative magnitudes of each.

The performance of the human eye as a sensor is very sensitive to the nature of the task it is assigned. It is vastly inferior to photometric devices for measuring intensity magnitude, but it is fairly good at detecting discontinuities. Therefore, it can be expected to locate discontinuities and points of change much more accurately than it can detect thresholds or half-maximum intensities. Approximate estimates of eye performance for several locators are also listed in Table 6-I for comparison.

TABLE 6-I  
COMPARISON OF VISUAL HORIZON LOCATORS

Source of Variation	Variability of Locators*				
	1	2	3	4	5
Air Density	2 km	0.7 km	0.7 km	0 km	0.1 km
Ozone	1	0.5	1	0	0
Albedo	3	0.5	0.5	0	1
Clouds	1	2	0.5	4	3
Aerosols	0.5	0.7	0.5	2	2
Sun Angle	2	1	1.5	0	1
Phenomenon Subtotal (bias error)	4.5	2.5	2.2	4.5	4
Eye Detection (random error)	3 km	3 km	2 km	0.3 km	1 km

\* Locators:

- 1: upper threshold
- 2: half-maximum intensity
- 3: mid-purity point
- 4: lower discontinuity
- 5: brightest point

Note that the phenomenon error behaves as a bias. The correlation distance is probably a few thousand miles. The eye detection error should be random with near-zero mean. The probable minimum sun elevation angle constraint is 10 to 15 degrees. From the point of phenomenon stability, a middle altitude (10 to 12 km) locator is desirable. The best locator at this altitude is probably the mid-point of purity change. This is the point where the horizon appears to change from bright orange to dim white. (See Figure 6-4.) While the eye response is most accurate using the low altitude discontinuity locator, the phenomenon variation of that locator makes it a poor navigation reference.

The dichroic beamsplitter filter affects the profile in several ways. The principal effect is that the wavelength range transmitted to the eye is narrower than it would be if a neutral beamsplitter were used. This reduces color contrast, thereby degrading the accuracy of locators that depend on color. This is partially offset by the fact that locators which depend on intensity are enhanced if color contrast is not present to confuse the scene. Another effect of the filter is altitude selection. The long wavelengths transmitted by the dichroic originate low in the atmosphere where the profile is very susceptible to cloud interference. If a neutral or blue filter was used, the profile would originate higher up where the phenomenological stability is better.

### 6.2.3 Selection of Locators

In order to use the horizon as a navigation reference, some identifiable visual feature must be selected. A number of possible locators are listed in Table 6-1. The most salient low-altitude locator is the low-altitude discontinuity. This is the apparent horizon caused by a cloud or aerosol layer that appears to stand out in the white part of the profile. Actually the filter would make this part look orange or pink but the discontinuity should stand out equally well.

The best middle altitude locator is the point where the color change from white to blue is half complete. With APOLLO dichroic filter 2, the color change is so ill-defined that a different locator must be described. The point where the intensity falls to one-half its maximum intensity could be used. However, the eye is not well suited for this type of task so this locator could not be identified as accurately as the color change locator.

The high-altitude locator, the upper threshold, is the highest point where light from the atmosphere can be detected against the blackness of space. This locator is affected less than mid-altitude locators by beamsplitter variations but more than

the low-altitude locator. The threshold identification task is the most sensitive to psychological factors such as adaption level, visual sensitivity, and judgment.

The altitude and variability numbers presented in Table 6-II indicate the approximate magnitude of the effects referred to in the above discussion.

TABLE 6-II  
DESCRIPTION AND SUMMARY OF LOCATORS WITH TYPICAL  
BEAMSPLITTERS

Altitude Beamsplitter	Low (apparent horizon)	Medium (color change)	High (upper threshold)
Neutral	Discontinuity $h = 0$ km $\sigma = 4$ to 6 km	White to Blue $h = 17$ km $\sigma = 2$ to 3 km	Threshold $h = 35$ km $\sigma = 3$ to 5 km
APOLLO No. 1 Beamsplitter	Same as above	Fed to Pink Not Usable	Threshold $h = 32$ km $\sigma = 3$ to 5 km

#### 6.2.4 Geometric Aspects of Navigation Sighting

Several geometric aspects of the navigation sighting situation are of interest because they limit measurement opportunities and define the envelope of conditions that must be analyzed and verified by tests. The typical midcourse navigation situation is shown in Figure 6-8. Two system constraints are very critical in this situation. The line of sight to the earth passes very close to the sun, so scattered light from the sextant objective and structure can saturate the image in certain situations. Figure 6-9 is a projected view of the sun and earth from the spacecraft in a representative navigation situation. Figure 6-9a shows the anticipated constraints and 6-9b shows the effect of pessimistic values for the constraints.

The second constraint illustrated in Figure 6-9 is sun elevation angle. This is defined as the angle of the sun above the local horizon measured at the point where the landmark line of sight is tangent to the earth. (The apex of the angle is at the earth and not at the spacecraft.) This constraint is necessary because the visual appearance of the atmosphere is different when the sun is low (near twilight) rather than when the sun is high.

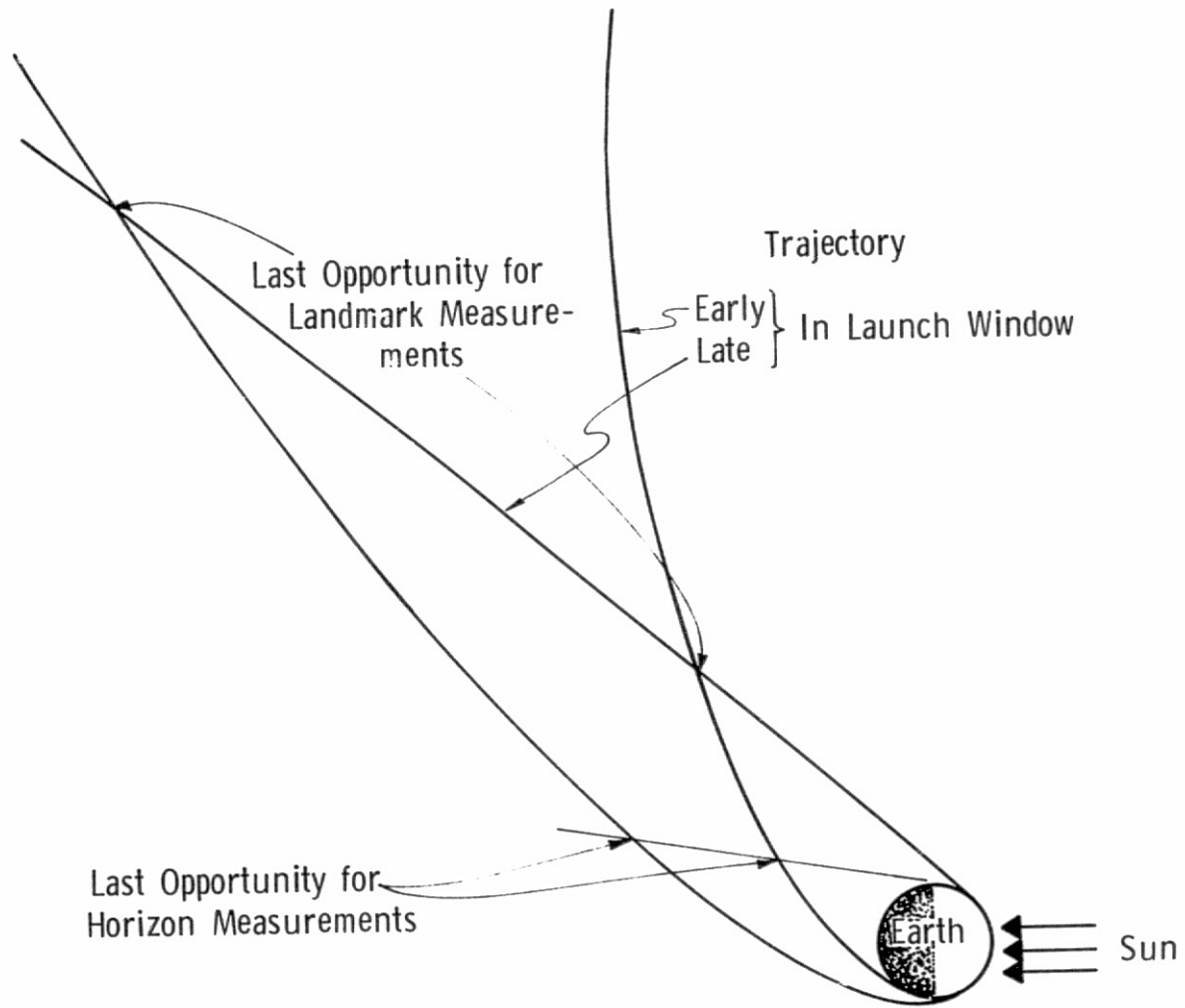


Fig. 6-8 Typical Midcourse Navigation Situation

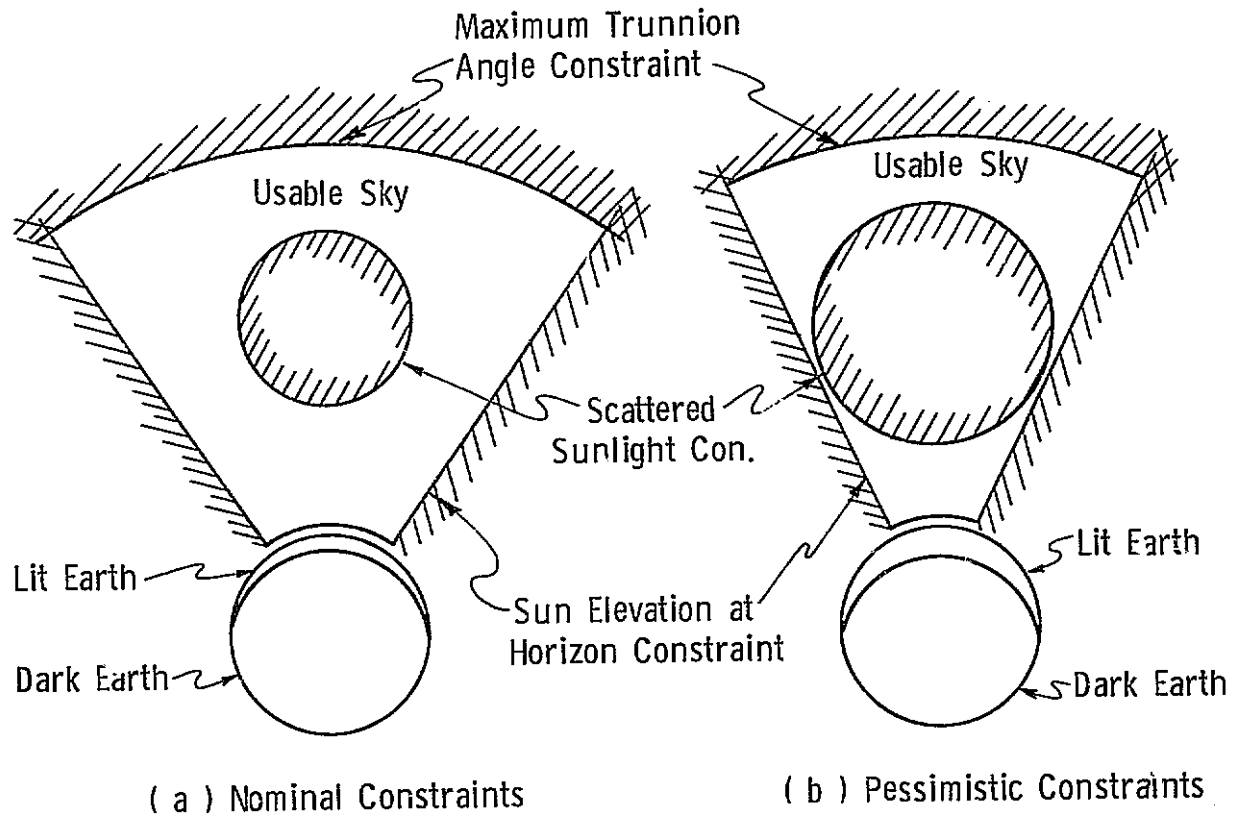


Fig. 6-9 Projected OSS Field of View in Typical Navigation Situation

The scattered-light constraint limits sky area in which stars can be sighted and in some cases excludes use of the earth. The sun elevation constraint limits use of the horns of the illuminated earth crescent. (With the geometry shown in Figure 6-8, the illuminated earth is a narrow crescent.) Since the star used must lie on the plane defined by the spacecraft, the center of the earth and the horizon, this constraint also limits the sky area in which stars can be used. The result of this sky area limitation is a limitation on the probability of finding a usable navigation star in a given situation. These effects become more severe as the spacecraft approaches the earth, so the constraints limit the last measurement opportunity. Since navigation accuracy is a function of measurement opportunity, these constraints directly affect reentry accuracy.

### 6.2.5 Summary of Sighting Constraints

If sextant measurement is to be feasible, the following constraints must be met:

1. Trunnion Angle—The trunnion angle must be greater than 2 degrees and less than 50 degrees, unless the sun is within 45 degrees of the landmark line of sight in which case the maximum trunnion angle is 45 degrees.
2. Star Magnitude—The star must be bright enough to be acquired against the background and tracked across the landmark line-of-sight target. The minimum star intensity is shown in Table 6-III.

TABLE 6-III  
MINIMUM STAR INTENSITY

	Earth	Moon
Horizon	3	3.5
Landmark	1	2.5

The advantage of horizon measurements is that they can be made with dimmer stars than can landmark measurements because, in the case of the earth, the upper threshold locator is only 1/10 as bright as the lower atmosphere or a landmark. In the lunar case, the interface at its edge and black space defines the locator.

Another advantage of horizon measurements is that, by moving the landmark line of sight through a small angle (1/2 degree or so), acquisition can be done against space rather than against a bright earth or moon background in the landmark case.

3. Scattered Light—The background illumination due to sunlight scattered off the optical elements must not be so bright that it obscures either the star or the horizon image. Star availability tables for various missions were prepared using an empirical model based on contour plots of solar simulator data to calculate the scattered light criterion as a function of star magnitude as well as geometry.
4. Sun Elevation—The local sun elevation angle at the tangent point for horizon measurements or at the landmark must be high enough to illuminate the target without distortion, as shown in Table 6-IV.

TABLE 6-IV  
MINIMUM SUN ELEVATION ANGLE

	Earth	Moon
Horizon	10°	5°
Landmark	10°	5°

5. Landmark Slant Angle—Due to optical foreshortening and atmospheric thickness, landmarks with large slant angles are unusable. See Table 6-V. (The angle is between vertical at the landmark and the landmark line of sight.) This constraint does not apply to horizon measurements.

TABLE 6-V  
MAXIMUM SLANT ANGLE

Earth	Moon
45°	60°

### 6.2.6 Optical Simulation Results

Three types of simulation tests are reported: 1) star visibility against a uniform background, 2) stars against a horizon or landmark, and 3) the horizon or landmarks against scattered light.

#### 6.2.6.1 Stars Against Uniform Background

The most significant factor in evaluating star visibility is the specific nature of the task. Detection, tracking, and acquisition each involves significantly different

physiological mechanisms. Tests show that the thresholds differ by up to two star magnitudes from one task to another while the repeatability of any one task seldom varied by one-half star magnitude between subjects or tests.

Figure 6-10 presents star magnitude visibility threshold versus background brightness for three tasks. The equivalent brightness of lunar and earth features is noted on the plot. The brightness unit on the plot is scene brightness times sextant transmission expressed in foot-lamberts.

The fact that the tests were conducted viewing this equivalent scene through APOLLO optics which have an objective area and magnification different from the naked eye is implicit in the plot and should be considered when comparing it with other data.

The lower set of lines is derived from Tiffany data (corrected for objective and exit-pupil area, magnification, and one-eye observation). These data represent a detection task. The subjects knew exactly where the star would appear and were asked to guess whether it was on or off. Although this task is not relevant to the APOLLO situation, the data are useful as a comparison with the other tests and as an indication of the effect of focus (image size).

The acquisition test data are shown by the upper cross-hatched band in Figure 6-10. This test determined the star magnitude that the subject could, without difficulty, acquire in any unknown part of the field of view and track without fear of losing it.

The tracking test data, plotted between the acquisition and Tiffany data, represent the dimmest star that can be tracked successfully. A star this dim is very difficult to acquire unless the subject knows exactly where to look. Tracking is possible only if the subject keeps his eye on the star at all times. The star magnitude criterion listed in Section 1 is shown by solid lines in Figure 6-10.

#### 6.2.6.2 Stars Against Horizon and Landmarks

Tests using a star and GEMINI photographs of the horizon showed that the upper threshold could be marked easily and accurately with a third magnitude or brighter star. Stars as dim as fourth magnitude can be used with a slight increase in operator effort and a small decrease in mark accuracy. When lower altitude locators, such as apparent ground level or cloud-top altitude were used, stars of 0.5 to 1.5 magnitude were required.

Tests on landmarks were very sensitive to scene-brightness factors such as ground albedo and the presence of oceans or clouds. The minimum star magnitude ranged from 0.5 to 3.0 magnitude depending on these factors.

#### 6.2.6.3 Horizon Against Scattered Light

These tests showed that the edge of the earth or moon could be detected even though the scattered light intensity was many times greater than target intensity. The most sensitive factor is a shift in the apparent upper threshold altitude due to the upper part of the horizon profile being obscured by scattered light before the brighter, lower part is affected. The criterion selected to define the constraint is the scattered light level that causes a shift of 5 to 10 km in the altitude of the locator. This effect was found to occur where the scattered light intensity reached about one-half the normal profile maximum intensity.

While the upper threshold is obscured by scattered light sooner than landmarks or lower altitude horizon locators, use of the upper threshold does not restrict measurement opportunities because scattered light generally obliterates the star before the locator is affected.

#### 6.2.7 Scattered Light Intensity

The scattered light data presented here were taken from tests performed with an actual APOLLO optical subsystem (completed with ablative cover) illuminated by a solar simulator. The scattered light intensity was found to be a very complicated function of geometry and no simple definition could be found. Previous models using 15-degree circles and 5-degree sectors are over-simplifications. No format less complicated than the series of contour plots presented here are adequate to represent the data.

Figures 6-11 through 6-17 present the scattered light test data in the form of contour plots. The landmark line of sight is in the center, trunnion angle is measured radially from the center, and shaft angle between the sun plane and the measurement plane is represented in the azimuth coordinate of the polar plots. For each figure the sun was placed at a different angle to the landmark line of sight. The contours map the scattered light intensities sufficient to obscure stars of the indicated magnitude. The threshold criterion used is the acquisition criterion plotted as a dotted line in Figure 6-10.

The scattered light data are expressed in star magnitudes rather than in conventional photometric units for two reasons. First, star visibility is the relevant factor;

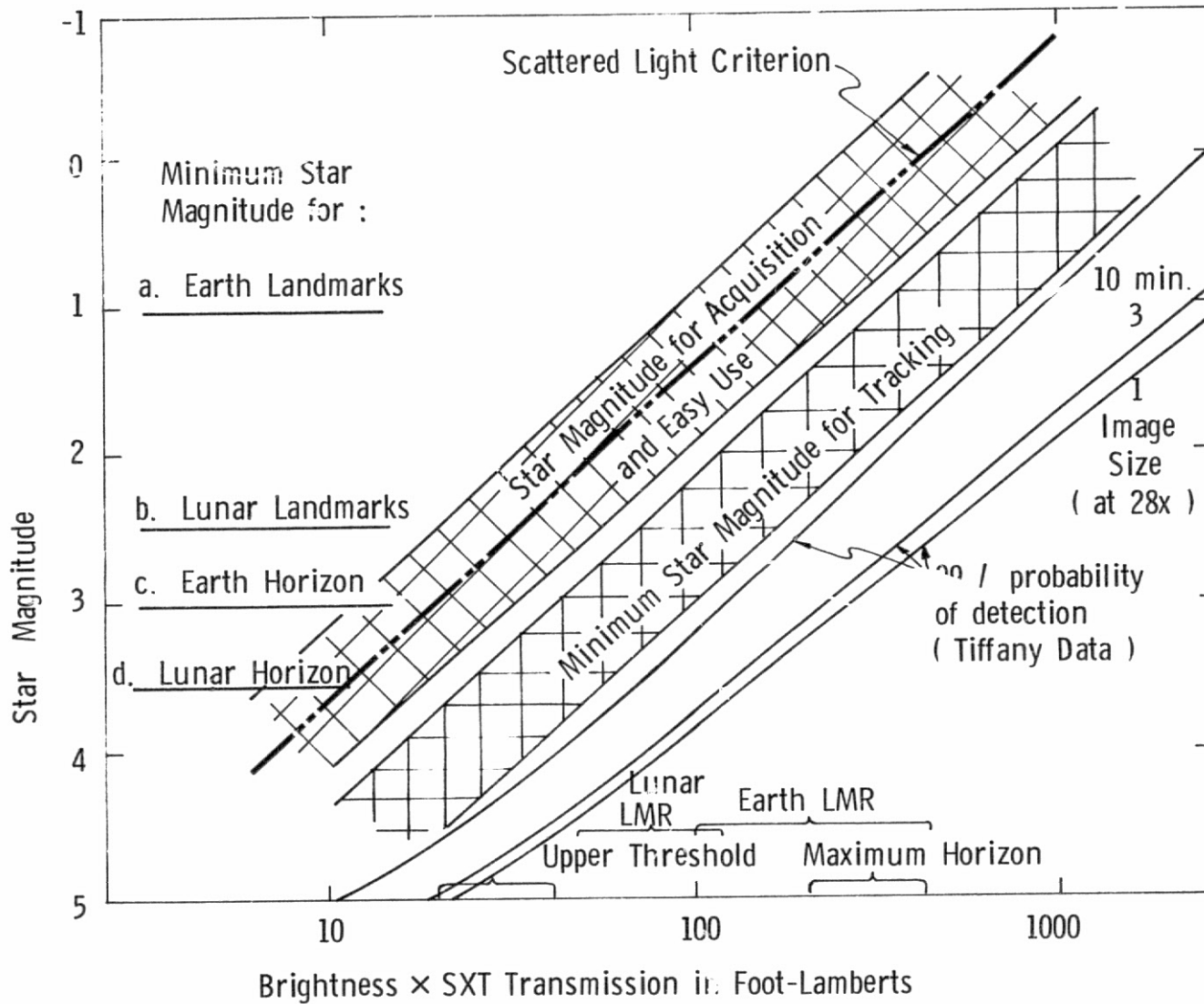


Fig. 6-10 Star Visibility Test Data

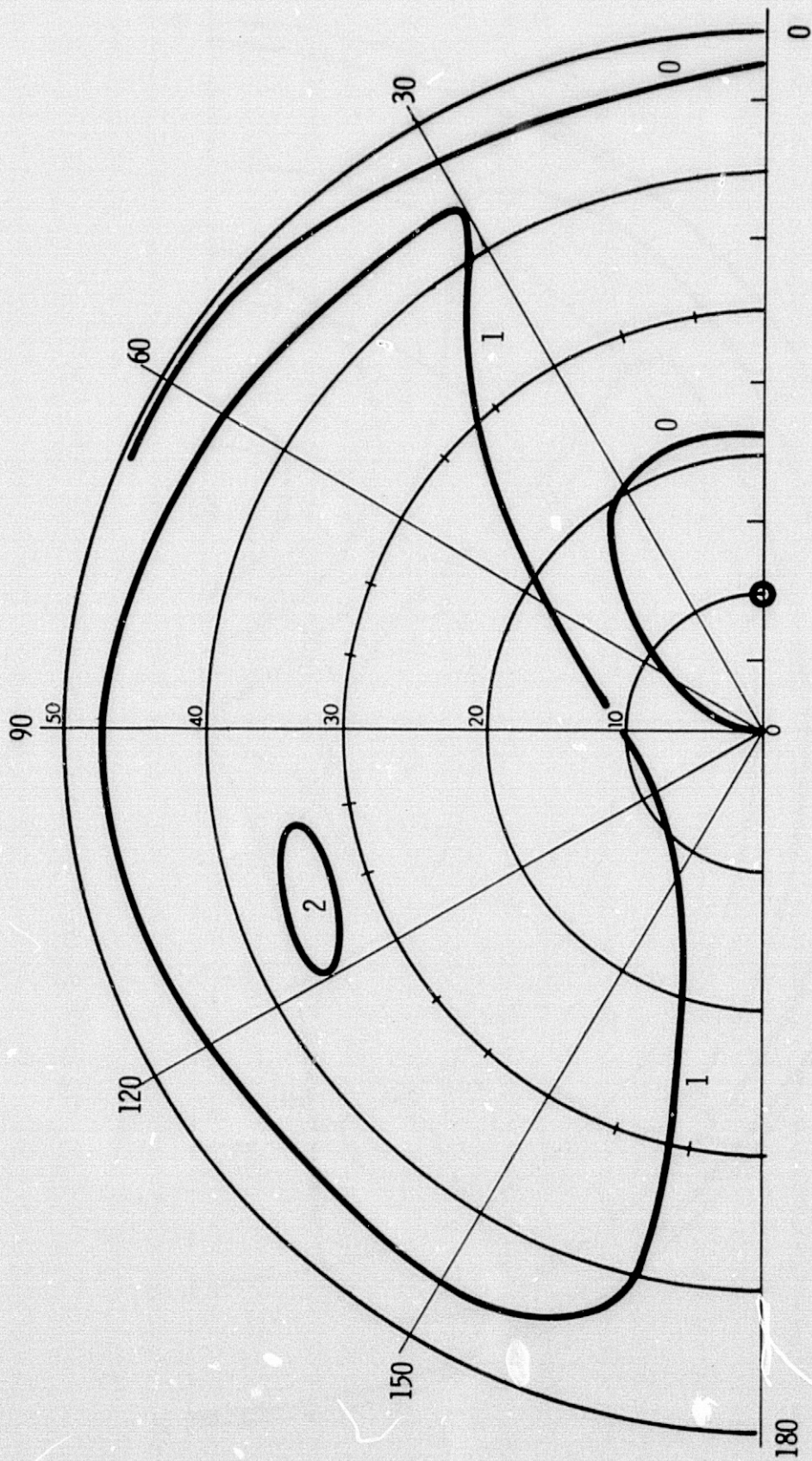


Fig. 6-11 Sextant Star Visibility Contours for Sun  $10^\circ$  from LLOS

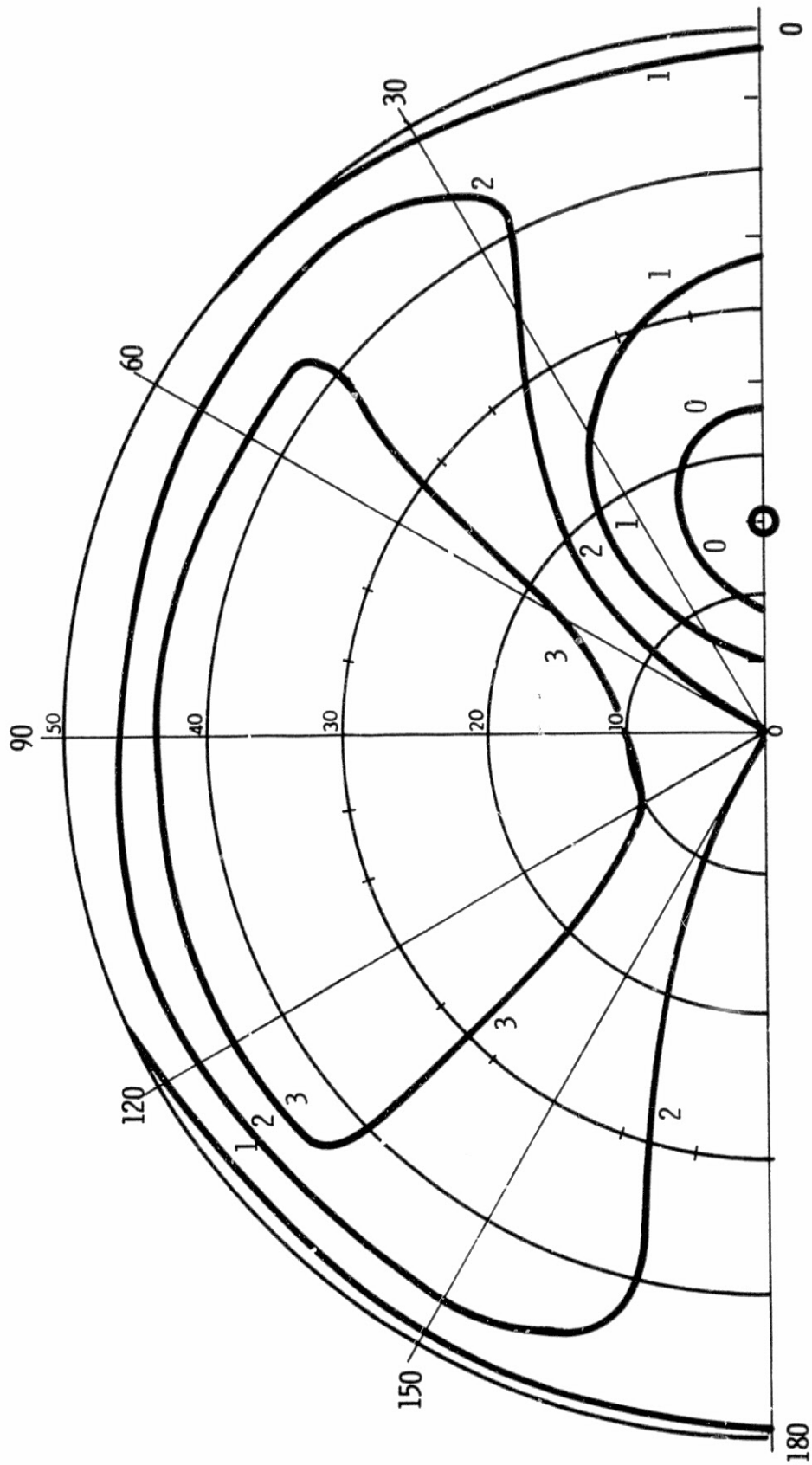


Fig. 6-12 Sextant Star Visibility Contours for Sun  $15^\circ$  from LLOS

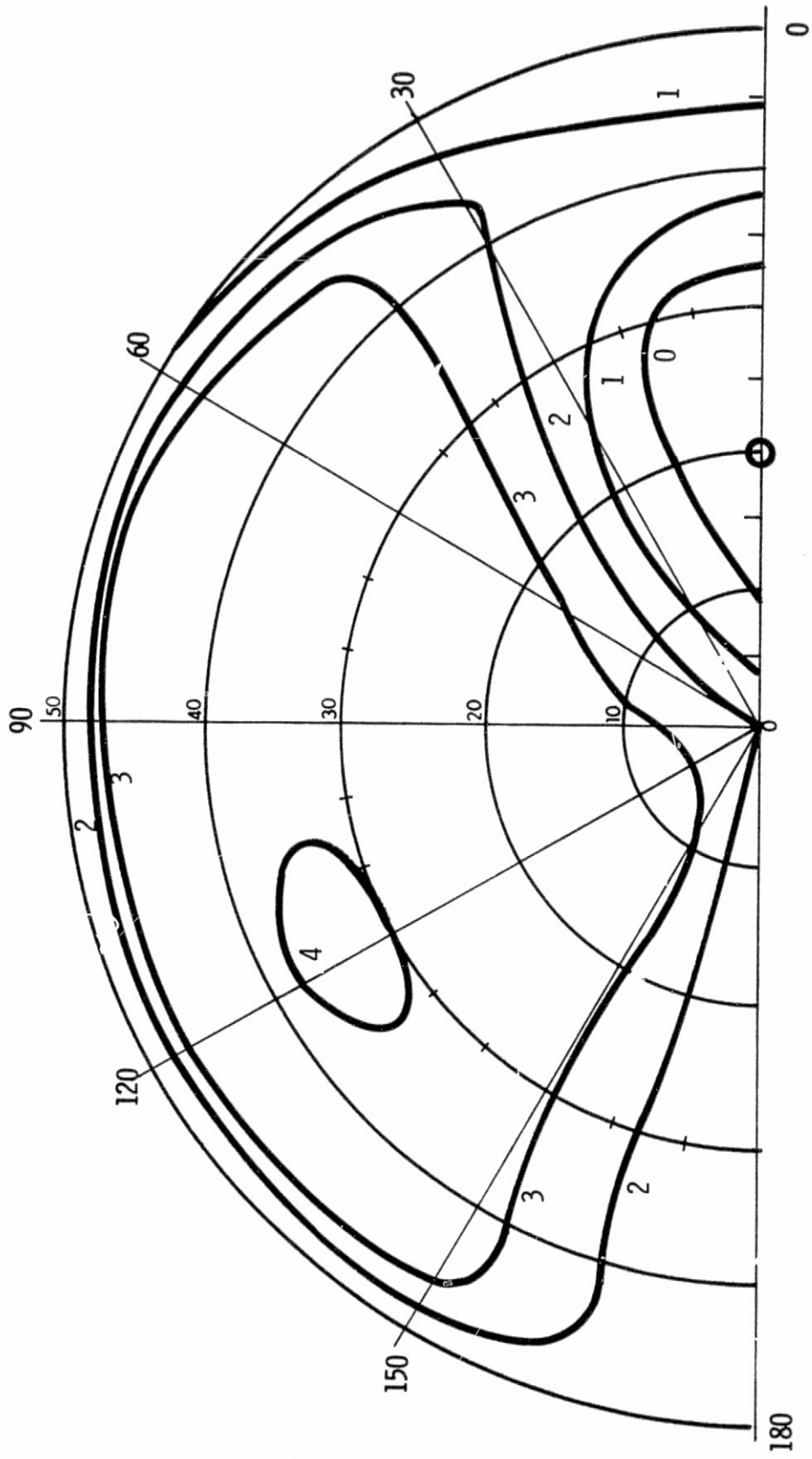


Fig. 6-13 Sextant Star Visibility Contours for Sun 20° from LLOS

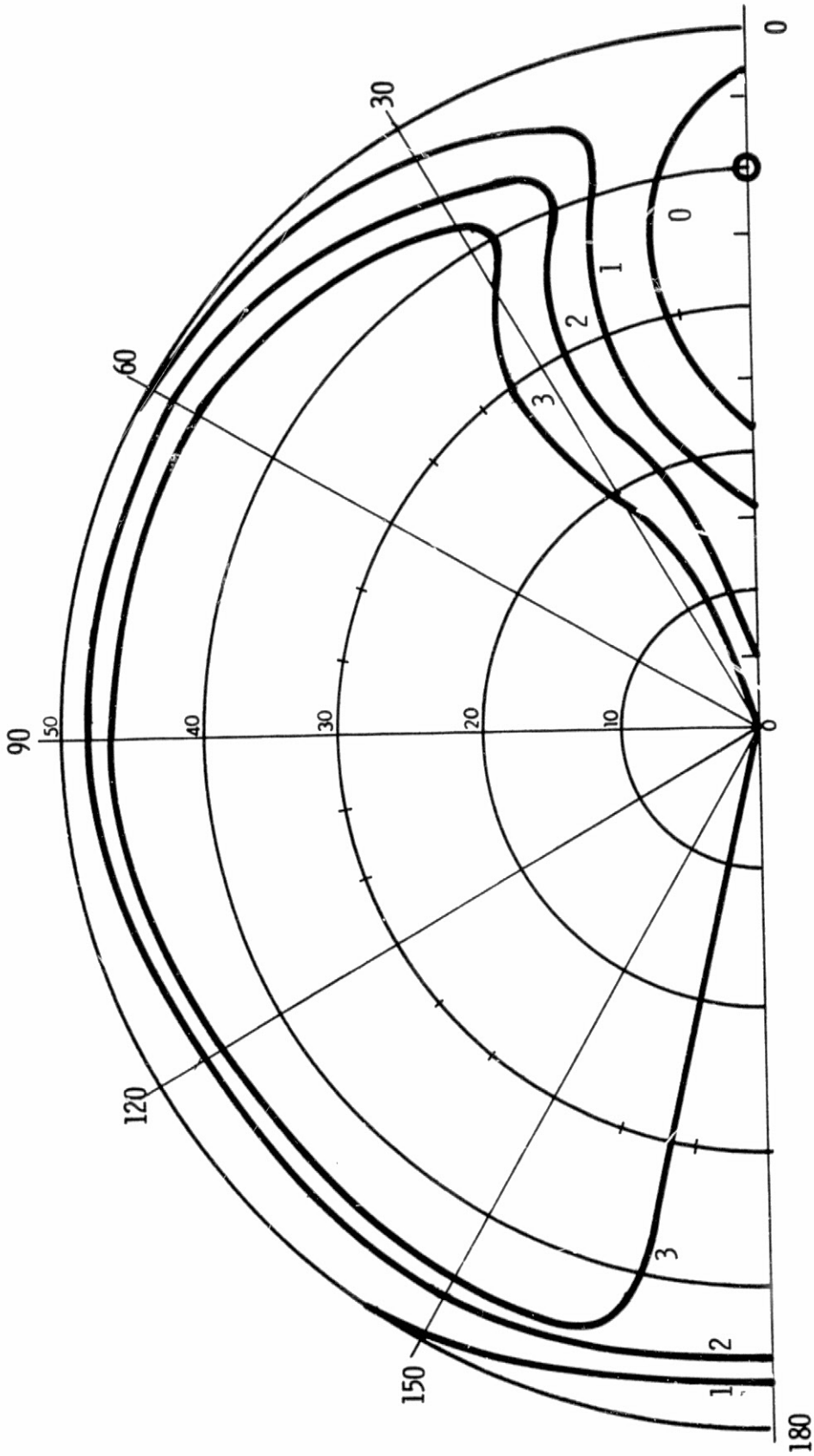


Fig. 6-14 Sextant Star Visibility Contours for Sun 30° from LLOS

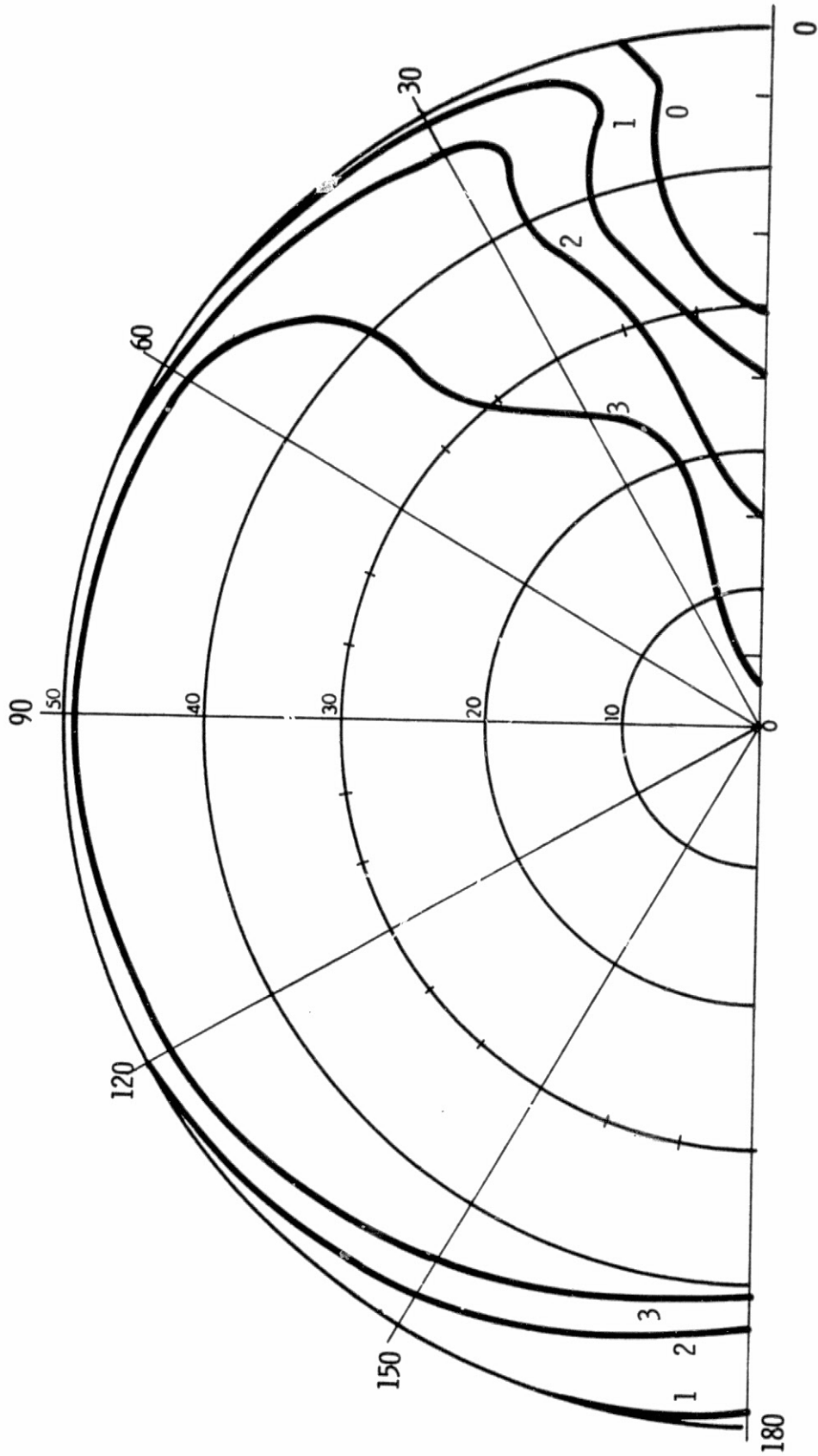


Fig. 6-15 Sextant Star Visibility Contours for Sun  $40^\circ$  from LLOS

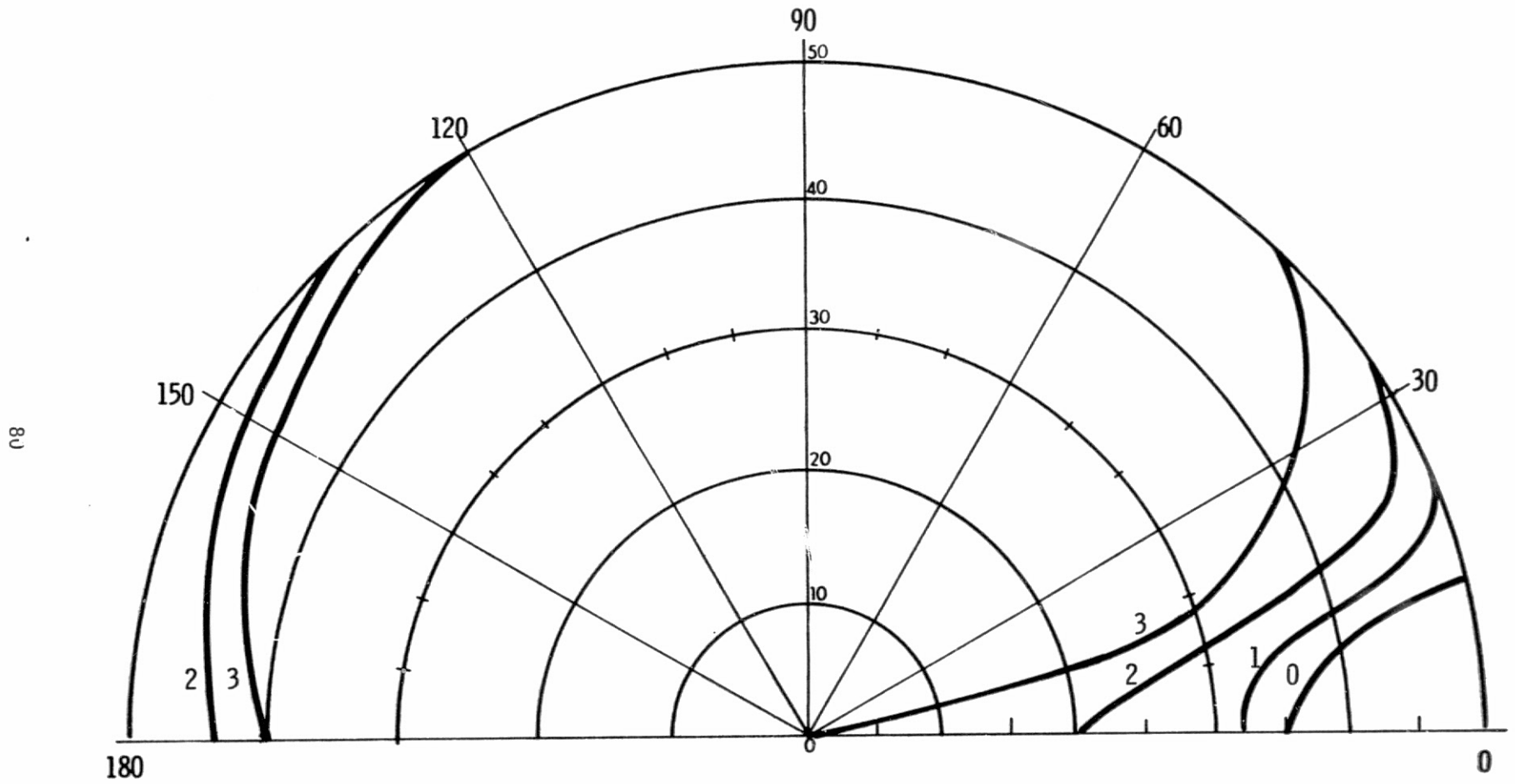


Fig. 6-16 Sextant Star Visibility Contours for Sun  $45^{\circ}$  from LLOS

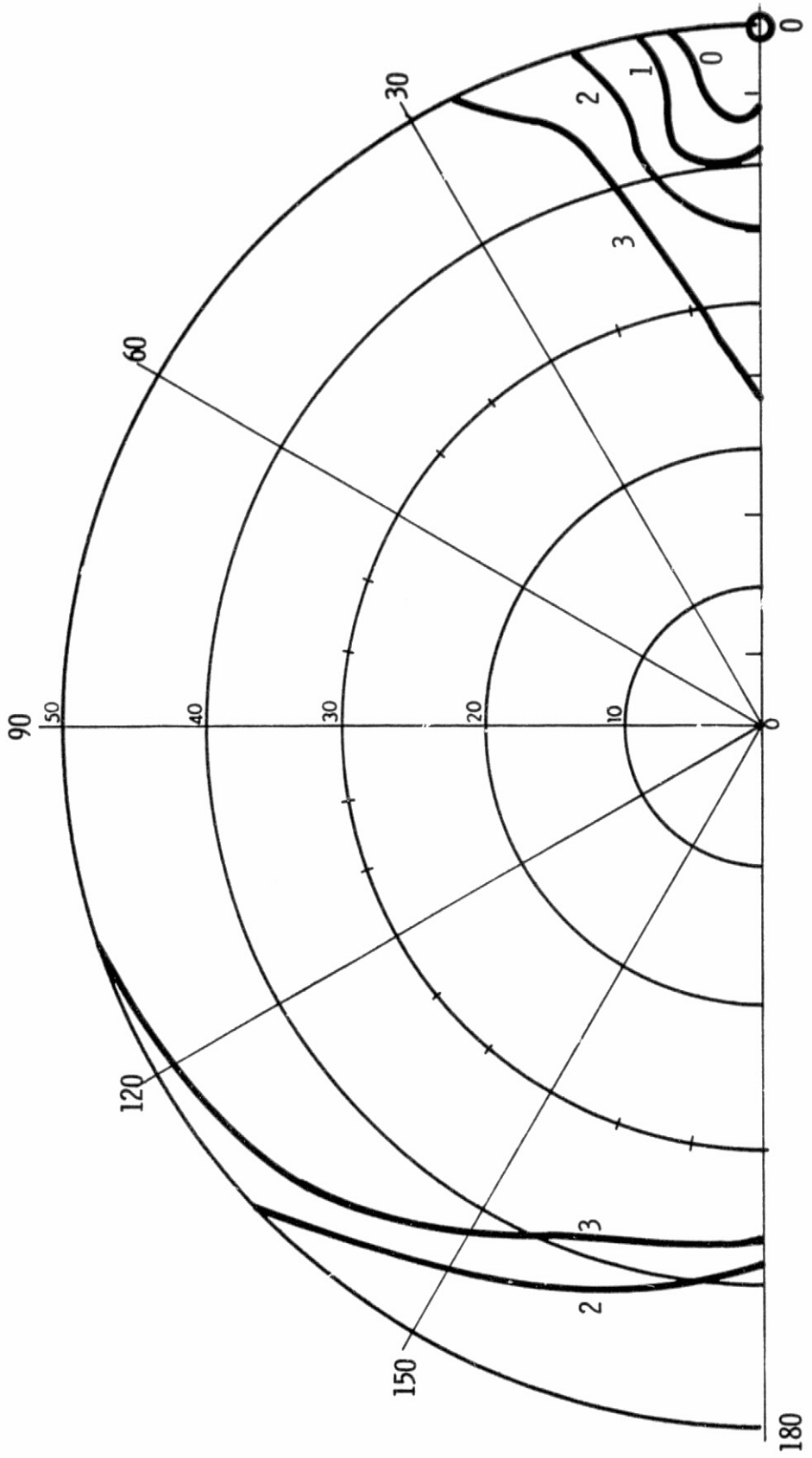


Fig. 6-17 Sextant Star Visibility Contours for Sun 50° from LLOS

second, conventional photometric units are difficult to apply since the scattered light is not focused at any image plane in the optics path and does not pass through the normal exit pupil. The data were calibrated by star visibility tests similar to those described in Section 6.2.6.

### 6.3 POSTFLIGHT MEASUREMENT EVALUATION

Figure 6-18 shows the schedule of cislunar midcourse navigation measurements, computer program P23, for the G-Mission (APOLLO 8) plotted on a diagram of the translunar and transearth trajectories. Fifteen state vector updates were scheduled in all: 2 early in translunar coast and 13 at intervals throughout the transearth return. Three marks were specified on each of three to five stars for each update, each mark requiring an individual P23 entry. In all, cislunar navigation during G-Mission transearth coast entailed 177 performances of P23, producing a total of 177 marks on 59 stars. (Note that one star in each sequence was usually marked on twice.) The figure gives the nominal time of each sequence of program activity, the decimal star code of each 3-mark star-horizon measurement in the sequence, three initials (e.g., NEH, FEH, signifying near-earth horizon and far-earth horizon, respectively; NMH, FMH, signifying near-moon horizon and far-moon horizon) and the times of the three midcourse corrections that would have been computed onboard using the return-to-earth program, P37, had communications failed. (Note that, before taking measurement marks and at half-hour intervals while marks are being taken, it is necessary to calibrate the sextant optics to compensate for measurement errors due to trunnion bias.)

Figure 6-19 shows the change in perigee that resulted from a group of 15 sightings made on the lunar horizon at a distance of 45 000 n. mi. during the translunar leg of APOLLO 8. At the end of this group of measurements, the indicated perilune was 67.1 n. mi., about 1.8 n. mi. less than the value later reconstructed from Manned Space Flight Network radar data from earth. Perigees computed onboard using either the return-to-earth program or orbit parameter display, R30, should converge in the manner shown during a sequence of midcourse navigation star-horizon measurements, whether earth- or moon-centered.

ORIGINAL PAGE IS  
OF POOR QUALITY

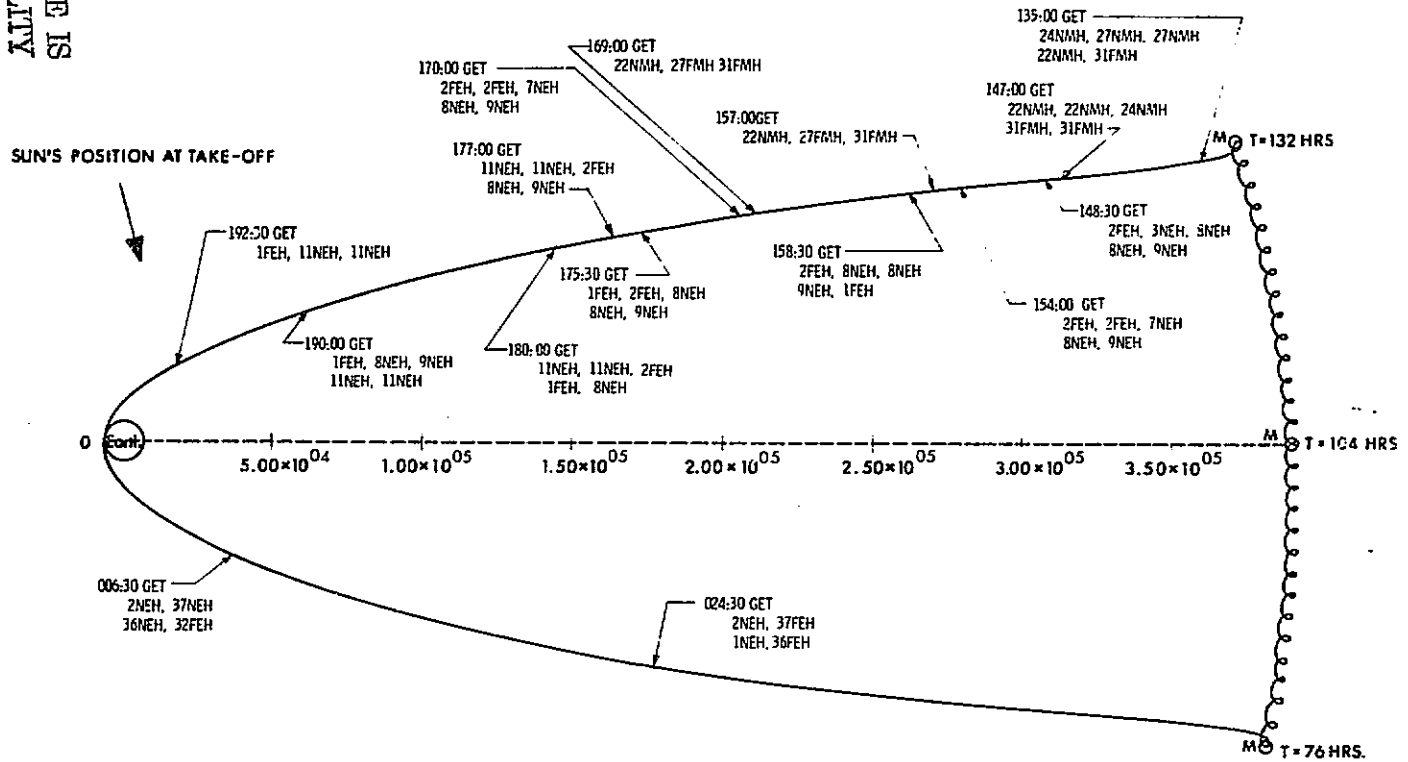


Fig. 6-18 P23 Activity for G-Mission Translunar and Transearth Trajectories

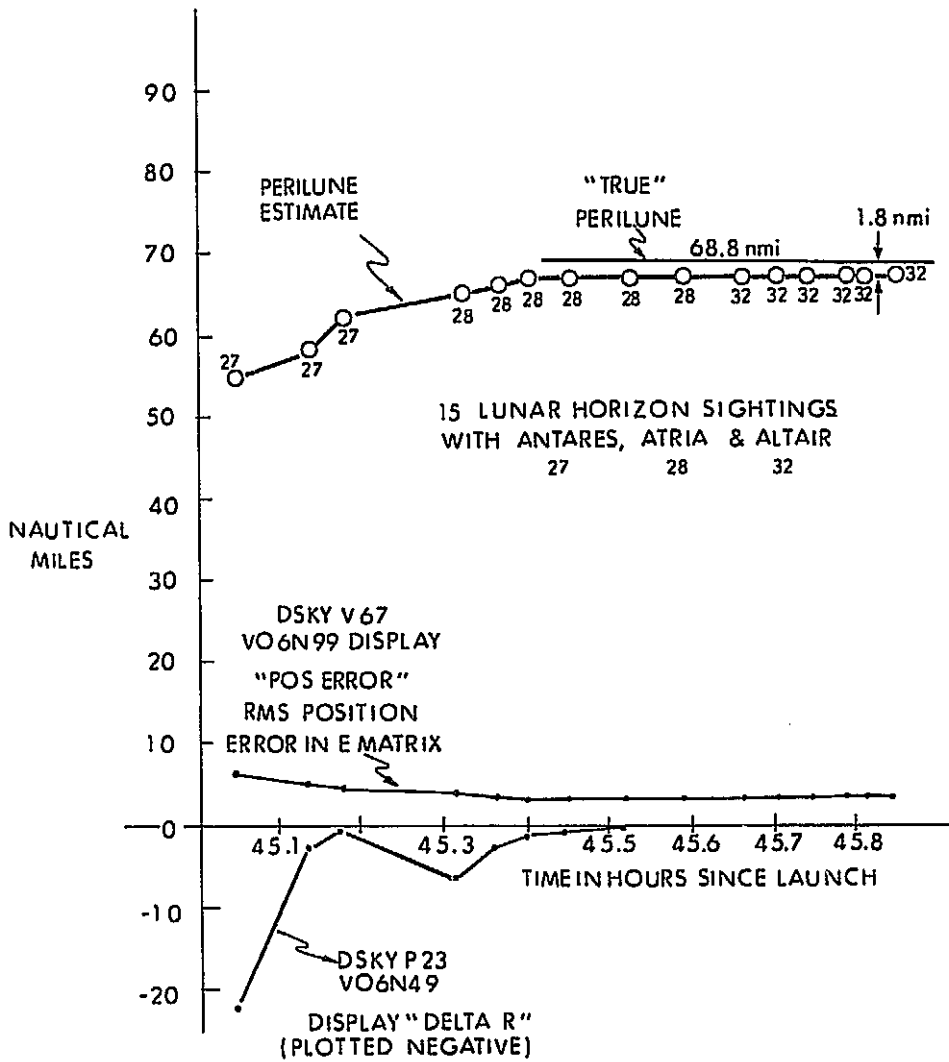


Fig. 6-19 Apollo 8 Translunar Midcourse Navigation

CHAPTER II  
RADAR SUBSYSTEMS

ACKNOWLEDGEMENT

The following individuals have contributed significantly to this chapter: Earle P. Blanchard, Leonard B. Johnson, William Saltzberg and Walter E. Tanner.

PRECEDING PAGE BLANK NOT FILMED

## CHAPTER II RADAR SUBSYSTEM

### SECTION 1.0 INTRODUCTION

The lunar mission relies on measurements from three independent radars, each of which interfaces with its respective Guidance, Navigation, and Control System for improvement of the vehicle state-vector estimate. The lunar module carries two radars: a landing radar (LR) for terminal guidance measurements during the powered descent and a rendezvous radar (RR) for tracking the command module in free-fall descent to the lunar surface and during ascent rendezvous. The command module is equipped with a VHF ranging system. These radar interfaces with the GN&C system involve both hardware and software in a relatively complex inter-relationship, the evolution and current status of which is described in subsequent sections. Table 1-I is a chronological listing of the milestones in radar development.

TABLE 1-I  
CHRONOLOGY OF HARDWARE DEVELOPMENT  
AND EQUIPMENT EVALUATION

June 1964 to March 1965	Development of landing radar simulator for use in the MIT/IL hybrid simulation. Two signal data converters were received in March 1965 from RCA, one for incorporation in the hybrid simulator and the other for preliminary evaluation of the landing radar data interface with the computer. The second unit was later transferred to Grumman.
July 1965 to March 1966	Evaluation of digital interface characteristics of landing and rendezvous radars. Prototype units of each digital interface were received from RCA in July 1965. The two units were later incorporated in a radar data input simulator for the lunar module guidance computer and installed in the System Test Laboratory.
March 1966	Design and assembly of test facility for playback of recorded landing radar signals and for processing of these signals through the radar electronic assembly and computer.

TABLE 1-I (Continued)  
CHRONOLOGY OF HARDWARE DEVELOPMENT  
AND EQUIPMENT EVALUATION

June 1966	Evaluation of the rendezvous radar's angle interface, using RCA's angle interface simulator, a stripped radar antenna with breadboard type servo circuits.
November 1966	Use of the landing radar prototype 2L for study of simulated signals. Recordings of signals were procured from Ryan Aeronautical. The 2L radar system was later used for recordings of tracker noise.
January 1967 to November 1967	Use of 4L landing radar for processing and evaluation of the 1966/67 flight test data.
June 1968	Adaption of landing radar digital data simulator for simulation of VHF ranging data. This simulator was used in October for COLOSSUS program evaluation.
August 1968	Use of 10L landing radar electronic assembly for evaluation of simulated radar signals.
November 1968	Evaluation of interface characteristics of the VHF interface circuits provided by RCA. These circuits were later incorporated in a simulator for command module software testing.
January 1969 to June 1969	Use of 10L and P32 landing radar electronic assemblies for evaluation of 1968 flight test data. The P32 radar was received on April 23, 1969.
February 1969	Integration of rendezvous radar routine R29 with the navigation system to study effects of gyro voting and of gyro failures.

## SECTION 2.0 ORIGINAL RADAR REQUIREMENTS

The present radar performance and interface characteristics reflect several basic system requirements that were defined in 1964 when NASA adopted the two-vehicle command-lunar module concept for the lunar mission. Two major mission premises at this early point in APOLLO development strongly affected radar requirements:

1. The vehicles should have a self-sufficient, onboard capability to perform their respective tasks.
2. The command module should have the capability of rescuing the lunar module from a clear orbit.

In practical terms, premise 1 required onboard sensors on the lunar module, both to assure successful rendezvous with the command module by continuous measurement of the relative state vector between the two vehicles, and to provide terminal guidance measurements in altitude and velocity with respect to the lunar surface for the necessary soft landing.

Satisfaction of the rendezvous sensor requirement was ultimately achieved through the present two-gimbal rendezvous radar. Initial consideration, however, was given to a radar design utilizing a body-fixed antenna that was pointed by attitude control of the lunar module. Such an arrangement, however, provided no opportunity for lunar module tracking of the command module from the lunar surface, thus failing to fully satisfy the self-sufficiency ground rule. Subsequently, the concept of a two-gimbal tracking radar capable of range, velocity, and angle measurements evolved and was adopted to meet this requirement. This two-gimbal concept became the rendezvous radar specification. An identical radar was specified for the command module to satisfy the requirement that this vehicle be able to rescue the lunar module.

To satisfy premise 1 for the lunar landing, several terminal guidance sensors were originally considered. However, the most promising candidates were a laser ranging system pointed at the intended site during the powered descent, and a combined radar altimeter and velocity sensor. The eventual choice of a landing radar approach was based primarily on the then much more highly developed and demonstrated radar state-of-the-art compared to the relatively new laser technology, as well as on the less critical pointing requirements of a landing radar system.

In regard to the command module, reconsideration of mission requirements and hardware problems in later periods of APOLLO development led first to the removal of the command module rendezvous radar, then ultimately, to the restoration of a radar capability in the form of a VHF ranging system. This arrangement was backed up by the optical subsystem and command module computer for the rendezvous function.

## SECTION 3.0 EVOLUTION OF THE RADAR SPECIFICATION

Initial specification of the APOLLO radars for MIT/IL purposes was based on the results of early mission analysis at MIT/IL and on an appreciation of the performance limits of radars that could be developed to meet the program schedule. The specification task was complicated by the fact that the radars were to provide measurements to several users, including the astronauts, and would have to meet performance requirements satisfying other systems in addition to the GN&C system.

The first documented statement of radar requirements and specifications at MIT/IL was made in APOLLO Report R-404 which defined operating limits and general performance requirements, and specified the electrical interface characteristics between radars and the GN&C system for both vehicles.<sup>1</sup> The report defines the two-gimbal tracking capability of the rendezvous radar and the multi-beam landing radar, both of which are easily recognized in their final implementation on flight-qualified spacecraft.

Complementing and expanding the general requirements described in R-404 were a series of interface control documents (ICDs) negotiated between MIT/IL and the respective vehicle prime contractors. The purpose of the control documents was to define the physical, electrical, and functional characteristics of the interfacing systems in sufficient detail to permit the various contractors to proceed independently with the design, development, and testing of the system elements.

To make possible the opportunity for a lunar landing prior to 1970, development of the APOLLO hardware and evolution of the ultimate mission plan proceeded simultaneously during the 1960's. The criteria for hardware were therefore originally based on very early mission analyses and concepts likely to be modified by later refinements. To provide a relatively stable design basis for detailed definition of radar requirements, particularly in the area of utilization and function of the radars, MIT/IL assembled and published two documents that greatly expanded the information presented in R-404, and that effectively defined a reference mission for use of the radars in an onboard automatic guidance, navigation, and control context for the

---

1. See Vol. I, Appendix A, Abstracts, R-404.

lunar mission.<sup>2</sup> These two documents (E-1903 and E-1904) specified the radar characteristics necessary for support of the GN&C system during lunar descent, stay, and ascent. The specifications were predicated on mission plans described both in R-404 and R-446.<sup>3</sup>

Although E-1903 and E-1904 did not become controlling documents directly, they illustrated the need for an inclusive, definitive, radar-interface control specification, reviewed and approved by NASA. Reports E-1903 and E-1904 subsequently served as the basis for the radar portions of the "Lunar Module Primary Guidance, Navigation, and Control Subsystem, Equipment Performance and Interface Specification," Grumman document LSP-370-3A, approximately 30 percent of which is devoted to specification of the rendezvous and landing radar interfaces with the GN&C system. The interface between the VHF ranging system and the command module computer is similarly defined in a North American Rockwell document, based on mutual negotiation of interface requirements between MIT/IL and North American for subsequent review and approval by MSC. Both performance and interface specifications also incorporate all interface control documents by reference.

---

2. See Vol. I, Appendix A, Abstracts, E-1903 and E-1904.

3. See Vol. I, Appendix A, Abstracts, R-404 and R-446.

## SECTION 4.0 RENDEZVOUS RADAR (RR)

### 4.1 RADAR FUNCTIONAL REQUIREMENTS

The primary task of the rendezvous radar is to measure range, range rate, and line-of-sight (LOS) angle information with respect to the transponder on the command module and furnish it to the GN&C system. The rendezvous radar is capable of providing data during all mission phases, except when the lunar module is attached to the command module and during the powered descent.

During ascent and rendezvous, the GN&C system uses the radar data to update or improve the estimated value of the lunar and command modules relative velocity and position vectors (state vectors). At other times, rendezvous radar data are used for comparison with measurements from other independent sources, such as the lunar module abort guidance system (AGS), the command module VHF ranging system, or Manned Space Flight Network (MSFN) data, for subsystem failure detection. During the docking phase, rendezvous radar measurements are employed by the lunar module crew to facilitate the critical maneuvers prior to hard contact. The rendezvous radar is operated either with the lunar module guidance computer or in a manual mode under crew control.

The GN&C system is capable of angle-designating the rendezvous radar antenna to the predicted command module line of sight, and issuing the auto angle-tracking enable signal when the indicated line of sight is within 0.5 degree of the computed target position. In addition, the GN&C system protects against rendezvous radar sidelobe acquisition within electrical tracking limits, and slews antenna gimbals from one angular coverage mode to another. The angle reference interface between the rendezvous radar and the GN&C system is at the navigation base, with all radar angle data referenced to this interface.

### 4.2 OPERATING LIMITS

The operating limits of the rendezvous radar are based on mission plans and requirement analyses described in R-404 and R-446, which assumed an 80 n. mi. command service module lunar orbit during rendezvous radar tracking from the lunar surface, and a direct ascent for the lunar module in rendezvous. Some of the

limits, such as the 400 n. mi. maximum radar range, were predicated on satisfaction of abort requirements. Full specification of the operating limits is given in Grumman document LSP-370-3A. However, the following are among the more important limits.

Operational range . . . . . 500 ft to 400 n. mi.  
Range rate . . . . .  $\pm 4900$  ft/sec  
Range acceleration . . . . .  $50 \text{ ft/sec}^2$  for lunar overfly  
LM angular velocity . . . . . 10 deg/sec per axis with degraded  
dynamic angle accuracy;  
1 deg/sec per axis with full angular  
accuracy

The flight plan for the actual lunar landing mission differed from the reference mission of R-446 in two principal ways: first, the command module lunar orbit altitude was 60 rather than 80 n. mi. as originally assumed; and second, the ascent rendezvous followed a concentric flight plan rather than a direct ascent. These changes served to expose the rendezvous radar to slightly greater velocity and acceleration limits than originally specified, and to increase somewhat the total operating time of the radar during rendezvous. However, ample design margins made possible the safe extension of radar operating limits to meet the needs of the actual lunar landing mission plan.

#### 4.3 ANGULAR COVERAGE

The rendezvous radar antenna is mounted on the inner gimbal of a two-axis gimbal system as shown in Figure 4-1. This design provides the necessary capability for angle-track of the target transponder within wide angular limits despite variations of the line of sight with respect to the spacecraft, both during free-fall of the lunar module and during the command module overfly of the landed lunar module. The order of the gimbal system and its orientation with respect to the lunar module permit controlled tracking through the zenith, in anticipation of lunar module tracking of the command module from the lunar surface. For this reason, the pole of the gimbal configuration lies parallel to the Y axis of the lunar module.

Historically, the names assigned to the radar gimbal axes were influenced by command module sextant nomenclature. Early plans for the command module called for a radar mounted on the service module with radar gimbal order identical to that of the sextant and with axes correspondingly parallel. Thus, the rendezvous radar inner axis was named the trunnion axis and the outer axis was called the shaft axis. This radar gimbal order, however, was not suitable for landed lunar

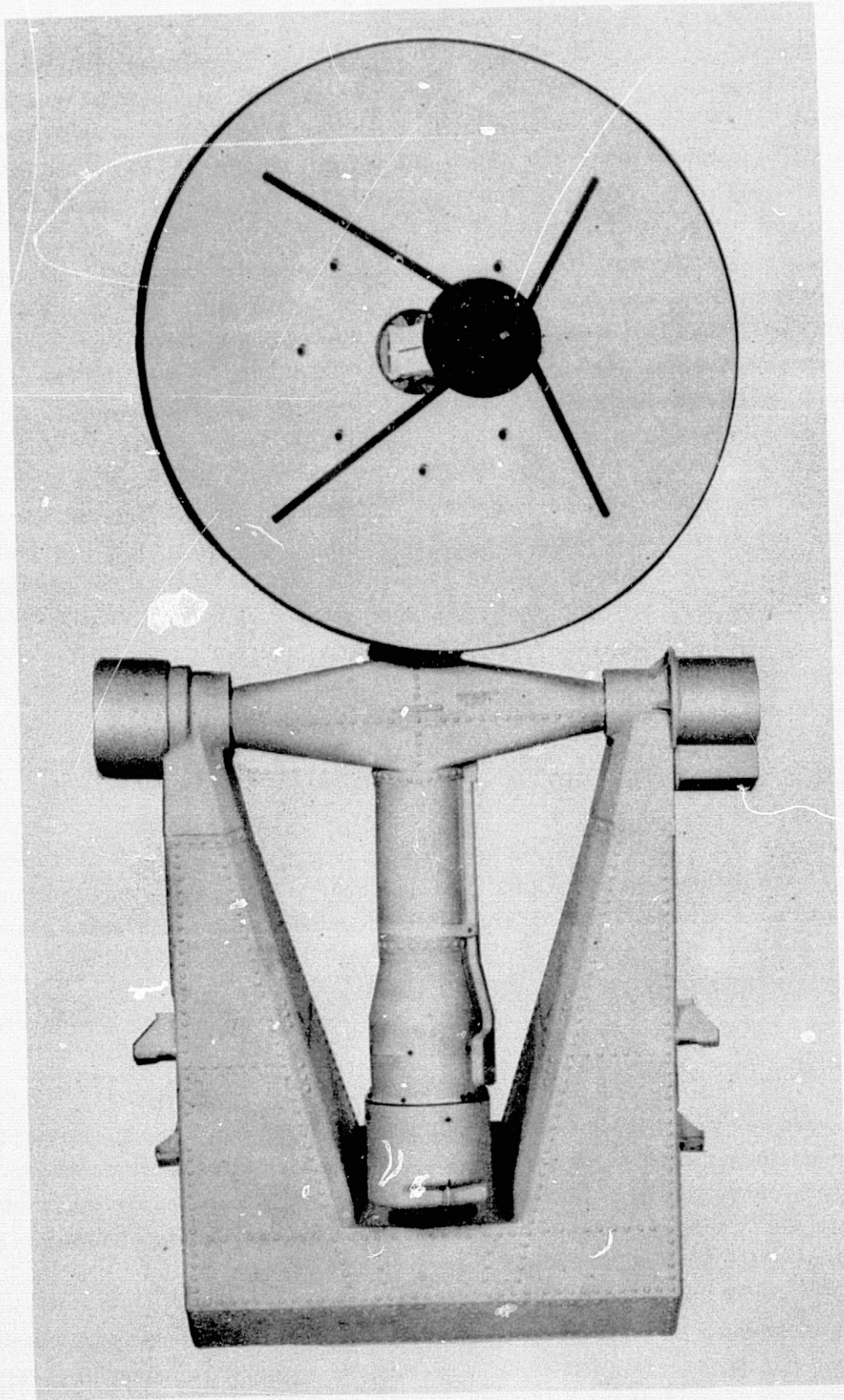


Fig. 4-1 Rendezvous Radar Antenna Assembly

module tracking of the command module overfly, and the rendezvous radar gimbal order was later reversed. However, use of the original radar gimbal terminology persisted. Thus, contrary to convention, the outer gimbal axis of the rendezvous radar, which is supported by the yoke of the antenna mounting pedestal, is referred to as the "shaft" axis, while the inner radar axis is designated "trunnion" axis.

From a purely mechanical standpoint, the double gimbal system allows wide antenna angle coverage over approximately three-quarters of a sphere. To avoid possible problems of gimbal-servo marginal stability, however, the region over which the rendezvous radar may be electrically positioned and controlled by the computer is somewhat more limited, and is achieved in two modes, as illustrated in Figures 4-2 and 4-3.

The rendezvous radar is constructed with mechanical stops to prevent the radar from inadvertent contact with the spacecraft in the regions of physical interference. The stops are of the energy absorbing variety, i.e., springs backed by hard stops. The sectors nominally occupied by the hard stops are indicated by the shaded regions in Figure 4-3. Shaft gimbal contact with the springs occurs approximately 5 degrees before the hard stop is encountered. In the shaft axis, the Mode 1 spring encounter angle is 60 degrees, while for Mode 2 the angle is 27 degrees.

#### 4.4 MEASUREMENT ACCURACY

The measurement accuracy of the rendezvous radar for purposes of automatic guidance, navigation, and control is specified in detail in Grumman Specification LSP-370-3A. A summary of measurement performance is given in Table 4-1.

#### 4.5 DESCRIPTION OF RENDEZVOUS RADAR

##### 4.5.1 Summary

The rendezvous radar (Figure 4-4) designed for the APOLLO mission is a lightweight, highly reliable and accurate space-stabilized continuous wave tracking radar that functions in moon, space, or earth environments, as well as in the presence of the reaction control system. In the lunar module, the rendezvous radar supplies data in three system modes of operation: Primary, Abort, and Manual.

In service, the radar is angle-designated to, and acquires coherently, its associated transponder in the command module, thereafter tracking it automatically. In the LGC mode, the radar supplies angle, digital range, and range rate data to the GN&C

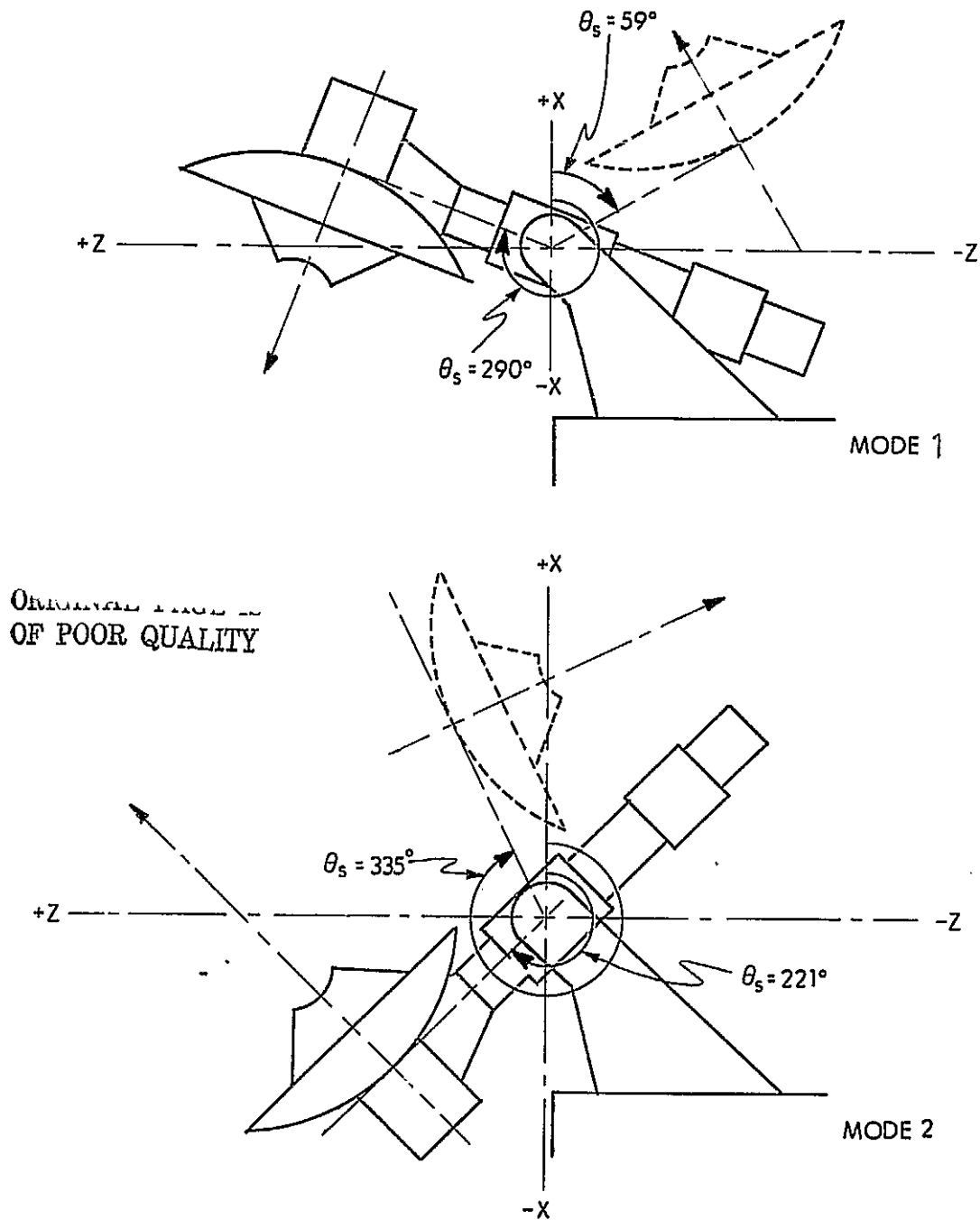


Fig. 4-2 Shaft Mode Limits Expressed in Shaft Resolver Angles

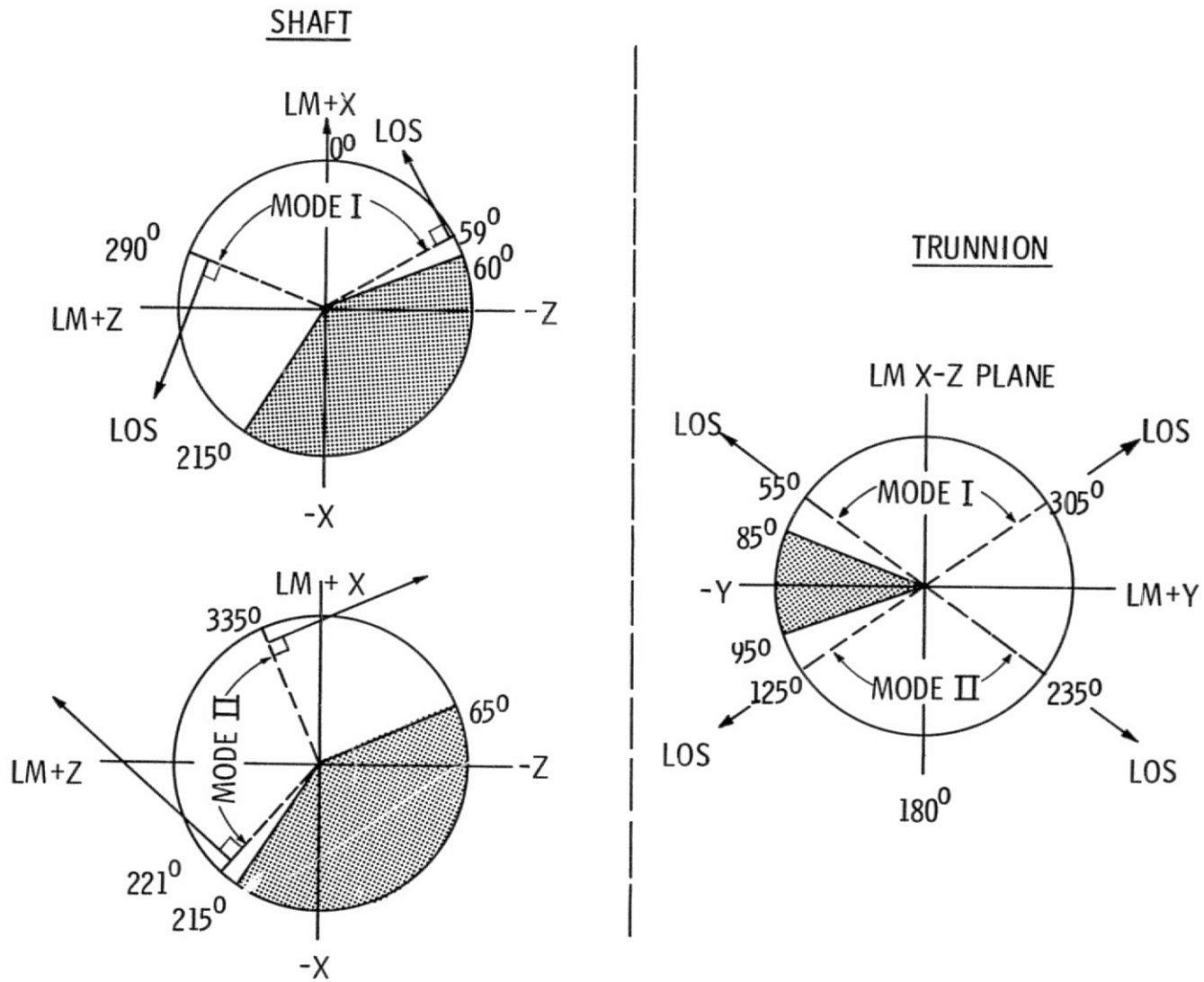
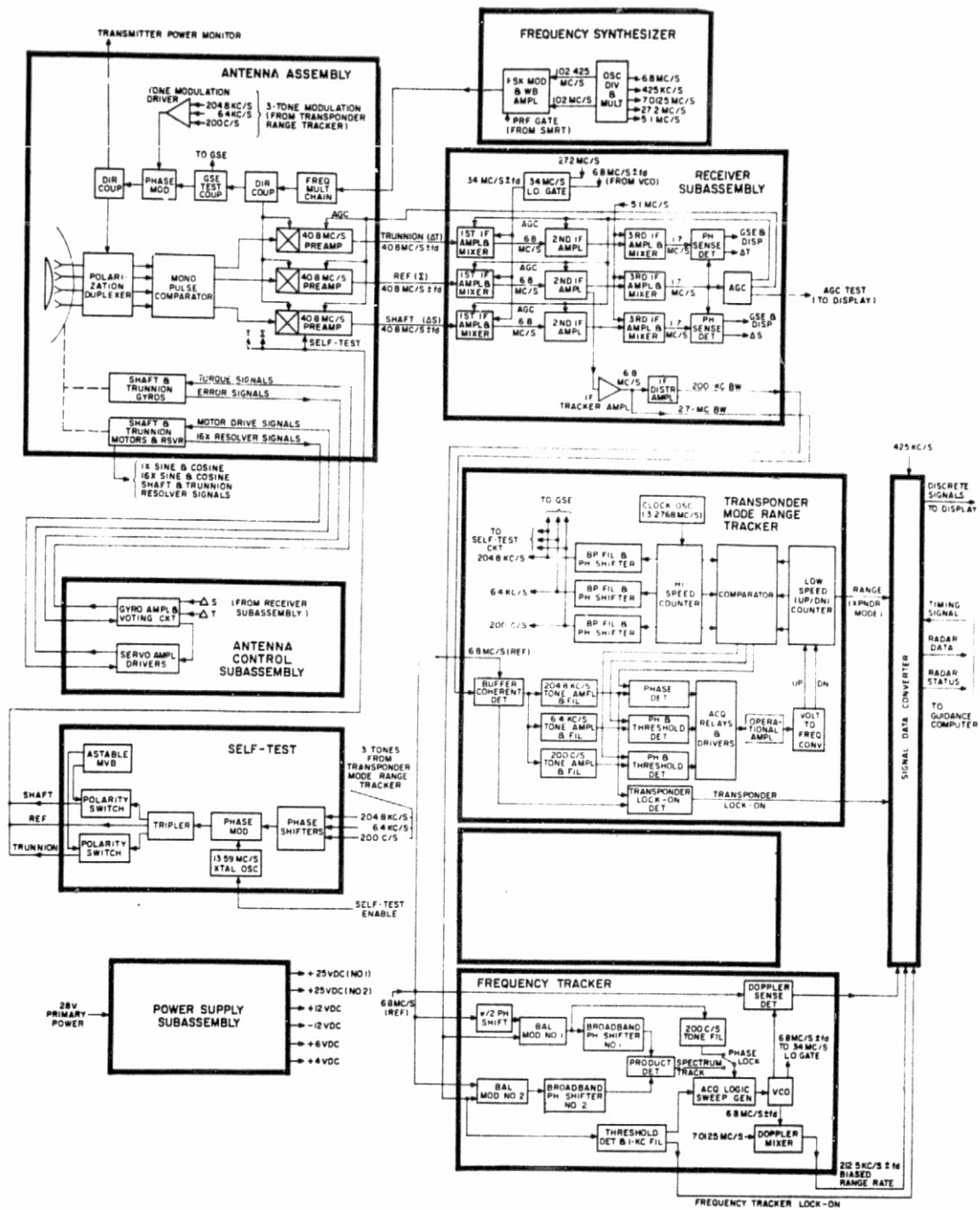


Fig. 4 3 Mode Limits and Hard Stop Locations Expressed In Resolver Angles



ORIGINAL PAGE IS OF POOR QUALITY Fig. 4-4 Rendezvous Radar Block Diagram

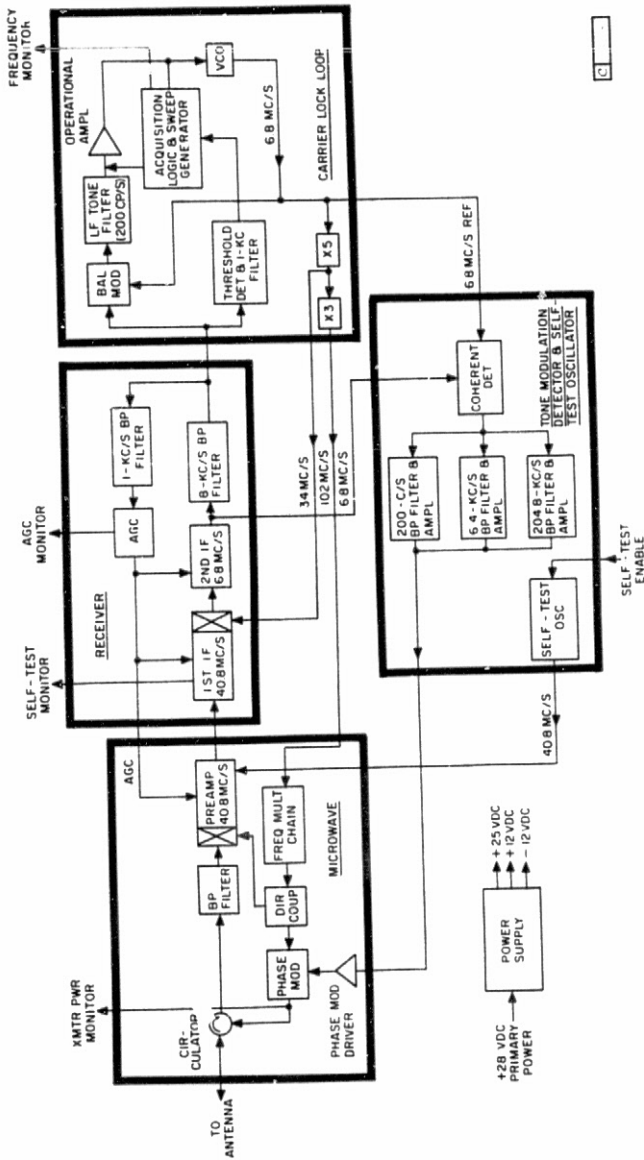


Fig. 4-5 Transponder Block Diagram

TABLE 4-1  
RENDEZVOUS RADAR MEASUREMENT ACCURACY

Parameter	Operating Interval	Error	
		3 $\sigma$ Random	Max. Bias
Range	400 n. mi. to 120 ft 400 n. mi. to 50.6 n. mi. 50.6 n. mi. to 80 ft.	1% of range or 80 ft	0.05% of range or $\pm 500$ ft.  $\pm 120$ ft
Range Rate	400 n. mi. to 80 ft	1.3% of range rate or 1.3 fps	$\pm 1$ fps
Angle (Vector sum of uncertainty in both axes)	400 n. mi. to 100 n. mi.  100 n. mi. to 5 n. mi.  5 to 1 n. mi.  1 n. mi. to 80 ft	<p style="text-align: center;">Linear decrease</p> (a)* 6.3 mr. to 5.8 mr. (b)* 4.8 mr. to 4.5 mr. (a) 5.7 mr. (b) 4.3 mr. <p style="text-align: center;">Linear increase</p> (a) 5.7 mr. to 11.0 mr. (b) 4.3 mr. to 8.2 mr. (a) 11.0 mr. (b) 8.4 mr.	System:           15 mr. (LM & RR)  RR only:           8 mr.

\* (a) For gimbal rate  $< 0.2^\circ/\text{sec}$

(b) For narrow-band limit cycle

system. In the Manual mode, these data and also inertial line-of-sight angular rate are supplied to the astronaut display panels.

#### 4.5.2 Rendezvous Radar Parameters

The following table lists significant radar parameters:

Radiation frequency . . . . .	9832.8 MHz
Received frequency . . . . .	9792.0 MHz
Radiated power . . . . .	300 mW
Antenna design . . . . .	Cassegrain
Tracking method . . . . .	Amplitude monopulse
Antenna diameter . . . . .	24 in.
Antenna gain . . . . .	32 dB
Antenna beamwidth . . . . .	3.25—4.0 degrees
Antenna sidelobe level . . . . .	-13 dB adjacent to main lobe
Angular coverage . . . . .	±70 by 225 degrees
Number of gyros . . . . .	4 (2 redundant)
Modulation . . . . .	Phase Modulation by 3 tones: 200 Hz, 6.4 kHz, 204.8 kHz
Receiver channels . . . . .	3
Receiver noise figure . . . . .	10 dB max.
Receiver intermediate frequencies	40.8 MHz, 6.8 MHz, 1.7 MHz
Unambiguous maximum range . . . . .	405 n. mi.
Minimum range . . . . .	50 ft
Maximum range rate . . . . .	±4900 ft/sec
Range data output . . . . .	15 bit serial format
Range scale factor . . . . .	(400 to 50.6 n. mi.)—75.04 ft/bit
Range scale factor . . . . .	(50.6 n. mi. to 50 ft)—9.38 ft/bit
Range rate scale factor . . . . .	-0.6278 ft/sec/bit
Power consumption (while tracking) . . . . .	170 W
Weight . . . . .	77.5 lbs

#### 4.5.3 Operation

The rendezvous radar is designed to track a cooperative transponder. The radar and the transponder each use varactor semiconductors as the multiplier and transmitting elements. Due to the high duty cycle characteristics of varactor multipliers, transmission and reception are on a CW basis for achievement of range performance. Gyros on the rendezvous radar antenna stabilize the line of sight against the effects of lunar module body motions, and permit accurate measurements of line of sight angular rate.

Angle tracking is accomplished by using the amplitude-comparison monopulse (or simultaneous lobing) technique to obtain maximum angular sensitivity and boresight accuracy. Range rate is determined by measuring the two-way Doppler frequency shift on the signal received from the transponder. Range is determined by measuring the time delay between the transmitted signal's modulation waveform and the received signal's waveform.

#### 4.5.4 Antenna

The rendezvous radar antenna assembly includes not only the usual microwave radiating and gimbaling elements, but other internally mounted electrical components including gyros, resolvers, multiplier chain, modulator, and mixer-preamplifiers. In lieu of microwave transmission elements such as waveguides and rotary joints, flexible low-frequency coaxial cables connect the outboard antenna components to the inboard electronics assembly. Flexible cable is used at each of the rotary bearing points.

The antenna is of the four-horn amplitude-comparison monopulse configuration. The Cassegrain type antenna is used to minimize the total depth of the antenna structure. The antenna transmits and receives circularly polarized radiation to minimize the signal variations resulting from attitude changes of the linearly polarized transponder antenna. Components are distributed inside the antenna to achieve balance around each axis. Each axis is controlled by a brushless servomotor that is driven by pulse-width modulated drive signals.

Four rate-integrating gyros are used for space stabilization and angle-rate measurement of the line of sight. They are located in the lower section of the trunnion axis to act as a counterweight. Only two of the gyros are used at any one time and a voting logic system, not located on the antenna, transfers control to the other two gyros in the event of a failure in either of the two gyros being used. The voting logic system compares the two active and one of the redundant gyro outputs. A two-speed resolver is mounted on each axis for high accuracy angle-data pickoff for the computer and for display.

The multiplier chain, phase-modulator, and mixer-preamplifiers are mounted internally behind the antenna dish. The multiplier chain supplies X-band power for radiation and local oscillator excitation. This is made possible by the fact that the transponder replies with a frequency side-step equal to the first IF of the radar. The heat dissipated by the multiplier chain is radiated back into space by the dish. The phase modulator employs a ferrite rod that is mounted inside the waveguide.

An externally mounted solenoid stresses the magnetic field in the rod. The ranging tone signals are then applied to the solenoid, varying the electrical length of the rod to phase-modulate the X-band carrier. Three balanced mixers and three preamplifiers are included in the antenna assembly, one for each of the three channels: reference, shaft error, and trunnion error.

#### 4.5.5 Receiver

The receiver is a highly stable three-channel, triple-conversion superheterodyne. It has intermediate frequencies of 40.8, 6.8, and 1.7 MHz. The bandwidth of the first and second IF amplifiers is approximately 3 MHz and the bandwidth of the third IF amplifier is approximately 1 kHz. Two channels are provided for amplifying the shaft and trunnion axis error signals and one channel is provided to amplify the sum or reference signal. The receiver also includes phase-sensitive detectors for generating angle error signals, an AGC circuit for controlling the gain of the three receiver channels, an IF distribution amplifier unit for supplying reference channel signals to range and frequency trackers, and a gated local oscillator-mixer for generating the second local oscillator signal. The second local oscillator frequency is obtained by beating the frequency-tracker voltage-controlled oscillator output with a reference frequency to produce a sum frequency exactly 6.8 MHz lower than the incoming 40.8 MHz Doppler-shifted frequency. After the second mixer, the Doppler frequency is removed and all subsequent signal processing is accomplished at fixed carrier frequencies. The most stringent requirement on the receiver is that the three channels must gain-track within  $\pm 2.5$  dB and phase-track within 27 degrees over a dynamic range greater than 70°C.

#### 4.5.6 Frequency Synthesizer

The frequency synthesizer generates all the fixed frequencies required for coherent signal transmission and reception. A single 1.7-MHz stable crystal oscillator and a system of multiplication, division, and mixing are used to produce the required frequencies, including a CW output signal for excitation of the transmitter multiplier chain. The synthesizer also generates various receiver, local oscillator, clock, and reference frequencies used by the receiver, the signal data converter, and the trackers.

#### 4.5.7 Frequency Tracker

The frequency tracker tracks the coherent narrow-line spectra received from the transponder by phase-locking the voltage-controlled oscillator (VCO) with the

incoming narrow-line spectrum. The phase detector for the phase-locked loop uses a 6.8-MHz signal from the frequency synthesizer as a reference. The error signal drives the oscillator to such a frequency that, when it is used as a local oscillator signal for the second IF mixer after being mixed with a 27.2-MHz synthesizer signal, it removes the Doppler frequency shift from all signals in succeeding IF stages and ensures passage of the signal through the 1.7-MHz filters. These filters have a bandwidth of 1 kHz. The tracker employs a frequency sweep circuit for sweeping the oscillator frequency across the Doppler frequency range ( $\pm 100$  kHz) to search for the received signal. A threshold detector senses the presence of a carrier signal within locking range, stops the sweep, and permits the voltage-controlled oscillator to phase-lock.

#### 4.5.8 Range Tracker

The range tracker determines the range to the transponder by measuring the phase angle between the transmitted tones and the received tones. It operates in the following manner. The 6.8-MHz signal received from the transponder is demodulated in a coherent product detector that uses a 6.8-MHz quadrature reference. The individual sine-wave tones are extracted from the receiver noise using bandpass filters. Range phase delay is measured independently on each of the three tones in a closed tracking loop. Three reference square waves are locally generated, each having variable phase with respect to the transmitted tones. This phase delay is adjusted until the reference square waves have matching phase with respect to each of the received tones. The reference square waves are produced digitally by comparison between a running high-speed counter and a low-speed, forward-backward range counter. The low-speed range counter is driven forward or backward until phase null is achieved in each of three phase detectors. The range counter is then driven forward or backward by incremental range pulses obtained from a dc-to-PRF converter that is controlled by weighted integration of the three-phase detector error signals.

#### 4.5.9 Servo Electronics

The antenna servo electronics contain amplifiers for driving the antenna shaft and trunnion axis servomotors, amplifiers for driving the gyro torquer coils, and voting logic for selecting the correct gyro pair. The servo electronics, in connection with the antenna components and radar receiver, form an inner and outer closed loop for each axis. The inner or stabilization loop maintains the antenna boresight on the target, based upon tracking error signals from the monopulse receiver. In the angle designate mode, this loop is open and accepts the lunar module computer

designate data, which commands the antenna boresight to the target supplying an automatic track enable signal for the rendezvous radar when within 0.5 degree of the computed target line of sight. This signal, together with frequency lock-on, closes the tracking loop. The antenna continuously tracks the target by maintaining the monopulse receiver angle error signals at null. The antenna may also be slewed manually at fixed inertial rates. The enable signal necessary to close the auto track loop is supplied by a manual switch in Manual mode.

The antenna shaft and trunnion motors are 32-pole, brushless, permanent-magnet rotor types driven by pulse-width modulated drive signals applied to the sine and cosine windings of each motor. Reversal of the direction of rotation is accomplished by reversing the motor windings across the pulse-width modulated drive voltage obtained by on-off switching of the 28-Volt dc power at a 1.8-kHz rate.

A gyro voting system, consisting of performance comparison and logical switching circuits, automatically detects and removes a malfunctioning gyro. Of the four gyros, two are used to stabilize the antenna. Each pair can perform the control function. The voting system determines whether the active pair contains a failed gyro by comparing the output of each of the active pair and one of the redundant pair. If a failure or degradation occurs, the other pair is switched in to stabilize the antenna.

#### 4.5.10 Signal Data Converter

The signal data converter accepts range and range rate data from the range and frequency trackers for conversion to the 15-bit serial format required by the computer. Data are shifted out to the computer on range or range rate output lines on command. The rendezvous radar also sends various discrete radar status indications to the computer, selects radar modes, and processes display data for activation of the astronaut display panels.

#### 4.5.11 Self-Test

Radar self-test circuits are located in the frequency tracker subassembly. These circuits permit testing of the radar without a cooperating transponder. The self-test circuit permits a check of transmitter power, phase-lock at minimum signal level, angle error detection, AGC action, and range and range rate measurement. Insertion of single values of range and range rate permit quantitative checking via the displays.

## 4.6 TRANSPONDER

### 4.6.1 General

The transponder (Figure 4-5) receives the rendezvous radar's transmitted CW signal and generates a phase-locked reply signal for transmission back to the rendezvous radar. The ranging modulation on the received signal is also retransmitted to the radar. The transponder, like the radar, uses a single multiplier chain for transmitter and local oscillator. This is made possible by designing the transponder to reply with a carrier frequency exactly  $240/241$  times the received carrier frequency, which results in a transmitted frequency 40.8 MHz lower than the received frequency. A small portion of the transmitter output is used for local oscillator excitation, resulting in a first IF of 40.8 MHz. Since the transmitted and received frequencies are separated, use of a duplexer permits operation with a single antenna.

### 4.6.2 Transponder Parameters

The following table lists the significant parameters of the transponder:

Received frequency . . . . .	9832.8 MHz
Radiated frequency . . . . .	9792.0 MHz
Radiated power . . . . .	300 mW
Modulation . . . . .	PM by 3 tones 200 Hz, 6.4 kHz, and 204.8 kHz
Weight . . . . .	15.2 lb

### 4.6.3 Operation

The transponder phase-lock operation is as follows. The carrier signal from the rendezvous radar is received and converted to the first IF of 40.8 MHz. The signal is amplified and mixed with a 34-MHz second local oscillator signal to produce a 6.8-MHz second IF. A voltage-controlled oscillator is pulled in frequency in an automatic phase control loop to phase-lock the incoming 6.8-MHz IF carrier to the oscillator signal. Multiplication of the oscillator frequency by a factor of 1440 produces the transmission and first local oscillator frequency. Acquisition is accomplished using an oscillator sweep and threshold circuit similar to the one used in the radar.

The ranging tones are extracted from the 6.8-MHz received signal in exactly the same manner as in the radar. After bandpass filtering and amplification, the tones are applied to the phase modulator for retransmission to the radar.

#### 4.6.4 Transponder Self-Test

Circuits are included to permit testing of the transponder without the rendezvous radar. A test oscillator operating at a single frequency permits the transponder to phase-lock without an external input. The transmitter power and AGC action may be checked, in addition to phase-lock, at a minimum signal level.

#### 4.7 TRANSPONDER ACQUISITION SEQUENCE

The normal acquisition sequence for the rendezvous radar and transponder is automatic. In simplified form, this sequence is as follows:

1. The radar antenna, under computer control, is designated in angle so that its transmitted CW radiation can be received at the transponder.
2. The transponder, which was previously sweeping in frequency, senses this radiation, stops its sweep, and phase-locks to the received radar signal. It then retransmits this signal side-stepped by 40.8 MHz.
3. The radar receiver, which was previously sweeping in frequency, stops its sweep and phase-locks to the received transponder signal. The maximum completion time of steps 2 and 3 is 4.4 sec.
4. The lunar module computer transmits AUTO TRACK ENABLE when antenna resolvers indicate that the boresight line of sight is within 0.5 degree of the computed target line of sight.
5. The radar angle tracking loop is closed upon completion of steps 3 and 4 and the error is nulled.
6. The radar activates ranging modulation and the range tracking error is nulled within a maximum of 10.6 sec after step 3 is completed. The coherent loop is now closed.
7. The radar indicates a DATA GOOD condition to the computer, based on both range and range rate lock-on completion. Angle, range, and range rate data are now available to the computer and the astronaut display panel. Angle rate also is available to the display panel.

#### 4.8 RENDEZVOUS RADAR-COMPUTER ANGLE INTERFACE

The lunar module computer controls the rendezvous radar antenna assembly in angle, and the radar communicates angular measurements of the line of sight to the computer by means of the rendezvous radar-computer angle interface. The performance and electrical characteristics of this interface are specified in Grumman P&I document LSP-370-3A and Grumman-MIT/IL LGC-RR Angle Interface Control Document, LIS-370-10006.

Each rendezvous radar gimbal axis mounts a precision dual (1 and 16) speed resolver. When the radar is under lunar module computer control, the resolvers are excited from a stable 800-Hz signal furnished by the GN&C system power and servo assembly (PSA). The sine and cosine outputs of each resolver are fed to the GN&C system coupling data units (CDUs), which perform an analog-to-digital transformation of this information into 15-bit binary words with a bit weight of approximately 0.01 deg/bit. In this way, the computer is advised continuously and unambiguously of radar shaft and trunnion angle with respect to the spacecraft to a resolution of approximately 0.01 degree.

The computer controls the pointing of the radar antenna in each axis by establishing the desired rate to the coupling data unit, which, in turn converts it to a proportional 800-Hz command derived from the power and servo assembly 800-Hz reference. The coupling data unit analog signal is transmitted to the radar electronic assembly, where it is demodulated. The resulting signal is applied to the torquer of the gyro corresponding to the gimbal being commanded. A displacement of the gyro float occurs, producing an output from the gyro microslyn, which in turn is amplified to excite the direct-coupled gimbal torquer. The gimbal accelerates, reaching a steady-state angular velocity such that the gyro precession torque nulls the command torque, except for a small imbalance necessary to overcome friction and losses. A fixed digital command from the computer thus induces a steady-state angular rate of the gimbal.

During the process of positioning the antenna, the computer repeatedly checks the angular location of the gimbal and adjusts its command to be proportional to the displacement of the gimbal from the desired final position. The radar and computer, in combination, comprise a position servo with no steady-state position error.

The angle interface proper evolved from larger considerations relating to the performance characteristics of the integrated rendezvous radar-computer positioning closed loop. Two design considerations were particularly important:

1. To evolve a design, each portion of which could be developed and tested independently.
2. To evolve a design with a non-critical interface, allowing the subsystem on either side of the interface to be interconnected to form a complete closed loop without stability or performance problems.

In the case of the angle interface, one key to satisfaction of these criteria was the presence of stabilization gyros in the radar gimbal servos. By torquing these gyros

from the lunar module computer with an 800-Hz command signal, a simple, reliable interface design was achieved. Within the radar, it was possible to design the gimbal stabilization subloops to possess wide bandwidth compared to the data sampling rate established by the computer for closed loop angle positioning, thus avoiding problems of marginal stability.

Another important factor in meeting the basic interface design criteria was the adoption of a previously proven design for angle readout of the radar gimbals. The resolvers selected for the radar are identical, both electrically and physically, to those used by MIT/IL for inertial measurement unit angle readout. Furthermore, the radar resolvers interface with coupling data units identical to those employed with the inertial platform. This commonality of design greatly reduced the potential angle interface problems and assured performance of known precision and reliability.

#### 4.9 RENDEZVOUS RADAR-COMPUTER DIGITAL INTERFACE

In addition to the angle interface, the rendezvous radar responds to and communicates with the GN&C system by means of an entirely digital interface existing between the radar signal data converter and the GN&C computer. This interface is described in the previously referenced R-404 and E-1904, and is specified in Grumman document LSP-370-3A and in Grumman MIT/IL Interface Control Document LIS-370-10004, "LGC-LM Electrical Interface."

The digital interface is the means by which the computer digitally commands and controls the radar, as well as the path by which the radar transmits digital measurement and status information to the computer. The signal paths comprising the interface are indicated in simplified form in Figure 4-6.

The radar interface circuits contained in the signal data converter consist of:

1. A gate, controlled by the computer, feeding a binary counter with a parallel transfer output capability for accumulation of range rate data.
2. A reversible range register and parallel transfer circuits for range data.
3. A 15-bit shift register capable of accepting the parallel transfer of a word from either the binary counter or the reversible register, and controlled for serial shift-out by the computer.

Upon receipt from the computer of a readout command in the form of a pulse train, the contents of the radar shift register are serially shifted across the interface to

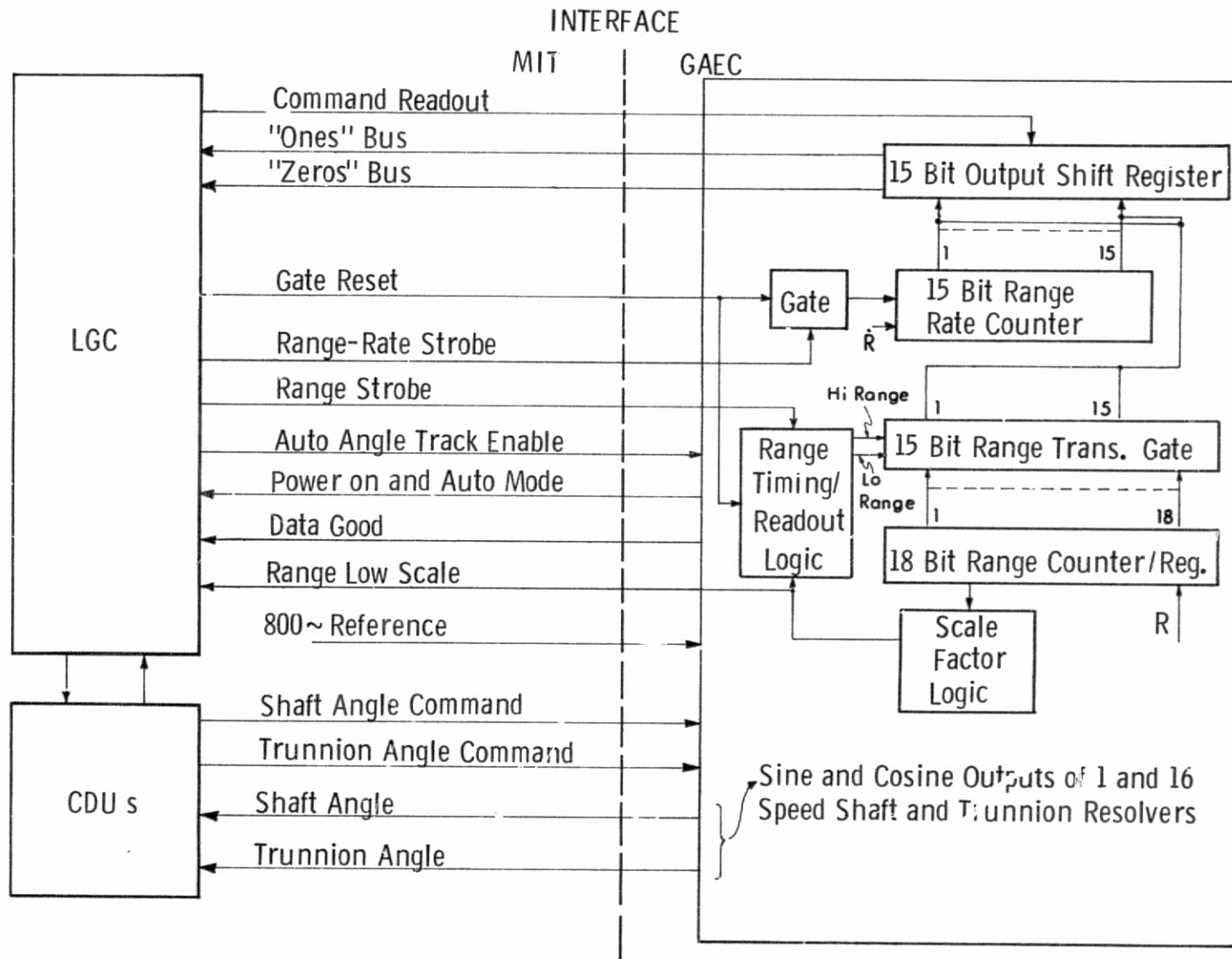


Fig. 4-6 RR/LGC Interface Block Diagram

the computer, the 1 bits being transferred on a 1's bus and the 0 bits being transferred on a 0's bus. The most significant bit is shifted out first.

A continuous pulse train gate-reset is transmitted to the radar whenever the computer is operating. Selection of the data to be read out (range or range rate) and the time of readout are accomplished by the computer through activation of the appropriate gate-strobe pulse train to the radar.

To read out range rate, the computer transmits the range rate strobe pulse train which causes the range rate gate in the radar to turn on (open), thus permitting the range rate signal in the form of a bias frequency plus Doppler frequency to enter the binary counter and accumulate a count that is a function of line-of-sight range rate. Upon withdrawal of the gate strobe pulse train, the gate is turned off (closed) when the next pulse of the gate reset pulse train is received. Range rate is furnished to the computer interface by the radar as a digital word:  $S_{RR} = [f_d + f_{BRR}] \tau_{RR}$  where  $f_d$  is a frequency in the radar proportional to range rate;  $f_{BRR}$  is a bias frequency; and  $\tau_{RR}$  is the counting interval generated by the gating action of the computer.

In the computer, range rate is calculated as follows:  $V_{RR} = k_{RR} (S_{RR} - f_{BRR} \tau_{RR})$ , where  $V_{RR}$  is range rate of lunar module with respect to the command module, and  $k_{RR}$  is the scale factor to convert the range rate count obtained from the radar to ft/sec.

To read out range, the same type of strobe pulse train is transmitted by the computer except that it causes the parallel transfer of a complete range reading to the shift register from the reversible range register internal to the rendezvous radar. The range measured by the radar along the radar boresight is computed in the lunar module computer by the following equation:  $R = K_n r_{RR}$ , where  $K_n$  is the bit weight and  $r_{RR}$  is the range count obtained from the radar upon computer readout command. Two range scales, used by the computer to convert the range count into range in feet, cover the required operating range. The scale change occurs at 50.6 n. mi. and the quantization bit sizes for the high and low range scales are  $K_1 = 75.04$  and  $K_2 = 9.38$  ft, respectively. The range scale change from high to low is indicated by the radar to the computer by a Range Low Scale Factor discrete signal that is issued when the range counter is rescaled. The radar accepts from the computer a status discrete (see Figure 4-6) designated AUTOMATIC ANGLE TRACK ENABLE, that enables the radar to initiate automatic angle track of the target once the computer has completed its angle designation. Removal of this discrete by the computer causes the radar to return to angle control by the computer. The radar provides the computer with the status discretions detailed in Table 4-II.

TABLE 4-II  
RENDEZVOUS RADAR-COMPUTER STATUS DISCRETES

Item	Description	Function
1	Power On and Automatic Mode	Indicates radar power is on and radar is in Automatic mode of operation (under computer control).
2	Data Good	Indicates to a high probability that range, range rate, and angle data from the radar are within accuracy specifications and are valid for computer use.
3	Range Low Scale	Indicates that computer should use radar scale factor specified for close-range measurements.

Note: All discrete signals are unipolar dc.

The radar-computer digital interface employs standard circuit designs that are common to interfaces between the computer and other subsystems.

The computer pulse transmitter circuits are transformer-coupled to the cable harnesses leading to the radars, and provide driving point impedance at the transformer outputs of approximately 50 ohms during transmission. The transformer coupling affords dc isolation for reducing ground loop problems, and provides line balance that tends to minimize electromagnetic interference difficulties. Pulses are transmitted in the cable harness on twisted pairs of approximately 62 ohms characteristic impedance. The low source impedance of the pulse transmitter circuits was originally intended to drive higher impedance loads through short cable lengths. However, in the development of the lunar module cable harness, some of the lines conveying pulse waveforms across the digital interface reached nearly 40 ft in length. To avoid the possibility of anomalous circuit behavior resulting from pulse waveform distortion due to reflections on the pulse lines, it appeared desirable to impedance-match these lines at both ends. The computer pulse transmitter circuits exhibit a nominal source impedance of 50 ohms over a wide range of loads and were already adequate for this purpose. Modifications of the signal data converters of both the rendezvous and the landing radars were subsequently carried out to provide cable terminations of nominally 65 ohms.

The radar signal converters contain pulse driver circuits whose output impedances vary somewhat with load, due to the non-linear characteristics of the output transformer. When loaded with the 200-ohm nominal impedance of the computer receiver circuits, pulse driver source impedance was measured as 20 ohms. Under these conditions, the pulse characteristics at the computer exhibited some overshoot at the leading edge and ringing on the trailing edge. The computer pulse receiver circuits, however, were designed for special immunity to pulse distortion and degradation. After being switched to the ON condition by the leading edge of the applied pulse, the circuits remain on for approximately  $3\mu$  sec before returning to the OFF condition. For a period of approximately  $12\mu$ sec following turn-on, the computer logic maintains the receiver circuits insensitive to further inputs and eliminates false triggering on transients as well as dependence on a trailing edge for turn-off. For these reasons, no adjustment of receiver circuit impedance level to match cable characteristic impedance was necessary.

The digital interface proper worked very reliably throughout the flight tests, the ground checkout activity, and the missions. However, in the course of the development, two idiosyncrasies which adversely affected the reliability of digital data transfer were discovered in the circuits communicating with the interface.

#### 4.10 RENDEZVOUS RADAR INTERFACE SOFTWARE

The radar subsystems provide the GN&C system with data essential to the successful performance of the mission. The task of developing the software to interface the radars with the GN&C system proved to be of major proportions, characterized by considerable complexity and sophistication. The magnitude of the computer routine and program task stemmed from the various steps required to provide the navigation inputs that, in the case of the rendezvous radar, included acquisition control, command of the desired measurements, transfer of data across interface from the radar to the computer, processing of data, testing data for reasonableness, generation of keyboard panel displays and alarms, insertion of radar measurements and status indications on the digital downlink telemetry, and protection of the radar functions. The software design task was further complicated by the fact that the radar was to be used in the mission as a dual-mode device; i.e., it was to be capable of either automatic or manual (astronaut) operational control. Under automatic control, the software design was required to advise the astronaut of certain conditions of radar function and malfunction to permit him to exercise his judgment and control of the radar through recycle and measurement-rejection capabilities. These factors, together with software accommodation of radar idiosyncrasies, resulted in software designs requiring a substantial portion of computer's permanent or fixed memory.

A detailed description of the radar software programs, routines, and downlink lists can be found in the Guidance System Operation Plan, Sections 2, 4, and 5.

#### 4.10.1 Computer Angle Control of the Rendezvous Radar

GN&C system control of the radar takes advantage of computer-contained knowledge of the line of sight from the lunar module to the command module. As a first step in activating the radar for computer use, the computer software is designed to determine the line-of-sight direction by differencing the lunar and command module state vectors to derive a pointing vector, designated  $r_{LOS}$ . This vector is then used as a reference for pointing the radar boresight toward the transponder mounted on the service module. There are two principal advantages to this approach: first, computer-commanded pointing of the antenna assembly obviates the need for a self-contained automatic angle-search mechanism which would complicate the radar, add to weight and power consumption, and raise associated reliability questions; second, the computer pointing protects the radar against sidelobe acquisition.

The problem of sidelobe acquisition is indigenous to any narrow-beam radar and always requires design consideration. In the case of this radar, four stable sidelobe lock-up points exist in Mode 1 at a radius of approximately 6 degrees from the boresight, as illustrated in Figure 4-7, and others at larger angular radii may exist under high signal strength conditions. To be assured of main beam acquisition, the radar electrical boresight must be pointed within 3 degrees of the true line of sight. In the process of angle acquisition, the computer monitors the radar gimbal angles with respect to those corresponding to the computer-calculated line of sight and issues commands to the gimbal servos, causing convergence on the commanded angles. When the radar approaches within 0.5 degree of the commanded angles, the computer issues the ANGLE TRACK ENABLE discrete that allows the gimbal servos to respond on a closed-loop basis to the microwave angle error signals of the antenna assembly rather than computer commands, provided the radar range rate tracking loop has acquired the transponder signal. The radar antenna slews to null the error signals by aligning its boresight to the true line of sight to the transponder. If the pointing error between boresight and true line of sight is less than 3 degrees at the time the ANGLE TRACK ENABLE discrete is issued by the computer, a radar angle pull-in on the main radiation lobe is assured.

Radar pointing uncertainties arise principally from inertial measurement unit misalignment, errors in the knowledge of lunar and command module state vectors, angle bias in the radar boresight, and tilt errors from misalignment of the radar in mounting to the lunar module. The combination of boresight and tilt error is

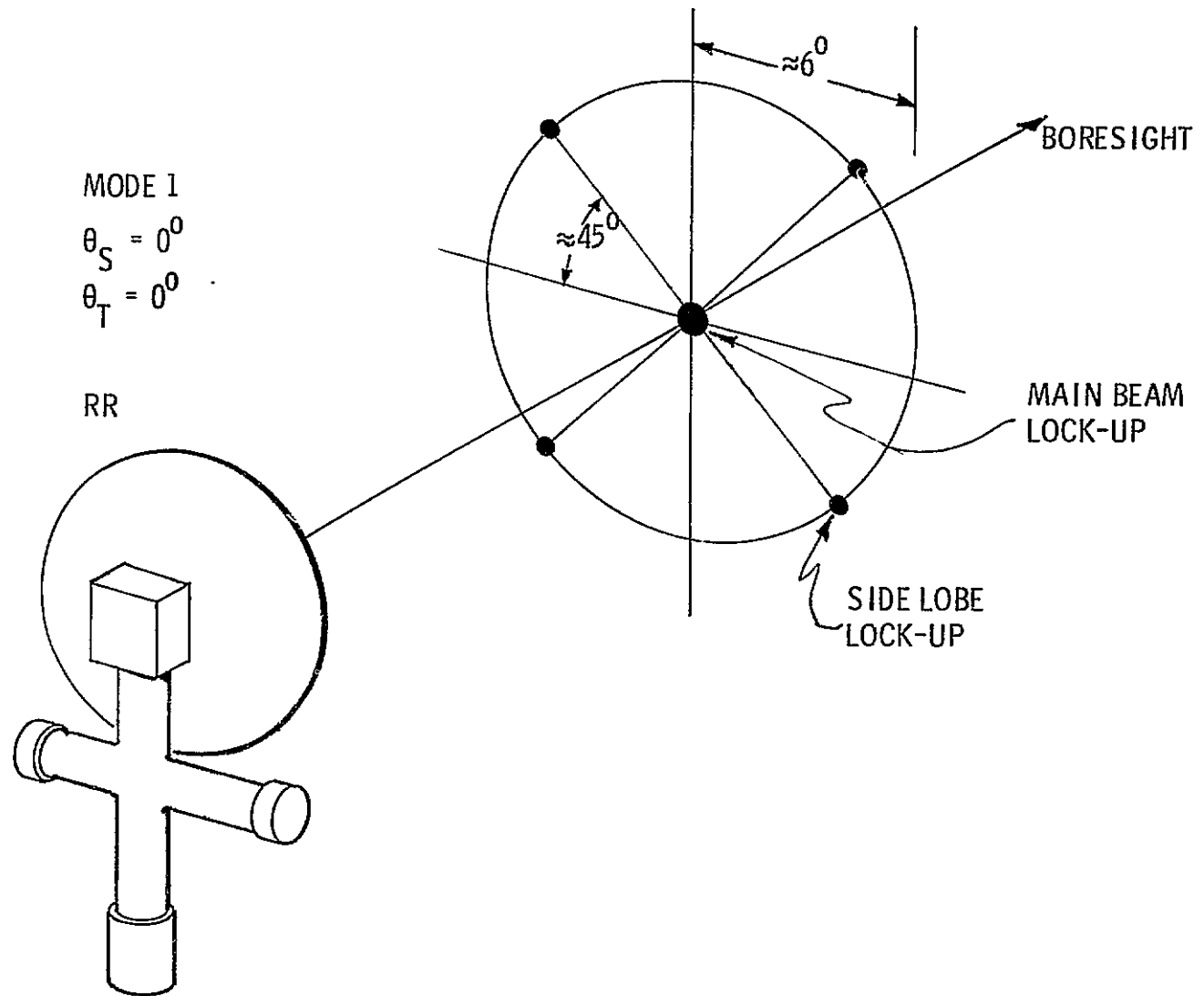


Fig. 4-7 RR Stable Angle Lock up Locations

controlled by the Performance and Interface Specification to 15 mrad maximum. To assure a 99.74-percent probability that the radar pointing error does not exceed the 3-degree limit at the time the computer gives the ENABLE discrete, the computer uncertainty in pointing must be 2.83 degrees or less.

The software design provides compensation for rate lag errors of the radar gimbal servos under steady-state angular-rate drive conditions. The gimbal servo velocity constant is controlled by the P&I Specification to be  $1.0 \text{ sec}^{-1}$  +25, -20 percent. When the radar is tracking the orbiting command module from the lunar surface, line-of-sight rates up to 15 mrad/sec are experienced and corresponding steady-state gimbal servo lag errors of up to 15 mrad develop. If not corrected, this condition would contribute to the radar pointing error. To eliminate this possibility, nominally exact compensation is provided in the software by actually commanding the radar to a pointing vector that leads the calculated line of sight by 1 second in time.

"Staleness" compensation is also built into the software to maintain radar pointing accuracy. The staleness condition arises because of the finite time required to integrate the relative state vectors of the spacecraft to current time prior to differencing for  $\underline{r}_{\text{LOS}}$ . In program P20, the Rendezvous Navigation Program, the Kepler integration requires about 0.5 sec to advance each state vector. In P22, the Lunar Surface Navigation Program, because only the command module state vector is calculated, the integration time is about 0.5 sec. To avoid staleness and associated angular errors in  $\underline{r}_{\text{LOS}}$ , the Kepler subroutines are performed for current time plus  $\epsilon$ , where  $\epsilon$  is the average time required to complete the Kepler integration.

The computer commands for angle designation of the antenna assembly are applied to the radar gyro torquers. The trunnion gyro is affixed to the radar inner gimbal and directly senses trunnion rate. The shaft gyro is also mounted on the inner gimbal, and rotates with the trunnion. Its sensitivity to shaft rate therefore is proportional to the cosine of the trunnion angle, being maximum for  $\theta_{\text{T}} = 0$  or 180 degrees and zero for  $\theta_{\text{T}} = \pm 90$  degrees. The software design recognizes this situation in computing gimbal commands.

Let  $C_{\text{S}}(1)$  and  $C_{\text{T}}(1)$  be the shaft (S) and trunnion (T) commands to the radar coupling data units for the antenna in Mode 1, and  $C_{\text{S}}(2)$  and  $C_{\text{T}}(2)$  be the corresponding commands for the antenna in Mode 2. Initially, the unit vector  $\underline{u}_{\text{D}}$  defining the desired direction of designation in navigation base coordinates is obtained from stable member coordinates as follows:  $\underline{u}_{\text{D}} = [\text{SMNB}] \text{ UNIT}(\underline{r}'_{\text{LOS}})$ , where  $[\text{SMNB}]$  is the stable member to navigation base transformation and  $\underline{r}'_{\text{LOS}}$  is the lag-compensated line-of-sight vector. The commands are then computed as follows:

$$C_S(1) = K \left[ \underline{u}_D \cdot \begin{pmatrix} \cos S \\ 0 \\ -\sin S \end{pmatrix} \right] \quad (1)$$

$$C_S(2) = -C_S(1) \quad (2)$$

$$C_T(1) = C_T(2) = -K \left[ \underline{u}_D \cdot \begin{pmatrix} \sin T \sin S \\ \cos T \\ \sin T \cos S \end{pmatrix} \right] \quad (3)$$

where S and T are the present shaft and trunnion angles and K is a scale factor used to establish the proper number of bits in the radar coupling data units. A limit check is made by the computer to ensure that no more than 384 bits are sent to the coupling unit.

The  $C_S$  command produces rotation in the shaft axis until the trunnion axis becomes perpendicular to  $\underline{u}_D$ . The  $C_T$  command produces rotation about the radar trunnion axis until the shaft axis is also perpendicular to  $\underline{u}_D$ . If the gimbal servos are linear with identical gain, the simultaneous application of  $C_S$  and  $C_T$  causes designation along a great circle containing  $\underline{u}_D$  and the radar boresight.

In the region of linear control, each gimbal of the radar responds to the 800-Hz command from its associated coupling data unit with a sensitivity of 2 deg/sec/Vrms  $\pm 12.5$  percent. Maximum coupling unit command corresponds to 384 bits scaled at 13.18 mV/bit, or 5.06 Vrms  $\pm 10$  percent. The linear region of control is defined as that for which the coupling unit output lies between 12 mV and 3.0 Vrms, where 12 mV is the approximate quantization level of the unit. For coupling unit commands above 3.0 V, the gimbal servo may saturate but must drive at least 7 deg/sec for an arbitrary command level of 5.4 Vrms.

In instances where the angular separation between the radar initial pointing and the desired pointing,  $\underline{u}_D$ , is approximately 10 degrees or greater, the computer may command full slew in one or both gimbal axes, causing drive saturation. The designate path of the boresight will then not follow a great circle route until commands to both gimbals have been reduced to within the linear range.

The basic technique of angle designation utilizes the computer and radar as a sample data servo system, with a sampling period of approximately 0.5 sec. Typical performance for one gimbal under linear control is illustrated in Figure 4-8. At

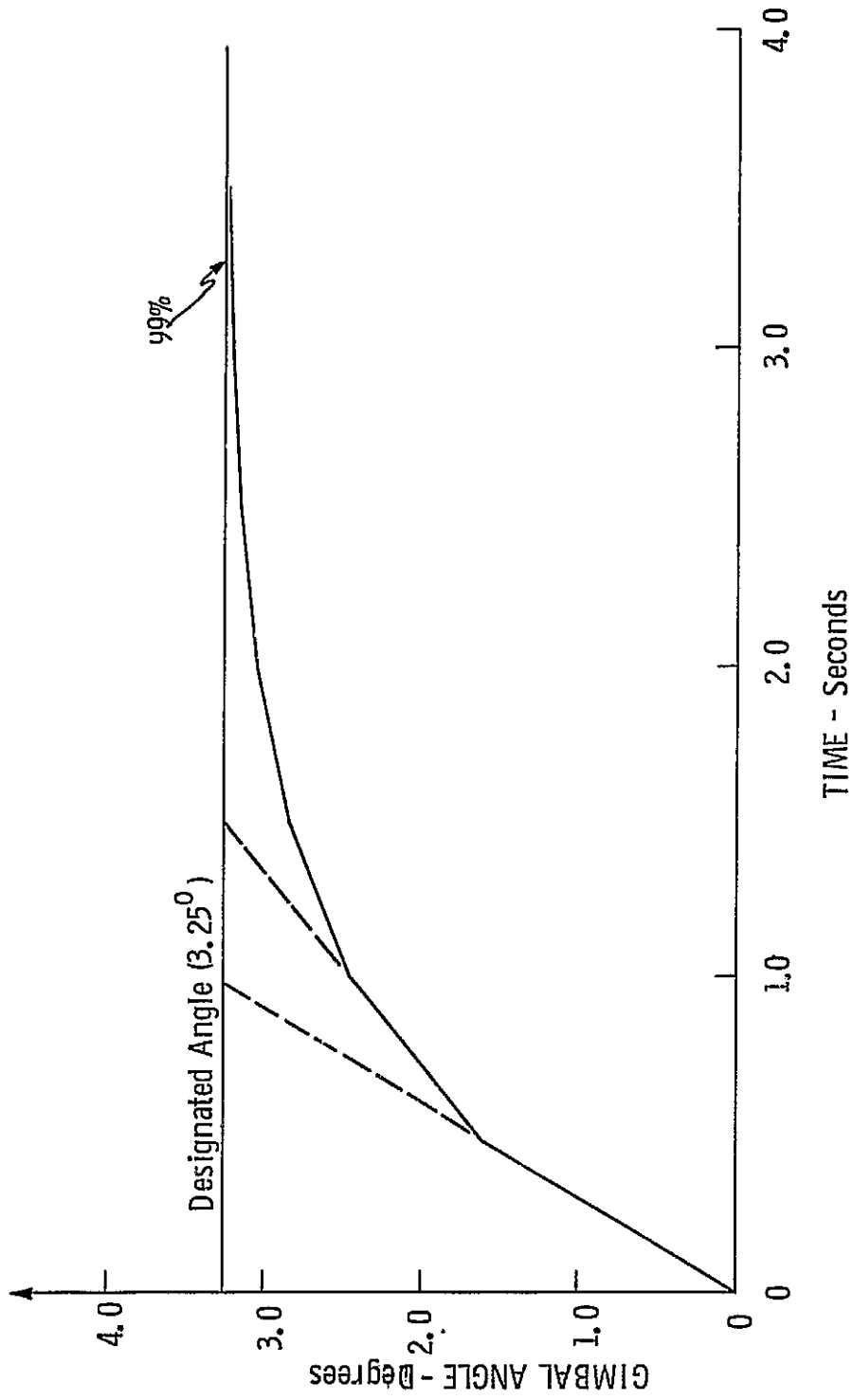


Fig. 4-8 Typical RR Angle Designate

sampling time, the computer computes the angular separation between the present and desired gimbal angles and issues a command rate that would null the error in 1 second. This process repeats approximately every half-second, so the remaining angle error is approximately halved within each sampling interval and the commanded rate is approximately halved at the time of each sample. The actual gimbal angle converges asymptotically with time on the desired angle and the rate converges asymptotically toward zero. Because the sampling period is long compared to the duration of transients in the wideband gimbal servo, and because of the asymptotic reduction in commanded rate, the stability of the complete computer-radar gimbal closed loop is assured, and the possibility of angle overshoots is virtually eliminated.

This basic angle designation technique is used in coasting flight, during the command module overfly of the landed lunar module, and for positioning the radar with respect to the lunar module body axes. In the first two instances, the dynamic problems of the moving line of sight are obviated by suitable lead compensation of the designate vector,  $\underline{u}_D$ , as previously explained.

#### 4.10.2 Rendezvous Radar Search Routine

In the early stages of radar development, several radar and GN&C system performance uncertainties affected the acquisition capability of the radar. In the radar, these uncertainties included the final main beam gain and beamwidth of the antenna, the minimum discernible signal (MDS) capability, and the transponder power, antenna gain, and pattern. In the GN&C system, the unknowns were platform alignment error and state-vector errors at the specific time of first angle designation of the radar. The extent of lunar and command vehicle attitude constraints was also an unknown at this time. Because the combined effects of these factors on the radar, the probability of acquisition at maximum range of 400 n. mi. could not be accurately forecast. The concept was therefore evolved of a search routine for exploring a volume of space in the vicinity of the calculated line of sight, with the intent of increasing radar acquisition probability. The subroutines necessary to achieve this search were designed into the software, identified as R24, the RR Search Routine.

The astronaut may select the RR Search mode if the normal RR Designate Routine fails to acquire the target. The RR Search Routine then designates the radar antenna in a hexagonal search pattern about the estimated line of sight. This pattern is hexagonal where dimensions between parallel sides are 5.6 deg, as shown in Figure 4-9. At the beginning of this mode the radar is designated for 6 seconds along the estimated line of sight to the target defined by the unit vector  $\underline{u}_{LOS}$ . Afterwards, the computer sequentially designates the radar to each corner of the hexagon for a

period of 6 sec before repeating the process, starting with a new designate along the line of sight unit vector ( $\underline{u}_{LOS}$ ) for 6 seconds. The time required to generate this search pattern is approximately 42 seconds.

Approximately every 6 seconds, the position and velocity vectors of the command and lunar modules are used to compute  $\underline{u}_{LOS}$  in the basic reference coordinate frame and the relative velocity ( $\underline{V}_{LC}$ ) in stable member coordinates. The routine then computes the desired radar pointing direction ( $\underline{u}_D$ ) which may be along  $\underline{u}_{LOS}$  or to one corner of the search pattern (see Figure 4-9). The routine proceeds to designate the radar by issuing rate commands to the radar gyros approximately every 0.5 second with approximate corrections being made each time for lag error and target motion.

The advantage of the search activity may be seen from Figure 4-10. The notched hexagon represents the path traveled by the center of the antenna beam. The concentric circles about the origin indicate angular displacement from the designated line of sight, and the irregular contours reveal beam dwell time. The boundary marked 5 sec encloses all pointing angles with respect to the designated line of sight that have been continuously exposed for at least 5 sec during the search to the radar main beam; i.e., that region of the main beam within 2 degrees of electrical boresight. This exposure provides at least the nominal acquisition probability of 85 percent at 400 n. mi. in one search of the velocity tracker for every pointing angle within the contour. In effect, the region for specified long range acquisition probability has been expanded by the Search Routine from a cone of 4 degrees total angle, under normal designate conditions, to a cone of 9 degrees average total angle.

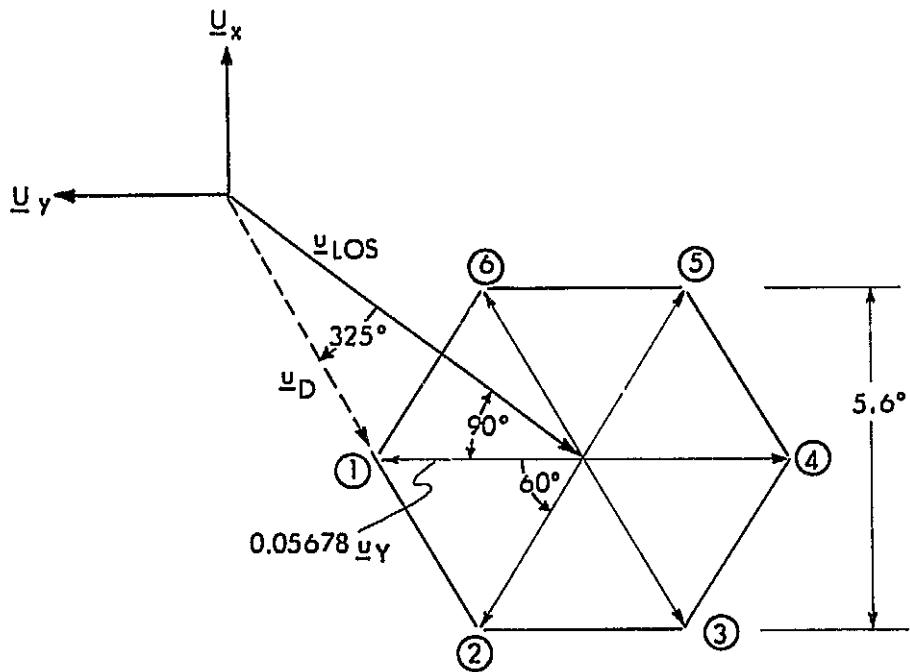
An acquisition achieved by use of the Search Routine offers no protection from sidelobes, since the 3-degree criterion described in Section 4.10.1 may obviously have been violated. Such acquisitions must be verified for main beam lock by manual procedures referred to in paragraph 5.2.4.1.3 of R-567<sup>1</sup>.

#### 4.10.3 Rendezvous Radar Angular Mode Control and Limits

From a purely mechanical standpoint, the two-gimbal design of the radar antenna assembly permits the radar boresight to be physically positioned over an angular range in excess of three-quarters of a sphere. As a practical matter, however, because of areas of mechanical interference between the antenna and the lunar module, and to maintain the quality of computer control of the radar as well as the accuracy

---

1. Guidance System Operation Plan for Program LUMINARY, MIT/IL Report R-567.



Note: Search pattern as viewed from CSM.

Fig. 4-9 RR Search Pattern

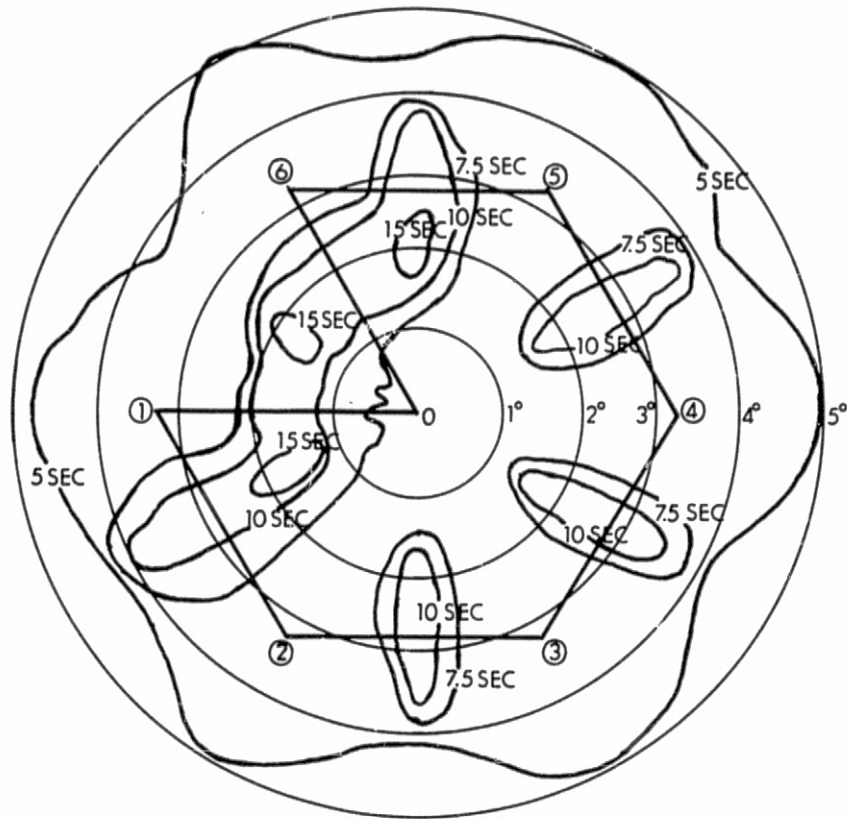


Fig. 4-10 RR Search Mode-Maximum Continuous Exposure Time(s) vs Angle from Designated LOS

of radar angle measurements, the region of radar utilization while interfacing with the GN&C system is somewhat more limited. The coverage regions are represented in Figure 4-11, and occur in two modes, depending on the trunnion angle:

$$\text{Mode 1: } 270^\circ \leq \theta_T \leq 90^\circ$$

$$\text{Mode 2: } 270^\circ > \theta_T > 90^\circ$$

where  $\theta_T$  is the angle read by the coupling data unit from the trunnion resolver. When the radar is under GN&C system control, it may be pointed and released or pointed and held with respect to the spacecraft at any angular position within the dashed lines. This capability, called up by astronaut request through the computer was designed into the software primarily to permit the radar to be positioned for minimum field-of-view interference during optical sightings with the alignment optical telescope and to allow orientation of the antenna for minimum heat loading during the lunar stay. It is also of great convenience in pre-flight checkout. The regions within which the radar may be angle-designated by the computer for transponder acquisition and within which the radar must measure to specified accuracies are shown by the solid lines.

Since the Mode 1 and 2 regions do not overlap, it is evident that some means must exist to command the radar from one mode to the other. Under computer control, this capability is provided by a routine designated as R25, the Radar Monitor Routine, that is designed to accomplish the mode changing functions despite marginal stability in the radar shaft gimbal servo during this transitional period. The marginal stability condition arises from the fact that to transfer to the other mode, the radar boresight must pass through the pole of the gimbal system; i.e., the radar boresight becomes parallel to the shaft axis. At this time, the input axis of the shaft gyro is perpendicular to the shaft axis and is insensitive to shaft rotation. Thus, in the vicinity of the pole, rate feedback from the gyro is negligible and the shaft servo is marginally stable.

In the design of the software, moding instabilities are alleviated in two ways: first, only the trunnion axis is driven during pole passage, preventing cross-coupling disturbances that could exist if both axes were driven during mode change. Second, the trunnion axis is commanded at maximum rate during pole passage to minimize the time duration of negligible shaft-axis-rate feedback and prevent the development of undesired shaft-angle perturbations.

#### 4.10.4 Radar Angle Limit Protection

The computer software is designed to protect the radar gimbal system from damage when the radar is in use as part of the overall GN&C system and the gimbal angles

exceed the limits shown in solid lines in Figure 4-11. The desirability of computer-continued protection was recognized early in the radar development program: because radar inertial stabilization of the boresight can result in gimbal impact onto the radar mechanical stops due to vehicle attitude changes. To forestall any possibility of physical damage due to mechanical impact of the gimbals with the stops, R25 performs a gimbal-angle check every 0.48 sec. This check also prevents serious power drain and dissipation problems resulting from attempts by the gimbal servo to maintain the inertial heading of the boresight if a gimbal were into its stop. If one or both gimbal angles reach or exceed the allowable limit, R25 assumes control of the antenna assembly and commands the radar boresight to the vehicle X-axis in the case of Mode 1, or to the vehicle Y-axis, in the case of Mode 2 type of operation. Once the reposition has been accomplished, R25 relinquishes control of the antenna assembly and allows the radar either to revert to its self-contained inertial stabilization mode or to be angle-designated by another software routine for a new acquisition attempt.

#### 4.10.5 Aided Acquisition

In the design of the radar and the interface functions, the maximum gimbal rates possible by computer command were deliberately constrained to relatively low values; i.e., a maximum of 10 to 12 deg/sec, to avoid possible dynamic and transient overshoot problems associated with high-speed servos and to make certain that the coupling data unit analog-to-digital maximum conversion rate of approximately 70 deg/sec was not exceeded. Slow radar slew rates pose no problem in free-fall phases of the mission where the time required, even for a change of mode, is not critical. However, during the command module overfly of the landed lunar module, the time available for accurate tracking of the transponder by the radar is less than 3 minutes, and quick acquisition is imperative. The design of the software materially assists in this situation by providing a pre-positioning function in anticipation of subsequent entry of the line of sight within the angular tracking limits of the radar. The computer commands and holds the radar boresight close to the mode edge for earliest intercept of the target line of sight. As soon as the line of sight enters the Mode 2 tracking limits, the computer initiates the Normal Designate Routine for the earliest acquisition.

#### 4.10.6 Angle Bias Estimation

One of the unique features of the software design is the inclusion of a Kalman filter for estimation and compensation of angle measurement bias inherent in the lunar module-rendezvous radar system. Under ideal conditions, the Kalman estimator

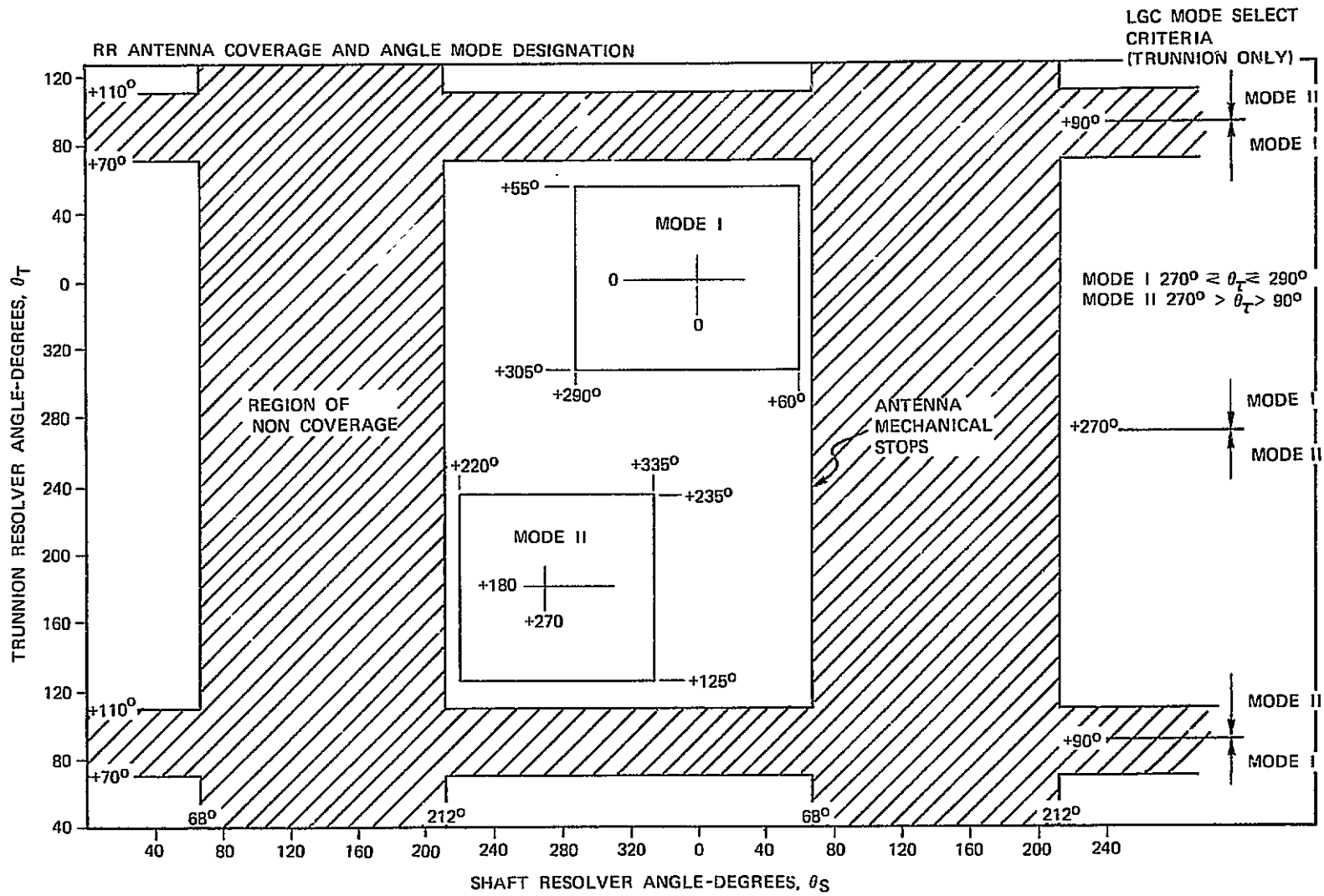


Fig. 4-11 RR-LM Angle Coverage

eliminates bias errors in the radar angle measurements, leaving only the random uncertainties. Three sources of possible bias error exist in the lunar module- rendezvous radar configuration:

1. Bias due to deviation of the antenna electrical boresight from the line of sight indicated by the resolvers
2. Bias due to tilt of the radar reference coordinate frame with respect to the lunar module navigation base, as might occur in the mounting of the radar to the spacecraft
3. Bias due to lack of orthogonality in the radar gimbals.

In the manufacture of the radar, gimbal orthogonality is maintained to better than 20 arcseconds, eliminating non-orthogonality as a practical source of bias error. However, boresight and tilt biases may be substantial, although the total bias is limited by the P&I Specification to 15 mrad.

At the time the Kalman estimator was first considered, it was not realized that the two principal categories of bias—boresight and tilt—would generate different error behavior as a function of antenna pointing. The computer was sized to include 9 x 9 matrix operation for estimation of vehicle position, velocity, and radar angle bias. A 3 x 3 matrix which was part of the 9 x 9 capability provided the estimation of individual shaft and trunnion angle bias. Bias estimation, however, was restricted by this design to a single category; the estimation process was capable of assessing either tilt bias or boresight bias, but not both. The introduction of a more sophisticated estimator with the ability to sort out both tilt and boresight bias was not feasible since the requirements for a 12 x 12 matrix operation would have imposed unacceptable demands on design of the computer in terms of increased storage and computation needs.

Another problem in bias estimation was related to the radar angle error model that, for several practical reasons, assumed that the radar angle measurement errors could be very simply characterized as bias and random types. The Kalman bias estimator was synthesized on this model. As a practical matter, however, the radar never exhibited bias in the ideal, time-invariant sense. A variation with time in the average angle measurement error always occurs during periods of radar usage, produced principally by such factors as temperature change in the radar electronics assembly, polarization variation, mechanical deflections of the radar pedestal and lunar module mounting point caused primarily by temperature changes, and electrical boresight variations accompanying changes in antenna pointing with respect to the lunar module structure. These variations are influenced by vehicle attitude history

during the mission and, although generally systematic, are very difficult to predict. The time variation of the average error suggests two questions:

1. What is considered as bias under these conditions?
2. What degree of stationarity in bias is required to allow the Kalman estimator to converge on stable predictions of usable accuracy?

The answers to these questions were based on the minimum time interval in which trajectory geometry changes could be expected to allow for good estimation of both state vector and bias. A satisfactory working definition stipulated that bias was the mean value of the measurement error in any 10-minute tracking interval. Random error was then defined as the variation about the mean of the measured parameter based on a 10-minute averaging interval.

Simulation studies of typical Kalman bias estimator designs established a stationarity criterion limiting the bias time rate of change to 0.5 mrad or less in any 10-minute interval. The performance characteristics of the radar itself do not permit the satisfaction of this requirement. For example, movement of the radar boresight from one edge of Mode 1 to the other may be accompanied by a boresight deviation of several milliradians, while a 90-degree polarization change can produce a boresight variation of as much as 2 mrad. The problem of satisfying the bias stationarity condition is therefore a system problem of controlling vehicle attitudes and attitude rates to prevent rapid changes in bias in the radar.

During mission analysis and planning phases at MIT/IL, it became evident that the difficulty of both the single-class bias estimation limitation of the computer's  $9 \times 9$  matrix and the bias stability requirement could be dispelled by establishing a constraint on the pointing angles permitted the radar during periods of utilization of radar angle measurements for state-vector update. Such a constraint was introduced in the SUNDANCE program assembly by causing the lunar module to re-orient its Z-axis toward the command module whenever the angle between the Z-axis and calculated line of sight exceeded 30 degrees during radar tracking periods. The effect of this design feature was to limit antenna assembly pointing to a portion of a 60-degree cone centered around the lunar module Z-axis. Within this region, the boresight variation is less than a milliradian and, under mission conditions, the stability criterion is satisfied. Because of the small boresight deviation, the Kalman estimator performs well in determining the angular bias, whether the filter is designed for tilt or for boresight bias estimation.

For reasons not connected with the radar, the LUMINARY programs are designed to maintain the lunar module Z-axis within a degree or two of the calculated line of

sight during the ascent rendezvous. The departure of the radar pointing from the 0,0 direction ( $\theta_{\text{shaft}} = 0^\circ$  and  $\theta_{\text{trunnion}} = 0^\circ$ ) is also no more than 1 or 2 degrees, and the performance of the Kalman bias estimator is further enhanced by this close attitude control. Note that radar pointing constraints become effective only after acquisition has been achieved, and do not prevent the initial angle designation of the radar anywhere within its specified angular control limits for purposes of target acquisition.

While it is possible to control lunar module attitude for the benefit of the radar during free-fall phases of the mission, this option does not exist when the radar is tracking the overflights of the command module from the lunar surface. In this application, the radar boresight may sweep from edge to edge of Mode 2 in 3 minutes with boresight bias deviations of 4 to 5 mrad. In addition, the tilt of the radar coordinate system with respect to the navigation base after the shock of landing is unknown. There is little chance of satisfying the bias stationarity condition, and the Kalman estimator is confronted with an unknown mix of tilt and boresight bias. Under these circumstances, there is no feasible remedy for bias uncertainties, and the computer software is designed to utilize only range and range-rate information for state-vector updating.

#### 4.10.7 Functional Protection of the Rendezvous Radar

The computer programs are designed to include several features to ensure optimal use of the radar. One such provision is a calculation of range to the command module, based on lunar and command module state vectors. If the calculated range exceeds 400 n. mi., the computer refuses to proceed with the radar routines and displays an alarm. The intent of this feature is to prevent the radar from being used beyond its 400 n. mi. design limit, which could result in degraded range measurement accuracy or in ambiguous range readout.

Another software feature automatically changes the radar angular mode, if necessary, to allow the radar designation along the calculated line of sight, or prevents designation if the line of sight does not lie within either mode limit. This latter characteristic prevents the radar from driving into the gimbal mechanical stops and it avoids excessive repositioning of the antenna.

PRECEDING PAGE BLANK NOT FILMED

SECTION 5.0  
LANDING RADAR

5.1 FUNCTIONAL REQUIREMENTS

The landing radar is employed during the latter portion of the lunar-module powered descent. It is a terminal measurement device providing range and velocity measurements for final update of the lunar module state vector in the computer as the vehicle approaches the lunar surface. The radar provides slant range and orthogonal velocity components with respect to the lunar surface, referenced to the antenna coordinate system.

The tracking circuits of the radar measure the Doppler shifts along three velocity beams and the range along an altimeter beam. By appropriate coordinate transformation within the radar electronic assembly, the desired velocities and range in antenna coordinates are obtained. Within the guidance computer, a further transformation relates the measurements to platform coordinates prior to update computations.

5.2 OPERATING LIMITS

The operating limits for the radar as originally derived and as currently specified in the Performance and Interface Specification are based on MSC Design Reference Mission Number 1 and on a very cautious estimate of minimum lunar radar reflection coefficients. Among the more important limits are the following.

Maximum Altitude . . . . . 25 000 ft for range data;  
15 000 ft for velocity data

Minimum Altitude . . . . . 10 ft for range data;  
5 ft for velocity data

Velocity limits on antenna axes:

$V_{xa}$  . . . . . -2000 to 500 fps  
 $V_{ya}$  . . . . .  $\pm 500$  fps  
 $V_{za}$  . . . . . 3000 to -500 fps

### 5.3 MEASUREMENT ACCURACY

The radar measurement accuracy for purposes of automatic landing is specified in detail in LSP-370-3A together with conditions applicable to the specification. A summary of measurement performance is given in Table 5-1.

TABLE 5-1  
LANDING RADAR MEASUREMENT PERFORMANCE SUMMARY

a. Range accuracy ( $3\sigma$ )

Altitude Range	25 000 to 3000 ft	3000 to 2000 ft	2000 to 10 ft
Accuracy	2%	3%	1.5% + 5 ft

b. Velocity accuracy ( $3\sigma$ )

Altitude Range Velocity Parameter	15 000 to 6000 ft	6000 to 2500 ft	2500 to 200 ft	200 to 5 ft
$V_x$	1.5%	1.5%	1.5%	1.5% or 1.5 fps
$V_y$	2.0%	3.5%	4%	2.5% or 2.5 fps
$V_z$	2.0%	2.5%	3%	2.5% or 2.5 fps

### 5.4 DESCRIPTION OF THE LANDING RADAR

The following paragraphs describe the operational landing radar.

#### 5.4.1 Antenna Coordinate System

The radar antenna coordinate system is defined in Figure 5-1. Lines 0-1, 0-2, and 0-3 represent the principal radiation axes of velocity beams 1, 2, and 3 respectively, and line 0-4 represents the axis of the altimeter or range beam. The radar measures velocity with respect to this coordinate system, but measures slant range along the axis of beam 4. In the flight radars,  $\epsilon = 20^\circ 38$  degrees and  $\theta = 24.55$  degrees.

The radar antenna coordinate system is related to the GN&C system navigation base by a specified set of Euler angles ( $\alpha, \beta$ ) for each of two radar antenna positions. Definition of the Euler angles is shown in Figure 5-2.

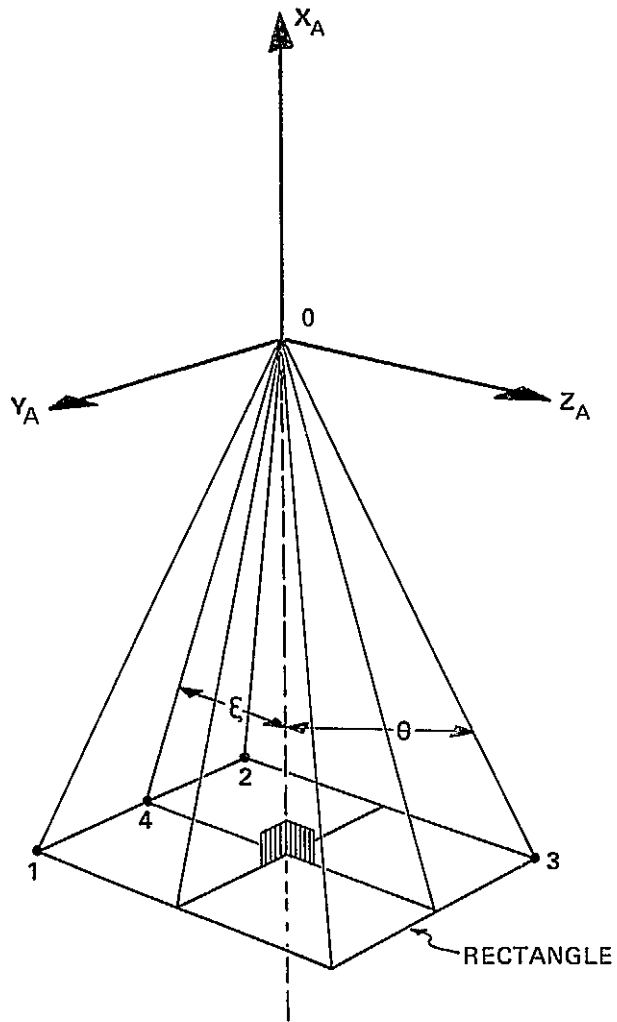


Fig. 5-1 L. R. Antenna Coordinate System

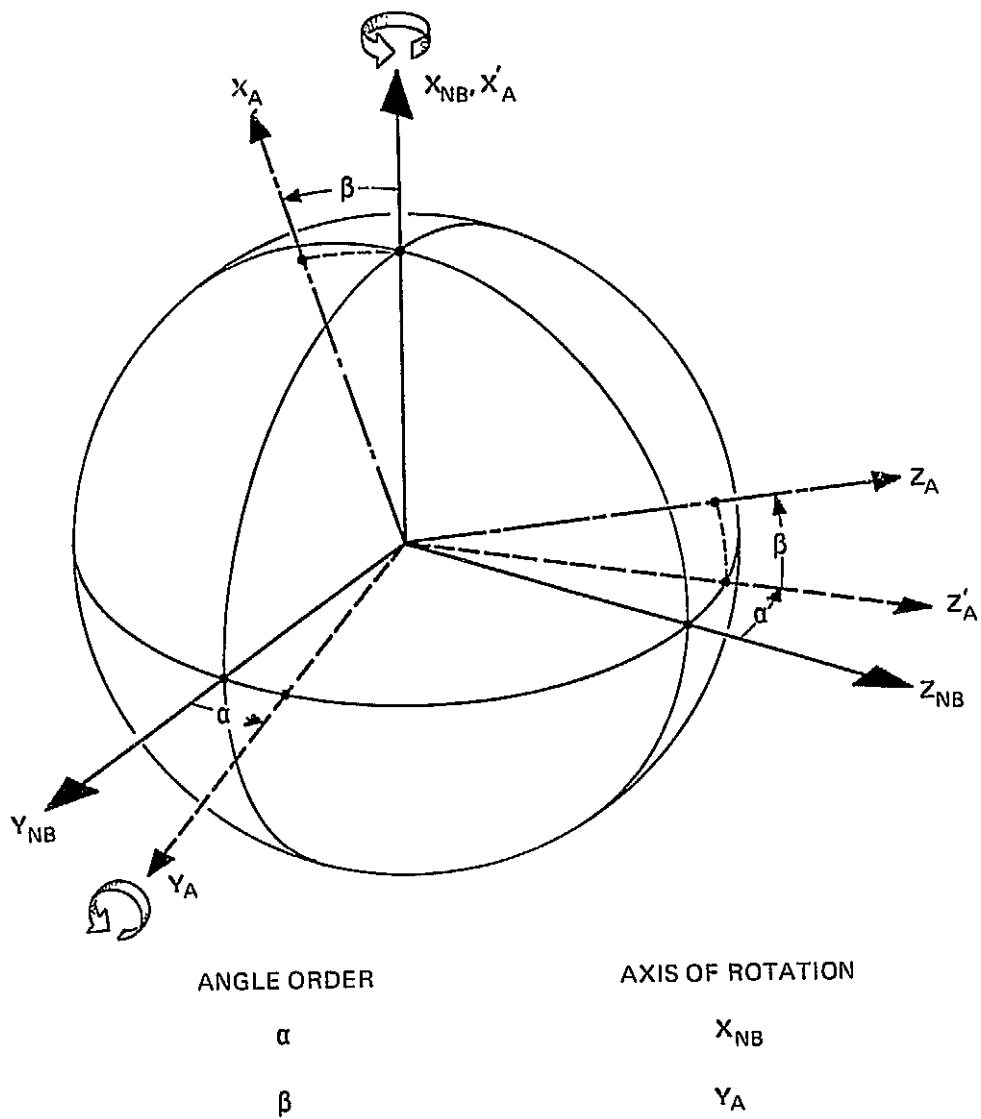


Fig. 5-2 Angles Defining Orientation of LR Antenna Axes with Respect to the Navigation Base Coordinate System

#### 5.4.2 Physical Description

The radar is composed of two assemblies with a total weight of 43.3 lb and a maximum power consumption of 132 Watts. A photograph of the two assemblies appears in Figure 5-3. The antenna assembly is located external to the lunar module descent stage on the underside of the spacecraft, adjacent to the retrorocket skirts. Thermal finishes and protective coatings are applied to the antenna assembly to control temperature during all phases of the APOLLO mission. Vacuum-deposited aluminum is used in conjunction with selected thermal-paint patterns to carefully control the ratio of thermal energy absorptance to emittance.

The antenna assembly contains a three-beam, CW, velocity-sensor, receiver-transmitter and a single-beam, frequency-modulated, CW altimeter receiver-transmitter. The transmitting and receiving antennas are planar arrays. The velocity sensor and altimeter transmitting arrays are mechanically interlaced into a common aperture. The beam angles are fixed in the antenna coordinate system.

#### 5.4.3 Landing Radar Operation

The radar senses the velocity and slant range of the lunar module relative to the lunar surface by means of a three-beam Doppler velocity sensor and a radar altimeter. The velocity and range information is processed and made available to the computer in serial binary form.

The radar, located in the descent stage of the lunar module, is packaged in two replaceable assemblies shown in the block diagram, Figure 5-4. The antenna assembly (AA) serves to form, direct, transmit, and receive four narrow microwave beams. To perform this function, the antenna assembly is composed of two interlaced slotted waveguides for transmission, and four space-duplexed planar arrays for reception. The transmitting arrays form a platform on which are mounted four quadrature-pair balanced microwave mixers, four dual audio-frequency preamplifiers, two solid-state microwave transmitters, a frequency modulator, and an antenna pedestal tilt mechanism. The electronic assembly (EA) contains the circuitry required to track, process, convert, and scale the Doppler returns that provide the velocity and slant range information to the lunar module computer.

The CW microwave energy from the velocity sensor's solid-state transmitter is radiated toward the lunar surface by the transmitting antenna. Reflected energy is received by three separate receiving antennas. The received Doppler-shifted energy

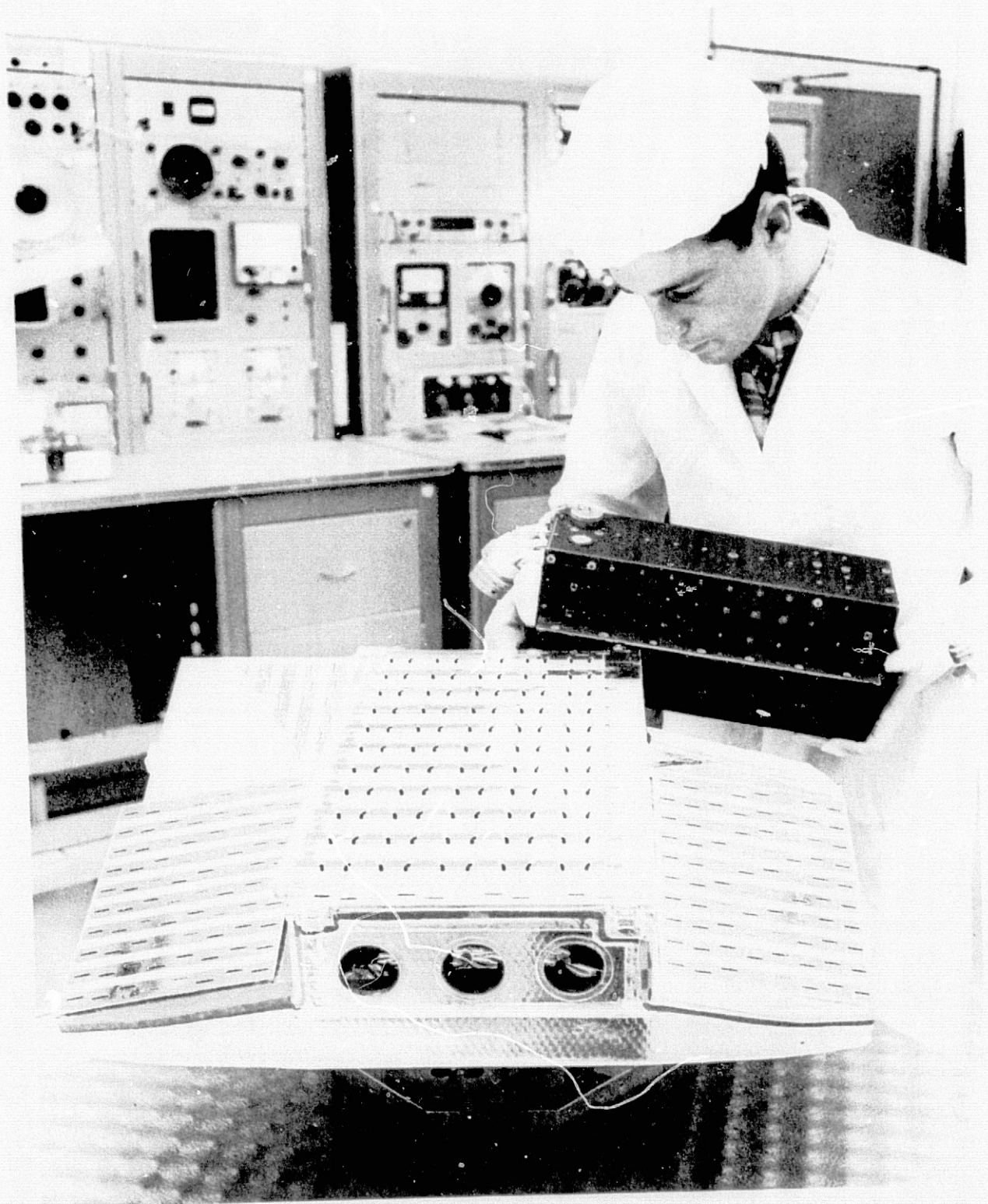
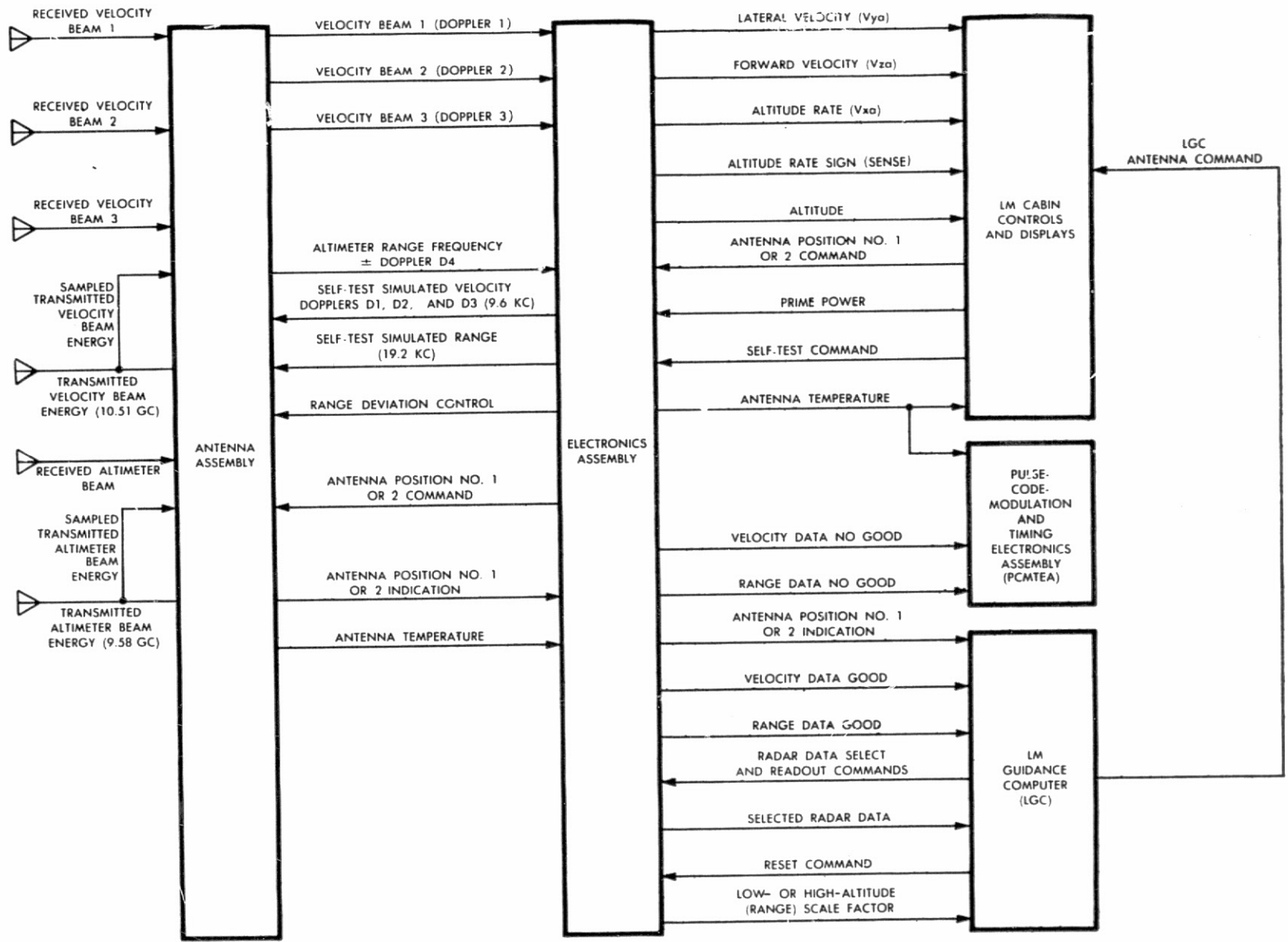


Fig. 5-3 LR Antenna and Electronic Assemblies



137

Fig. 5-4 LR Antenna and Electron Assemblies Block Diagram

is homodyned<sup>1</sup> in the balanced mixers to yield an output-difference frequency that is the Doppler shift between the received and transmitted signals. The difference is directly proportional to velocity between the lunar module and the lunar surface along the beam axis.

The altimeter transmitter is frequency-modulated in a sawtooth manner at a repetition rate of 130 Hz. The altimeter microwave energy is applied to the altimeter transmitting antenna and directed at the lunar surface. The backscattered received energy is also homodyned to produce a difference frequency at the output of the balanced mixers, proportional to the slant range along the range beam, plus the Doppler shift. A Doppler correction, derived from Doppler measurements of beams 1 and 2, is made in the range computer of the electronic assembly before transmission of range data to the lunar module computer.

The quadrature outputs of the three velocity sensors and the altimeter mixers are applied to associated audio preamplifiers containing automatic gain switching based on received signal strength.

The signals at the preamplifier outputs are applied to the frequency trackers in the electronic assembly. After searching and acquiring the signal over the expected frequency range with a narrow-band tracking filter, the frequency trackers track the centroid of the signal spectrum. The output of each velocity tracker is a signal of 153.6 kHz plus a frequency corresponding to the power centroid of the velocity-beam Doppler spectrum. The output of the range tracker is a signal of 153.6 kHz plus a frequency corresponding to the centroid of the Doppler-shifted spectrum of the range-beam return.

The velocity tracker outputs are routed to the velocity data converter/computer for resolution into components corresponding to the antenna coordinate system. To facilitate indication of the sign of the velocity, each of the resolved signals is presented to the signal data converter in the form of a pulse train deviated from a 153.6-kHz center frequency by an amount proportional to the coordinate velocity. The signal data converter interfaces with the lunar module guidance computer by accepting strobe signals from the computer for gating and readout of velocity data in serial binary form. The serial binary radar output information is fed to the computer.

---

1. A heterodyning process used in a receiver with zero intermediate frequency. The function of the local oscillator in a conventional superheterodyne receiver is replaced by a portion of the transmitted signal that is leaked into the balanced mixer to produce the output difference frequency.

The range tracker output enters the range data converter for compensation of beam 4 Doppler shift and emerges as a pulse train whose frequency is proportional to slant range. This output is applied to the signal data converter for gating and transfer to the computer.

Radar status signals, which include Range Data Good, Velocity Data Good, Antenna Position Indication, and Range Scale Factor, are provided to the computer in the form of discrete relay contact closures.

#### 5.4.4 Landing Radar Design Features to Counter Vehicle Effects

Of necessity, the radar antenna assembly is mounted on the underside of the lunar module descent stage to provide both a view of the lunar surface during the powered descent and maximum available mechanical mounting rigidity. However, the environment is unfavorable for best operation of the radar.

One problem encountered early in the design of the lunar module was interception of part of beam 1 by the rear leg and foot of the module. To minimize this difficulty, the antenna assembly mounting point was relocated and the antenna coordinate system was skewed with respect to the module body axes to displace beam 1 from the rear leg. The skew angle,  $\alpha$ , is -6 degrees (Figure 5-2).

In the powered descent, during the period of desired usage of the radar, the lunar module changes pitch angle (i.e., rotates about its Y-axis) by a total of approximately 75 degrees, a change that is too extreme to allow acceptable incidence of the radar beams with the lunar surface. By providing the radar antenna assembly with a two-position pedestal and the capability of quickly reaching either position by rotation about the antenna Y-axis, the effect of vehicle pitch variation is circumvented, making possible acceptable radar performance. The angles specifying the two fixed antenna assembly positions are  $\beta_1 = -24$  degrees and  $\beta_2 = 0$  degree (Figure 5-2).

Another problem for the radar was potential spurious signal inputs arising from modulation of reflected antenna sidelobe energy. Modulation was possible from mechanical sources such as vibration of the descent engine bell, vibration of the lunar module rear leg and foot, and movement of the thermal blanket on the underside of the module descent stage. There was a possibility also that weak spurious signals could be produced by the scattering of radar energy from the descent engine plume. Considerable analytical and experimental work was expended both by the radar supplier (Ryan) and Grumman to determine the magnitude of these problems. Subsequently, several features were included in the radar design to preclude these

difficulties in the radar environment. RF shields were added to the radar antennas to reduce sidelobe sensitivity. A non-vibratory reflector was interposed between the antenna assembly and the engine bell to divert radar sidelobe energy from the bell and thus prevent modulation. The radar acquisition circuits were designed to distinguish between the desired single-sideband, Doppler-shifted return, and double-sideband, amplitude-modulated return. The circuits thereby rejected acquisition and track of much of the vibration-induced spurious signals, which are often of the double-sideband variety. Finally, the passbands of the Doppler preamplifiers were substantially attenuated at low frequencies to decrease receiver sensitivity to vehicle-induced noise signals strongest in the low frequency region. This protection against spurious lock-up was achieved, however, at the price of enlarging the zero-Doppler dropout region because of receiver insensitivity to low frequency Doppler signals.

#### 5.4.5 Landing Radar-Computer Interface

The radar responds to and communicates with the GN&C system by means of a digital interface between the radar signal data converter and the GN&C system computer. This interface is described in R-404 and R-1904, and is specified in LSP-370-3A and in ICD LIS-370-10004, "LGC-LM Electrical Interface."

The digital interface is the means by which the computer digitally commands and controls the radar, as well as the path by which the radar transmits digital measurement and status information to the computer. The signal paths comprising the interface are indicated in simplified form in Figure 5-5.

The radar interface circuits contained in the signal data converter include:

1. A gate for each radar measurement ( $S_{XA}$ ,  $S_{YA}$ ,  $S_{ZA}$ ,  $S_{RA}$ ), controlled by the computer, feeding a binary high speed counter.
2. A high speed counter capable of accumulating a count controlled by the selected gate, and of serially transferring the count to the computer on command.

Selection of the data to be read out (range or velocity) and the time of readout are accomplished by the computer through activation of the appropriate gate strobe-pulse train to the radar. A gate-reset continuous pulse train is transmitted to the radar whenever the computer is operating. To read out, the computer first transmits the desired strobe pulse train that, in combination with the gate-reset pulse train, causes the associated gate in the radar to turn on (open), permitting the measurement signal

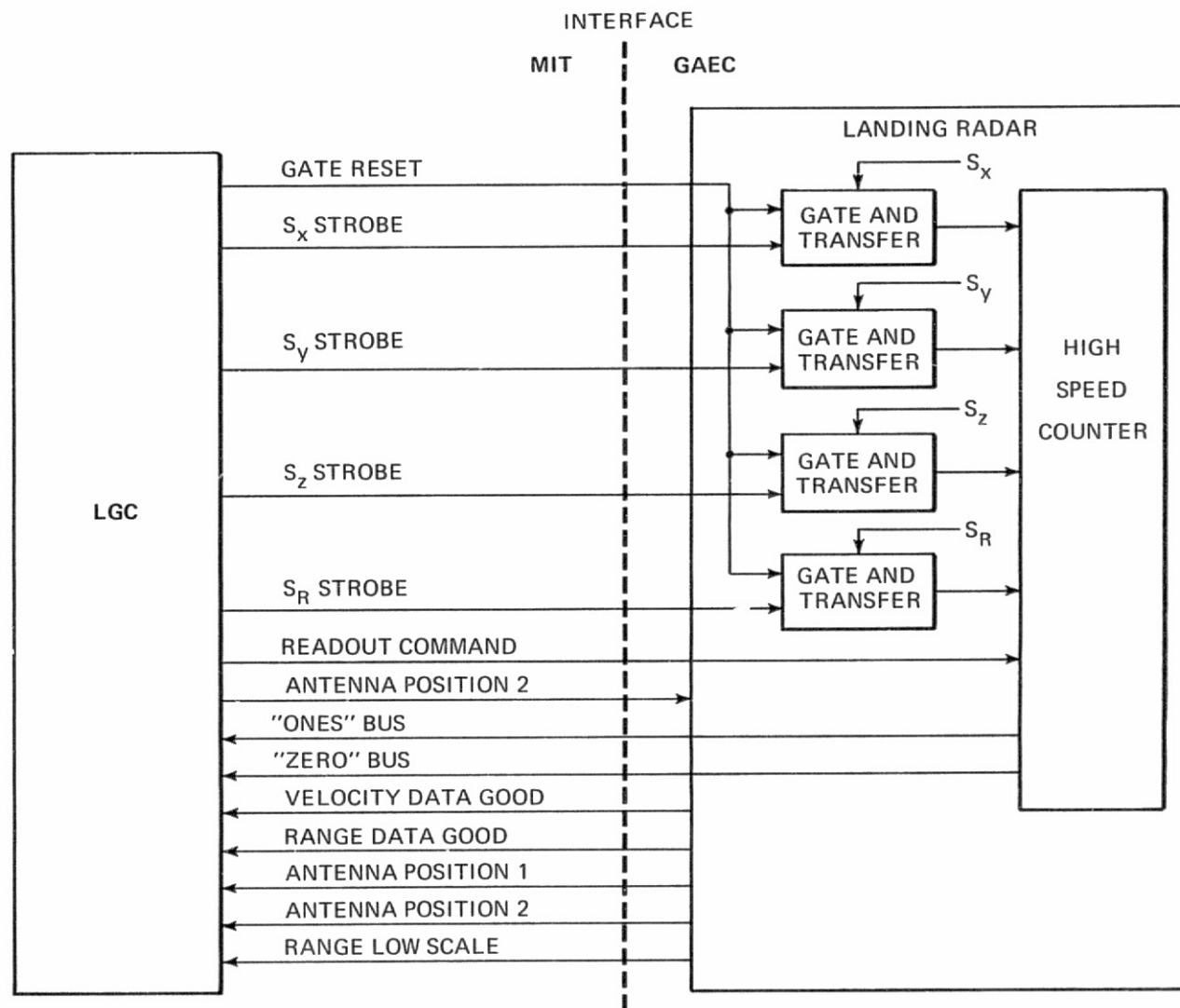


Fig. 5-5 LGC - LR Interface

to enter the binary counter and accumulate a count that is a function of the selected parameter. Upon withdrawal of the gate strobe pulse train, the gate is turned off (closed) when the next pulse of the gate-reset pulse train is received. Upon receipt from the computer of a readout command in the form of a pulse train, the contents of the radar shift register are serially shifted across the interface to the computer, the 1 bits being transferred on a 1's bus and the 0 bits being transferred on a 0's bus. The most significant bit is read out first. No more than one parameter gate is commanded open by the computer at any one time, and another gate will not subsequently be commanded open until the gate strobe counter readout cycle of the first data transfer has been completed.

The radar accepts from the computer a discrete command designated Antenna Position 2, causing the radar to move the antenna to Position 2 in the absence of an overriding manual command.

The radar provides to the computer the discrete status signals shown in Table 5-II. All discrete signals are unipolar dc.

TABLE 5-II  
LANDING RADAR STATUS DISCRETES

Status Discrete	Function
VELOCITY DATA GOOD	Indicates that velocity data from the radar are within accuracy specifications and are valid for computer use except for a period of 4 sec after first appearance or reappearance
RANGE DATA GOOD	Indicates that range data from the radar are within accuracy specifications and are valid for computer use, except for a period of 4 sec after first appearance or reappearance
ANTENNA POSITION 1	Indicates that the radar antenna occupies position 1
ANTENNA POSITION 2	Indicates that the radar antenna occupies position 2
RANGE LOW SCALE	Indicates that the computer should use the radar scale factor specified for close range measurements

The landing radar-computer interface employs standard computer circuit designs common to interfaces between the computer and other subsystems. A description of the salient electrical characteristics of this interface and circumstances affecting its design appear in Section 4.10.

## 5.5 LANDING RADAR INTERFACE SOFTWARE

A considerable body of subroutines is carried in the computer specifically for use with the landing radar. The software selects the measurement desired from the radar at the appropriate time, commands and controls the readout, extracts the bias count from the velocity data, applies scale factors, tests the data for validity, transforms the data into appropriate coordinate systems, weighs the data, updates the state vector with weighted measurements, generates panel displays and alarms, commands the radar antenna to Position 2, responds to DATA GOOD status, and applies radar outputs to the telemetry downlink.

The velocity data are obtained from the radar with respect to the radar antenna coordinate system of Figure 5-1, and are transformed by the computer into the navigation base coordinate system.

The velocity data furnished at the computer interface by the radar comprise three binary data words of the following form:

$$S_{XA} = \left[ (f_1 + f_3) / 2 + f_B \right] \tau_{LR}$$

$$S_{YA} = \left[ (f_1 - f_2) + f_B \right] \tau_{LR}$$

$$S_{ZA} = \left[ (f_3 - f_2) + f_B \right] \tau_{LR}$$

where  $S_{XA}$ ,  $S_{YA}$ , and  $S_{ZA}$  correspond, respectively, to the velocity components along the  $-X_A$ ,  $+Y_A$ , and  $+Z_A$  antenna axes of Figure 5-1. The quantities  $f_1$ ,  $f_2$ , and  $f_3$  are the beam Doppler frequencies,  $f_B$  is the bias frequency used in the radar, and  $\tau_{LR}$  is the time interval used by the radar when counting the cycles of the above frequencies so as to produce the data words  $S_{XA}$ ,  $S_{YA}$ , and  $S_{ZA}$ . The time interval  $\tau_{LR}$  is 80.000 msec.

In the computer, the velocity along each antenna coordinate axis is computed from the above data words as follows:

$$v_{XA} = k_{XA} (S_{XA} - f_B \tau_{LR})$$

$$v_{YA} = k_{YA} (S_{YA} - f_B \tau_{LR})$$

$$v_{ZA} = k_{ZA} (S_{ZA} - f_B \tau_{LR})$$

where  $v_{XA}$ ,  $v_{YA}$ , and  $v_{ZA}$  are the radar measured velocities along the positive antenna coordinate axes, and  $k_{XA}$ ,  $k_{YA}$ , and  $k_{ZA}$  are the corresponding scale factors used to obtain the above velocities in feet-per-second.

The range data obtained from the radar are measured along the range beam shown in Figure 5-1. These data are sent to the computer from the radar as a binary data word,  $R_{LR}$ , which represents the count of a certain frequency in the radar during the time interval  $\tau_{LR}$ . Within the computer, the range  $r_{LR}$  along the range beam is computed as follows:

$$r_{LR} = \begin{cases} k_{LR1} R_{LR} \\ k_{LR2} R_{LR} \end{cases}$$

where  $k_{LR1}$  and  $k_{LR2}$  are the bit weights, respectively, for the long and short range scales in order to obtain  $r_{LR}$  in feet. When the radar range low scale discrete is being received from the radar by the computer,  $k_{LR2}$  is used.

A summary of the processing constants required by the computer for radar operation follows:

- $f_B$  . . . . . Velocity bias frequency.
- $\tau_{LR}$  . . . . . Counting interval of the radar.
- $k_{XA}$  . . . . . Scale factor to convert  $(S_{XA} - f_B \tau_{LR})$  to velocity along the radar antenna coordinate  $X_A$  (Figure 5-1) in feet-per-second for the counting interval  $\tau_{LR}$ .
- $k_{YA}$  . . . . . Scale factor to convert  $(S_{YA} - f_B \tau_{LR})$  to velocity along the radar antenna coordinate  $Y_A$  in feet-per-second for the counting interval  $\tau_{LR}$ .
- $k_{ZA}$  . . . . . Scale factor to convert  $(S_{ZA} - f_B \tau_{LR})$
- $\alpha_1, \beta_1$  . . . . . Respective angles between the radar antenna coordinate system in Position 1 and the navigation base coordinate system (Figure 5-2).
- $\alpha_2, \beta_2$  . . . . . Respective angles between the radar antenna coordinate system in Position 2 and the navigation base coordinate system (Figure 5-2).

$k_{LR1}$  ..... Bit weight in feet for long range scale.  
 $k_{LR2}$  ..... Bit weight in feet for short range scale  
 $\epsilon$  ..... Angle of range beam with respect to the  $-X_A$  axis  
of the radar antenna.

A complete description of the radar software is contained in Sections 4 and 5 of the SUNDANCE and LUMINARY GSOP series.

### 5.5.1 Computer Processing of Velocity Data

Early in APOLLO development, before the fine details of the interface between the radars and the GN&C system had been decided, the measurement accuracy of the landing radar was computed on the basis of data smoothing provided by 400-msec accumulation time in the radar high speed counter for velocity measurements, and 200-msec accumulation time for range. However, accumulation of the velocity bias frequency ( $f_B = 153.6$  kHz) alone in 400 msec exceeded the 15-bit capacity available for the landing radar-computer data transfer interface. Since provision for 400 msec of analog smoothing in the radar, or alternatively, the reduction of the radar bias frequency both implied substantial redesign of the radar, a decision was made to accomplish the smoothing task in the computer by an incremental technique. For this purpose, the standard computer radar read subroutine, consisting of an 80-msec gate pulse train followed shortly by the readout command pulse train, was invoked several times in succession; the individual measurements obtained were summed and averaged in the computer. Experimental investigation conducted at MIT/IL with a radar electronic assembly as part of the Phase II Integration Tests concluded that averaging of five 80-msec data samples to yield a single velocity measurement afforded an optimum trade-off between data smoothing and measurement error due to data staleness. Radar velocity measurements are therefore the average of five 80-msec samples. Because smoothing is not as important, all other radar readouts by the guidance computer (rendezvous radar, VHF ranging, and landing radar range) are accomplished with a single read subroutine cycle.

Although the special treatment of radar velocity readout furnishes the necessary smoothing, it also introduces larger quantization errors than those associated with a single continuous 400-msec accumulation interval. Results of analyses of these errors are given in the reports referenced below.<sup>2</sup> In the case of APOLLO 11 radar

2. "Velocity Errors in Lunar Landing Radar Caused by Digital Processing," E-1937; Janusz Sciegienny, March 1966 (See Part IV, Appendix A, Abstracts, E-1937); See also the results of "Quantization Error Studies," E. P. Blanchard; Enclosure 3, Minutes of Radar Integration Meeting No. RIM-115n; MSC-Houston; 6 May 1969.

implementation, the quantization bias was shown to be negligible, with random quantization error less than 0.5 fps peak under worst case conditions.

### 5.5.2 Landing Radar Reasonableness Test

One of the major uncertainties complicating the radar design was that of the lunar surface reflectance at the operating frequencies of the radar. For design purposes, best available information was used to define a conservative minimum reflectance as a function of beam angle of incidence; a maximum reflectance 12 dB greater than minimum was postulated. The radar was required to operate within specifications over this reflectance range. Analysis revealed that a radar of sufficient sensitivity to measure within specifications under minimum reflectance conditions would, under maximum reflectance, be vulnerable to cross-lobe lockup (tracker acquisition and track of a spurious signal), arising either from (1) receiver main-beam reception of surface-reflected transmitter-antenna sidelobe energy, or (2) receiver beam sidelobe reception of surface-reflected transmitter-antenna main-beam energy.

Full recognition of this problem occurred after much of the radar design had been completed. Because substantial design changes would have been required to protect against sidelobe lockup in the radar, a decision was made to implement a data reasonableness test in the computer for the exclusion of false data from sidelobe lockup. Consequently, all lunar module program assemblies have contained a radar reasonableness test that compares each radar measurement with the same quantity as determined from the lunar module state vector. In APOLLO 11, the velocity acceptance criterion was

$$|\delta q| \leq (7.5 + 0.125 V_T) \text{ fps}$$

where  $\delta q$  is the difference between the radar velocity measurement and the value estimated from the state vector, and  $V_T$  is the magnitude of the lunar module estimated velocity. The range acceptance criterion was

$$|\delta q| \leq (200 + 0.125 h) \text{ ft}$$

where  $\delta q$  is the difference between the altitude derived from the radar range measurement and the estimated altitude, and  $h$  is the estimated altitude with respect to the landing site. The altitude reasonableness test is omitted above high gate because of the possibility of improperly excluding valid altitude data that may be in error by several thousand feet when the radar is first employed in the powered descent. Although the reasonableness test was specifically designed to combat cross-lobe lockup, it will obviously reject any measurement that fails to meet the criterion, regardless of the cause of the error.

## SECTION 6.0 VHF RANGING SYSTEM

### 6.1 FUNCTIONAL REQUIREMENTS

The active vehicle during rendezvous is normally the lunar module that performs its navigation measurements with the inertial measurement unit during maneuvers and with the rendezvous radar during coasting phases. Early APOLLO planning contemplated an identical radar on the command module to act as a backup system by providing range, angle, and range rate measurements to the command module computer and to the lunar module via voice link, but this scheme was eliminated from the program as mentioned in Section 2.0.

In July of 1967, MSC directed that the existing backup capability of the command module-based navigation system be augmented by modification of the existing VHF communications link to measure range, thereby supplementing angle data available from the optical subsystem, i.e., the scanning telescope and the sextant.

During a lunar mission, it is intended that while the lunar module, as the active vehicle, is performing its rendezvous navigation, the sensors in the command module provide an independent check on lunar module navigation. The command module may also assume the active role in rendezvous in the event that the lunar module GN&C fails or that the lunar module propulsion system is unable to perform the required rendezvous maneuvers.

### 6.2 OPERATIONAL CHARACTERISTICS

The range measurement capability of the VHF communications equipment was achieved by modifying the transceivers in both the command and lunar modules. The modifications affected the interface with the GN&C system in the command module only.

Basically, the ranging system is implemented by incorporating a ranging unit (digital ranging generator) in the command module and a range tracker (range tone transfer assembly) in the lunar module. Operationally, the ranging mode is initiated by astronaut call-up in the command module. The transceiver in the lunar module acts as a transponder; it receives, demodulates, and re-keys the lunar module

transmitter with the recovered and reconstituted modulation. The signal is received at the command module receiver and demodulated. The time delay between the transmitted and received modulated signal is measured in the command module ranging unit. The time delay is a measurement of the two-way propagation time, including equipment circuit delays. The fixed circuit delays are compensated for in the measuring process and the time delay is converted to a range measurement. A three-tone modulation system eliminates ambiguity at long range and provides the required accuracy at short range.

Ranging activity is astronaut-initiated in the command module and begins an automatic sequence using the three ranging modulation tones. The acquisition phase, which takes between 10 and 15 sec to complete, is followed by a tracking phase employing only the high frequency tone. Valid range data are obtained only in the tracking phase. Simultaneous operation of voice modulation and range measurements is possible only during the tracking phase. Potential voice transmission interference with the lower two ranging frequencies used during acquisition is automatically inhibited during this period. As an operational procedure, voice transmission is not used when the VHF system is developing range data for use in updating the command-to-lunar module state vector.

Upon completion of proper acquisition as verified by internal tests, the tracking phase begins and a DATA GOOD discrete is issued by the VHF system to denote that valid range data are available for use in the guidance computer. The DATA GOOD tests are performed automatically during the acquisition sequence and prior to transferring range data upon computer command. The VHF range data are utilized for state vector update at approximately 1-minute intervals.

### 6.3 OPERATING LIMITS

The VHF ranging system is designed to measure range to specified accuracies over a range interval from several hundred feet to 200 n. mi. for all range rates and accelerations occurring during rendezvous. In addition, in the interval between 200 and 327 n. mi., the VHF system in conjunction with the command module computer is capable of unambiguous measurement to unspecified accuracies.

### 6.4 MEASUREMENT ACCURACY

VHF ranging accuracy is nominally 450 ft,  $3\sigma$ , within the operating limits. Ranging accuracy is determined primarily by uncertainties in the signal delays occurring within the VHF circuitry. These delays vary principally with temperature and

somewhat with signal strength about a mean value that can be determined for an ensemble of VHF ranging systems and compensated for in a calibration procedure. Thermal noise is a relatively small contributor to total measurement uncertainty. These properties of the system result in measurement uncertainty that is nearly independent of range.

## 6.5 COMPUTER-VHF RANGING INTERFACE

Figure 6-1 is an interface block diagram of the added digital ranging generator (DRG). The connections to the guidance computer are shown encircled.

The governing document defining the interface characteristics of the VHF ranging equipment and the guidance computer is North American ICD No. MH01-01380-216. Signal waveform and timing requirements, circuit source and load impedances, as well as wiring and shielding of interconnections, are detailed in this document.

Five pairs of leads interconnect the computer to the VHF ranging equipment. The computer generates two outputs: a Range Strobe signal and a Readout Command signal. Each signal is transmitted to the VHF system on a pair of leads. Range data between the command and the lunar modules are furnished by the VHF ranging equipment on two pairs of lines in the form of a 15-bit binary word. A DATA GOOD discrete signal is furnished to the computer when the data from the VHF equipment are suitable for use by the computer.

To initiate the transfer of range data, the computer transmits to the VHF equipment a range strobe consisting of a train of 256 pulses at a 3.2-kHz rate, occupying a total time interval of 80.000 msec.

Approximately 5 msec after completion of the range strobe, the computer transmits a COMMAND READOUT signal which is a train of 15 pulses at a 3.2-kHz rate.

The VHF equipment utilizes the range strobe to initiate the transfer of data to the range output register and uses the COMMAND READOUT signal to sequentially shift the data from the range register to the computer on each of two data lines, one line for binary 0's and the other for 1's. The most significant bit is shifted first.

## 6.6 INTERFACE EVALUATION TESTS

During October 1968, MIT/IL was furnished with a simulator of the VHF ranging digital interface unit for three specific purposes: 1) to evaluate the ranging unit

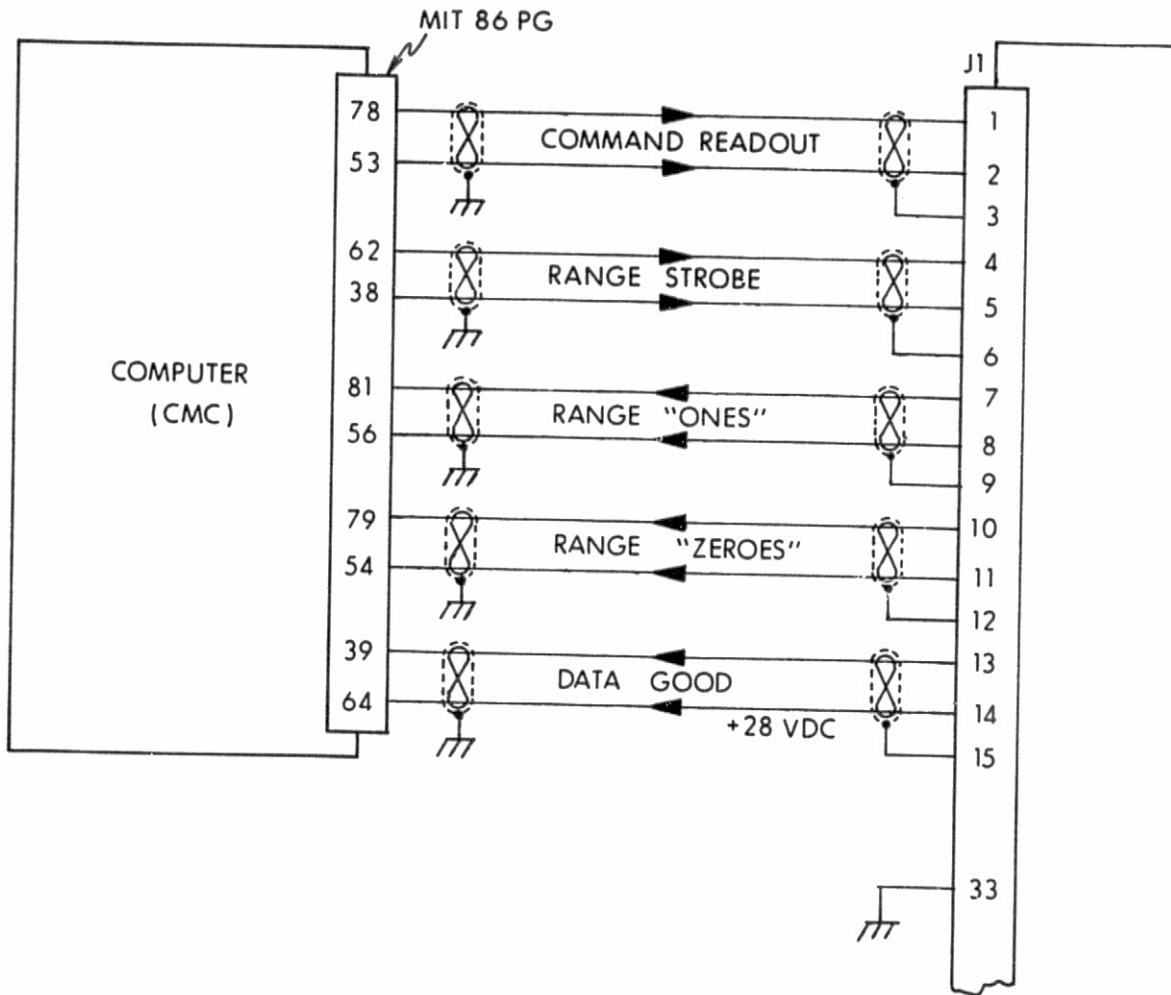


Fig. 6-1 DRG Interface Block Diagram

design to ensure functional compatibility between the VHF ranging system and the navigation system, 2) to verify compliance with the interface control document, and 3) to provide a ready means of injecting precisely defined data into the computer for purposes of software program verification.

#### 6.6.1 VHF Interface Simulator

Figures 6-2 and 6-3 show the general configuration of the unit after minor modifications were incorporated at MIT/IL.

The circuitry of the unit is located on two boards, one designed to simulate the readout register of the VHF digital ranging generator and the other to simulate the interface circuits between the digital ranging generator and the guidance computer. The interface circuit board was adapted from a production type unit and is an excellent simulation of the operational equipment both mechanically and electrically. The unit was furnished with an 8-foot cable representative of the spacecraft harness.

The VHF ranging interface simulator is fully representative of the operational equipment from a functional point of view. The binary range switches which establish the range data to the computer replace the logic levels furnished by the three-tone range tracker of the actual equipment. The front panel DATA GOOD switch gates a representative excitation signal to the interface discrete circuit. The resulting static range signal transferred to the computer from the preset storage register is precisely defined.

#### 6.6.2 Evaluation

The simulator was subjected to a variety of tests under laboratory conditions to ensure compatibility with the computer and compliance with the interface control document including evaluation of such operational characteristics as signal waveform, signal timing, input and output impedances, and the effect of transmission lines typical of those expected in the spacecraft configuration.

The tests showed fully compatible operation between the simulator and the computer.

### 6.7 VHF RANGING SYSTEM INTERFACE SOFTWARE

Rendezvous Tracking Data Processing Routine R-22 is the computer routine that periodically processes the sextant and/or VHF ranging data to update the state vector of either the command or the lunar module. R-22 is automatically called by Rendezvous Navigation Program P-20.

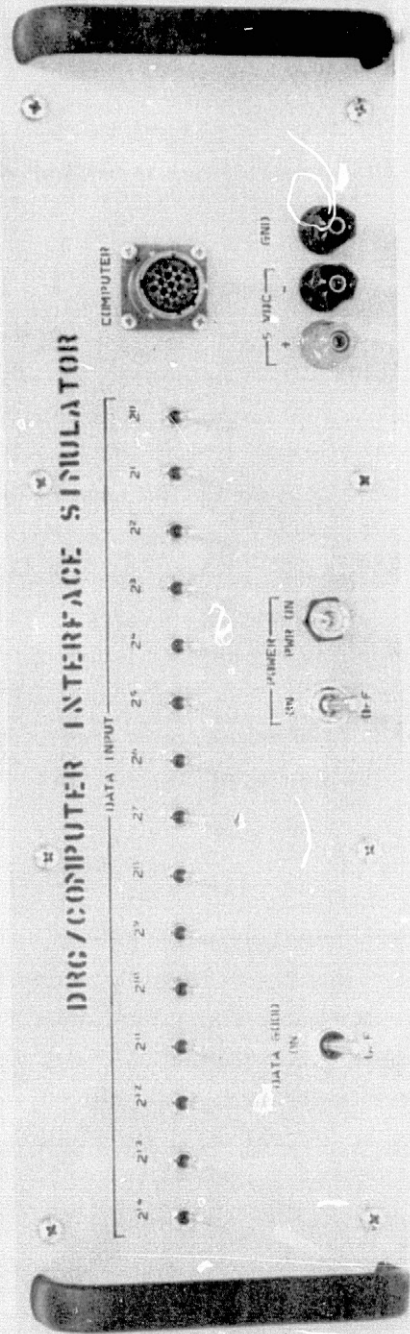


Fig. 6-2 General Configuration of VHF Interface Simulator

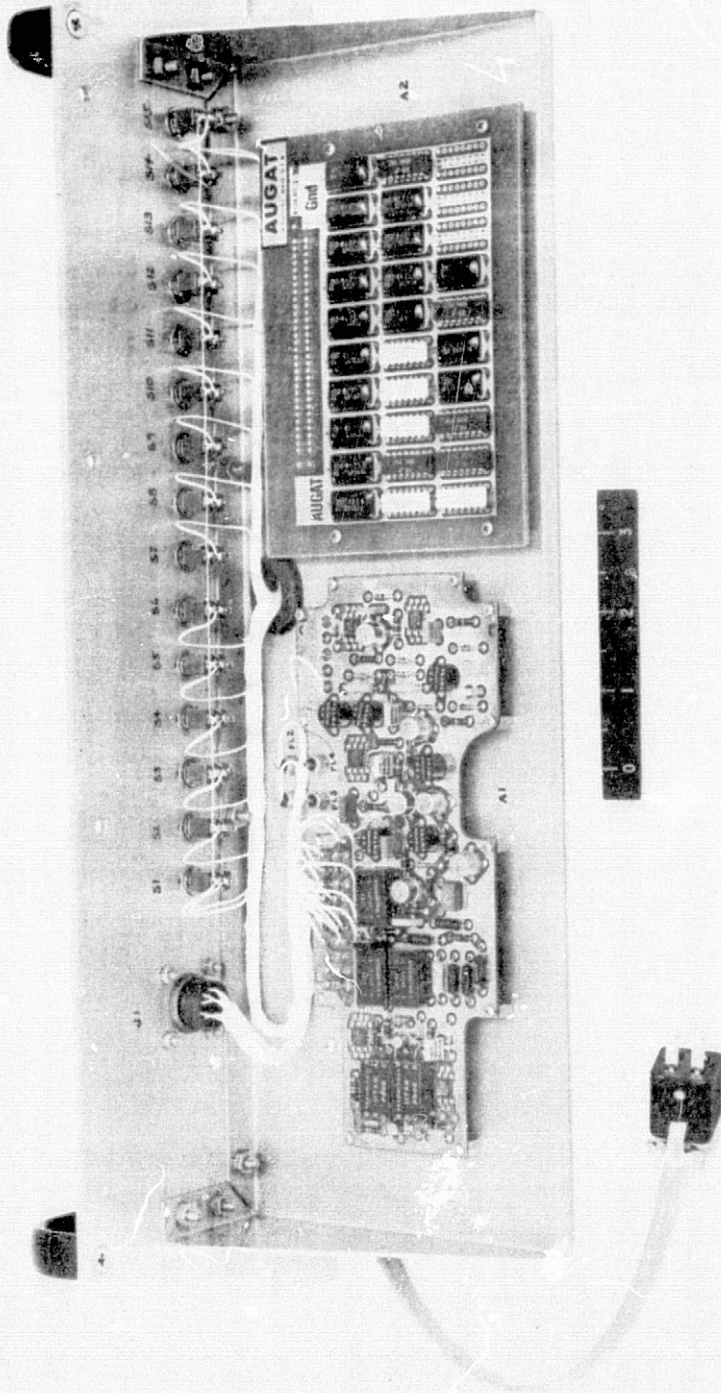


Fig. 6-3 General Configuration of VHF Interface Simulator

Prior to utilization of VHF ranging data, P-20 calls Preferred Tracking Attitude Routine R-61 that controls the attitude of the command module with respect to the line of sight to the lunar module to assure proper coverage of the lunar module by the sextant field of view, the rendezvous radar transponder antenna pattern, and the VHF antenna pattern.

Once the astronaut has set the VHFR flag, indicating his desire to utilize range measurements in the state vector update process, R-22 reads VHF data no oftener than once per minute, provided the VHF DATA GOOD discrete is present, and interleaves these measurements with angle data obtained from the sextant. However, neither sextant nor VHF data are employed for update during periods of command module maneuver to avoid possible measurement errors. The software includes an update check that signals an astronaut alarm in the event that the incorporation of measured data would produce a change of state vector in excess of predetermined limits, and automatic update is suspended pending astronaut disposition.

R-22 counts the number of VHF measurements that have been used for update purposes and displays this information to the astronaut via the keyboard and display panel on command. The software also places VHF range measurements and all status information associated with the VHFR-command module computer interface on the telemetry digital downlink.

A more detailed description of the VHF ranging software is contained in subsection 5.2.4 of the COLOSSUS GSOP.

## SECTION 7.0 FLIGHT TEST PROGRAM

### 7.1 GENERAL

MIT/IL participated in an APOLLO Radar Flight Test Program conducted at the White Sands Missile Range (WSMR), New Mexico.

Flight testing was undertaken to assist in the engineering evaluation of both the rendezvous and the landing radars. Certain tests were performed to directly measure the performance characteristics of the radars themselves. Other tests were performed to gain information basic to the math models for describing each radar in order to predict performance in the mission regimes which could not be tested in flight or by any other means. Such flight test data as accuracy, angle biases, signal strength, beam dropout regions, and sidelobe acquisition were invaluable in developing the math models.

MIT/IL required flight test data for the Phase II GN&C radar system integrated tests in order to verify computer programs and evaluate the combined subsystem data-processing performance. The trajectory and test evaluations were designed to provide radar data over as wide a range of probable mission profiles as possible in view of a number of practical constraints associated with the flight program, and were designed to duplicate, insofar as was practical, the trajectory interrelationships of range, range rate, and acceleration, and angle, angle rates, and acceleration that were anticipated for the pertinent phases of the APOLLO mission.

### 7.2 FACILITIES

The WSMR facility was selected for radar flight testing because of the inherent advantages of a large operating area already possessing most of the required instrumentation and enjoying a close proximity to Holloman Air Force Base. The Army provided cinetheodolite and ground radar tracking coverage at many locations within the confines of the range itself. WSMR also had available extensive facilities for reducing the vast number of cinetheodolite photographs needed to establish the aircraft state vector accurately. These refined tracking data, along with the data from the radars, were then processed by Computing and Software, Inc., at Holloman Air Force Base. This organization developed the final data-reducing and printout

formats for the flight tests. In addition, WSMR provided timing equipment in support of the IRIG timeline and office facilities for NASA and contractor personnel.

Two test aircraft were acquired by NASA, a T-33 jet aircraft and an SH-3A helicopter. These two vehicles, while not capable of the high velocities that would be encountered during the lunar landing, could provide a significant portion of the flight conditions required for acceptable landing radar testing. Although the long distances at which the rendezvous radar was to operate could not be duplicated, the existing aircraft capability facilitated evaluation of the rendezvous radar-computer performance over a considerable range of radar operation.

Interfacing between the radars and the data recording equipment was accomplished by Grumman manufactured support equipment that simulated computer interrogation or strobing of the radars and then processed the radar data for recording.

The flight testing program required over two years for completion. During this period several major operational and equipment problems were encountered, most of which were associated with the landing radar tests. Early testing was initiated with prototype radars that did not possess the performance or reliability characteristics of the final production units. Later testing utilized radars highly representative of the mission hardware and demonstrated both improved performance and reliability.

Mounting constraints on the aircraft restricted the extent of mission simulation tests. The landing radar, for example, required enclosure within a radome pod to protect it from the airstream. However, specific fixed orientation of the pod with respect to the aircraft was necessitated by aerodynamic considerations, and the possibility of tilting the landing radar to simulate major portions of the descent profile was precluded.

One outstanding problem that caused many delays and a great deal of retesting was the slipping of the time reference on the flight vehicles. In the case of the landing radar, timing errors quite seriously degraded the coordinate transformation required for cine and radar data correlation. Occasional weather conditions — cloud cover, blowing dust, etc. — hampered operation, requiring many tests to be rescheduled or repeated.

### 7.3 MIT/IL RENDEZVOUS RADAR TESTS

The radar was mounted on a lunar module mockup and an adjustable pedestal located at the origin of the WSMR flight test range. The transponder was mounted on the

underside of either the T-33 jet aircraft or the SH-3A helicopter. From the flight data, IBM-compatible magnetic tapes were prepared containing rendezvous radar interface digital data and WSMR theodolite tracking data in the same coordinate system and parameters (range, range rate, and angle) as the raw radar data. Because the Kalman filter was unable to estimate more than one type of bias (tilt or boresight) prior to initiation of the tests, the radar antenna tilt bias, with respect to the pedestal, was adjusted to less than 1 mrad, making possible later checks on the ability of the Kalman filter to estimate boresight bias.

### 7.3.1 Rendezvous Radar Lunar-Stay Simulation Tests

These tests simulated the portion of the mission where the command module, in lunar orbit, passes over the landed lunar module with the radar in antenna Mode 2 for acquiring and tracking the command module transponder through the module trajectory over a 90-degree line-of-sight sector nominally centered at the lunar module's zenith.

The aircraft altitude and speed were selected to achieve a line-of-sight angle rate of 1 deg/sec maximum (the required tracking rate of the radar) at the zenith. Lateral offset was introduced in some tests to approximate the conditions that might exist with the lunar module tilted or out of the command module orbital plane. The effect of reduced signal strength at orbital ranges between lunar and command modules was simulated by attenuation of the transmitted power between the radar and its transponder. WSMR cine tracking facilities were employed during these tests. Many over-flights were accomplished in directions that tested radar tracking accuracy under conditions where angular rates were produced about the trunnion axis only, the shaft axis only, and both axes together. Over the angular regions covered, the radar exhibited a small bias (approximately 3 mrad) with a bias variation of 1 or 2 mrad over most trajectories.

The range-rate data from the radar exceeded accuracy specifications; however, during the early tests with the prototype radars, evidence of cycle slip in the range tracker appeared in some cases, particularly in the long range (300 n. mi.) flight tests. This difficulty disappeared after the prototype radars had been replaced with production units.

### 7.3.2 Rendezvous Radar Rendezvous Simulation Tests

Within practical limits, these tests simulated conditions that the radar would encounter during descent from and ascent to the command module. For these tests,

the Pearl Site lunar module mockup was rotated upward about the Y-axis of the radar coordinate system, with the radar placed in angle Mode 1 and tracking the flight vehicle over the trajectories indicated in Figures 7-1 and 7-2. The transponder transmitter power was sufficiently reduced to simulate the signal-to-noise conditions anticipated during rendezvous.

A series of semi-circular flight patterns were flown, using both the T-33 and SH-3A at altitudes varying from 3000 to 24 000 feet above ground level (AGL) and of differing radii (see Figures 7-1 and 7-2). The intent was to develop range rates and angular rates simulating those expected to exist during the lunar module free-fall part of the mission. Observations of range, range rate, and, in particular, angular tracking accuracy were made. Test results indicated that, at line-of-sight angles greater than 30 degrees above the horizon, the radar had angular biases of the order of 2 to 3 mrad with a bias variation of slightly over 1 mrad. At line-of-sight angles below 30 degrees above the horizon, the radar angular accuracy requirements were not expected to be met because of multipath problems from ground bounce. Range and range-rate data were within specifications over the complete path of the trajectories flown. In many cases, however, the test flight profile was not optimum for radar evaluation.

An additional series of tests was performed in which the SH-3A helicopter flew a straight-line course in front of the radar site. The parameters for this trajectory were chosen so that the actual range and range rate could be extrapolated to match the true rendezvous values. Essentially, the entire trajectory was contained within 30 degrees of the lunar module Z-axis. Data from these flights were employed in a computer simulation at MIT/IL for the purpose of evaluating the Kalman filter with actual radar data. Figures 7-3 and 7-4 show typical results of the Kalman filter estimation utilizing the WSMR flight test data. The results of the simulation proved that the filtering process converged quickly and was accurate.

### 7.3.3 Polarization Tests

These tests were conducted to determine the relationship between polarization shift and boresight bias shift. The flights passed in front of the radar, which had its pedestal elevated 30 degrees about the Y-axis. East-to-West and West-to-East flights were criss-crossed with North-to-South and South-to-North flights and with flights at 45 degrees relative azimuth, all at the same altitudes to display different aspects of the transponder antenna to the radar at specific line-of-sight angles. Radar shaft and trunnion angles were compared to the WSMR cine readings in the radar coordinate system. Results of this test were entirely consistent with the

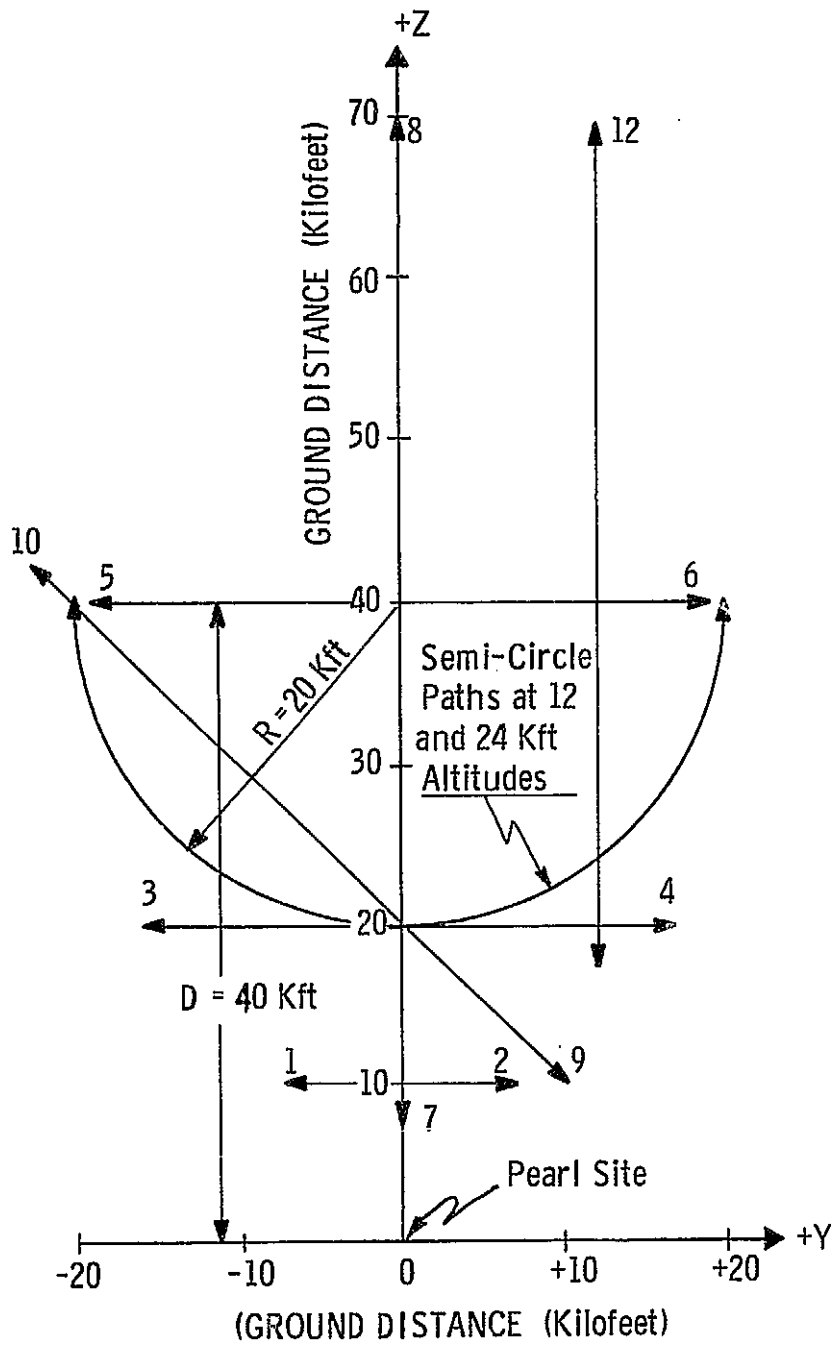


Fig. 7-1 T-33 Flight Trajectories—Alt. 12k ft (except as noted)

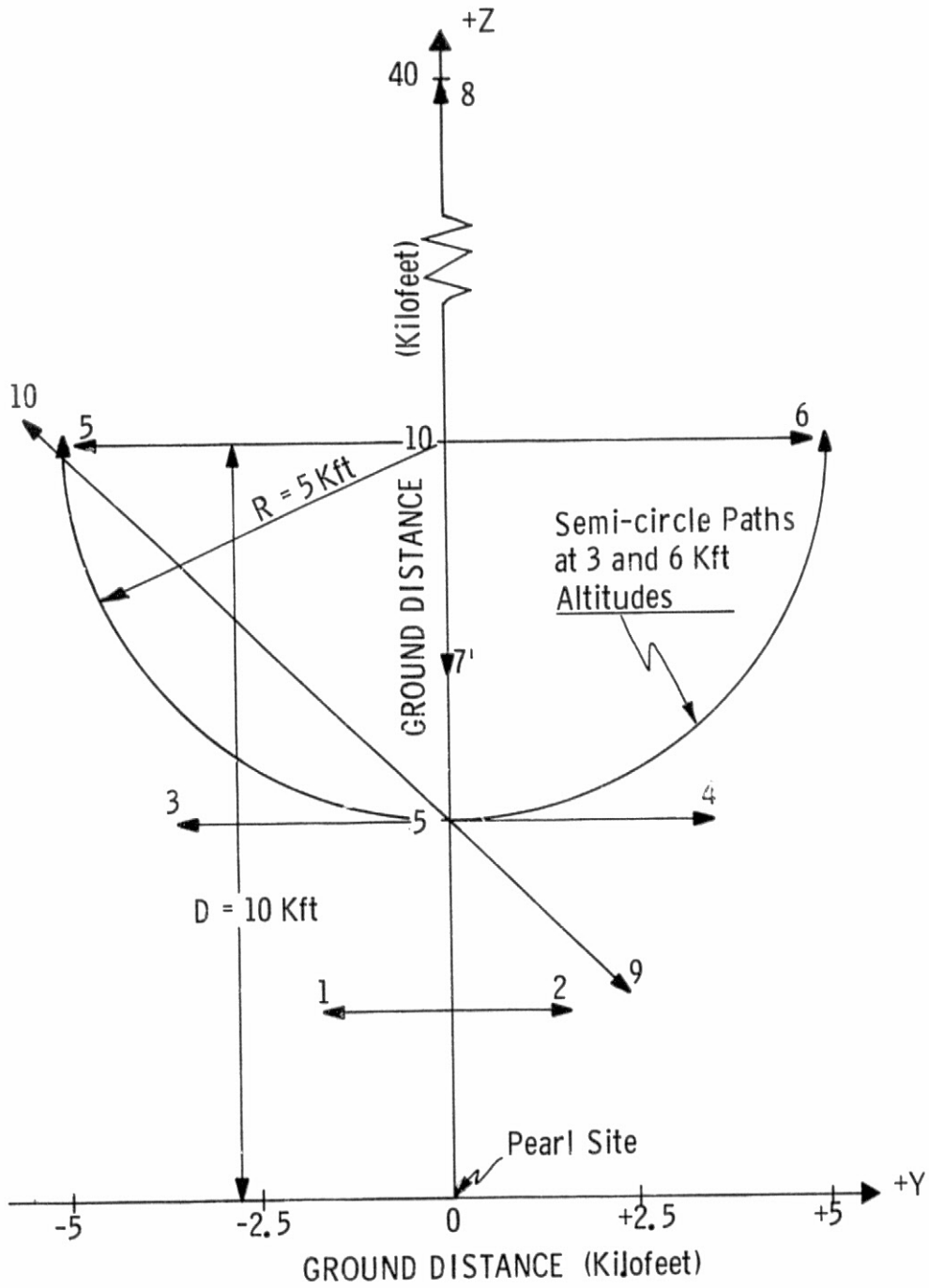


Fig. 7-2 SH-3A Flight Trajectories—Alt. 3k ft (except as noted)

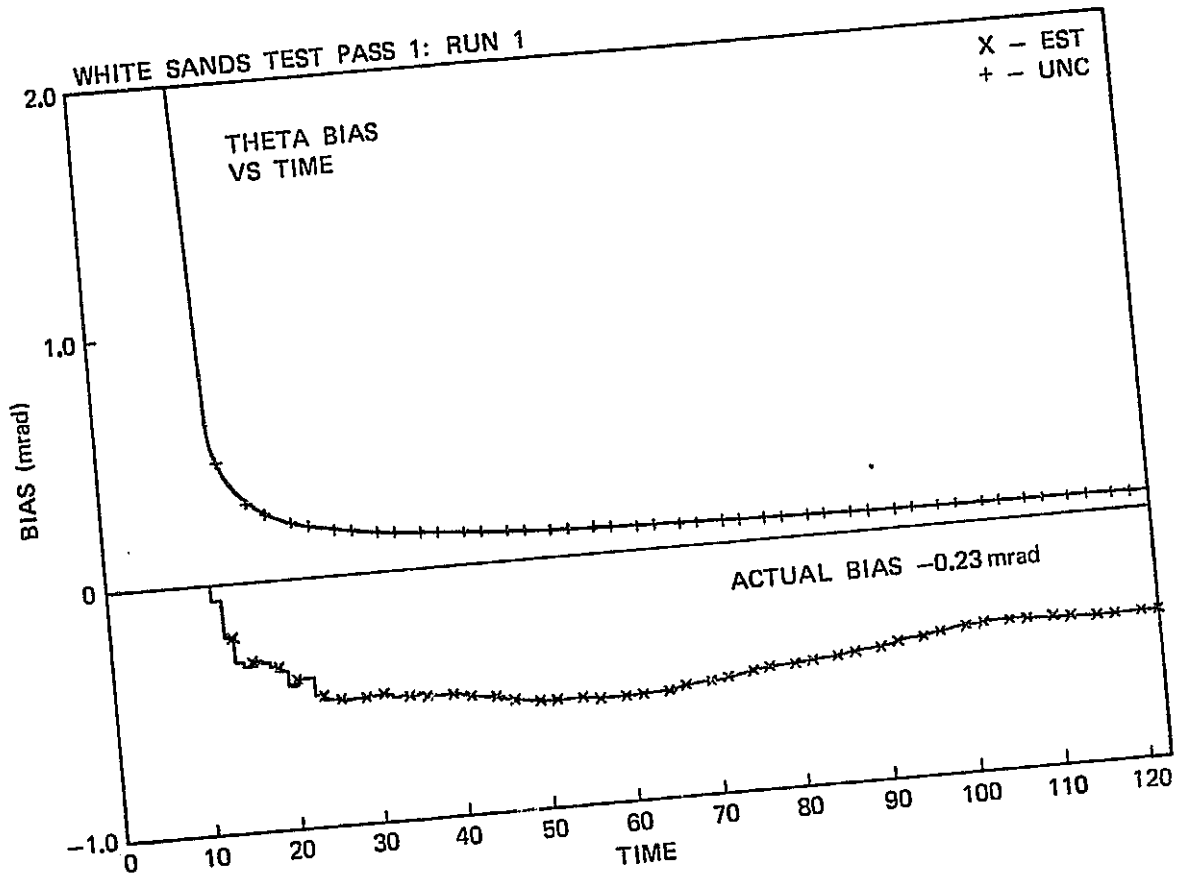


Fig. 7-3 White Sands Test Pass 1: Run 1 Theta Bias vs Time

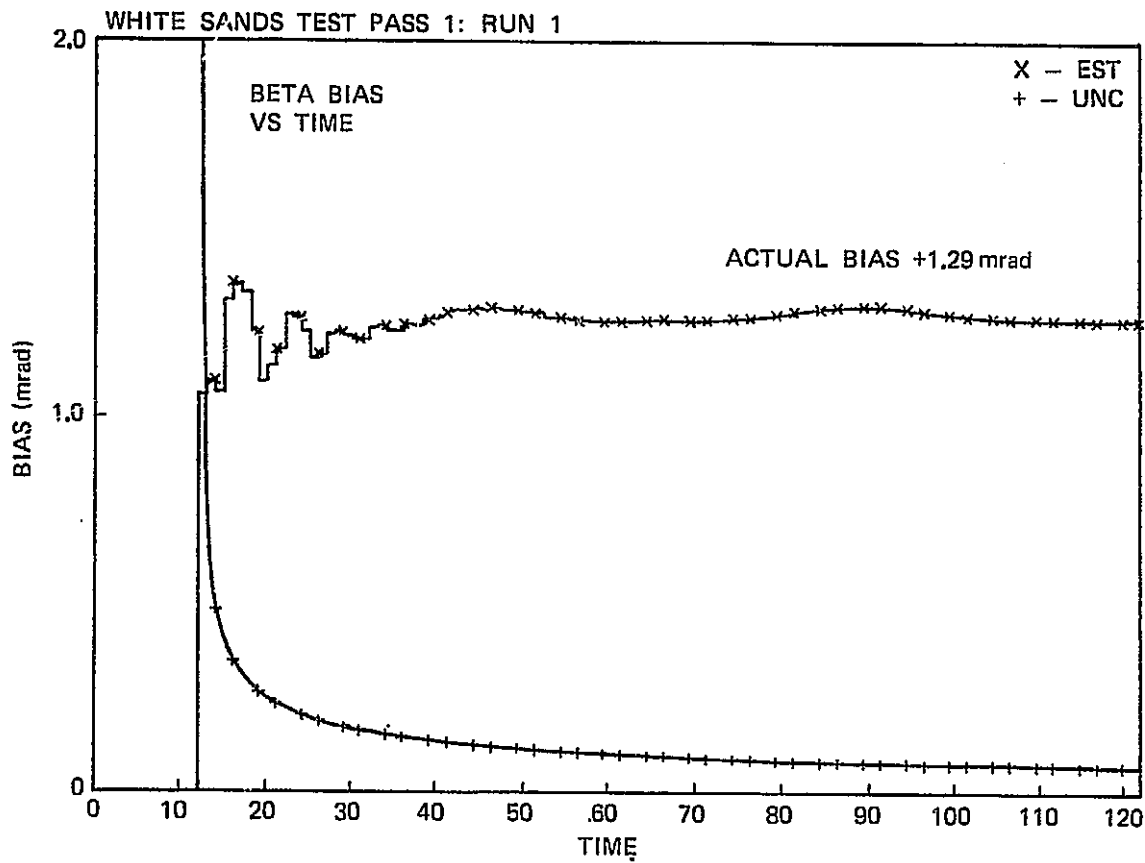


Fig. 1-3 White Sands Test Pass 1: Run 1 Beta Bias vs Time

predicted polarization effects. Maximum boresight deviations observed were of the order of 2 mrad.

#### 7.3.4 Rendezvous Radar Pearl-X Test

The Pearl-X test was devised to test the tracking ability of the rendezvous radar at long ranges by calling upon a radar based at WSMR to track a transponder on board the APOLLO 7 command module during overflights closest to the White Sands area. The radar was slaved in angle to the precision tracking Rampart radar at the WSMR site to establish radar angle acquisition. The radar performed extremely well, acquiring and tracking at ranges, range accelerations, and range rates substantially beyond the design specifications, leading to high confidence in its ability to support the missions.

#### 7.4 LANDING RADAR TESTS

As far as the landing radar was concerned, the WSMR flight tests were of the utmost importance simply because there was no other satisfactory method for measuring landing radar accuracy and observing its performance under varied conditions.

The radar was mounted on the underside of the T-33 or the SH-3A, with its Z-axis forward and its X-axis down. An attitude reference system (Litton LN12A) was installed on each aircraft to provide pitch, roll, and yaw information, permitting transformation of cinetheodolite data into the radar coordinate system. An IRIG timeline base was used as time reference, enabling correlation between radar and cine data to within 5 msec. The data derived from the radar were in two forms: analog Doppler data derived from the radar preamplifier outputs recorded on 14-channel magnetic tape, and data read from the electronic assembly digital interface circuits and recorded on IBM-compatible tapes. The transformed cinetheodolite data were also taped in the same format as the radar digital data. Of particular significance in these tests was the fact that up to the time of flight test conclusion, the flight test radar did not contain the more recent modifications of the mission flight models simply because the modifications did not exist at that time. One such modification was the reduction of the 80.001-msec gate strobe to 80.0001 msec. Another was the reduction of the pulse width of the radar internal readout pulses. These changes had the effect of reducing the velocity bias introduced by the readout configuration from 0.4 to 0.015 count. In the case of the Y-velocity component, the changes reduced the bias attributable to these causes from 0.5 to 0.018 fps. Hence, the radar velocity readouts in the mission flight equipment should be slightly more accurate than indicated from assessment of the flight test data.

#### 7.4.1 Landing Radar Mission Simulation Tests

Because of antenna mounting constraints on the T-33, simulation of that portion of the descent profile within the velocity range of the T-33 could not produce meaningful results.

The SH-3A helicopter, however, was employed to duplicate portions of the descent profile below 600 feet altitude where the landing radar antenna is in Position 2. The purpose of the test was to duplicate the angular relationship between the four antenna beams and the velocity vector, and to observe data accuracy, beam dropouts, and possible cross-lock re-acquisitions.

Although the stipulated trajectory was exceedingly difficult to fly, test results showed that many tracker dropouts occurred, and were valuable in verifying the radar math model. Cine accuracy at the low altitudes deteriorated such that radar accuracy could not be ascertained. No radar cross-lock acquisition was evident during these tests.

#### 7.4.2 Zero-Doppler Dropout Tests

Tests were made with the SH-3A helicopter at various altitudes calling for the vehicle to initiate a straight and level flight path, wait for the radar trackers to lock up, and then, at different climbing attitudes, slow down until the trackers unlocked. Cine and radar data were compared at each point where any one of the velocity beam trackers lost signal. Figure 7-5 shows the tracker dropout regions as a function of altitude and velocity.

#### 7.4.3 Cross Beam Lock-on Tests

Although an occasional cross-lock condition occurred between beams during some of the flight tests, a special test was developed to intentionally induce cross-beam lock-on. The test was a circular course with the SH-3A in a 15-degree left bank and pitched between +21 and -21 degrees, placing either Beam 2 or 3 vertical at each end of the pitching excursion. The radar was turned on, allowed to achieve acquisition, and a readout of the range beam and each orthogonal velocity was performed. The radar tracking was then re-interrupted and the entire procedure repeated. All reacquisitions were studied, and each cross-lock case was noted. In this series of tests, cross-lock was observed in about 30 percent of the acquisitions.

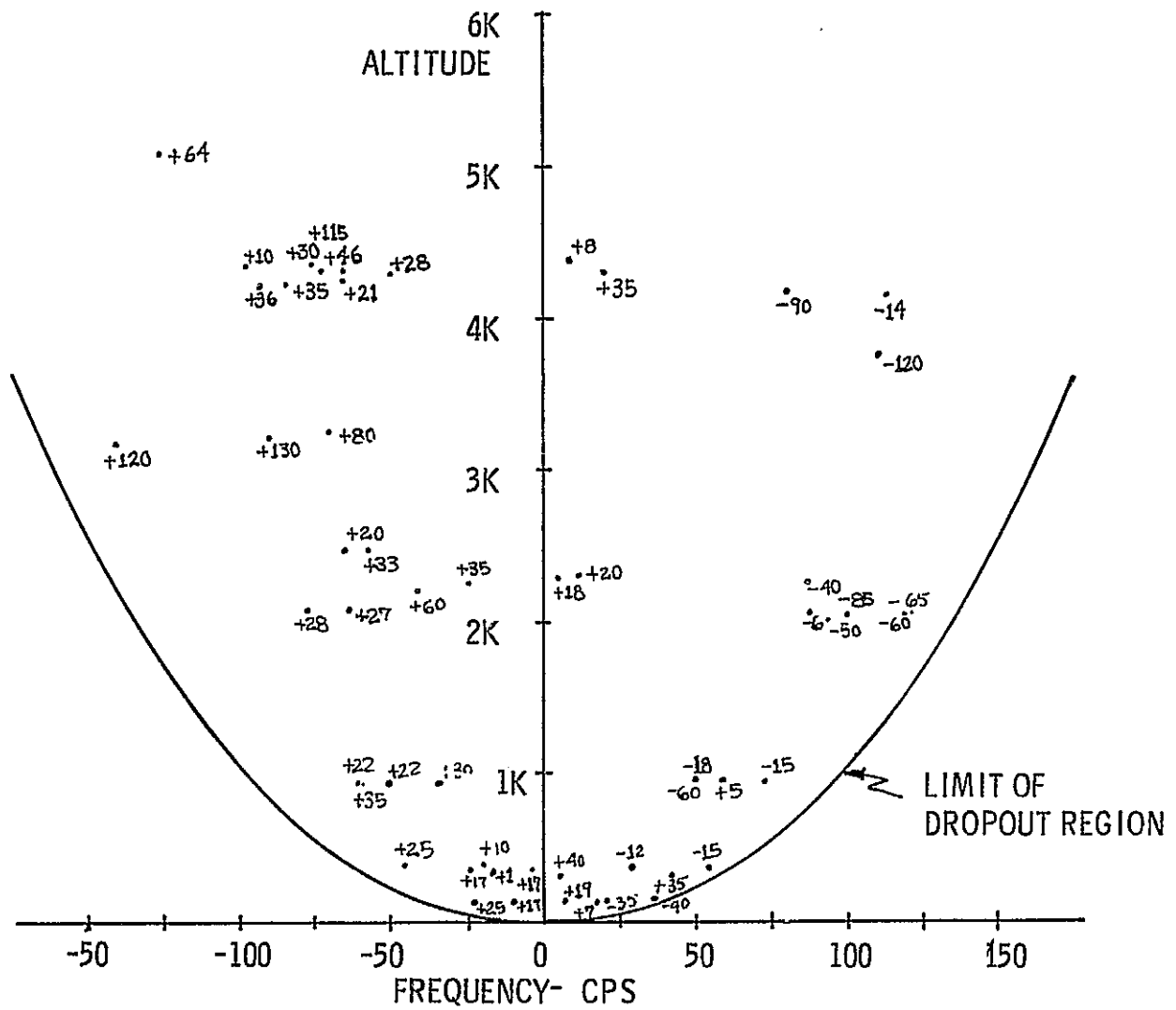


Fig. 7-5 LR Dropout Points

#### 7.4.4 Deceleration and Attitude Angle Rate Tests

These tests were designed to assess radar performance during a vehicle slowdown and vehicle attitude change rates that are consistent with those expected during the mission.

Verification was obtained of radar performance during the slowdown, when angular rates were low. However, as the vehicle went through the larger rates (at lower speeds), timing differences between the cine data and the attitude reference readout, which were not accounted for in the data reduction program, introduced errors in the calculation of the reference data and prevented assessment of radar performance.

#### 7.4.5 Range Beam Tests

These tests were designed to induce a radar range-scale change. The aircraft was flown over Little Burro peak (an approximate 1500-foot change in range) to observe radar measurement behavior during scale-factor switching. Range scale-factor switching usually occurred when the range dropped to less than 2500 feet and returned to high scale when the range increased to greater than 3000 feet. These results verified that the radar design met P&I Specification switching-hysteresis requirements.

### 7.5 FLIGHT TEST REFERENCES

The following documents are flight test references:

1. GAEC Document LTP-370-205 dated 15 July 1965, "Lunar Excursion Module Recommended Radar Flight Test Plan and Control Document."
2. GAEC Flight Measurements List, LMO 372-477, dated 1 Dec. 1965.
3. "LEM-PGNCS P&I Specification (Draft)," LSP-370-3, 17 Feb. 1966.
4. GAEC Test Data Memorandum LMO-822-198 dated 28 Feb. 1966, "PEARL Computer Programing Status."
5. MIT/IL Report 23R-660328, "Specification of MIT/IL Data Form Requirements for WSMR Radar Flight Tests," dated 28 Mar. 1966.
6. "Flight Test Control Document for Project APOLLO Lunar Excursion Module Radar Systems Boresight and Flight Tests," NASA/MSC, dated 26 April 1966.
7. "MIT/IL Flight Trajectory Requirements and Recommendations for LEM Radar Tests at WSMR," Document 23R-660622, 6 June 1966.

8. TRW Project Technical Report TASK ASPO-34A, "Rendezvous Radar Flight Test Plan," NAS 9-4810 (05952-H035-R0-00) 15 Sept. 1966.
9. TRW Project Technical Report TASK ASPO-34A, "LM Landing Radar Aircraft Flight Test Plan," NAS 9-4810 (05952-H0-23-R0-00), 7 Sept. 1966.
10. TRW Project Technical Report ASPO Task 34B, Geometric Transformations Associated with Project PEARL," dated 14 July 1967.
11. "MIT/IL Flight Trajectory Requirements and Recommendations for LEM Radar Tests at WSMR," Document 23R-660622 Rev. A, 28 Dec. 1968.
12. GAEC Document LTR 372-010, dated 11 Nov. 1968, "Lunar Module Test Report for Rendezvous Radar Flight Tests at White Sands Missile Range."
13. Ryan Report 53966-112, "Analysis of Low Altitude Flight Tests LM Landing Radar Model P-11X," dated 21 March 1969.
14. Ryan Report 53966-114, "Analysis of High Altitude Flight Tests LM Landing Radar Model O-11X," dated 7 April 1969.
15. WSMR National Range Data Reports Prepared by Computing and Software, Inc, Holloman, New Mexico.

PRECEDING PAGE BLANK NOT FILMED

## SECTION 8.0 INTERFACE TESTING PROGRAM

### 8.1 INTRODUCTION

To assure electrical and functional compatibility of the radar design with the GN&C system, MIT/IL was initially provided with prototype models of the digital interface circuits of both the landing and the rendezvous radars. The evaluation of these interface units and their integration with a laboratory model of the lunar module guidance computer constituted the Phase I portion of the MIT/IL test program. Phase II of the test program encompasses the evaluation of the rendezvous radar angle interface with the coupling data units and the lunar module computer, together with the verification of the computer programs that control readout processing and interpretation of digital and angle data from both radars. In addition, the Phase II program included the processing and evaluation of flight test data from White Sands Proving Grounds to verify radar characteristics and the mechanization and programming of the computer.

### 8.2 PHASE I TEST PROGRAM

The Phase I test program started in July 1965 with the delivery of the landing radar and the rendezvous radar digital interface units from RCA, Burlington, Massachusetts. The principal test objectives were satisfied by early March 1966, when operation of data and discrete-signal transfer into the first available lunar module computer (600M) was demonstrated. Portions of the AURORA software program, which contains all the subroutines for system testing of the navigation equipment, were used to control the computer.

The evaluation tests of the radar digital interface equipment were designed to examine the circuit performance and to ensure that both the literal requirements and intent of the governing interface specifications were met.<sup>1</sup>

The interface circuits were evaluated under laboratory conditions and covered the following topics:

---

1. GAEC-MIT/IL Interface Control Document LIS-370-10004; See also Performance and Interface Specification LSP-370-3A.

1. Electrical circuit characteristics,
2. Timing requirements and tolerances under conditions of deteriorated pulses,
3. Effects of transmission cables of different characteristics and lengths on performance of pulse circuits, and
4. Operational performance of interface circuits and verification of the computer programs.

Figure 8-1 is a simplified block diagram showing the equipment components of the Phase I interface tests. In each test it was necessary to stimulate the interface units with signals representing the raw data of the three velocity components and of the altitude of the landing radar as well as of the range and the range rate of the rendezvous radar. Stimulation was obtained in one channel at a time from a pulse generator with a precise crystal-controlled PRF. A number of typical stimulation frequencies are available covering the range of the raw frequencies of all data channels.

Discrete data, such as DATA GOOD, RADAR IN AUTOMATIC MODE, and ANTENNA IN POSITION 2, were simulated by the operation of switches. Discrete data from the computer to the radars were checked with an indicating meter. (Most discrete signals to or from the computer are dc voltage levels of either 0 or 28 Volts.)

The interplay between the computer and the two radar signal data converters (high-speed counters) is under control of the lunar module computer or equivalent simulation equipment. For the evaluation of the effects of pulse timing and pulse degradation, it was necessary to use special test equipment to generate the gate control pulses, S1 and S2. For system performance tests, cable measurements, and verification of computer programs, the digital interface equipment was connected to the computer and to the display and keyboard. A core rope simulator provided the programs and also controlled the computer until permanent core rope memories were available. For some of the laboratory tests, a computer simulator was also used to provide the necessary timing signals (S1 and S2) and to permit readout of data on an oscilloscope.

### 8.2.1 Phase I Test Equipment

Several major pieces of equipment were especially designed for use during the Phase I test. Figure 8-2 shows the rendezvous radar digital interface unit, a modification of the original unit delivered to MIT/IL by RCA. The control panel was equipped with switches for the stimulation of the discrete inputs. A running-time counter

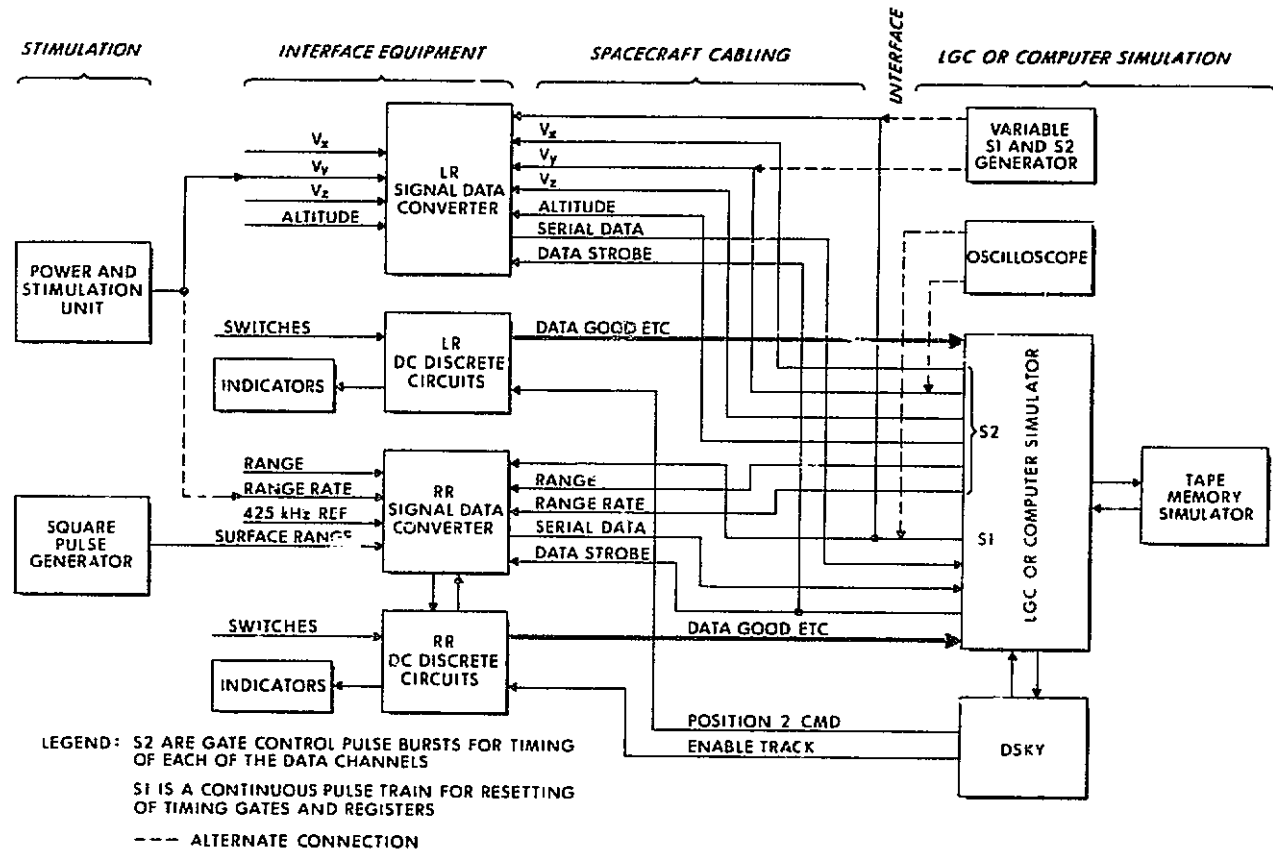


Fig. 8-1 Block Diagram of Phase I Interface Tests

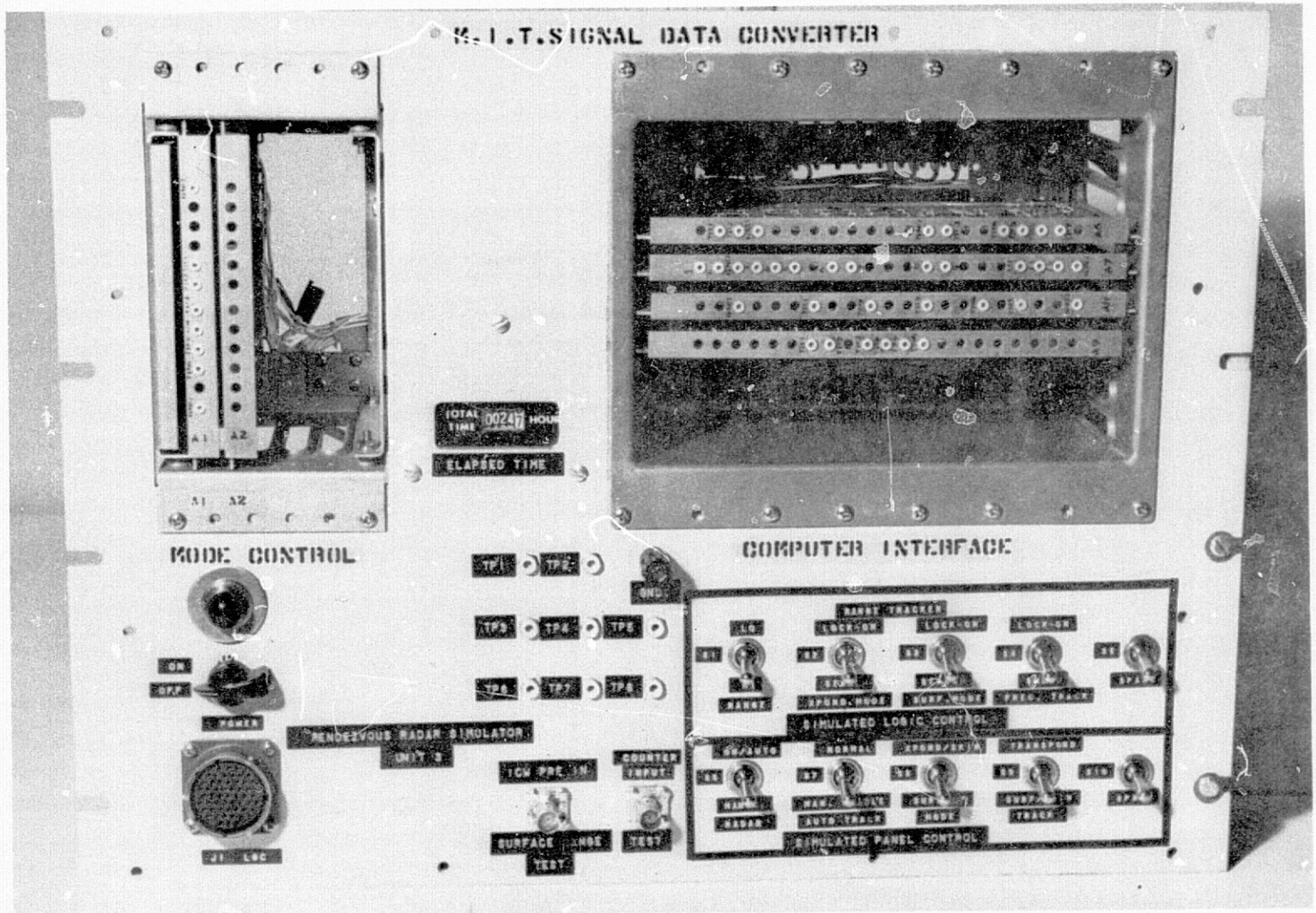


Fig. 8-2 Rendezvous Radar Digital Interface Unit

was added to keep track of the operating hours for the purpose of equipment reliability evaluation.

The landing radar digital interface unit (Figure 8-3) was assembled at MIT/IL, using the RCA signal data converter and the discrete circuits. The control panel was organized the same way as that of the rendezvous radar.

Figure 8-4 depicts the entire digital interface simulator, consisting of the interface units of both radars and a power and stimulation unit. The latter provided power to the simulation equipment and contained on the right side the precision PRF generator, capable of stimulating any one of the data channels with a calibrated pulse train corresponding to the raw frequencies developed by the radar systems.

For laboratory evaluation of the radar interface circuits and of pulse transmission problems, MIT/IL made use of a computer simulator (Figure 8-5) developed by the MIT/IL Computer Group. This simulator contained all the circuits for addressing any one of six radar data channels, and provided for timing the readout of two signal data converters. Driving and load circuits were identical to those of the lunar module guidance computer.

### 8.2.2 Problems Encountered In The Phase I Tests

The governing interface control document is a general document specifying the types of standardized circuits available in the computer for interfacing with other subsystems. Dynamic characteristics of these interface circuits are specified for arbitrary resistive loads and the specifications refer to conditions at the computer connector. The interface control document was conceived and written to pertain to a lumped-parameter interface.

In the lunar module however, the radars are tied to the computer connector through substantial lengths of line: 20 ft for the rendezvous radar, and 40 ft for the landing radar. For the pulse waveforms of the interface, these interconnections behave as transmission lines and present distributed parameter characteristics at the computer connector.

An incompatibility exists between the interface control document and the conditions actually present at the interface in the integrated configuration, and contributed to the difficulties of verifying interface characteristics against control document specifications. In some cases, disparity between specified and actually obtainable conditions prevented a direct verification. The situation was further complicated

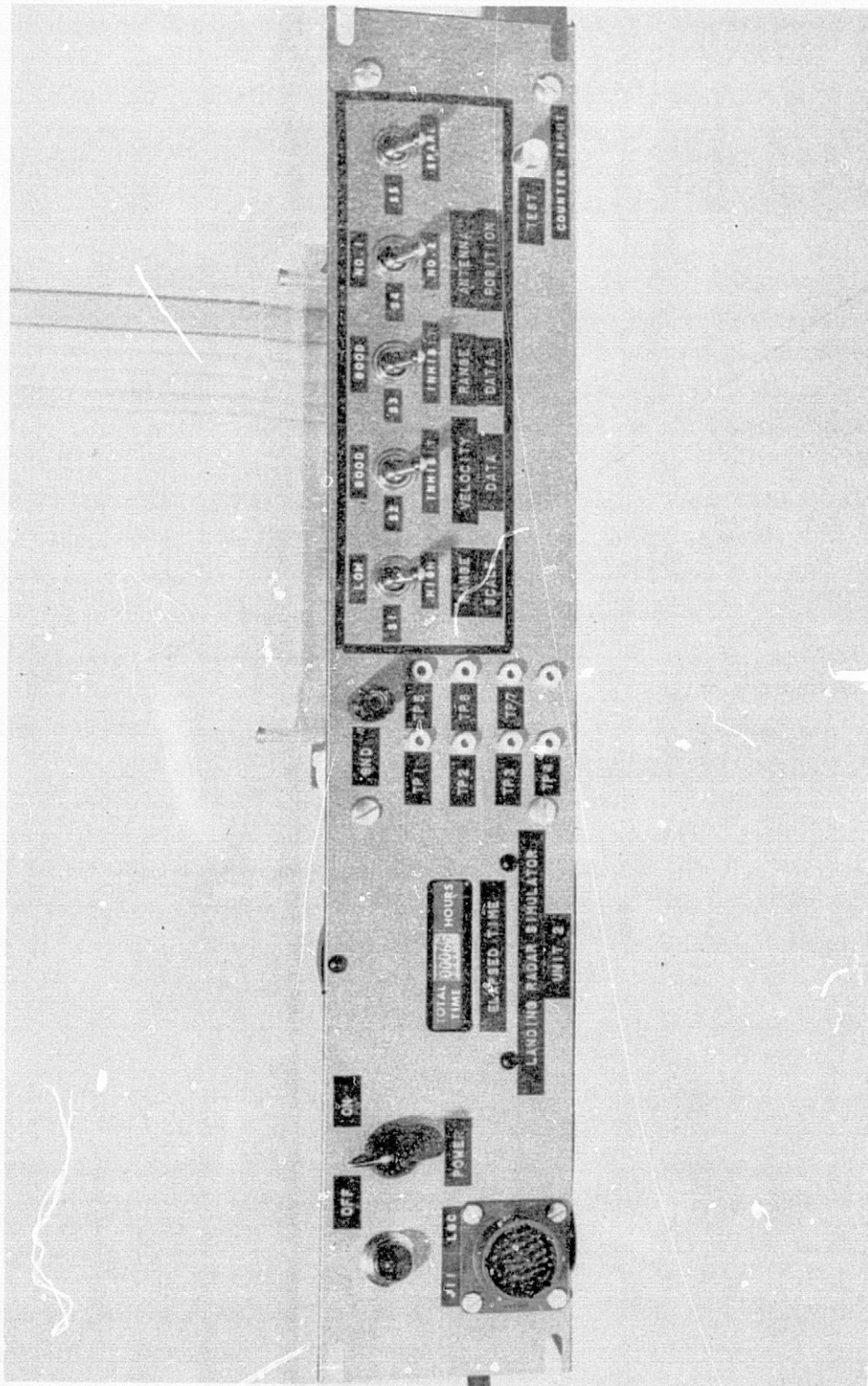


Fig. 8-3 Landing Radar Digital Interface Unit

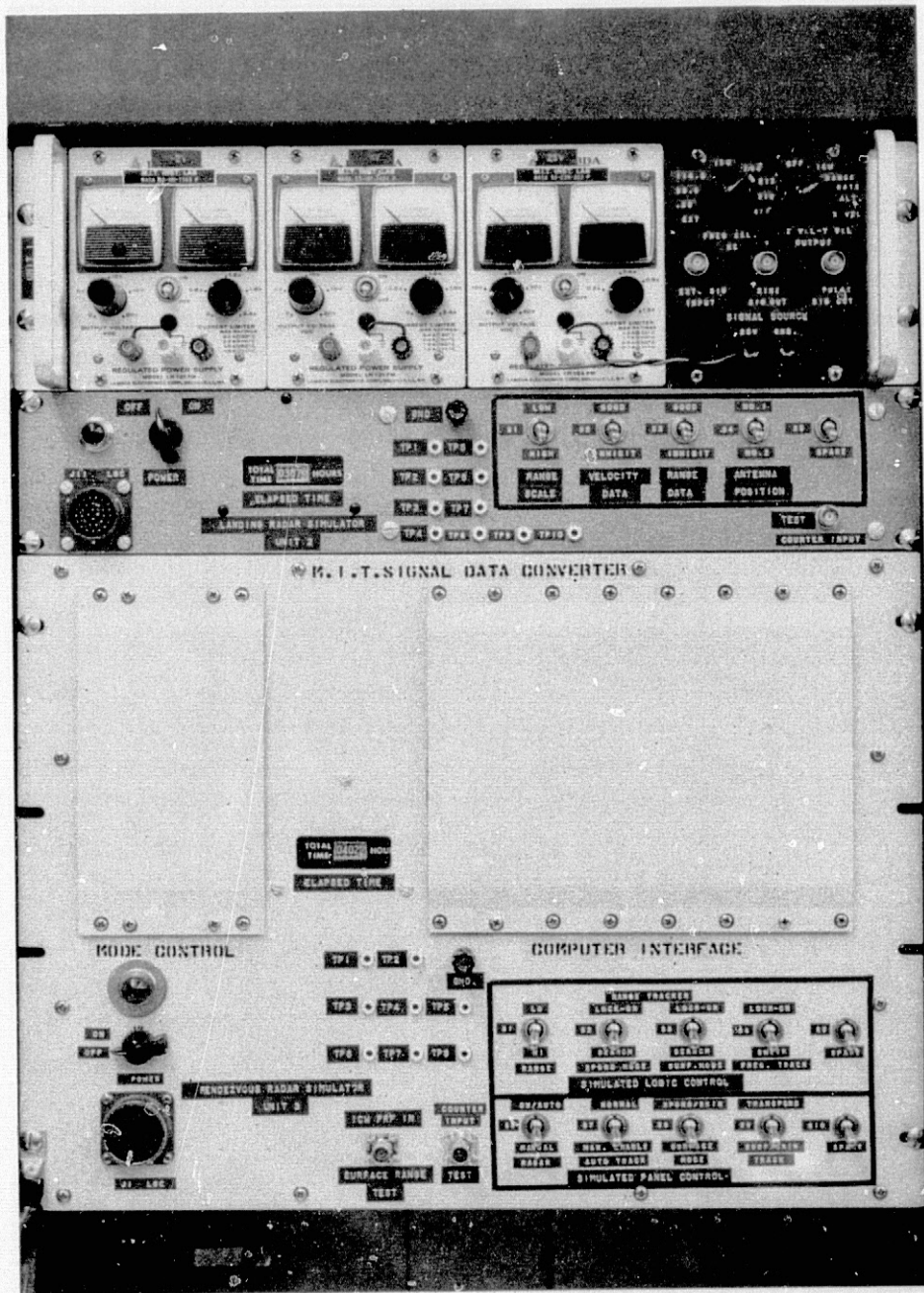


Fig. 8-4 Digital Interface Simulator



at the start of the Phase I tests by the fact that neither the computer nor the radar pulse circuits matched the characteristic impedance of the interconnecting transmission lines, with the result that considerable waveform distortion occurred from line reflections. This condition was later ameliorated by redesign of some of the radar pulse interface circuits.

### 8.2.3 Test Results

The results of the Phase I interface testing program were reported in MIT/IL Document No. E-1976, Evaluation Phase I, Final Test Report (May 1966).<sup>2</sup>

A few of the more pertinent conclusions are detailed in the following paragraphs.

The Phase I interface tests demonstrated that, under laboratory conditions, the digital interface circuits of the engineering prototypes of both radars met the applicable requirements of interface specification LIS-370-10004. The equipment functioned properly for the entire running time, about 400 hours. Even with simulated 40-ft spacecraft cabling on the landing radar and 20-ft cabling on the rendezvous radar, all the pulse and dc discrete circuits worked without error.

The radar digital interface equipment was used with the Model 200 LGC for computer program verification of the radar digital interface portion of the AURORA programs. Since the rendezvous radar range-data output uses all 15 available digits, the decimal readout capability of the display and keyboard was found unsuitable for range testing because of its 14-digit limitation. However, either binary panel readout or the downlink printout can be used.

A valuable aspect of the Phase I tests and experiments was the exchange of design data and test information that may have bearing on reliable operation of the mating pieces of equipment. The tests brought out that the radar interface circuit designers chose to use the trailing edge of the reset pulses and the leading edge of the selected gate strobes to develop the timing gates for the measurements of radar parameters, despite the fact that the pulse trailing edge is undefined in the interface control document. This design did not, however, lead to any malfunction, even though the trailing edges of the pulses could be substantially distorted by transmission through long, unterminated cables. Since the cable experiments were a joint (Grumman-MIT/IL) effort, data were exchanged with Grumman on the engineering level as soon as they became available. The results led to circuit revisions of the radar

---

2. See Part IV, Appendix A, Abstracts, E-1976.

interface units to provide terminations of nominally 65 ohms, resistive, on the transmission lines from the computer; the interface control document was updated to reflect the change. This proper termination eliminated waveform rise and fall problems.

The evaluation of the pulse transmission cables demonstrated the specially designed immunity of the lunar module guidance computer to pulse distortions, primarily because the computer circuits work from the leading edge of the pulses, which are within specifications.

In the course of the transmission experiments with a simulated spacecraft harness, a problem of feedback across unshielded cables was encountered. Proper operation was obtained when all shields of pulse transmission cables were tied to spacecraft ground at both ends. This grounding has since been established by Grumman as a requirement to be covered by installation specifications rather than by the electrical interface specifications.

The evaluation of the landing radar interface design also indicated the following:

1. The overlap of Strobe 1 and 2 is critical in assuring accurate data readout.
2. Timing delays inside the signal data converter are produced by one-shot multivibrators. Measured delays did not agree with given timing diagrams and the question arose as to whether the critical sequence of "data transfer" and "counter reset" that occurs with the signal data converter could be maintained over the entire temperature range and from production unit to production unit. A recommendation was made to Grumman that the timing of these one-shot delay circuits be carefully checked on each unit.
3. Timing of the signal data converter timing gate is from leading and trailing edges of the S2 and S1 pulses, respectively. Satisfactory operation was obtained in the laboratory environment, but it would be desirable to standardize on the leading edge, as is done throughout the GN&C system equipment.
4. The input impedance of the signal data converter pulse circuits was 200 ohms on the 2L prototype. Following an MIT/IL recommendation, Grumman authorized a design change on later units that reduced the impedance to a nominal value of 65 ohms, providing good termination for the pulse lines from the computer.

5. While the rendezvous radar digital interface unit examined in the Phase I tests served the purpose of exercising the lunar module guidance computer and verifying the compatibility of the interface design, the unit could not be considered representative of the later production equipment.

### 8.3 PHASE II TEST PROGRAM

#### 8.3.1 Evaluation of Rendezvous Radar Angle Interface

In June 1966, a special model of the rendezvous radar antenna with prototype servo circuits was received at MIT/IL to evaluate the interaction between the radar and the coupling data units, inertial measurement unit and computer. This evaluation examined 1) the stability of the servo circuits, 2) the accuracy of angle readout under conditions of vehicle motion (base motion), and 3) the accuracy of antenna angle designation for different routines of target acquisition. There were also questions of electrical compatibility, involving, for example, the signal polarity of interfacing circuits.

The prototype antenna is shown in Figure 8-6, installed on a rate table that provides angular rates and accelerations about a vertical rotation axis. The antenna is tilted 45 degrees so that base rotation provides equal inputs to both the shaft and trunnion axes of the antenna. In the prototype antenna a counterweight was substituted for the reflector dish. The ball below the antenna is the inertial measurement unit, and in the background on the right is the cabinet containing the servo circuits.

The performance of the prototype equipment confirmed the soundness of equipment specifications. The equipment also permitted testing of the radar-related computer routines during their development. There was one shortcoming in the prototype, however, that later proved to be very significant. The production type radars contain a redundant set of gyros that had been left out on the prototype for economy. The voting logic associated with the complement of four redundant gyros caused servo instabilities when the radar was slewed at high angular rates. Detection of these problems at Kennedy Space Center led to a joint effort between the radar manufacturer and MIT/IL to assess the extent of the problem and to evaluate hardware and software fixes. In February 1969, MIT/IL evaluated a flight type radar (P-9) in its System Test Laboratory in a setup similar to that of Figure 8-6. The results of these special tests are reported in a separate section.

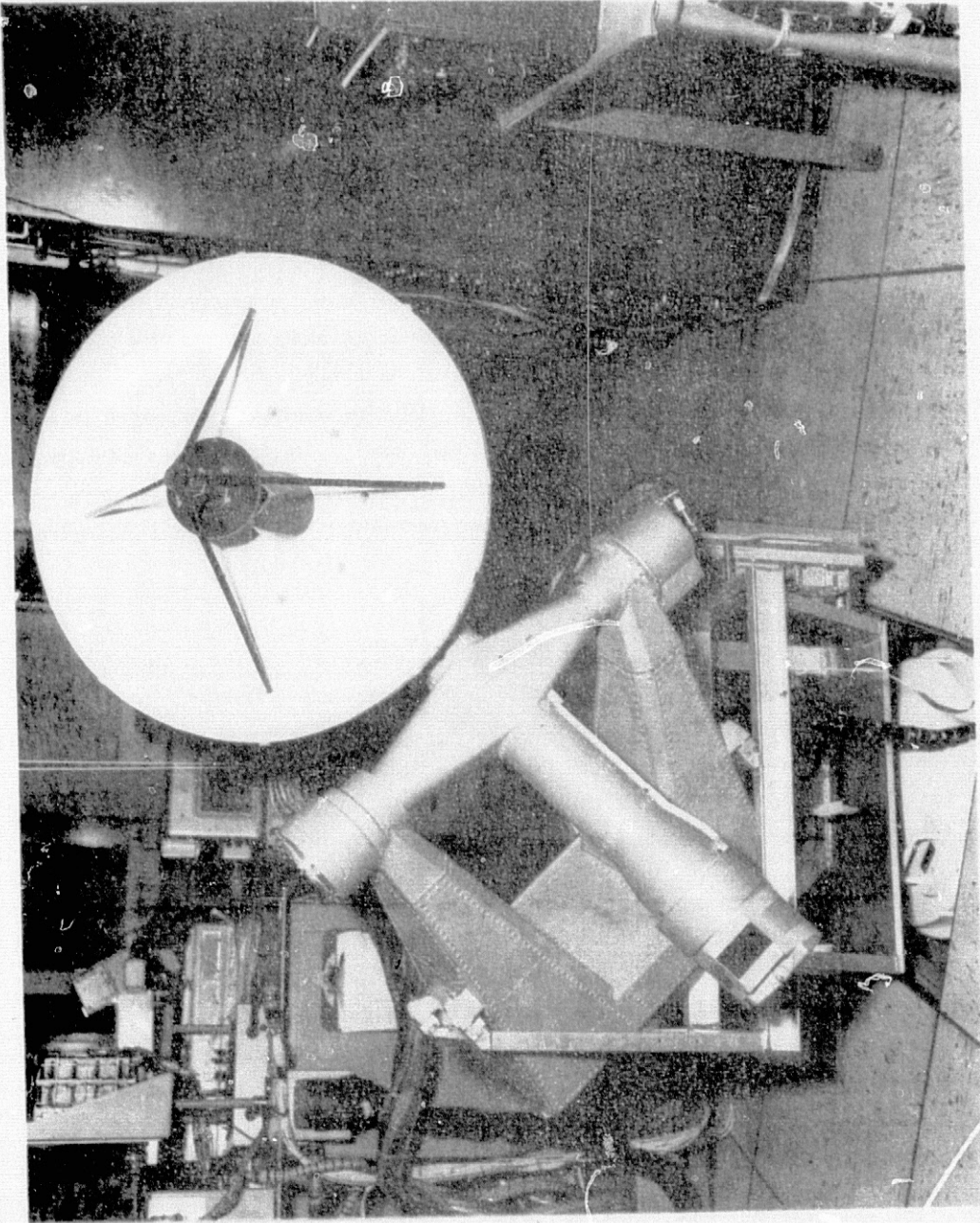


Fig. 8-6 Rendezvous Radar Antenna Simulator

### 8.3.1.1 Servo Evaluation

The radar antenna is a two-axis, gyro-stabilized platform with its own stabilization circuits. The computer controls the orientation of this platform relative to the inertial angular reference provided by the inertial measurement unit or relative to the vehicle reference frame. Control of the radar servos is required for the angular acquisition of the target (command module transponder). When the radar is in its Angle Tracking mode, the computer reads the shaft and trunnion angles of the antenna upon demand from the navigation routines.

During angle designation, the computer closes two servo loops, one for each gimbal axis. At a sampling interval of 0.5 sec, the angles are measured, error angles are computed, and an inertial slew rate is commanded to each platform axis for the duration of the sampling interval. The slew rate is proportional to the error angle and is set to reduce this error to one-half in the next half-second interval. This very conservative approach was selected to allow for gain tolerances in the outer servo loop. A gain increase by more than a factor of 2 would be required to cause an overshoot in the angle designation servo. Gain is also affected by the relative length of the sampling interval and the gain tolerances of the digital-to-analog converters and of the analog circuits. Transients of the stabilization system at the time of angle readout might also prevent proper operation of the digital servo.

Laboratory experiments quickly showed that anticipated gain tolerances and the transients of the stabilization loops were acceptable and that the outer loop gave very smooth angle designation.<sup>3</sup> However, the good results preceded the introduction of gyro voting circuits and the realization of excessive time delays in the computation routines.

A subject of early concern was the likelihood of servo instabilities when changing from one mode of angular coverage of the antenna to the other. Mode changes require "plunging" of the antenna trunnion angle through the gimbal system pole region in 90 degrees for which the shaft angle stabilization had gain compensation problems and was very sensitive to backlash in the error angle detectors. To overcome these difficulties, it was decided to plunge through the pole trunnion angle at a high angular rate of about 10 deg/sec while no shaft command rate was applied. This scheme had to be proven experimentally in the presence of base motion. The plunging

---

3. W. Tanner and W. Saltzberg, "Electrical Characteristics of Rendezvous Radar/Computer Angle Interface; Evaluation of Stabilization and Designate Servo Loop Interaction with Guidance System," Radar Group Memo, 1 September 1966.

procedure was satisfactory with the prototype antenna but later became a problem when failures of redundant gyros were simulated. Base motion, in particular base rate reversals, put a severe requirement on the antenna tracking servo and on its stabilization equipment. During such base reversals, the static friction of bearings and seals impart a jerk to the antenna. A highly bred servo had been designed to keep the antenna alignment within about 1 mrad during these jerks. But the large servo bandwidth of about 20 Hz required extreme stiffness in the mounting base and mounting structures. In the laboratory it was difficult to provide the necessary stiffness because of the limited weight capacity and the limited stiffness in the rate table itself. Base vibrations were sustained by the antenna servos when the trunnion angles were beyond 60 degrees. The base vibration had to be recognized as an instrumentation problem and separated from the performance data.

The results of the base motion tests<sup>3</sup> are shown in Table 8-I. Note that the angular errors are given for different values of static friction torque on the two axes. The first column in each case is for natural friction at room temperature. The friction was then increased by special adjustable friction devices that simulated conditions at low ambient temperatures. The angular errors were excessive for the trunnion axis servo and had to be corrected by later servo refinements.

#### 8.3.1.2 Comparison with MIT/IL Digital Simulation Model

Part of the MIT/IL digital simulation of the navigation and guidance hardware is a model of the rendezvous radar antenna servos and of the angle readout and slew control provided by the coupling data units. To decrease the complexity of this simulation, the high order antenna servo was approximated by a second-order system of differential equations. A block diagram of this approximation is shown in Figure 8-7. The approximation was based on the results of a detailed design analysis by the radar manufacturer (RCA) by matching the transient response of the stabilization loop for a step of slew rate input. It remained to be seen whether the performance of the real antenna was sufficiently different to require an adjustment of the parameters of the digital model.

Figure 8-8 shows the angular rate response of the simulated radar during a typical angle designation. The graph is for the trunnion of the two-axis system. Note the finite rise time of the command rate changes, produced by digital-to-analog converter of the CDUs. The transient response of the antenna system is essentially over after the half-second sampling interval.

The performance of the real antenna was close enough to the digital model so that parameter changes were not necessary. Using the worst tolerance buildup in loop

TABLE 8-I

## BASE MOTION DISTURBANCE

FRICTION		SHAFT AXIS			TRUNNION AXIS		
		18oz-in.	44oz-in.	108oz-in.	16oz-in.	39oz-in.	51oz-in.
Rotation Reversal per axis	Average Acceleration per axis	Peak Angular Error (mrad)			Peak Angular Error (mrad)		
0°/sec	0	±0.1*	-	-	±0.1*	-	-
0.7°/sec	14°/sec	0.3	0.4	0.8	1.2	2.0	2.4
1.4°/sec	17°/sec	0.3	1.1	1.2	2.0	2.5	3.0
2.8°/sec	40°/sec	0.5	1.4	1.2	2.0	3.0	4.8

\*Servo noise fluctuations in absence of base motion.

C-33

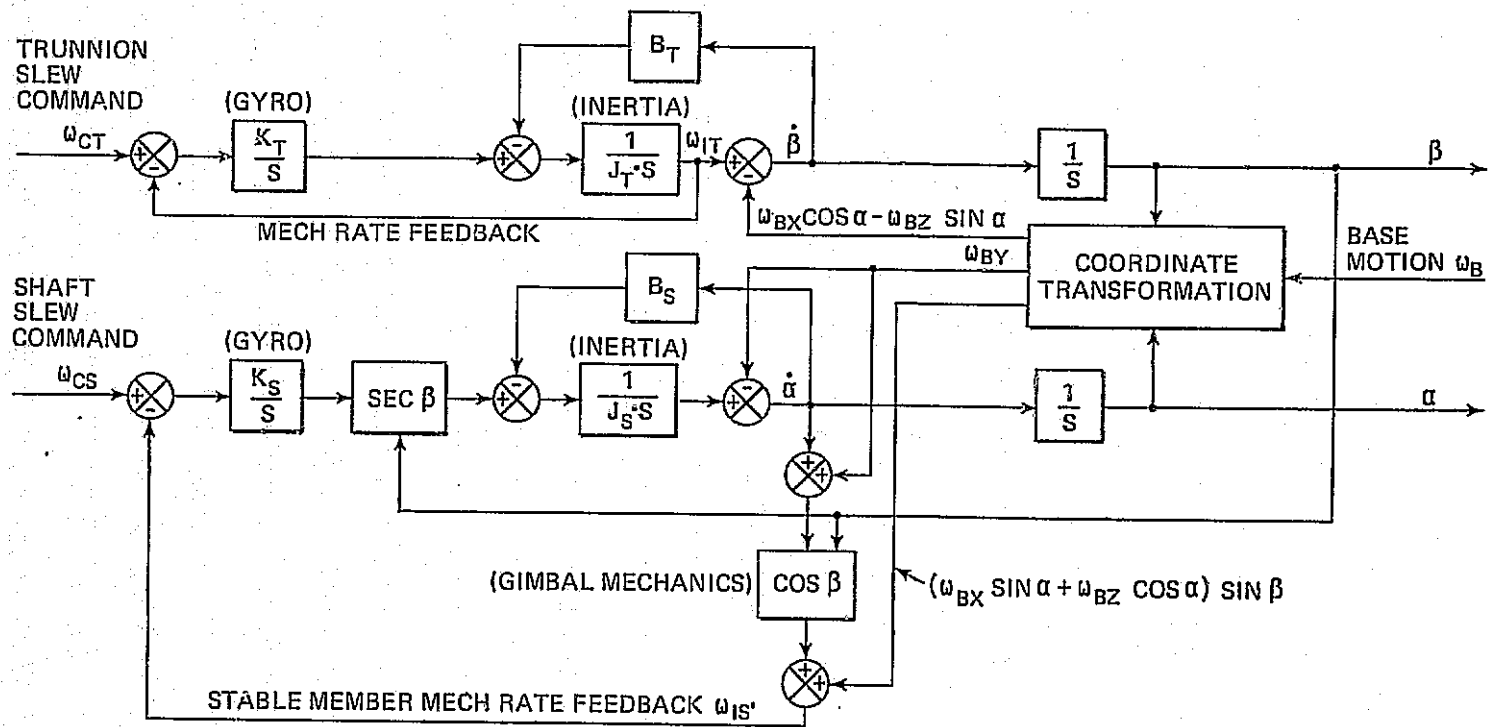


Fig. 8-7 RR Antenna Servo Digital Simulation

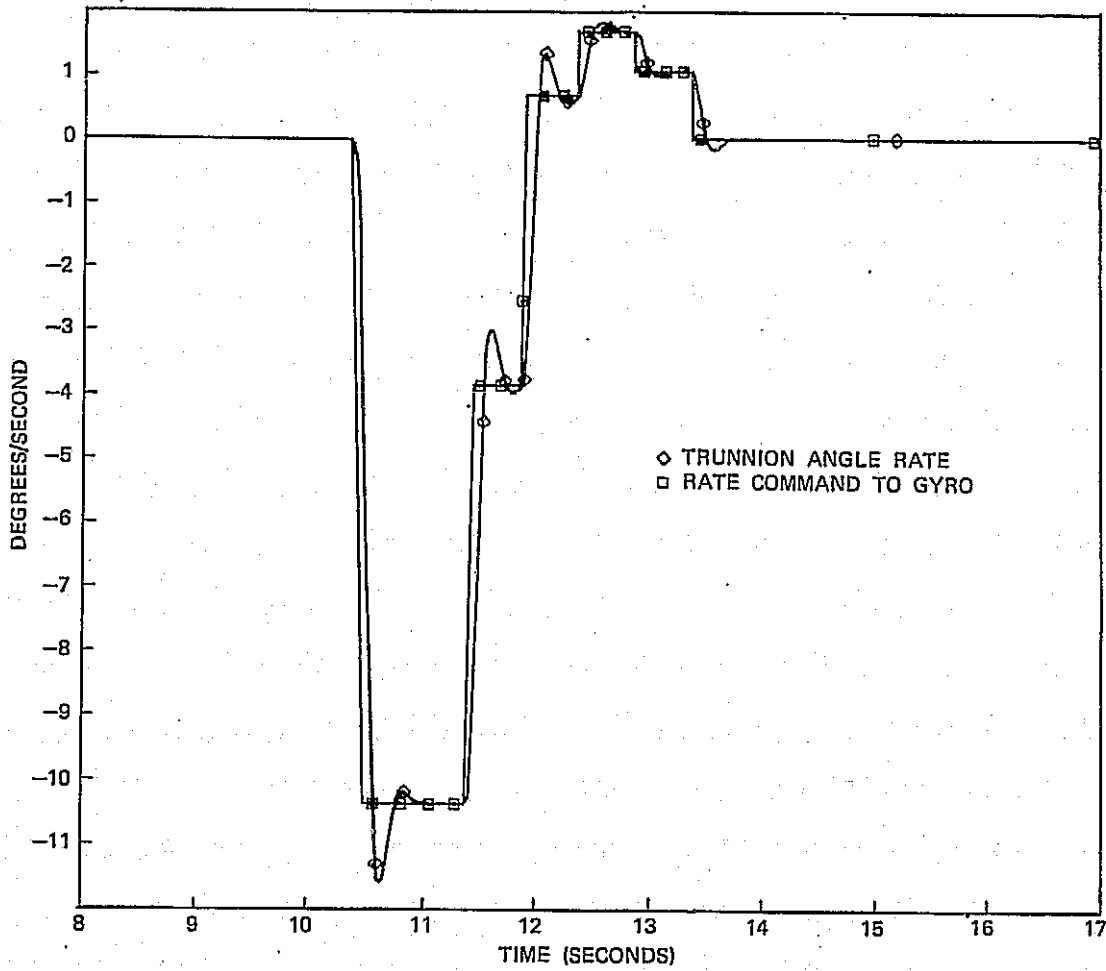


Fig. 8-8 Digital Simulation of Antenna Angle Designation (Trunnion Angle)

gain, the angular overshoot of the model was larger than that of the real antenna. Rise time and duration of the angle transient were reasonably well matched. Data on the servo performance and its comparison with the digital model are contained in the three radar group memos.<sup>3,4,5</sup>

### 8.3.1.3 Dither Problems

Production models of the radar antenna did not perform as well as the prototype. Excessive tracking errors were traced to backlash in the stabilization circuits. The problem was eliminated by introducing a 12-Hz "dither" signal whose purpose was to eliminate the electrical backlash in the modulation and detection circuits of the stabilization loop. It was expected that some of this 12-Hz signal would exceed the backlash and actually vibrate the antenna. This was verified by adding the proposed dither circuit to the equipment at MIT/IL and by recording angle outputs at high rate. A report was issued on this problem.<sup>6</sup>

The possibility of antenna vibrations was of lesser importance. Of prime concern was the capability of the high speed angle readout (resolver-CDU-computer) to follow these small vibrations and possibly put an unnecessary burden on the computer. In addition, angular rates exceeding 4 deg/sec caused by the vibration could not be tolerated. Exceeding this limit would cause the CDU to switch into another operating mode with insufficient readout accuracy. The problem was resolved by amending the interface specifications to require that the dither be applied only in the Auto-Track mode and that the total tracking error resulting from dither not exceed 2 mrad on the readout resolver.

### 8.3.1.4 Computer Program Evaluation

Up to January 1968, the radar interface tests were conducted with the experimental AURORA program in the guidance computer. This program permitted antenna angle designations relative to body coordinates and relative to the inertial measurement

---

3. Ibid.

4. W. Tanner and W. Saltzberg, "Rendezvous Radar Angle Interface Simulator, Investigation of 400/800 cps Jerk and Angle Designation with Base Motion," Radar Group Memo, 17 October 1966.

5. W. Tanner, K. Glick, W. Saltzberg, "Angle Readout Accuracy, Comparison of Rendezvous Radar Simulation with Experiments, Comparison of Interface Performance with Specifications," Radar Group Memo, 15 February 1967.

6. W. Tanner, "Effects of Dither on Trunnion Angle Readout," Radar Group Memo, 28 February 1967.

unit stable member. But the radar routines were not tied in with navigation computations, nor was there a capability to perform a search pattern with the radar. The prototype mission program assembly was called SUNDANCE. As early versions of this program became available in January, extensive evaluation began. While the effort of program evaluation in the System Test Laboratory is reported elsewhere, the following remarks relate to the interaction between computer and antenna servo.

Two items were of critical importance: 1) the antenna's mechanical axis had to be designated within a fraction of a degree toward a target moving at 15 mrad/sec and 2) angular acquisition of the target and performance of a space-stabilized search pattern had to be possible from any starting point within the two modes of angular coverage. Experiments to confirm pointing accuracy and search and acquisition performance used a light beam pointer for visual observation and an independent angle recording from the high speed resolvers of the two antenna gimbals. The mirror mounted on the trunnion near the crossing of the two gimbal axes is shown in Figure 8-6. This point was on the rotation axis of the rate table so that the mirror would not leave the optical aperture of a reference mark projector when base motion was applied.

In order to recognize lag errors of the designate servo, it was necessary to mark a time reference with the angle recordings of the gimbal angles. Special initialization of command and lunar module orbits for which the time of zero crossings of trunnion and shaft angles were known was entered in the guidance computer's navigation program. The computer memory simulator permitted countdown to the reference time and recording of the instant together with the angle readout.

Early in program development, investigation in the System Test Laboratory revealed an inherent lag error in the digital designate servo that required compensation. More important, some of the subroutines used for definition of the target location (in vehicle coordinates), particularly a Kepler integration routine, were putting delays into the designate loop and causing substantial overshoots of the antenna during target acquisition and search pattern generation. Eventually these problems were resolved by sophistication in the computer programs. The capability of exercising the computer programs on a hardware system, however, has saved time in recognizing the problems and in checking out corrective measures.

### 8.3.2 Evaluation of Landing Radar Data Readout

During Phase I testing, the electrical and functional compatibility of the interfacing circuits was established between landing radar and computer. Phase II testing started

in March 1966 and its purpose was to establish the statistical characteristics of landing radar readout by means of a realistic simulation of input signals to the radar, as well as by using radar signals that had been recorded during the flight tests at White Sands. These flight tests produced the first data in December 1966 and a second series of tests, conducted with production landing radar assemblies, provided final test data and terminated late in 1968. One major objective of the tests at MIT/IL was to verify the soundness of the technique of reading velocity data. The computer effectively controls the smoothing time applied to the radar data by selection of the counting interval of the frequency counter. This interval was to be 400 msec long but had to be broken down into five successive but separated 80-msec intervals for reasons of compatibility with computer architecture. The question remained as to whether or not the number of 80-msec samples should be changed to obtain the desired accuracy of the data.

The first effort of MIT/IL was the implementation of a test facility in the System Test Laboratory that could accept recordings of simulated radar signals as well as flight test signals. The equipment was assembled from commercial components and from special test equipment built at MIT/IL in the period between March and November of 1966. The setup is shown in Figure 8-9. The landing radar electronic assembly is shown mounted in its handling fixture and cold plate on the small table. To the left is the recirculation unit for the coolant. A 14-channel tape reproducer provides raw Doppler signals as well as reference and digital control signals for the radar.<sup>7</sup> The rack on the right contains radar power supplies and controls, signal conditioners and phase equalizers, telemetry discriminators, and decommutators for the multiplexed control signals. In addition, there is a time reader for the recorded IRIG-B reference time. The radar is tied into the lunar module guidance computer which, in turn, downlinks the radar data into digital recording equipment called the downlink simulator. A diagram of the system for flight data reduction is shown in Figure 8-10.

#### 8.3.2.1 Statistical Characteristics of Data Readout Using Simulated Input Signals

Based on an early descent trajectory and on the anticipated pitch angles of the landing radar, a specification was prepared to procure magnetic tape recordings of simulated radar signals. This specification is contained in the document referenced in footnote 7. Simulation and recording of the signals were carried out by Ryan, San Diego. The first tapes were delivered to MIT/IL in November 1966.<sup>8</sup>

---

7. E. Blanchard, "Requirements for MIT/IL Phase II Landing Radar Simulation Tapes," Document 23N-R 660930, 30 September 1966.

8. Ryan Aeronautical Company, Report No. 53974-46 of 27 January 1967, Data Package of M.I.T. Tapes 9 through 17.

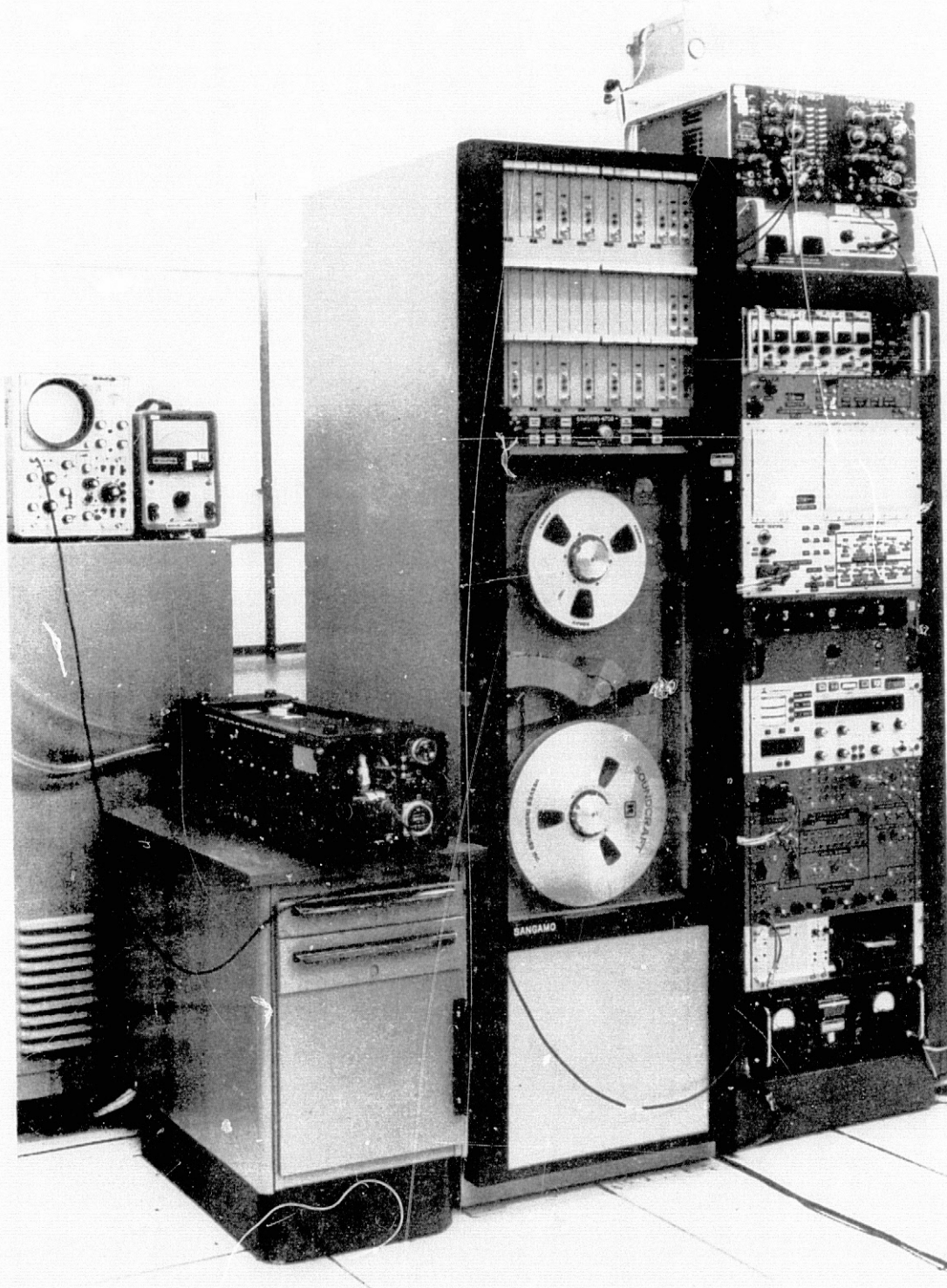


Fig. 8-9 Test Setup for Simulated Radar Signal

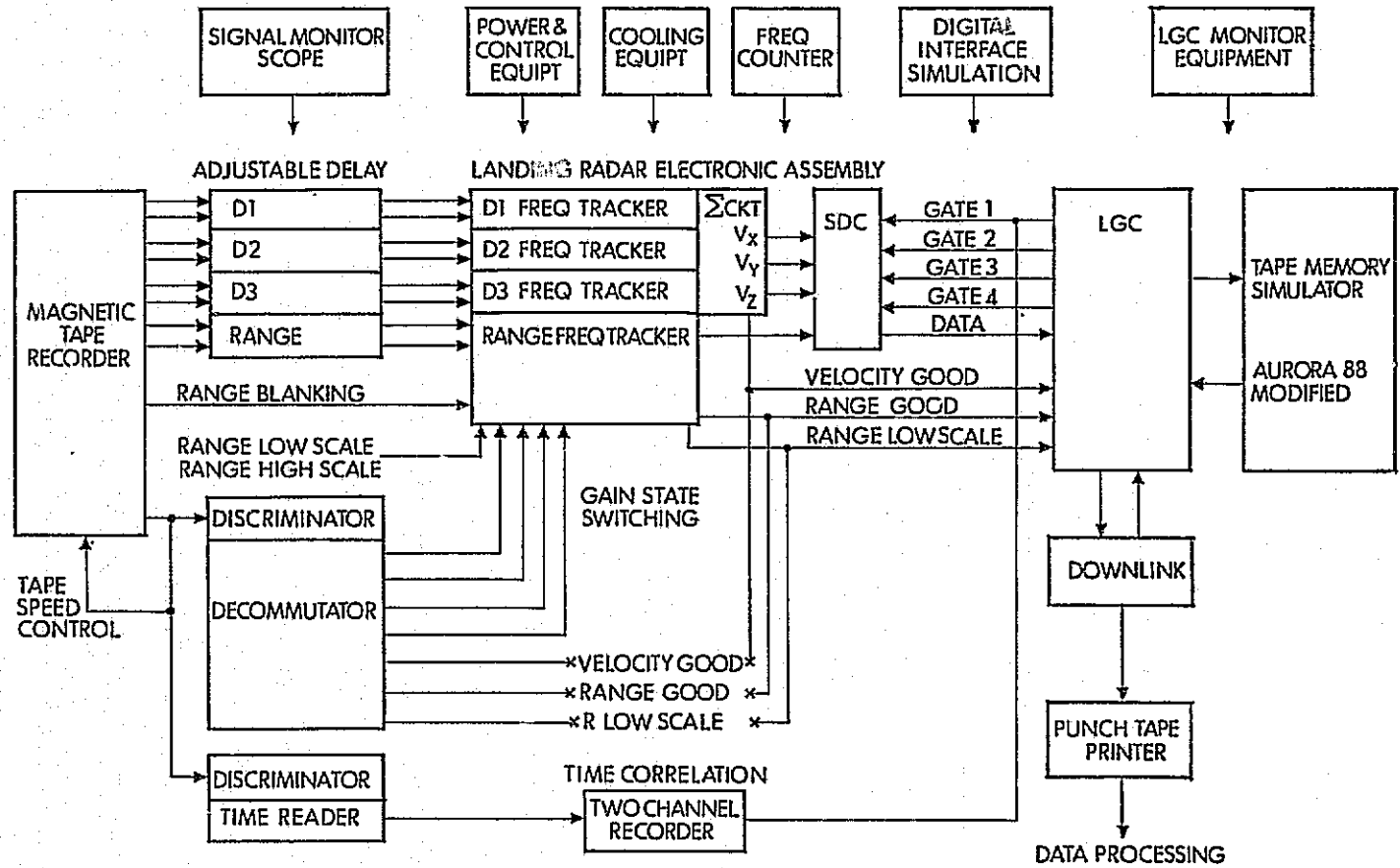


Fig. 8-10 Data Readout Simulation of Landing Radar

The magnetic tapes contained recordings of statistically independent signals for three Doppler trackers or for the three trackers involved in ranging. Superimposed on the signals was thermal and vibration noise that could be expected at the given simulated altitude. Also simulated was a so called "RF viewfactor noise" that represented interference from the engine bell and from the rear landing leg. These two objects were in "view" of some of the the radar beams and their vibrations produced signal noise. All interference signals based on the vehicle configuration of 1966 were analytical predictions and represented the most realistic model for a radar carried on a rocket-propelled vehicle. The later flight tests did not have the typical vibration and interference environment and, therefore, lacked a feature that only signal simulation could provide.

8.3.2.1.1 Random Errors and Readout Delays.—The basic source of random errors of a Doppler velocity sensor is the spatial distribution of radar reflectors within the footprint of each radar beam. This type of error is proportional to the square root of  $V/T$ .  $V$  is the velocity component across the beam axis;  $T$  is the smoothing time. There are other sources of error: thermal noise, tracking servo noise, interference noise, and quantization noise in the digital data readout. Under ideal conditions, a Gaussian error distribution is obtained and only then does the above relation of the error to smoothing time hold.

Table 8-II lists the total  $3-\sigma$  velocity errors that were seen by the guidance computer for three orthogonal axes. Simulated signals with a stationary center frequency were fed into the 4L landing radar electronic assembly. Special programing of the lunar module guidance computer permitted a five-sample (of 80 msec) readout of the radar's output counter (signal data converter) at a rate of one readout per second. The five samples were accumulated in the guidance computer and downlinked for recording. The data were then compared with reference signals that had also been recorded on the magnetic tape. The statistical sample in each of the tabulated results is about 100 to 120 error points. Range error data are based on a single 80-msec readout interval of the radar's output counter.

A more difficult task was the determination of lag errors. As the vehicle velocity changes or more important, while the vehicle changes attitude, the radar signal frequencies change at a rate that can be predicted. During pitch-up and site redesignation maneuvers, rapid changes can be anticipated in radar signal frequency that might either cause loss of tracking or at least a lag error in the velocity data. These rapid frequency changes were simulated by frequency up and down ramps. Precise time correlation between the readout of the radar data and the recorded reference signals permitted the measurement of bias error that could be attributed

TABLE II

COMPUTER-LANDING RADAR SYSTEM, SUMMARY OF DATA READOUT  
ERRORS FOR SIMULATED INPUT SIGNALS

TRAJECTORY IDENTIFICATION						LAG					RANDOM ERROR 3 SIGMA								
POINT	TIME (SEC)	ALT (FT)	SLANT RANGE (FT)	RANGE (FT)	TOTAL VELOCITY (FPS)	$\Delta V_X$ (FPS)	$\Delta V_Y$ (FPS)	$\Delta V_Z$ (FPS)	$\Delta R$ (FT)	$\Delta R$ (%)	$\Delta V_X$ (FPS)	%	$\Delta V_Y$ (FPS)	%	$\Delta V_Z$ (FPS)	%	$\Delta R$ (FT)	%	
BREAKING	1	3775	25190	171k	25570	1942	-	-	-	+145	+0.6	-	-	-	-	-	-	375	1.5
	2	3835	16407	80.4k	16506	1071	-	-	-	+ 48	+0.3	-	-	-	-	-	-	243	1.5
	3	3885	9253	37.3k	9275	654	-	-	-	+ 1	+0.0	-	-	-	-	-	-	129	1.4
PITCH UP	4	3889	8623	34.8k	9722	622	-	-	-	-	-	-	-	7.5	1.2	-	-	-	-
VISIBILITY	5	3899	7148	28.0k	7532	559	-2.5	-0.4	-2.8	+ 35	+0.5	2.4	0.4	8.7	1.6	6.3	1.1	80	1.1
	6	3939	3020	11.4k	3188	321	-0.7	-0.6	+1.9	+ 3	+0.1	2.1	0.7	7.8	2.4	5.7	1.8	74	2.3
	7	3959	1764	6.0k	1838	217	-1.4	+0.2	-0.2	+ 9	+0.5	3.0	1.4	6.0	2.8	8.7	4.0	13	0.7
	8	4012	188	251	18	26	-	-0.1	+0.3	-	-	-	-	3.6	-	3.6	-	-	-
LANDING	9	4049	52	53	56	5	-	-	-	-	-	-	-	-	-	-	-	-	-
SITE REDESIGNATION	10	3909	5856	20.8k	6418	486	-0.7	-0.0	-1.5	+ 4	+0.1	2.0	0.4	8.0	1.6	5.9	1.2	76	1.2
	11	3900	7040	52.0k	7061	559	-	-	-	-	-	-	-	-	-	-	-	-	-
	12	3919	4890	41.0k	4984	534	-	-	-	-	-	-	-	-	-	-	-	-	-
	13	3939	3417	31.3k	3419	490	-	-	-	+ 13	+0.4	3.0	0.6	13.5	2.8	5.1	1.0	102	3.0
	14	3949	2891	26.6k	2906	460	+1.5	-0.8	+1.1	+ 14	+0.5	2.4	0.5	11.1	2.4	4.8	1.0	114	3.9
	15	3969	2123	18.1k	2223	386	+1.8	+1.0	+4.7	-	-	2.7	0.7	9.6	2.5	7.8	2.0	-	-

ORIGINAL PAGE IS  
OF POOR QUALITY

to the lag in the frequency tracking servos. These errors are listed in the center portion of Table 8-II.

Some of the simulated data could not be processed because of explainable instrumentation difficulties. But with the low velocity flights, difficulties occurred (points 8 and 9) with the acquisition of the signals. As a result, the acquisition sensitivities of later radar systems were changed.

8.3.2.1.2 Frequency Tracker Noise Investigation.—All simulation recordings contained first a series of clean sinusoidal signals for functional testing of the system and to establish a performance baseline for the tests. For some simulation points, these baseline data showed large random deviations. After extensive experimentation these random errors were traced to a cross-coupling effect in the four frequency trackers of the 4L radar system, an early prototype. Figure 8-11 depicts the error distribution for one of the worst-case situations, a test point representing marginal radar signal amplitude and low vehicle velocity (26 fps). The lopsided error distribution is an indication of cross-coupling between the frequency trackers associated with beams 1 and 2. The large errors are attributed to servo noise. Precaution was taken to avoid instrumentation errors; the data were read with an independent counter, thus excluding the quantization error associated with the guidance computer. Painstaking analysis of the error data indicated that cross-coupling might cause excessive errors during lunar missions. The possibility of such error was later eliminated by adding shielding between the frequency trackers.

#### 8.3.2.2 Processing of Flight Test Data

The flight tests of both the rendezvous and the landing radars at WSMR were under direction of MSC. The portion pertaining to the landing radar evaluation had the objective of exposing the radar system to an operational flight environment and of measuring its performance over terrain that reasonably simulated the properties of the lunar surface. The high-speed, high-altitude portion of lunar descent was simulated by installing a landing radar on a T-33 jet trainer. The low-speed portions of the descent used an SH-3A helicopter as test bed. Radar and instrumentation were in packages that could be transferred from one test vehicle to the other.

MIT/IL participated in the definition of trajectories for the test flights. Some of the flights represented critical sections of "Design Reference Mission 1" trajectory of the lunar module; others were aimed at observing such radar functions as tracker acquisition and the switching of the range scale factor of the ranging system. A series of straight and level flights provided data on the statistical distribution of

SIGNAL SOURCE: RYAN SIMULATION OF POINT 8 (STATIC)

TOTAL VELOCITY: 26 fps  
 SLANT RANGE: 189 ft

	$f_D$	BW	S/N (100Hz)	LEVEL
BEAM 1	190 Hz	41 Hz	21.5 db	78 mV
BEAM 2	190 Hz	41 Hz	21.2 db	76 mV

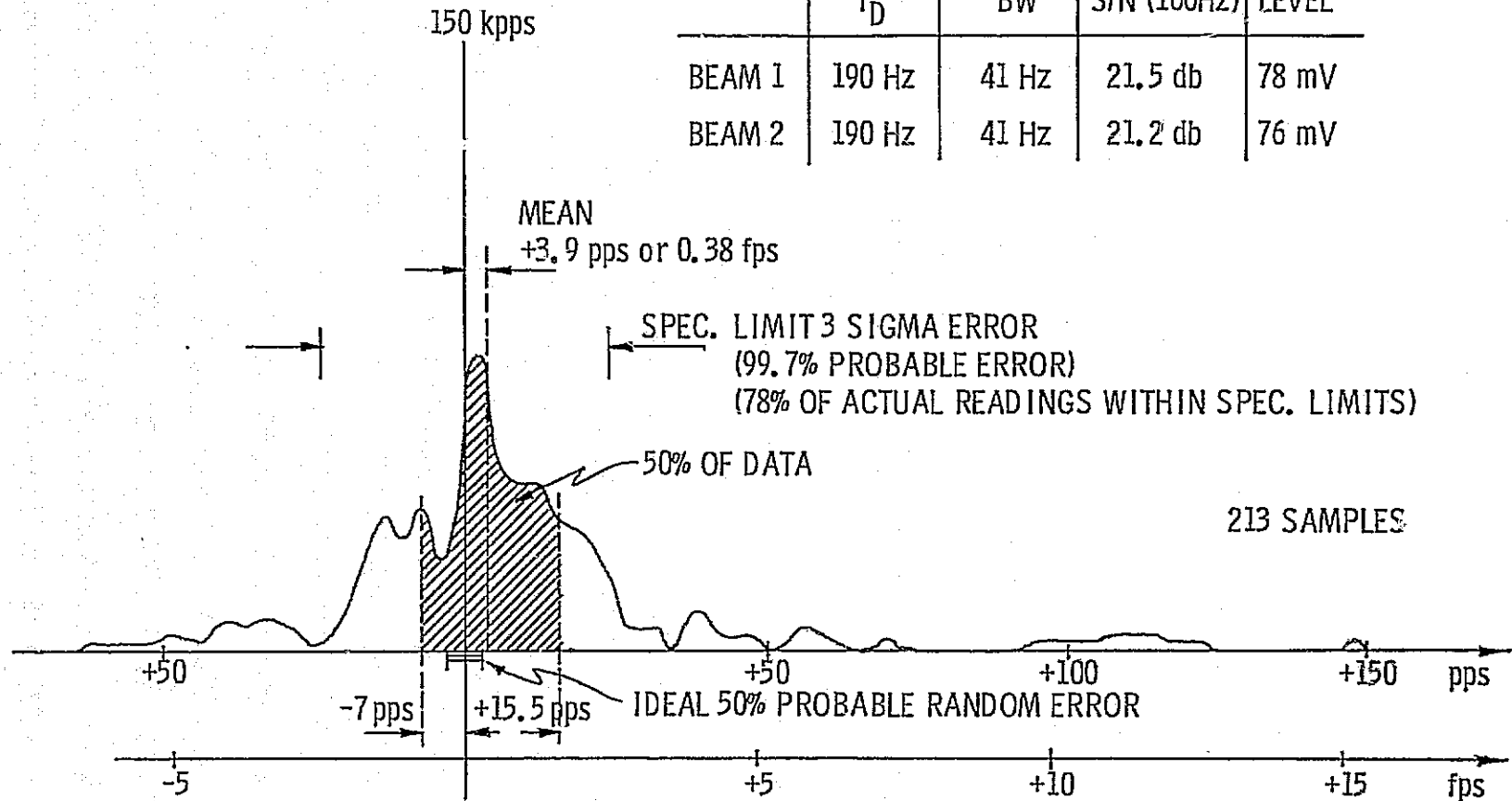


Fig. 8-11 V-Velocity Tracker Error—Probability Density

radar errors. Up and down flights by the helicopter simulated conditions just prior to the landing of the lunar module, and provided data on the probability of radar drop-out because of zero velocity along the Doppler beams.

Schedules did not permit instrumenting the test vehicles with components of the guidance system. Instead, a "3050" flight instrumentation computer was installed for radar data readout and a Litton type LN-12A inertial platform was used for the determination of vehicle attitude. Initially, a time reference was provided via a VHF link from the White Sands telemetry station, but a reference time generator was later carried onboard. Data from the radar and the reference platform, the timing signals, and a variety of environmental information were recorded by an onboard tape recorder.

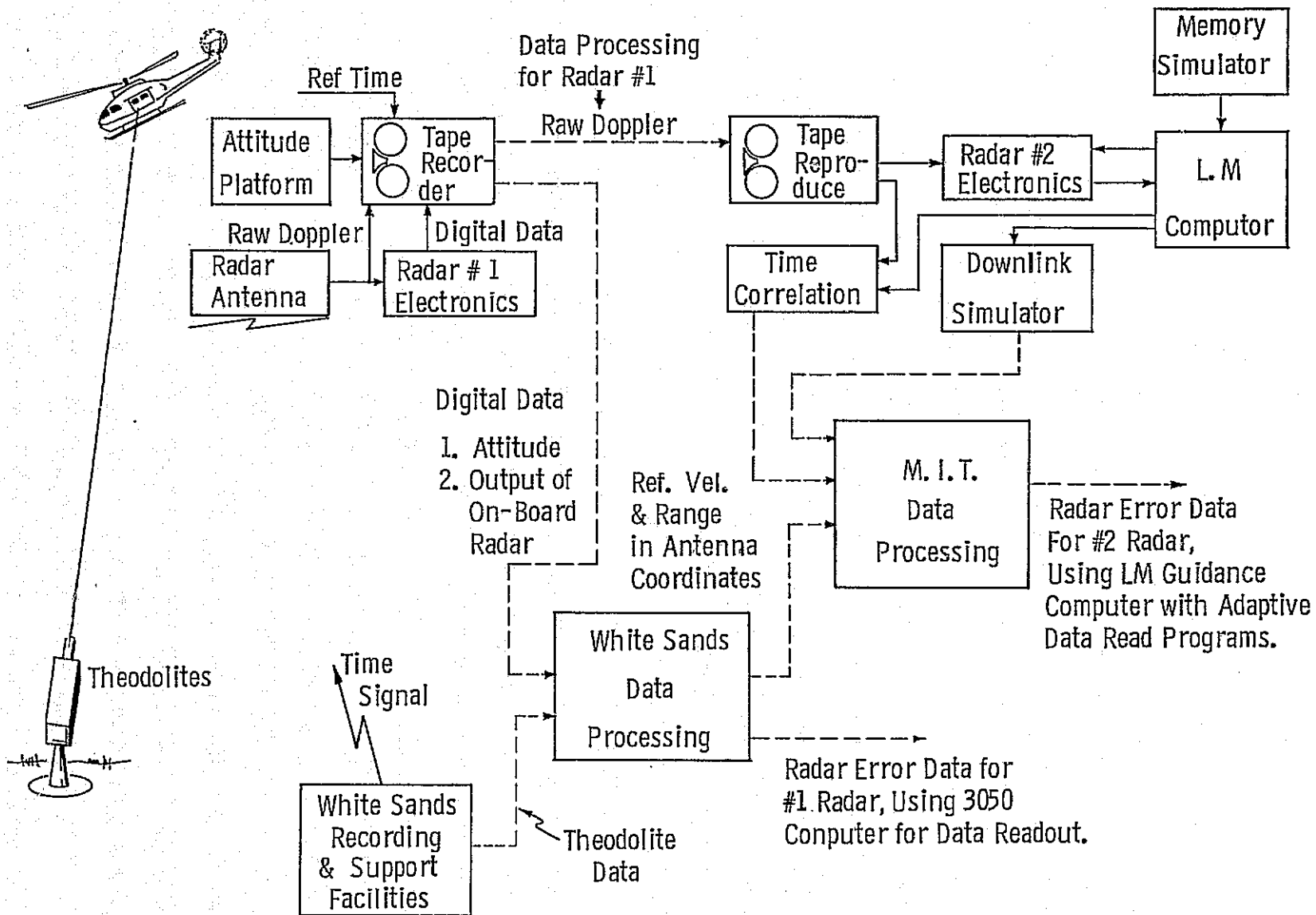
Flight trajectories were tracked by cinetheodolites. From tracking data and from attitude data recorded onboard the aircraft, Computer and Software Company of Holloman, N.M., prepared reports and data on magnetic tape. These data included the flight trajectory and reference range of the radar in its own coordinate system, and finally an error evaluation of the onboard digital data. All of these operations, as well as the instrumentation of the two test vehicles, were under direction of Grumman.

In anticipation of changes in the programming of the lunar module guidance computer and to permit end-to-end testing of the radar as integrated with the guidance system in its final hardware configuration, a second avenue of data processing had been planned. The raw data from the radar, consisting of three pairs of Doppler signals, one pair of range signals, and a number of signals defining the operating state of the radar, were recorded on board. These recordings were used at MIT/IL in conjunction with an independent radar electronic assembly to confirm on a real system the proper processing of radar data by the guidance computer. Figure 8-12 shows in block form the concept of recording flight test data, the reprocessing of the raw signals in a system configuration at MIT/IL, and the data processing required to compare the data of the navigation system with the original flight trajectory.

The reprocessing of the recorded analog radar signals was performed in the MIT/IL System Test Laboratory using the equipment shown in Figures 8-8 and 8-9. The use of the tape memory simulator in conjunction with the guidance computer permitted special programming of the computer. This was required to change the number of samples in the velocity readout, to accommodate the 10 word-per-second downlink, and to incorporate programs for recognition or updating of errors in the downlink transmission. Particularly difficult was the problem of time correlation between

FLIGHT TEST OPERATIONS

MIT SYSTEM EVALUATION



196

Fig. 8-12 Flight Test Operations

recorded data and the reference trajectory, since the computer readout was asynchronous with the time recording on the analog input tape. Correlation was obtained by recording timing signals from the analog tape and from the computer on a high speed paper recorder and by comparing the relative location of the traces.

The output of the signal processing in the System Test Laboratory was a punch tape (or later a "digistore" magnetic tape) that contained radar data and a time tag provided by the guidance computer. These data were then processed together with radar reference data, which were provided by Grumman on computer-compatible magnetic tape. Data processing at MIT/IL interpolated the trajectory data for the exact time of the radar data readout and produced the error data for velocity and slant range. The results were also plotted automatically. Typical data plots are shown in Figures 8-13 through 8-18.

8.3.2.2.1 1966/1967 Flight Test Data.—The first series of flight tests used 7L-type landing radar onboard the two aircrafts. In the laboratory, the data were consequently processed through the 4L electronic assembly and a lunar module guidance computer, using special programing that was compatible with the 10 word-per-second downlink simulator (latest downlink capacity is 50 words-per-second). After a long period of difficulties with flight instrumentation, recording levels, time recordings, and data processing problems, it was finally possible to get a realistic reproduction of radar signals into the system and to correlate the radar data with original trajectory data with a timing error of less than 5 msec.

E-2185 gives the results of the 1967 tests.<sup>9</sup> The errors of velocity and slant range measured by the radar were generally within specification limits. This was particularly true for high speed flights. Error data relating to the 4L radar and error data originating from the 7L onboard system were in agreement. However, there were a few low level and low velocity flights that showed random errors beyond specification limits in the order of 3 to 6 ft/sec as well as occasional errors of 15 to 20 ft/sec. Some of the larger errors could be associated with tracker acquisition after a dropout. Some of the smaller errors were the result of decorrelation by 1 second of the attitude and velocity data in computing the reference velocities. Unfortunately the data from low level, low velocity flights were sparse and did not permit clear identification of the error sources.

The relatively large random errors in velocity suggested consideration of an increase in the number of velocity samples. This would increase the effective smoothing

---

9. W. Tanner et al., "Landing Radar/LGC Interface Experiments, Part II, Flight Test Data Package," E-2185, 30 September 1967.

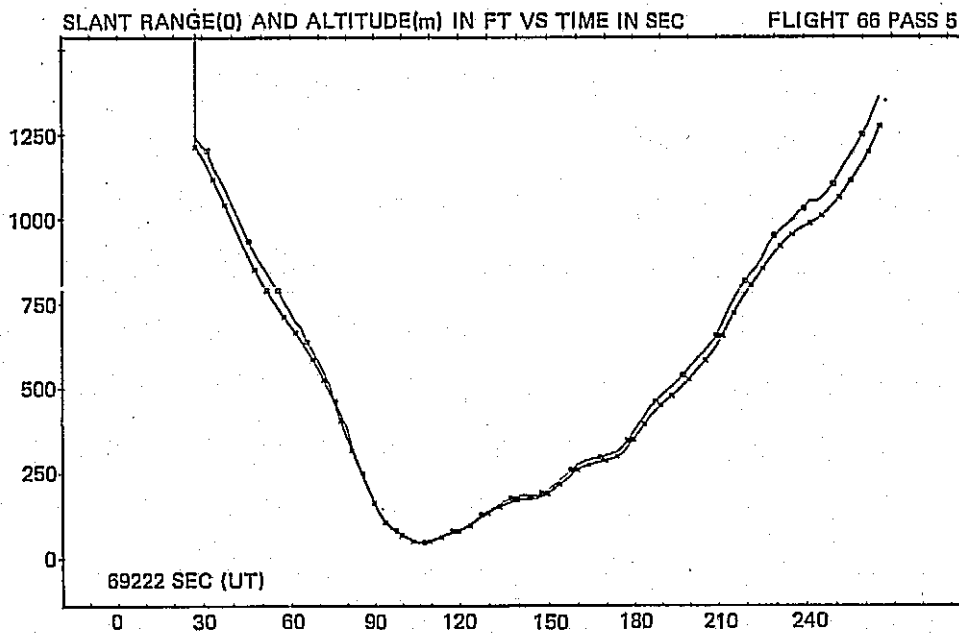
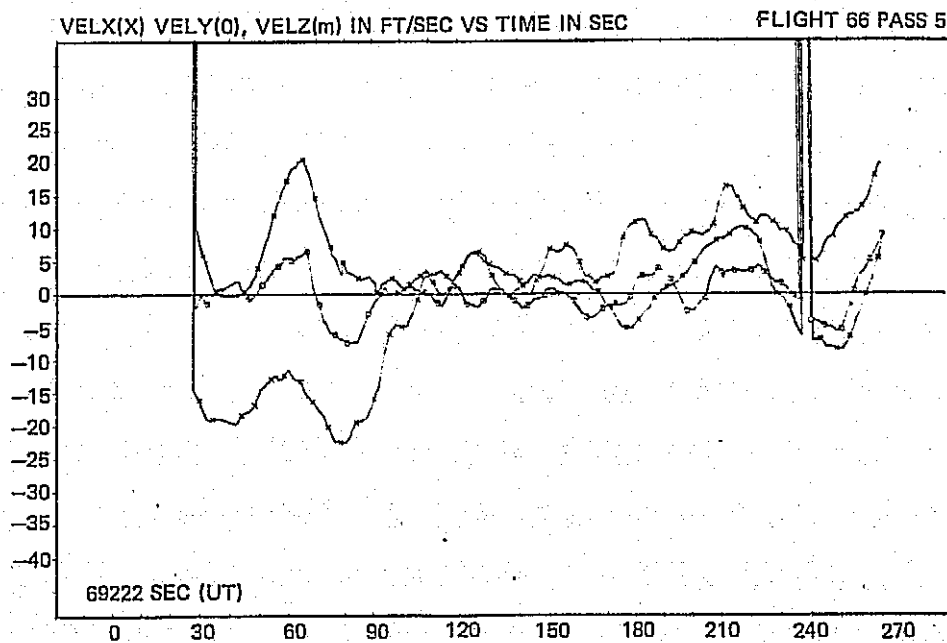


Fig. 8-13 LR Helicopter "Yo-Yo" Flight vs Time



THREE VELOCITY COMPONENTS IN ANTENNA COORDINATES

Fig. 8-14 Three Velocity Components in Antenna Coordinates

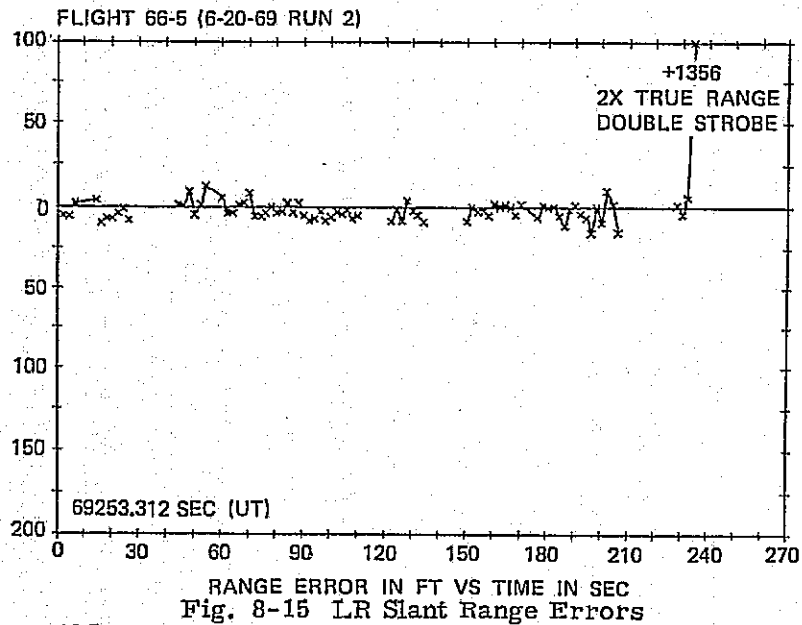


Fig. 8-15 LR Slant Range Errors

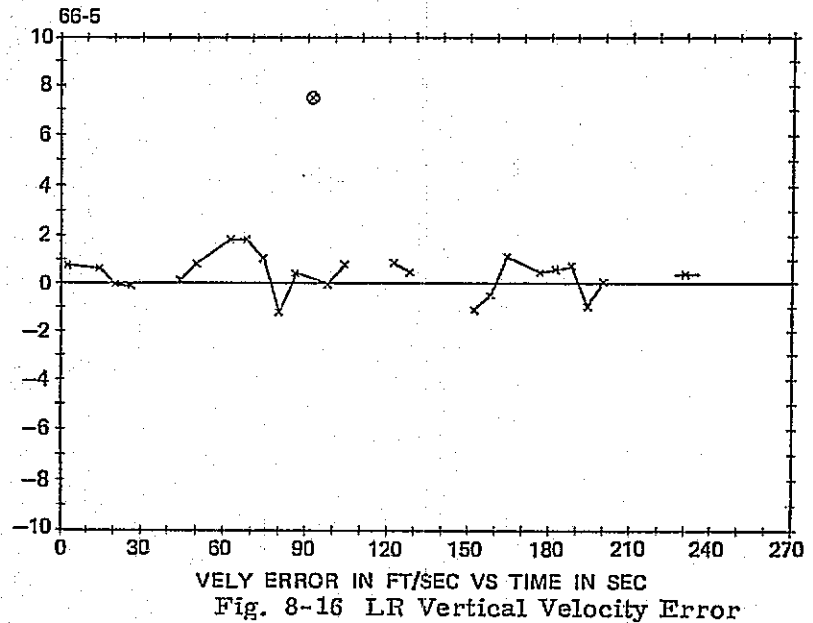


Fig. 8-16 LR Vertical Velocity Error

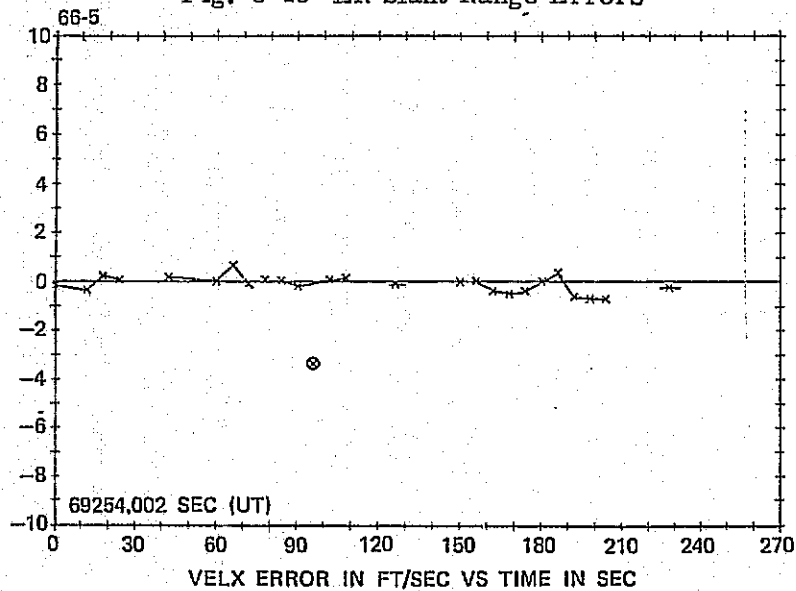


Fig. 8-17 LR Cross-Track Velocity Error

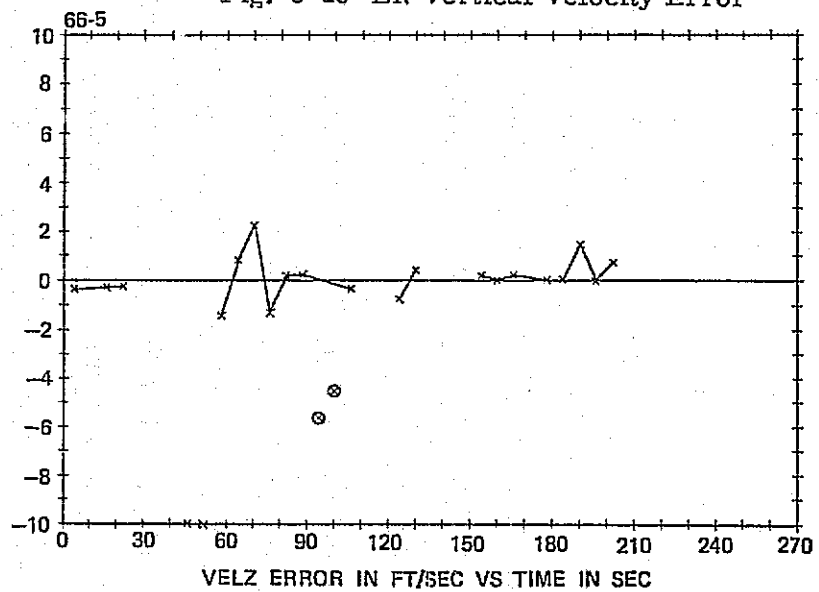


Fig. 8-18 LR Track Velocity Error

time and thus reduce the errors. To observe the effect of changes in smoothing time, the regular five-sample readout was complemented by reprocessing the analog tapes, using first three and then nine samples. Several typical flights were analyzed this way, only to find that the large random errors were hardly affected by the sampling technique. The distribution of errors was anything but Gaussian. These observations led to the conclusion that there was an erratic interference causing the errors. Until this interference was identified and substantially reduced, there was no reason to alter the data readout sequence of the radar.

Since there had been several changes incorporated in the production radars after the 7L system was built, it was decided to implement a second program of flight testing with special emphasis on low-level flights using up-to-date hardware. Another action taken as a result of the unsatisfactory tests at low velocities was the implementation of a reasonableness test for radar velocity and range data in the computer in order to recognize and discard bad radar data. In addition, a 4-second delay was incorporated before radar data could be used after re-acquisition following a dropout. The weighting of radar velocity data was reduced to 0.2 thereby reducing the contamination of navigation data by an erratic radar reading.

8.3.2.2.2 1968 Flight Test Data.—The new series of flight tests made use of the 11L landing radar system onboard the aircraft; the 10L electronic assembly was installed at MIT/IL shortly after it was received in August 1968. Installation tests using old flight test recordings showed noticeably improved sensitivity of the radar tracker at low velocity and better acquisition characteristics. However, there were occasional internal interference problems in the digital circuitry and consistent malfunction in the switching of the range circuits into low range. Since the 10L equipment was the best available, it was used for processing of the new high-altitude data taken with the T-33. On 25 April 1969, MIT/IL received a replacement unit, Electronic Assembly P32, that was used immediately to provide data on the critical low altitude, low velocity flights.

The results of radar system evaluation at MIT/IL were presented at the Radar Integration Meetings at MSC of 2 April, 6 May and 25 June 1969, and are contained in the minutes of these meetings.<sup>10,11,12</sup> An example of the data is given in Figures

---

10. W. Tanner, "Landing Radar Flight Test Data of 1968 G-Flights," (Presentation delivered at MSC Radar Integration Meeting, 2 April 1969).

11. W. Tanner, "Landing Radar Flight Test Data Processing at MIT/IL," (Presentation delivered at MSC Radar Integration Meeting, 6 May 1969).

12. W. Tanner, "Progress of Landing Radar Data Processing of 1968 Flight Tests (Final)," (Presentation delivered at MSC Radar Integration Meeting, 26 June 1969).

8-13 through 8-18. The first two graphs show slant range, altitude, and the three velocity components for the radar system versus flight time. The particular flight was an almost vertical "Yo-Yo," during which radar dropout followed by acquisition problems are expected. The next four graphs show the radar errors in range and velocity.

The range data are quite good even though they are "noisier" than on most flights. The last data point is an example of an error that was caused by a double pulse in the readout strobe of the serial data readout. Two such errors were identified in a total of about 1000 range readings. The same type error had been recorded during system tests at Kennedy Space Center in the readout of velocity data. Since there was a good chance for a higher rate of occurrence of this error, the double pulse was removed by a hardware fix called BOLD on the APOLLO 11 system, and by a program change in the computer of later flight systems.

The velocity data show several dropouts that are indicated by the interruption of the solid line. Vertical velocity (X-component) is usually very good and within a fraction of 1 ft/sec of the reference velocity. Horizontal velocities (Y and Z) have larger errors. There are a few data points out of line. They were removed since they could be correlated with an instrumentation problem associated with gain-state switching in the radar receiver.

Statistical analysis of the error data was difficult because of the low number of data points per flight. In order to increase the sample, flights of similar nature were combined into groups. The mean error and the standard deviation were then computed for the data of the entire group. Table 8-III is the summary of the errors for the high-altitude, high-velocity flights using the T-33 aircraft. These data were taken with the 10L electronic assembly. Each data block is given for a range interval in altitude and one in forward velocity. The numbers within the block identify the flight numbers. To the right are the bias and RMS errors for the three velocity components and for the range component.

All the previous radar data had been processed by using modified AURORA<sup>13</sup> programs in the computer and by recording of the data on punched paper tape. When the P32 electronic assembly became available, flight-type computer programs were used with the high speed (50 word-per-second) downlink with data recording on magnetic tape. The data processing also had to be adapted to the new data format.

---

13. AURORA was the first program for the lunar module guidance computer designed for hardware checkout.

The data on the low-altitude, low-speed flights were processed with this latest system configuration and represent an end-to-end test for the combination of radar system and the navigation computer. Table 8-IV is the summary for these low-level flight data.

The data obtained at MIT/IL by processing of recorded raw radar signals through an actual system contained slightly larger random errors than the data originating from the 11L onboard radar system. It is not known whether the increase in standard deviation is due to time correlation problems or to slightly different characteristics of the frequency trackers between the 11L and the P32 radar systems. The fact that two independent systems gave consistent results greatly enhanced confidence that the landing radar onboard the APOLLO 11 flight would perform well. The shakedown tests in the System Test Laboratory also revealed the possibilities of acquiring erroneous data. Protective measures such as the reasonableness tests could be incorporated into the computer programs on the basis of first-hand knowledge of the problem. It was demonstrated that system testing of a Doppler sensor system with recorded raw radar data is a workable approach, and that the actual flight trajectory can be correlated with the radar recording to better than 5 msec and can reproduce velocity to better than 0.5 ft/sec.

TABLE 8-III

## ERROR STATISTICS OF LANDING RADAR FLIGHT TESTS

Bias and RMS errors after removal of erratic data. Tabulation for groups of 1958 high speed flights (T-33). Data processing using EA-10L and modified AURORA programs. Data include errors of reference trajectory, quantization, lag time.

Altitude Range (FT)	Forward Velocity (FPS)	
	200 - 400	400 - 720
26000 - 36000 Climb	List of Runs VELX Bias/RMS VELY Bias/RMS VELZ Bias/RMS R Bias/RMS	75-1   +0.7/1.7 78-1   -1.2/3.1 -0.3/1.2 +38/85
15000 - 30000 Dive		72-1   72-2   72-3   +0.4/0.9 72-4   +1.7/3.3 72-4   +0.4/1.2 78-2   +5/103
12500 - 17000	75-7   +0.5/1.0 76-3   +5.4/2.5 76-3   +0.4/0.8 77/32	76-1   +1.2/1.8 76-2   +0.7/1.8 +0.4/1.5 +43/38
5000 - 9500		73-6   +1.7/2.2 73-6   +0.2/1.5 +4.0/4.4 +11/67
3000 - 4400	73-1   +1.1/1.8 73-7   +1.4/1.4 +1.7/2.8 -2/24	

TABLE 8-IV

ERROR STATISTICS OF LANDING RADAR END-TO-END FLIGHT TESTS

Bias and RMS errors after removal of erratic data, Tabulation for groups of 1968 low level G-Flights, M.I.T. data processing using FA-32, LGC 600 or 100M, LUMINARY 97 programs, 50 wps downlink, Data include errors of reference trajectory.

Altitude Range (FT)						
530 - 1200	List of Runs	VELX Bias/RMS VELY Bias/RMS VELZ Bias/RMS R Bias/RMS	67-1	+0.2/0.4 +0.2/0.9 -0.2/0.8 <u>+1/6</u>	57-3 64-1	+0.2/0.35 -0.23/0.8 +0.1/0.6 <u>+2/5</u>
400 - 800			67-4	+0.3/0.4 +0.1/0.4 -0.2/0.5 <u>+2/3</u>	57-3 57-4 64-3	+0.1/0.2 +0.1/0.7 +0.2/0.5 <u>1/5</u>
95 - 200	70-4	0.0/0.2 0.0/0.7 -0.1/0.4 <u>-4/3</u>	67-5 67-5	+0.3/0.8 -8.1/8.6 -0.4/1.1 <u>-1/3</u>	57-6 64-5	0.0/0.3 +0.1/0.6 -0.3/0.5 <u>0/3</u>
40 - 97					61-3	+0.7/0.4 +0.2/0.0 +0.4/0.6 <u>+12/10</u>
35 - 60	70-3	+0.1/0.6 -0.2/1.3 -0.4/0.9 <u>-3/4</u>	78-2	+0.1/0.4 0.0/0.8 -0.1/0.5 <u>-2/4</u>		

## CHAPTER III CANDIDATE SUBSYSTEMS

### SECTION 1.0 GENERAL INTRODUCTION

This chapter discusses the design and development of three candidate subsystems that were considered for use in APOLLO, but which, for the reasons stated, were not incorporated into the final guidance, navigation, and control (GN&C) system. The three subsystems discussed are the star tracker-horizon photometer, the map and data viewer and the lunar module optical rendezvous system.

## SECTION 2.0 TRACKER-PHOTOMETER

### 2.1 INTRODUCTION

The onboard measurement of included angles between selected stars and the earth's horizon or earth's landmarks is a required backup function for maintaining knowledge of spacecraft position and velocity.<sup>1</sup> To supplement this normally manual task, a star tracker and horizon photometer were designed as part of the Block I-100 and Block II optical subsystems (OSS). The star tracker was to provide automatic tracking of a preselected star along the sextant star-line-of-sight (SLOS). A horizon photometer was to serve as a reliable means of recording the acquisition of a well defined point within the earth's atmospheric horizon along the sextant landmark-line-of-sight (LLOS).

The tracker-photometer arrangement is particularly effective when the spacecraft is in a near-earth orbit from where atmospheric conditions may make it difficult for the human eye to accurately define a horizon locator or to see a cloud-obscured landmark. In addition, the tracker-photometer subsystem can make star/horizon angle measurements in much less time and with fewer display and keyboard (DSKY) operations than with measurements obtained manually.

The location of the star tracker and horizon photometer is shown in Figure 2-1. The star tracker line of sight is parallel to the sextant star line of sight and the horizon photometer line of sight is parallel to the sextant landmark line of sight.

### 2.2 STAR TRACKER

The star tracker provides precise star direction error information for the sextant trunnion and shaft servo loops when the optical subsystem is operating in the Tracking mode. The instrument is capable of tracking stars of third visual magnitude or brighter. Using the optics' servo loops, the star tracker functions as a nulling device that maintains a preselected star at the center of the sextant field of view. Synchronous demodulators generate X and Y servo error signals proportional to star image distance from the center of the field of view to drive the sextant trunnion and shaft.

---

1. See R-447 and R-495, Vol. I, Appendix A, Abstracts.

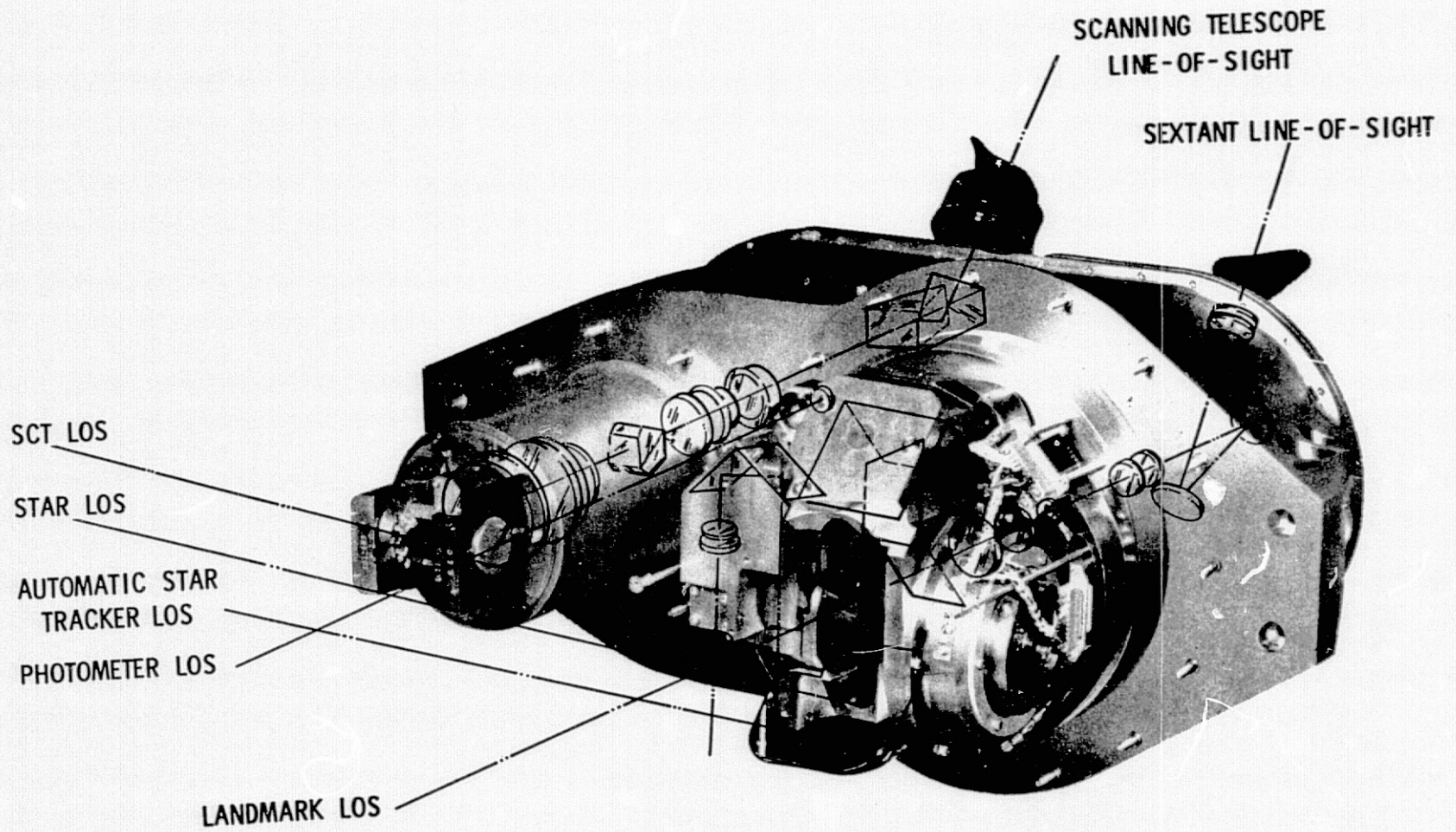


Fig. 2-1 V-30 Apollo Optical Unit

Figure 2-2 is a block diagram of the star tracker. Starlight is introduced to the tracker objective lens through an extension of the sextant indexing mirror and two orthogonal mirrors. The starlight is modulated by two tuning fork resonator assemblies. The modulated starlight is then collected by a condensing lens, and the image focused on the cathode of the photomultiplier tube (PMT). Electrical signals from the phototube are amplified, synchronously demodulated, and then modulated by an 800-Hz reference signal to produce the X and Y tracker output signals.

The light modulator assembly consists of two tuning forks, one for each sextant star line of sight degree of freedom, that vibrate with precisely controlled frequencies and amplitudes. Slits attached to the tines of the forks convert the continuous starlight into bursts of light that have unique phase and frequency components for the star position within the tracker's field of view. Electrical pulses carrying this position information from the phototube are then demodulated to drive the sextant motor-drive amplifiers.

The synchronous demodulators extract both the fundamental ( $f_1$  and  $f_2$ ) and second harmonic ( $2f_1$  and  $2f_2$ ) components of the modulated starlight as the star moves in the field. The fundamental components are modulated by the 800-Hz reference signal producing the X and Y outputs that are then transformed into shaft and trunnion servo error signals. The harmonics are summed to provide automatic gain control of the phototube and a star presence signal to the computer.

### 2.3 HORIZON PHOTOMETER

The horizon photometer uses the "signature" or "locator" phenomenon of the horizon profile as viewed from space at a known altitude above the limb of the earth. Analysis has shown that an accurately predictable relationship exists between the intensity of a sunlit horizon viewed from space and the intensity at a given altitude above the limb of the earth. This relationship, termed a horizon profile, has been determined to depend on such factors as the scattering of sunlight and extinction of aerosols (i.e., attenuation of sunlight) as a function of altitude. The half-power intensity of a given profile reliably occurs at approximately the same altitude above the limb for certain wavelengths. This phenomenon therefore defines a locator or signature within the profile. Theoretical considerations indicate that the variation of the horizon signature with altitude will vary as little as approximately  $\pm 0.5$  n. mi. for a scan performed in or near the ultraviolet region (to exclude interference from clouds) in the band 3700-3800A. This corresponds to a signature stability of approximately  $\pm 2$  arcminutes when viewing the horizon along a target line of sight from an orbital

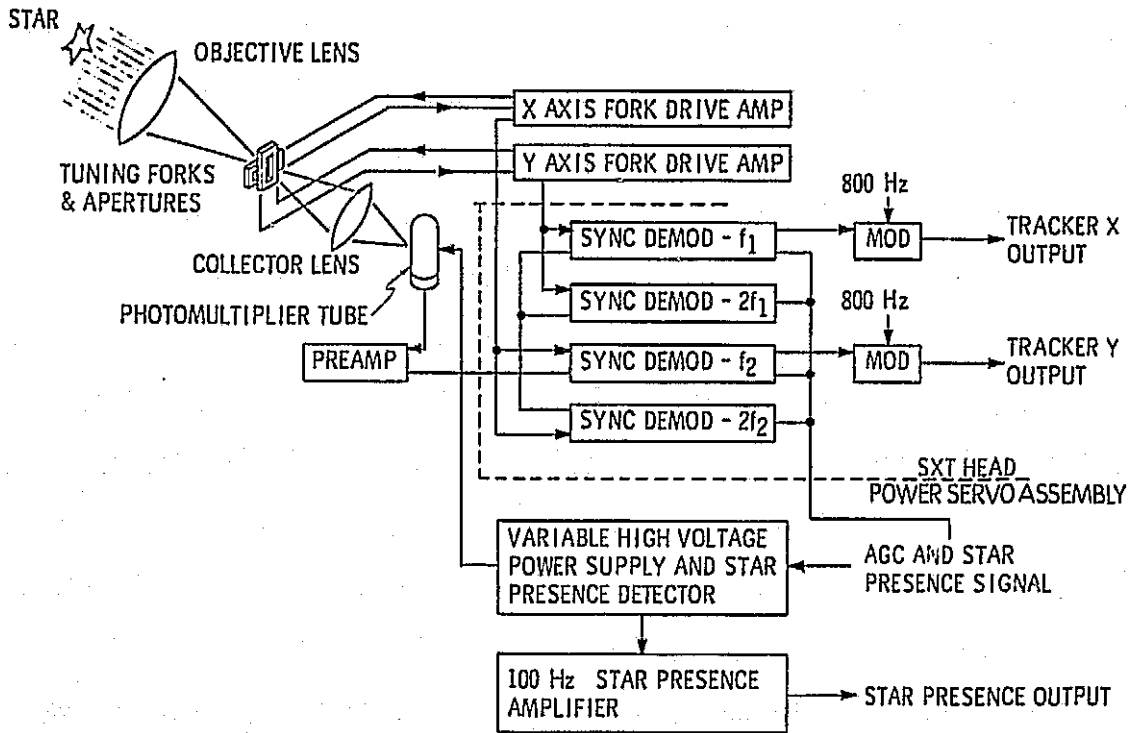


Fig. 2-2 Star Tracker, Block Diagram

altitude of 150 n. mi. See Figure 2-3. It has been determined experimentally, for example, that a horizon scan time of 10 seconds through the target at the center wavelength of 4200 Å produces a variation of signature with altitude of  $\pm 1.0$  arcminute.<sup>2</sup>

The horizon photometer which was designed to use this signature phenomenon is shown in the block diagram of Figure 2-4. Light from the earth's horizon passes through an ultraviolet filter and is collected by an objective lens that focuses the received light into a tuning fork precision oscillator assembly. Pulses of modulated light are then directed to a photomultiplier through a collector lens. The photomultiplier produces electrical pulses with timing corresponding to the modulated light pulses, and with amplitude corresponding to the radiance of that portion of the horizon profile being viewed. A narrow-band amplifier provides high-gain and low-noise amplification of the photomultiplier output. The peak detector stores the maximum value of the horizon intensity signal and, when the intensity drops to one-half peak value, the comparator, through the horizon gate, signals the computer to record the trunnion angle and time.

#### 2.4 NAVIGATION TECHNIQUE WITH THE TRACKER-PHOTOMETER

For a star-horizon angle measurement using the tracker-photometer, the navigator or computer first locates the desired navigational star in the sextant star line of sight, and the star tracker is used to keep the star precisely in the star line of sight during the ensuing maneuvers with the optical subsystem in the Track mode. Then, by appropriate spacecraft attitude changes, a point near the earth's horizon between the center of the earth and the horizon is acquired in the landmark line of sight. As the horizon is scanned along a line outward from the center of the earth toward the tracked star, the angle between the star line of sight and the landmark line of sight is monitored. When the horizon marks the half-power signature point, the trunnion angle is recorded by the computer as the star-horizon angle.

#### 2.5 CONCLUSIONS

The addition of the star tracker and horizon photometer to the existing optics would have permitted automatic sightings at low altitudes as well as in translunar flight, but component assembly, scheduling, and cost difficulties combined to cause removal of the tracker-photometer from the optics design in January 1968. Although a configuration incorporating the tracker-photometer into the Block II GN&C system was designed, it was not implemented in the flight hardware designated for mainline APOLLO flights.

---

2. C. Gray, R-648, M.I.T. X-15 Horizon Definition Experiment Final Report.

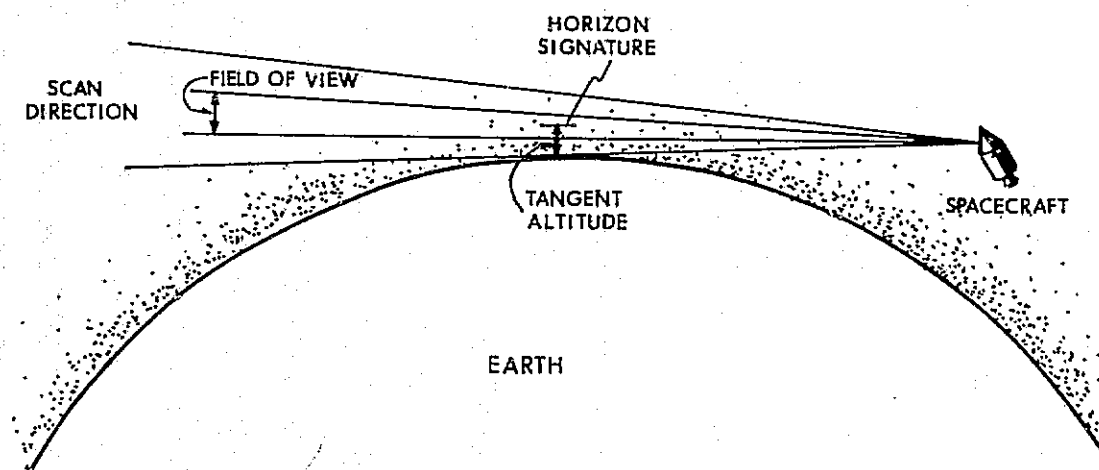


Fig. 2-8 Horizon Sighting Geometry

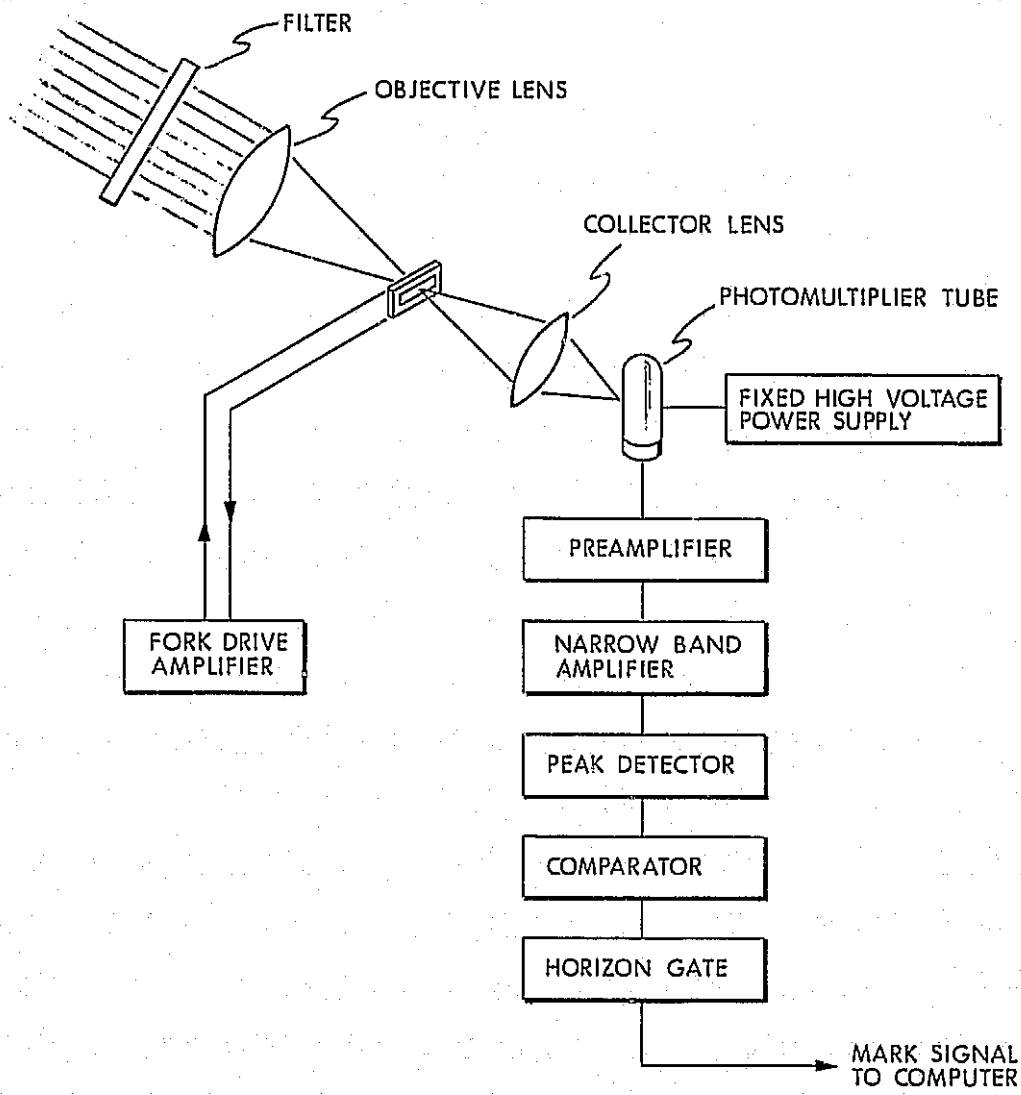


Fig. 2-4 Horizon Photometer, Block Diagram

Experiment M-439 has been under consideration for performance aboard APOLLO Applications Program flights to make use of the tracker-photometer. The proposed experiment has three objectives: validating the definition of a stable horizon signature and demonstrating its usefulness for onboard spacecraft navigation; validating the techniques of horizon position measurement; and providing a world-wide check on the horizon model. The implementation of these objectives is planned through the logical extension and synthesis of the APOLLO GN&C system. Applications of the tracker-photometer to future manned space flights, both for automatic inertial platform realignments and for automatic navigation, are discussed in MIT/IL reports E-2246 and E-2389.

PRECEDING PAGE BLANK NOT FILMED.

## SECTION 3.0

### LUNAR MODULE OPTICAL RENDEZVOUS SYSTEM

#### 3.1 INTRODUCTION

The lunar module optical rendezvous system, or LORS program, was initiated in 1965 as an alternative to the rendezvous radar (RR) subsystem. The optical rendezvous system was to replace the rendezvous radar and the alignment optical telescope on the lunar module and was to provide the following: star direction information for alignment of the lunar module inertial measurement unit (IMU), measurement of line of sight parameters between the lunar and the command service modules to derive range and range rate data for rendezvous guidance, and guidance information during the lunar module descent phase and during fixed site operations on the lunar surface. In addition, the optical rendezvous system could be used to help guide the lunar module to previous SURVEYOR or other preselected landing sites on the lunar surface.

The MIT/IL role in the optical rendezvous system development was that of technical advisor to NASA. In 1962, MIT/IL suggested that an optical tracker system be used for rendezvous of the command module with the lunar module. In 1964-65, MIT/IL compiled a list of requirements for a rendezvous system in response to a NASA request. A number of MIT/IL guidance and navigation personnel participated in the review of the airborne design, reliability, ground support equipment, and optical rendezvous subsystems integration with the GN&C system, including computer software. Hughes Aircraft Company was selected to build the optical rendezvous system, under subcontract to AC Electronics.

Due to increased confidence in the rendezvous radar as a more highly developed and demonstrated state-of-the-art system, the optical rendezvous system was canceled for use on mainline APOLLO flights and the role of MIT/IL ceased in its development. This section, therefore, describes the development of the system through early 1966.

#### 3.2 FUNCTIONAL CAPABILITIES

The optical rendezvous system consists principally of an optical tracker, mounted on the lunar module, and a luminous beacon, mounted on the command module.

The tracker was designed to detect and track specified targets to an accuracy of 0.15 mrad, one sigma, relative to the lunar module navigation base. One target is the command module luminous beacon, which should be detectable under ideal conditions at ranges up to 400 n. mi. Other capabilities include the tracking of the sun-illuminated command module to a distance of 400 n. mi. and the tracking of a third magnitude star in the presence of a fifth magnitude star. The beacon should be detectable against the sun-illuminated moon to a distance of 40 n. mi. The tracker is able to acquire and maintain track to the 0.15 mrad accuracy limit during lunar module body rates of up to 1.0 deg/sec. During lunar module body rates of up to 10.0 deg/sec, the tracker is able to maintain track, but not to the required accuracy. In a separate mode of operation, the beacon could be tracked by the lunar module flight crew using a hand-held sextant.

### 3.3 OPTICAL RENDEZVOUS SYSTEM COMPONENT DESCRIPTION

The following is a description of the operation of the optical tracker, the role of the lunar module guidance computer (LGC) in the optical rendezvous system operation, and the luminous beacon.

#### 3.3.1 Optical Tracker

The optical tracker (Figures 3-1 and 3-2) is a single line-of-sight instrument with two degrees of freedom (azimuth and elevation) that uses four photomultiplier tubes (PMTs) as optical sensors. It weighs approximately 30 pounds and consumes 80 Watts peak and 40 Watts average power. The tracker operates in two modes: Star Track and Beacon Track.

In the Star Track mode, light passes through a nutating wedge prism, which imparts a 5.0-mrad offset to the image light path. When the prism is rotated, the star image sweeps out a circle in the focal plane of the tracker's Cassegrain objective. A mask, located in the focal plane, divides the field of view into four axes, defined by two perpendicular sets of two colinear slits, in a cross pattern. (Refer to Figure 3-3.) Four relay prisms, located behind the mask near the focal plane, conduct light from the four slits to the four phototubes. The relay prisms thus act as sector division optics, with each photomultiplier generating an electrical pulse when the star image sweeps across its associated slit. The nutating prism is driven at a constant speed of 32 rps by an induction motor and is mechanically coupled to a phase generator that provides prism rotation angle information to the tracker's signal processing electronics.

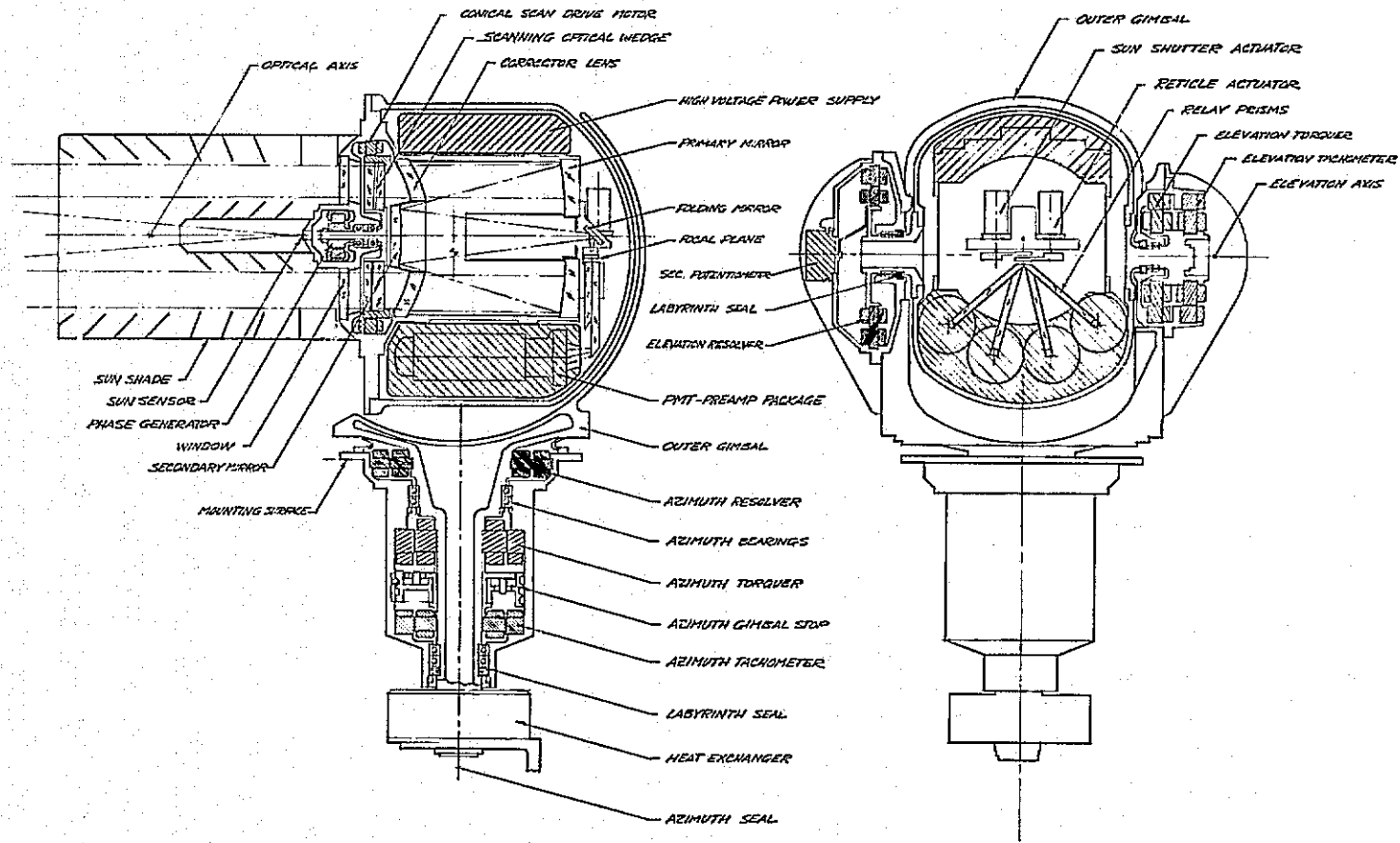


Fig. 3-1 Optical Tracker Cross Section

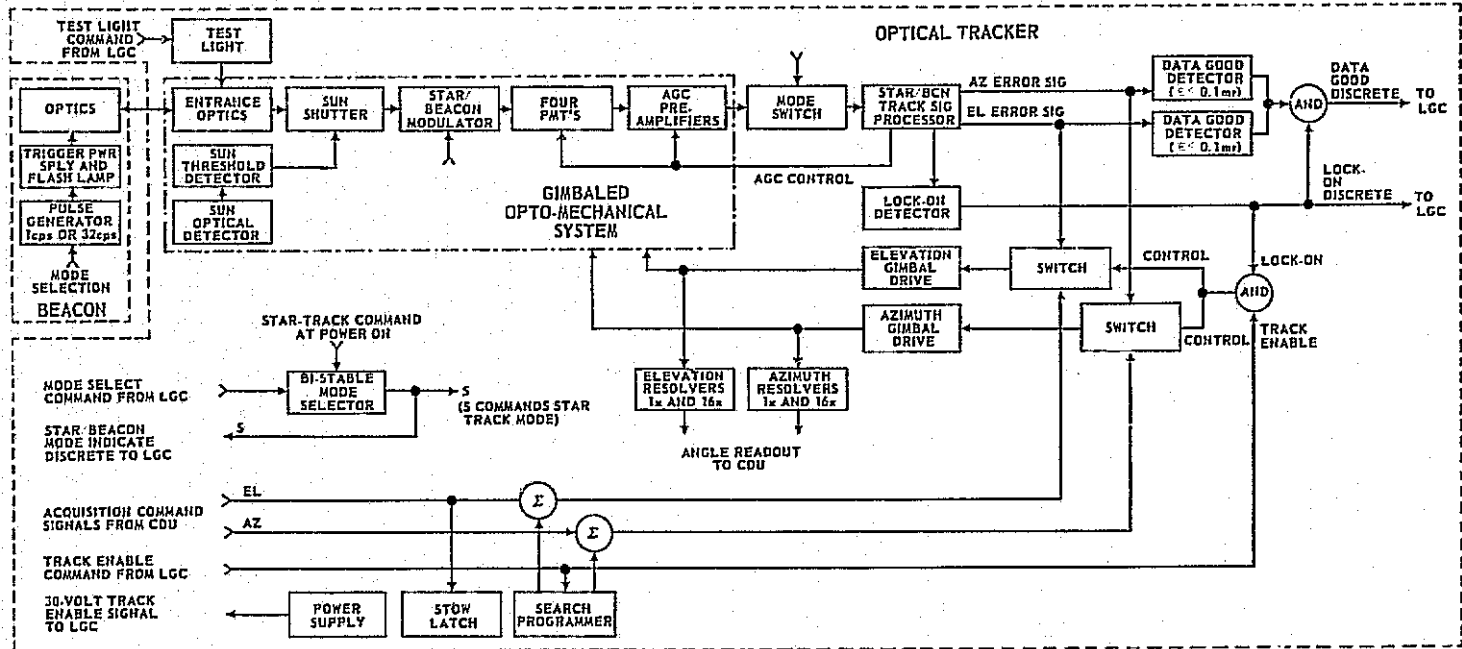


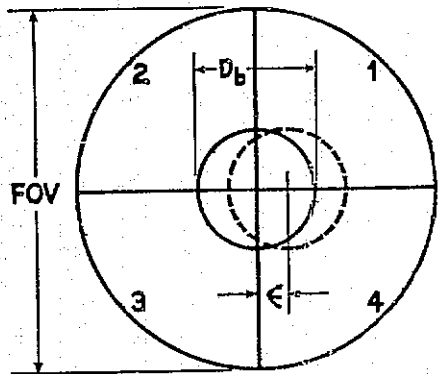
Fig. 3-2 LORS System Logic Block Diagram

Figure 3-3 shows the pulse position modulation technique used in the Star Track mode. With the target located at zero error angle, the target image describes a circular trajectory (indicated by the solid circle) that intersects each of the slits at equally spaced time intervals. The demodulation technique which is used for converting this target positioning information into an error voltage is shown at the right of Figure 3-3. Sine and cosine reference signals (from the prism phase generator) are also shown. The positions of the signals from the various photomultipliers, as indicated by  $S_1$ ,  $S_2$ ,  $S_3$ , and  $S_4$ , depend upon the error angle,  $\epsilon$ . For example, if  $\epsilon$  is zero, all four detector output pulses coincide with the zero crossings of the reference waveforms as shown. Signals from detectors 1 and 3 are summed and sent into one channel where the sum is compared with the reference sine wave; similarly, signals from channels 2 and 4 are summed and compared to the reference cosine wave in a separate channel. Thus, failure of any one phototube in no way diminishes tracking information if the image nutation rate is greater than 32 rps. When the signals are located in time position as shown by the solid lines, the reference waves are sampled at their zero crossings and zero error voltage is produced.

When an error angle  $\epsilon$  exists in azimuth, as indicated by the dotted target-image trajectory circle in Figure 3-3, the timing of signals  $S_1$  and  $S_3$  is not altered. On the other hand, the timing of signals  $S_2$  and  $S_4$  is altered in such a way as to bring  $S_2$  and  $S_4$  closer together in time. If  $S_2$  and  $S_4$  are multiplied by the cosine reference wave in a sampling circuit, a negative error voltage results. The opposite effect exists with an error angle in the opposite direction.

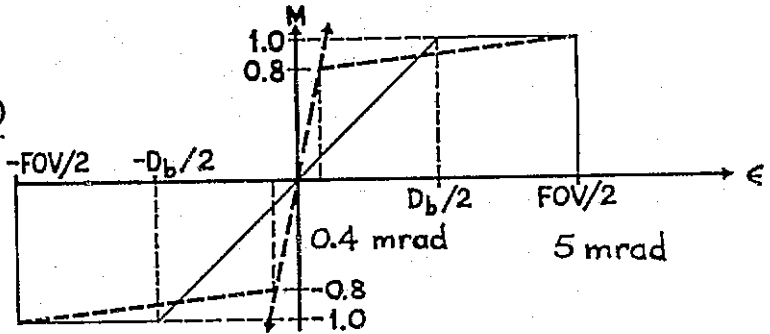
In the monopulse modulation mode (Beacon Track) four phototubes labeled 1, 2, 3, and 4 are arranged in the form of a four-quadrant array and the overall field of view is restricted by means of a circular field stop. The nutating prism is locked in a known position and the slit mask is removed from the optics focal plane by a rotary actuator. The beacon image is now nonrotating and slightly out of focus and falls directly on the faces of the four relay prisms. This type of monopulse system is analogous to radar monopulse systems that have been in use for many years. The angle error signal is proportional to the difference between the sums of the signals obtained on opposite sides of a quadrant array. The equations for the modulation index achievable in the system are indicated in Figure 3-3. At the right, a plot of the way this modulation index can be made to vary is shown as a function of the error angle  $\epsilon$ . The error angle is the amount of displacement of the target image from the center of the array. The slope of the modulation index versus error angle curve depends upon the size of the blurred image of the target. This blurred image of the target is indicated by the symbol  $D_b$  in the figure. For large

MONOPULSE SYSTEM ( SLIT MASK REMOVED FROM FOCAL PLANE )



$$M_{AZ} = \frac{(S_1 + S_4) - (S_2 + S_3)}{S_1 + S_2 + S_3 + S_4}$$

$$M_{EL} = \frac{(S_1 + S_2) - (S_3 + S_4)}{S_1 + S_2 + S_3 + S_4}$$



PULSE POSITION SYSTEM ( SLIT MASK IN FOCAL PLANE )

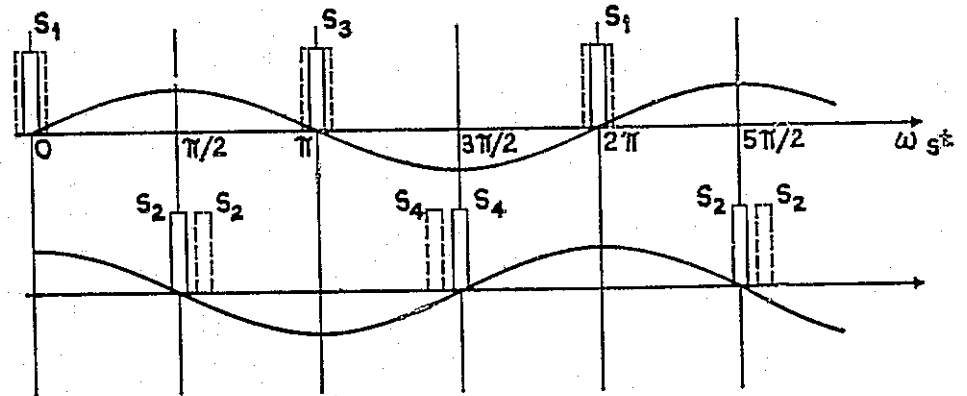
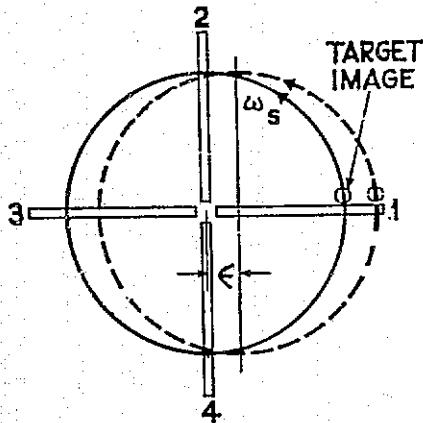


Fig. 3-3 LORS Modulation Techniques

values of  $D_p$ , the error angle curve rises approximately linearly until a value of error angle equal to  $D_p/2$  is reached; at this point the image is entirely contained on one side of the array and the modulation index is unity.

To complete the control loop, line-of-sight azimuth and elevation error signals, generated by the signal processor, energize the tracker optics gimbal drive motors, and dual speed resolvers supply angle information to the tracker coupling data unit. When the line of sight is within 5 degrees of the sun's limb, a sun sensor activates a sun shutter to block the optical path and protect the phototubes from direct solar illumination.

When the tracker is not in use, it is oriented by lunar module computer command into a stowed position, and the sun shade is capped by a protective cover. The cover contains, as a self-test feature of the optical tracker, a point light source that can simulate a flashing command module beacon and a steady star image. Each time the tracker is used, the computer initiates a self-test routine before the cover is removed.

The coupling data unit provides the position information link between the tracker and the computer. The unit provides the analog-to-digital conversion required to read the tracker gimbal angles into the computer, the digital-to-analog conversion to allow the computer to position the tracker gimbals, and an analog output proportional to the difference between the actual gimbal angle and the angle commanded by the computer.

### 3.3.2 Lunar Module Computer Control

The operation of the optical tracker, except for power application by the crew, is controlled entirely by the computer program, including tracker mode selection and evaluation of the azimuth and elevation angle information. When the tracker is turned on, the lunar module computer commands the Star Track mode, verifies that the azimuth and elevation angles indicate the stow position, and turns on the self-test light in the stowage cover. If no tracker failure is indicated (TRACKER WARNING on the display), the computer unstows the tracker and positions it to within  $\pm 1.0$  degree of the expected target line of sight. The computer may also command lunar module reorientation to select an appropriate target. A search program, generated internally in the tracker, is then started and, when a target of sufficient magnitude enters the field of view, the program is terminated and the automatic tracking process begins. The computer now accepts and processes the tracker angle data. If the tracker encounters a limit stop in azimuth or elevation,

the computer orients the tracker to reacquire the target when it leaves the stop, based on its computation of the target's path.

After the tracker is turned on, if the computer initiates the Beacon Track mode, the above sequence is followed, except that the self-test light in the stowage cover is pulsed at a 32-pps rate to simulate the flashing command module beacon. When the tracker is in the Beacon mode, a 5-mrad fixed bias exists in the line of sight; the computer removes this bias from the tracker line-of-sight coordinates as determined from the angle inputs to the computer.

When the computer has processed the necessary tracking information, it either commands the tracker to assume the stowed configuration or repositions the line of sight to acquire a new target. The crew is advised by the computer to turn off the tracker power after it is stowed.

### 3.3.3 Command Module Luminous Beacon

The major components of the luminous beacon are two xenon flash lamp and condenser units and a single electronics package consisting of two power supplies and a controller, all within a single housing. See Figures 3-4 and 3-5.

Two modes of operation, Autotrack and Visual, are selectable by the command module crew. In the Autotrack mode, the lamps are pulsed continuously at 32 pps with a pulse duration of 5 to 15 microseconds; in the Visual mode, the lamps are pulsed at 32 pps for 0.5 sec on followed by a 0.5 sec off-time. (The Visual mode was to be used for sightings by the lunar module crew, using a hand-held sextant.) Providing 8 Joules of optical energy in an 80-degree conical field, the beacon requires 350 Watts peak power. Telemetry signals indicate proper operation of each flash lamp channel.

## 3.4 REFERENCES

The functional operation of the optical rendezvous system and its testing at the GN&C level are more fully described in AC Electronics Division Experimental Design Exhibit XDE34-T-53. The LORS-LGC interface is described in XDE34-R-301.

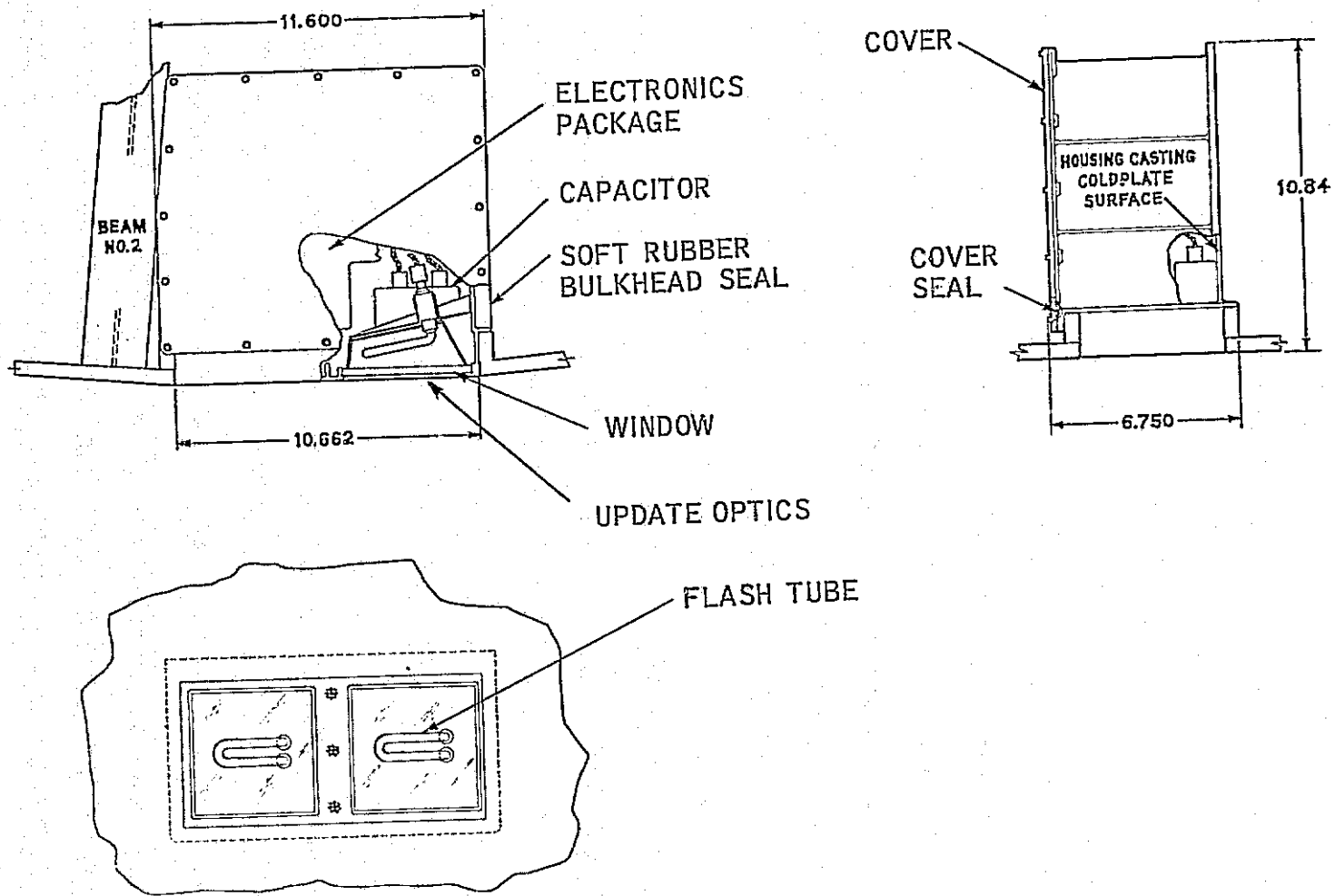


Fig. 3-4 Luminous Beacon

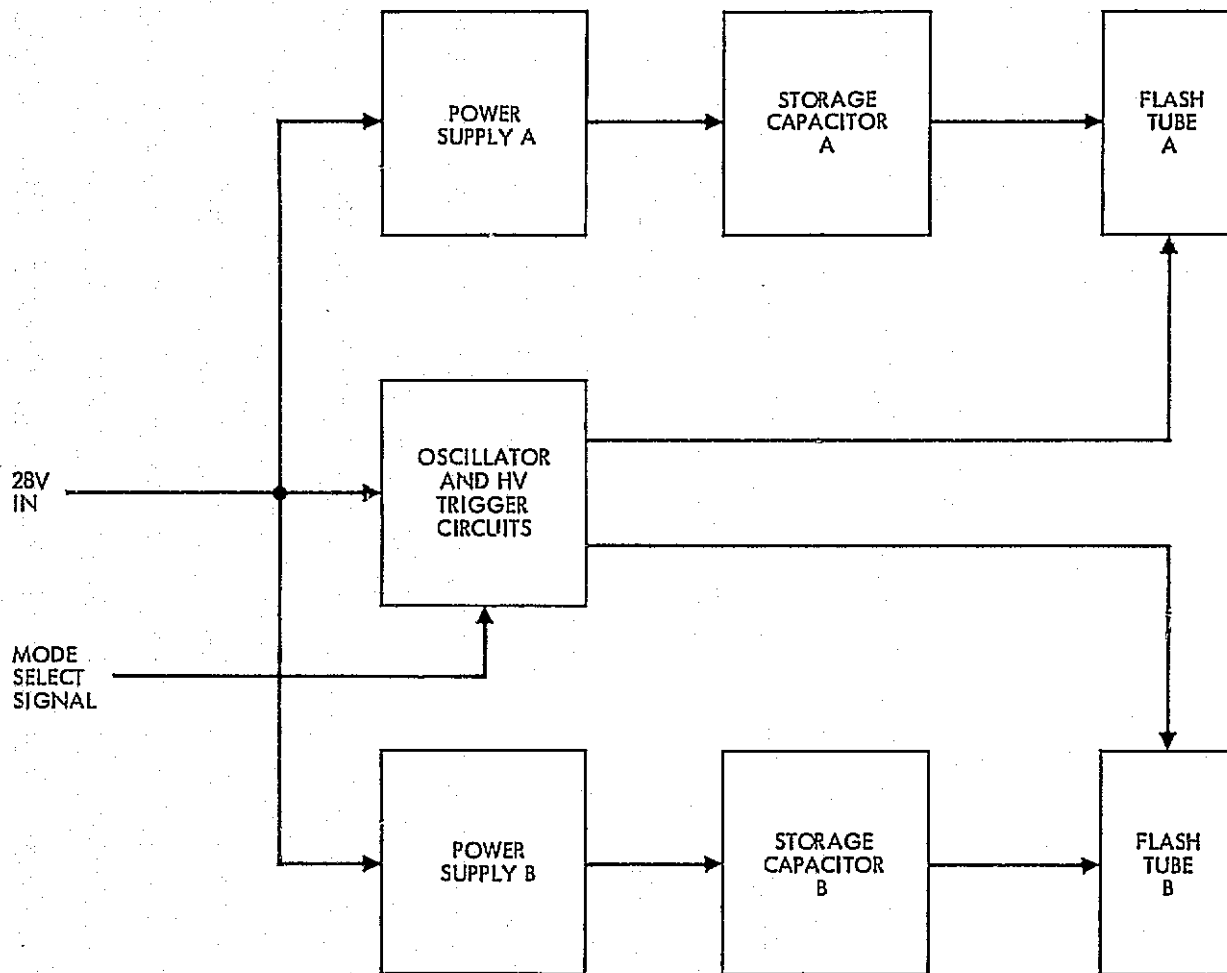


Fig. 3-5 Luminous Beacon Block Diagram

## SECTION 4.0 MAP AND DATA VIEWER

### 4.1 INTRODUCTION

The map and data viewer (M&DV) was designed and built as part of the Block I GN&C system for the command module. A second version was designed for the Block II configuration, but was not incorporated into that system because of weight, cost, and schedule limitations.

The function of the map and data viewer is to provide to the crew of the spacecraft visual access to such information as navigation charts, flight instructions, computer settings, and systems status by projecting images from a spool of 16-mm film onto a viewing screen above the optical subsystem optics panel. The astronaut accesses the information for display by operating controls on the indicator and control panel. In the Block I configuration, GN&C circuit malfunctions are automatically presented by 11 annunciator lights adjacent to the projection screen. Figure 4-1 shows the viewer and its associated controls on the indicator and control panel.

### 4.2 GENERAL DEVELOPMENT

Two configurations of the map and data viewer were designed by MIT/IL. The first design (Block I) was released to Kollsman and a number of units were manufactured. The second design for Block II was never released. With 90 percent of the design completed, NASA deleted the viewer from the GN&C system in February 1965.<sup>1</sup> However, since the design was so near completion, MIT/IL requested NASA support to finish design of the Block II configuration and to build one prototype.<sup>2</sup> This support was granted and completion of the Block II design effort began in March 1965. The prototype was finished in October and was functionally evaluated under 0-g flight conditions at Wright-Patterson Air Force Base in November.<sup>3</sup>

---

1. Contract Change Authorization No. 153-0009 to NASA Contract NAS9-153 (Removal of the Map and Data Viewer).

2. Task 3, Contract No. NAS9-4065 (M.I.T. DSR No. 55-358).

3. I.S. Johnson and W.E. Patterson, M.I.T. Internal DG Memo No. 585, "Zero G Flight Tests of G&N equipment; WPAFB, 15-18 November 1965" (29 November 1965).

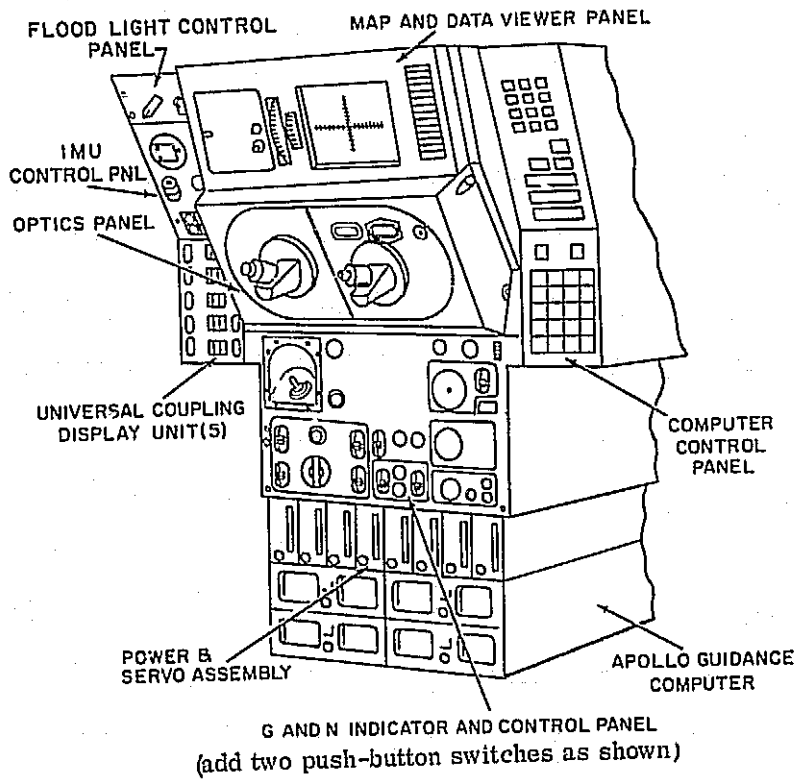


Fig. 4-1 Lower Display and Control Panel

The optical subsystem was designed to provide maximum resolution and magnification in the space available. System magnification was 18.5 and resolution exceeded 7 lines/mm on the screen. Under ideal conditions, the eye can resolve about 1.0 arcminute. At a 12-inch viewing distance, this is equivalent to 11 lines/mm. The optics were breadboarded and tests were run using NBS resolving power targets and strips of 16-mm film taken by the MIT/IL Photographic Laboratory. The maximum resolution of the test film was 96 lines/mm. On the view screen, the smallest target was resolved (i.e., 5.2 lines/mm) with no measurable difference in resolution between the center and edges. Screen luminance was uniform (75 percent of center luminance at corner of screen; this variation is not noticeable to the eye), and there was no noticeable distortion of the image. Subjective tests indicated that color rendition was good and that the image was clear and well defined. Ambient light levels for different viewing modes were satisfactorily defined.

#### 4.3 MAP AND DATA VIEWER PHYSICAL DESCRIPTION

This section describes the design features common to the Block I and II viewer configurations, with emphasis on Block II. Significant differences between the two configurations are given in Table 4-1.

The viewer was designed for viewing 16-mm color film on a 5.4 by 7.4 inch rear projection screen. In order to allow access to an unlimited amount of filmed data, the viewer used interchangeable cartridges, preloaded with 75 feet (3000 frames) of film.

Figure 4-2 depicts the viewer housing and a layout of the internal condition lights. Although not functionally related to the viewing screen, the condition lights are mounted in the viewer assembly; their function is to provide indications of specific GN&C system malfunctions (inertial unit temperature, accelerometer failure, etc.).

The Block II design allows for two modes of film positioning (slew and manual) and variable intensity for viewing under different ambient light conditions. Provision is provided for replacement of the projection lamp in case of failure. The weight of the unit (less external controls) is 8.25 pounds.

##### 4.3.1 General Construction

Most viewer structural components were fabricated from cast magnesium. Viewer construction may be described relative to its major components for greater clarification as the housing assembly, gearbox assembly, film cartridge, access door assembly, and electronics assembly.

TABLE 4-I  
CHARACTERISTICS OF BLOCK I AND BLOCK II MAP AND DATA VIEWER

Item	Block I M&DV	Block II M&DV
Lens	Ektar 2, f1.4, 25 mm	Same
Magnification	18.5	Same
Resolution	90 lines/mm (Kodachrome II) 4.8 lines/mm at screen	Same
Film	Standard double sprocket 16 mm film	Same
Lamp	Two filaments, 5W and 7W	2 Lamps - 2 filaments/lamp
Lamp Replacement	Manual Replacement	Rotating Turret
Screen	Polacoat, moveable	Mylar, sealed
Magazine Capacity	50 ft - 2000 frames	75 ft - 3000 frames (thin base Mylar)
Moisture Resistant	No	Breathing enclosures on projection system and lamp housing
Film Drive Modes	manual; single step, bidirectional slew - 20 frames/sec	manual; variable- slew - 0 to 70 frames/sec
Frame	Machined beryllium	Cast magnesium
Mirror	Machined beryllium	Cast magnesium, nickel coated
Weight (including magazine and film)	9.43 lb	8.25 lb
Magazine (including weight film)	10.6 oz (300.5 grams)	7.4 oz (208 grams)

~~PRECEDING PAGE BLANK NOT FILMED~~

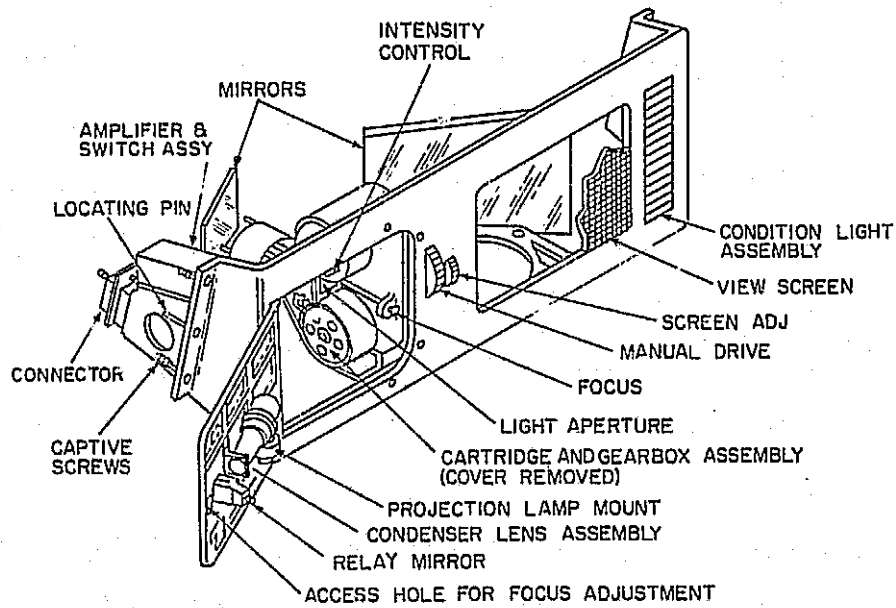


Fig. 4-2a Map and Data Viewer

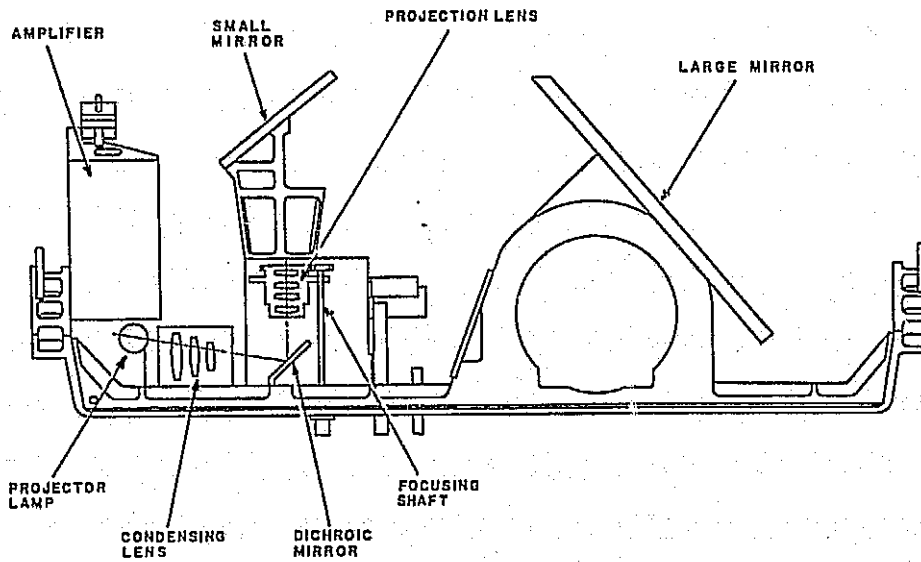


Fig. 4-2b M and DV, Top View

#### 4.3.1.1 Housing and Moisture Seal Assembly

The housing assembly, as shown in Figure 4-2, was fabricated from cast magnesium. It provides mounting facilities for the gearbox assembly, two mirrors, the condition light assembly, and view screen. A control is provided that permits manual vertical positioning of the film.

The view screen is made of Mylar and is attached to the viewer housing by a moisture-proof seal. Some models of the viewer included provisions for the screen to be scribed with vertical and horizontal indices to allow measurement of relative coordinate positions on projected maps, etc. A series of marks on the bottom portion of the screen, in conjunction with indices on the film, indicated approximate location in the total film strip of the frame being viewed. This was to enable rapid slewing to a particular section of the film strip for approach to the specific film data frame desired. A moisture seal shroud (Figure 4-2a), consisting of a lightweight cover sealed to the viewer housing and the gear box, is fitted with a pressure relief valve and desiccator to prevent moisture fogging and damage to the internal optical components.

#### 4.3.1.2 Film Cartridge

The film cartridge (Figure 4-3) consists of two spools with associated externally driven gears and sprockets that transport up to 75 feet of 16-mm film past a light aperture. The viewer gearbox provides a loading recess for the film cartridges. The cartridge is inserted through the access door and loaded into the gearbox recess. Gearbox and cartridge alignment is achieved by means of a locating pin and by reference surfaces on both the cartridge and projection lens.

The locating pin is embedded in the gearbox housing and mates with a slotted hole in the cartridge aperture block; this ensures correct positioning of the aperture relative to the projection lens and obtains correct meshing of the gears. The gearbox and cartridge sprocket drive gears are special 5-tooth, long-addendum gears. During loading, the film is aligned so that a frame is centered in the aperture when a tooth space of the sprocket drive gear is centered on the aperture opening.

#### 4.3.1.3 Access Door Assembly

The door (Figure 4-4) provides access to the gearbox for loading and unloading film cartridges. In addition, the door supports the projection lamp, condensing lens, and relay mirror.

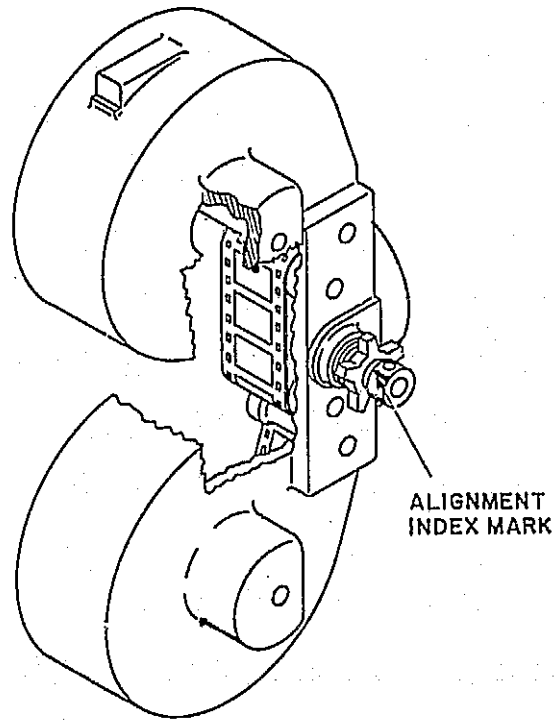


Fig. 4-3 Cartridge and Film Alignment

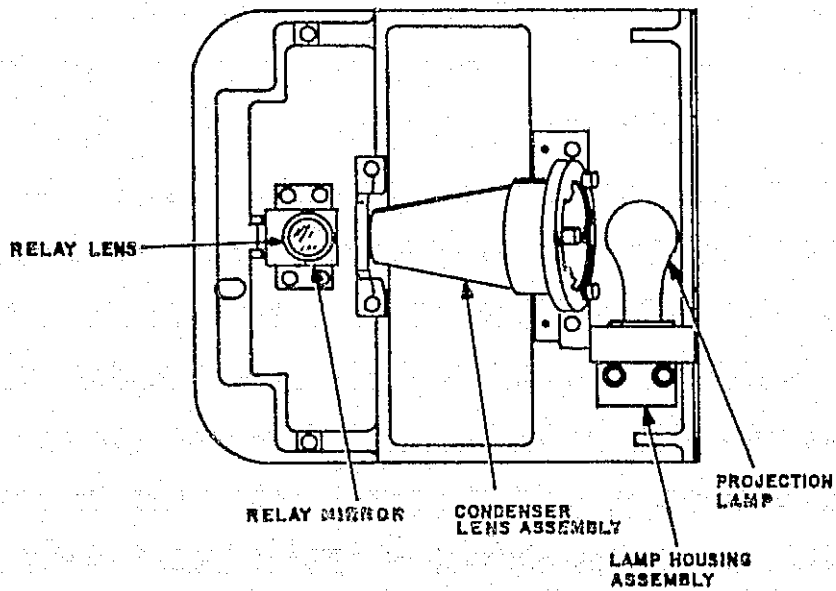


Fig. 4-4 Access Door Assembly

The specially designed projection lamp is mounted on the rear of the access door. The condensing lens, mounted adjacent to the lamp, receives the light and directs it to a dichroic relay mirror. The relay mirror reflects the visible light through 90 degrees and directs it through the cartridge aperture when the door is closed. Long wavelength radiation is transmitted through the mirror to a heat sink.

#### 4.3.1.4 Electronics Assembly

The original requirements for the viewer were based on a use concept that had much of the data stored in the same sequence as would be used during flight. Thus, the Block I film drive had two modes: a single frame step (forward or backward) and a slew mode of about 20 frames per second in addition to the manual drive mode. The slew mode allowed for changes in the sequencing required for flying alternate or abort missions.

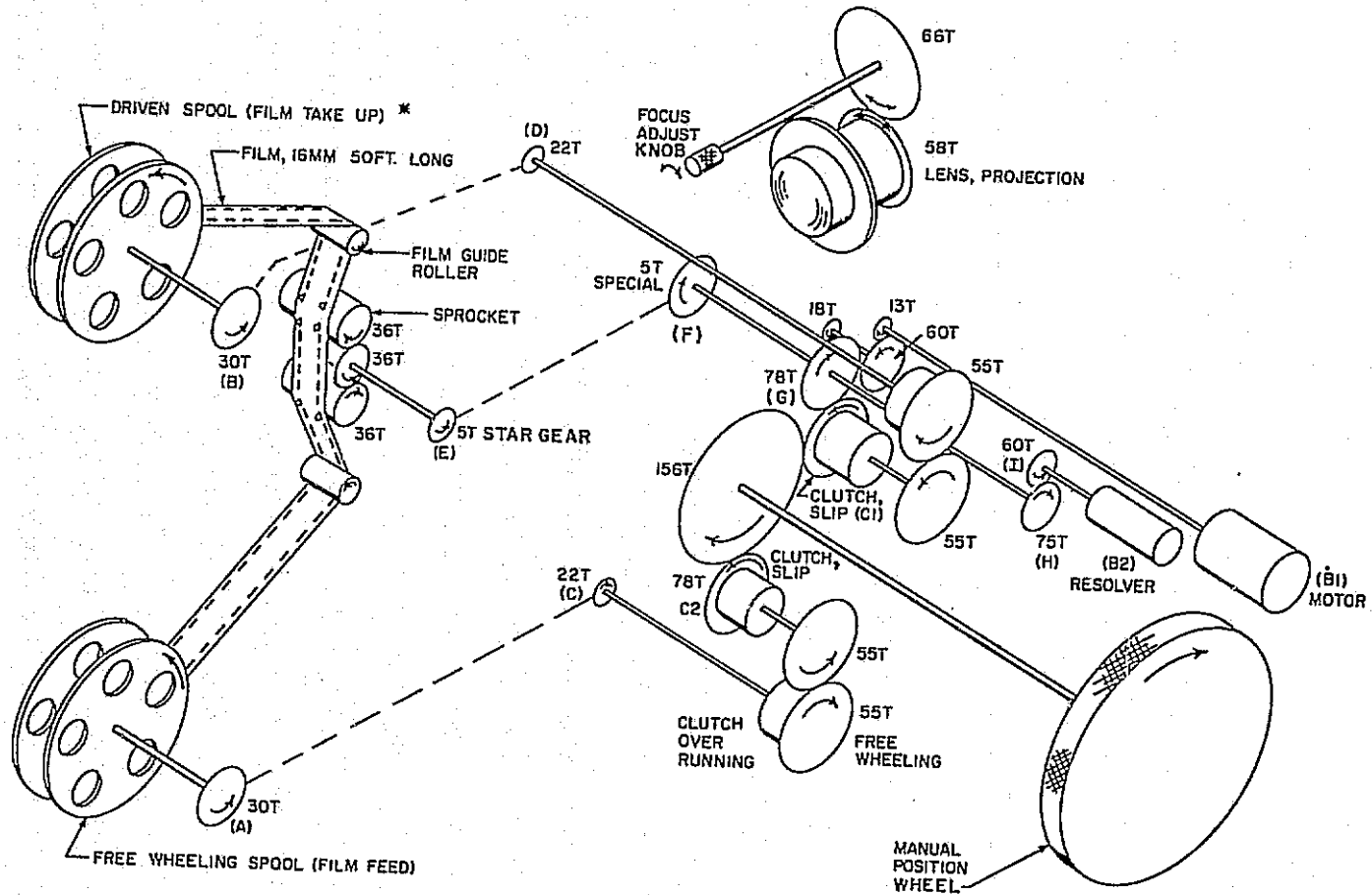
Later, mission planning tended away from the very vigorously pre-planned timeline to the more flexible modularized concept. The ability for rapid slew to allow random access then became a paramount requirement. To accomplish this, the film drive in Block II was redesigned to allow a continually variable speed from 0 to approximately 70 frames per second. This design greatly simplified the viewer electronics circuitry and decreased the weight of the viewer by 9 oz.

A linear resolver is attached to the data frame control lever on the G&N panel. Using the linear resolver as the command input and a tachometer as the feedback element, a simple rate control servo was designed for film drive control.

#### 4.3.2 Map and Data Viewer Mechanization

The viewer gearbox assembly drives the film cartridges in two directions, forward and reverse, and houses the projection lens that projects the light passing through the cartridge aperture. Simultaneously, the gearbox must permit angular film speed to vary as the effective diameter of the film spools changes, while maintaining a uniform rate of feed through the aperture.

Figure 4-5 illustrates the cartridge and gearbox drive system. The cartridge drive gears (A and B) extend beyond the housing to engage their respective gearbox drive components (C and D). The two cartridge sprockets on each side of the aperture block are driven by gear E that engages its gearbox drive components (gear F). Gearbox motor B1 provides constant drive to the pinned gear and shaft system (gears



\* SLEWING IN UP DIRECTION

Fig. 4-5 Gearbox and Cartridge Mechanization

F, G, and H), that drives resolver B2, slip clutch C1, and cartridge sprockets (through gears E and F).

The slip clutches (C1 and C2) are set at 0.85-inch-ounce torque. To protect the film, the clutches slip or disengage when frictional loading increases above this value. The overriding clutches (C3 and C4) are free-wheeling in one direction and transmit torque in the other. The cartridge drive spool gears A and B are driven directly through the override clutches by gears C and D. A slip clutch and overriding clutch are in series between the sprocket drive shaft and each spool drive shaft. The slip clutches allow variable angular speed with changes in effective spool diameter, thus maintaining a constant linear film speed. The overriding clutches permit forward and backward film movement by permitting the "feed" spool to unwind freely, while the "take-up" spool is being driven.

The manual film drive control serves as a backup in case of motor malfunction, and also permits incremental adjustment at each frame position. The control is mechanically connected to motor and drive gearing.

#### 4.3.3 Optical System

The viewer optical system (see Figure 4-6) consists of a projection lamp, reflector, a condensing lens system, a dichroic relay mirror, a projection lens, and two nickel-coated magnesium mirrors.

Two projection lamps are provided for the viewer; they are mounted on a rotating turret and, in the event of failure of one lamp, the other can be manually rotated into operating position. Each lamp contains two filaments to provide three levels of film illumination and an integral focusing reflector. Light emanating from the projection lamp is made convergent and is directed onto a dichroic relay mirror by the condensing lens system; the mirror is dichroic so that thermal energy from the lamp is removed from the optical path to provide some degree of thermal isolation of the film. The mirror turns the light 80 degrees and directs it through the cartridge aperture into the projector lens; that is, f1.4, 25-mm with a fixed aperture and geared focus ring. The lens is focused from the viewer front panel by turning a shaft and pinion that engages the lens focus ring gear. The image path from the projector lens is turned 180 degrees by two nickel-coated magnesium mirrors and directed onto the Mylar view screen.

The projection lamp, mounted on the rear of the access door, is designed for high filament strength and long life. It contains two 6-Volt filaments of 5 and 7 Watts,

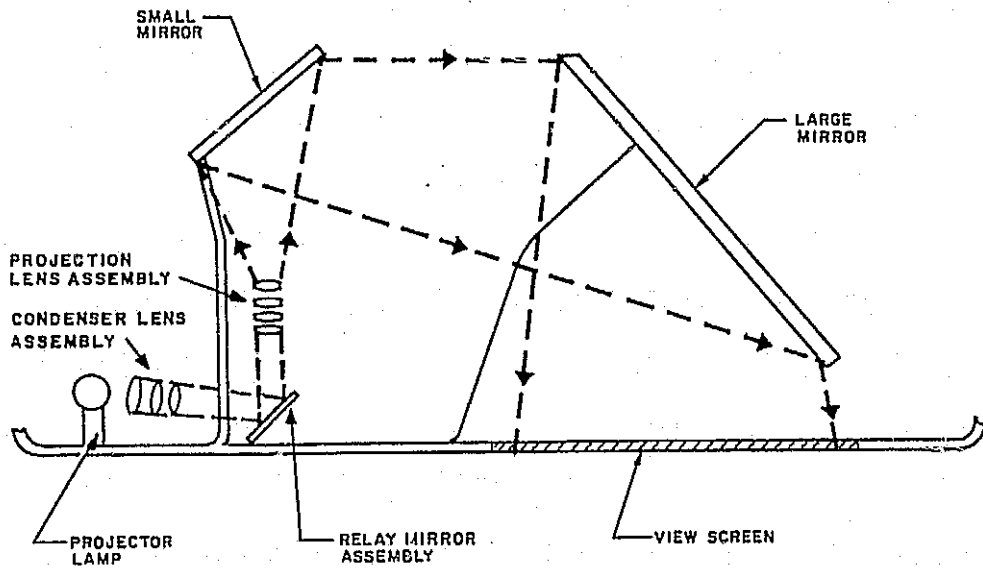


Fig. 4-6 M&DV Optical System Functional Diagram

with 12-Watt total capability using both filaments simultaneously. The dual filament design makes available three levels of light intensity at the filament design color temperature of 2870°K. This greatly enhances resolution of color film used in the viewer.

#### 4.3.4 Operation

The viewer is operated by controls on both the viewer and the indicator and control panel. The panel control provides remote film slewing; the viewer panel contains a manual input control that permits manual positioning of the film to the frame desired in the event of a failure in the remote capability.

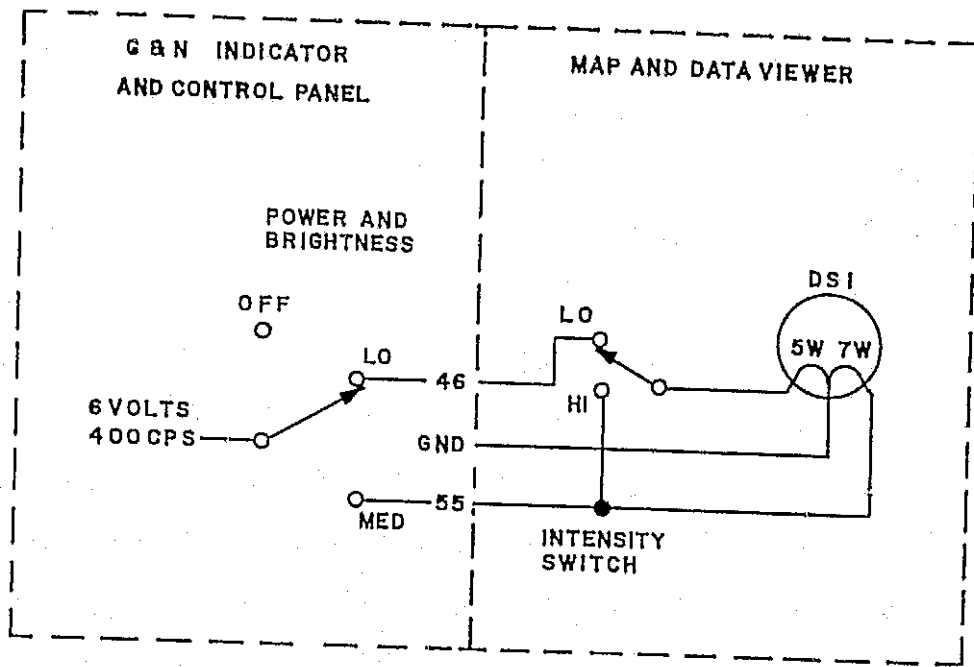
The G&N panel also houses the POWER and BRIGHTNESS switch that is used in conjunction with the viewer INTENSITY switch to control projection lamp input power. This switching arrangement provides the capability of varying the lamp intensity (adjustment of view screen brightness) without affecting lamp color temperature. This feature provides for optimum image definition under all anticipated ambient lighting conditions. Figure 4-7 shows the projection lamp control circuit with the switching sequence required for intensity control.

### 4.4 DEVELOPMENT TESTING OF BLOCK II CONFIGURATION

The final phase in the development of the Block II viewer was an evaluation of the design for selected environmental stresses. The viewer was subjected to modified tests of ND 1002037 (Environmental Qualification Specification) for sinusoidal and random vibration, pressure, humidity, and shock. The performance of the equipment was checked periodically during the tests and after each cycle and phase. Except for momentary degradation during short transient periods, the performance and image display quality were excellent. The condition and performance of the unit at the conclusion of the tests indicated an adequate tolerance to the stress levels of these tests.

#### 4.4.1 Sine-Wave Vibration Tests

Six sine-wave 1-g vibration test cycles were conducted for 8 minutes each along each of three orthogonal axes for a total of 18 tests. This controlled frequency was varied linearly from 15 to 2000 cps. Image quality was monitored during each test cycle, and mechanical performance was checked at the termination of each cycle. No failures occurred and image quality was degraded only at 130 cps. The maximum acceleration recorded on the primary structure was 6 g at a mid-point



PROJECTION LAMP INTENSITY

<u>POWER AND BRIGHTNESS SWITCH POSITION</u>	<u>INTENSITY SWITCH POSITION</u>	<u>TOTAL PROJECTION LAMP PWR (WATTS)</u>
OFF	HI	0
	LOW	0
MED	HI	12
	LOW	7
LOW	HI	0
	LOW	5

Fig. 4-7 Projection Lamp Control Circuit

between the end-support locations. The spring-loaded access door underwent a 15-g acceleration in one direction and a 12-g acceleration in the other. Because of the semi-secure condition of the door, this response was anticipated. The buffeting did not damage integral components such as the lamp turret, lamp-house enclosure, or condenser lens housing. The strap-on desiccator "breather valve" was vulnerable to breakage due to its location with respect to the center of gravity and the radius of gyration. It underwent 12-g acceleration near the frequency of 130 cps.

#### 4.4.2 Random Vibration Tests

Fourteen random vibration test cycles were run on the equipment while sensitive locations were monitored and recorded. The minimum time for each cycle was 6 minutes, with a constant, controlled input level of 7.86 g rms. During the sixth cycle, the filaments of the working lamp shorted and fused. Because each filament went "dead" on only the bypassed side of the fusion weld, there was no total illumination loss; the remaining "live" portion of the filaments provided limited and unsymmetrical illumination of the viewing screen. The spare lamp, which had been subjected to essentially the same vibration levels as had the working lamp, was then rotated 90 degrees into the working position. It restored the viewing screen luminance to its proper level.

During this series of random vibration tests, two marginal aspects were noted in the construction of the desiccating "breather valves." Only the valve which was provided with an auxiliary strap-down support was able to withstand the applied vibration. The other developed a fatigue fracture line along the root of the thread encompassing the boss by which it mounts into a tapped hole in the equipment. This weakness could be eliminated by a simple redesign of the valve body. Unless the retention spring maintains a positive load on the desiccant material, the granules of desiccant become loose and tend to pulverize. If this occurs, the resultant dust could present a contamination problem, even though the containment filters have prevented such occurrences thus far. This potential hazard can be avoided by using a sufficient quantity of desiccant so that the retention spring is compressed to one-half its free length. With sufficient installed compression in the retention spring, vibration will not compact the desiccant beyond its compressive reach.

#### 4.4.3 Pressure Tests

Three pressure chamber tests were run to verify the strength of the 0.030 magnesium sheet, moisture-sealing enclosure. To simulate mounts and rates of pressure change anticipated in the APOLLO command module, the chamber's pressure was

rapidly reduced to impose pressure differentials of 10 and 5 psi upon the equipment. After reducing the chamber's pressure by these values, the chamber was "released" back to approximately 15 psi. Due to the fact that a 5 to 10 psi positive, internal pressure might be imposed on the equipment during a mission, an internal pressure relief valve was tested for preventing damage to the optical enclosure and found to be adequate. Except for sudden surges of pressure, the desiccating "breather valves" are designed to balance internal-to-external pressure differentials to within 1-1/2 psi. The sheet metal enclosures are designed to withstand this level of pressure differential, externally, or internally. The rate of pressure drop was 5 pounds in 1-3/4 minutes and 10 pounds in 4 minutes. Pressure was increased at one-half this rate.

#### 4.4.4 Moisture Tests

Five moisture tests were conducted per MIL-STD-810 method 507.1 in an effort to determine the capacity of the seals and enclosures for preventing moisture migration in a condition of high ambient humidity. Each test cycle began with the relative humidity at 95 percent and a linear temperature increase from 70° to 120°F over a period of 2 hours; 120°F was then maintained for a period of 6 hours with the relative humidity held at 95 percent or more; finally, the temperature was lowered, uncontrolled, from 120° to 70°F over a period of 16 hours at approximately 95 percent relative humidity.

Throughout test 1 there was no indication of moisture migration and no degradation of the image on the viewing screen. The lamp was on continuously to permit constant monitoring of the viewing screen; this constant illumination might aid in humidity control and should be limited in further tests to operation when the screen image checks are to be made. Test 2, conducted on this basis, showed no moisture migration. Because ambient pressure was static during these moisture tests, pressure was varied during the remaining tests to induce moisture migration.

Moisture tests 3 and 4 included the moisture-temperature schedule of tests 1 and 2, plus periodic fluctuations in ambient pressure to cause the "breather valves" to aspirate under conditions of high humidity. The pressure was reduced from 30 in. Hg to 20.5 in. Hg in 4 minutes, held at 20.5 in. Hg for 15 minutes, then increased to 30 in. Hg in 2 minutes. This cycle was repeated five times in tests 3 and 4, with relative humidity occasionally reaching 97 percent. Checks of the image on the viewing screen were made at 4-minute intervals. At no checkpoint in either test was there any sign of image degradation on the view screen. These results were satisfactory. After test 4, the indicator gel in the "breather valve" of the projection

system's enclosure was removed, dehumidified, and reinstalled. It contained 3.12 grams of water.

The moisture tests were comprehensive. Humidity sensors indicated an absence of a dew point condition. Tests 3 and 4 were conducted within a potential dew point range, but failed to yield a true dew point effect. Unit design material and components prevent the dew point effect. The thin-walled moisture enclosures are constructed of magnesium, which has a high coefficient of thermal conductivity. Any temperature change in the ambient conditions is quickly transmitted by the magnesium to the atmosphere on the opposite side. This low thermal resistance reduces the temperature transfer, destroys the sharp gradient, and prevents the dew point effect.

It seemed mandatory, however, that the effects of a true dew point condition be known, especially at the viewing screen and other critical locations; e.g., interfaces between film magazine and illumination system and the magazine and the projection system.

To create a true dew point condition at the viewing screen and other parts of the optical system, a sharper temperature rise was instituted in test 5. The initial phase of the test cycle was modified so that the temperature rise from 70° to 120°F was accomplished in 1 hour and 40 minutes, rather than 2 hours. This sharper temperature rise caused a momentary fogging of the viewing screen. Because the image on the screen remained fogged for less than 2 minutes, it was apparent that the temperature gradient at the screen dropped suddenly. Visual inspection following this series of moisture-temperature-pressure tests disclosed evidence of some surface-grain corrosion as well as a small amount of blistering of finish paint (maximum diameter of blisters being 3/16 inch). There was no evidence of any impairment of the structure, seals, and enclosures, or the performance of the unit.

#### 4.4.5 Drop Test

The "qualification" drop test was conducted as a final test phase for the Block II viewer. This test conformed to ND-1002037 for 20 g. Visual inspection of the unit following this shock test disclosed no evidence of structural or operational impairment.

#### 4.5 PORTABLE CONFIGURATION

With the deletion of the viewer from the CN&C system, subsequent design efforts centered upon studies concerning the film drive mechanism to allow random access

(see paragraph 4.3.1.4); and a portable version of the viewer using the basic optics and film drive mechanism.

The interest in a portable version of the viewer grew from two considerations. The first requirement came from the 0-g functional tests at White Sands Missile Range. During these tests, it was noted that the viewer could easily be seen by all three astronauts when encouched in their usual operating position at the main display console. If the viewer was portable, its use could be expanded to cover both lower equipment bay and main display console operations, and the unit could be secured to the spacecraft for use in several convenient locations. The second requirement for a portable configuration arose when an eyepiece stowage unit was designed and installed in the space previously occupied by the viewer.

Starting with the present optics design and film drive mechanism, various arrangements were studied. The most promising one is shown in Figure 4-8. The optics design was not modified in order to maintain the same high resolution capability of the original design; namely, 90 lines per mm on color film. A wooden mockup was constructed to verify the convenience of the portable configuration. It appeared that by reducing the screen size to alter the size of the final package, the individual film frame data would have been reduced so as to become unintelligible.

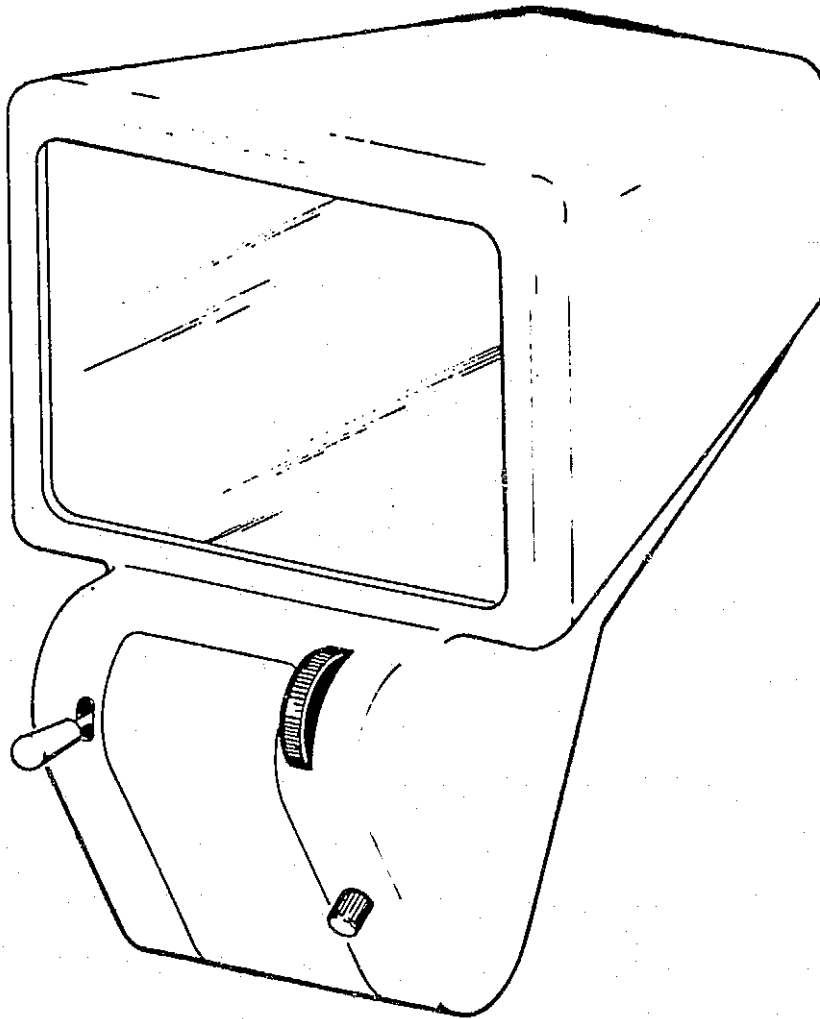


Fig. 4-8 Map and Data Viewer - Portable Configuration